

# Università Degli studi di Napoli “Federico II”

TESI DI DOTTORATO IN INGEGNERIA AEROSPAZIALE, NAVALE E  
DELLA QUALITÀ  
CICLO XIX

## Cloud Characterization in CIRA Icing Wind Tunnel



Relatori Ch.mi:  
Prof. Ing. G. M. Carlomagno  
Prof. Ing. T. Astarita

Matteo Bellucci  
Centro Italiano Ricerche Aerospaziali  
DETEC, Facoltà di Ingegneria

# INDEX

INTRODUCTION .....	6
CHAPTER 1 .....	9
WHY AIRCRAFT ICING IS DANGEROUS .....	9
1.1 ICING THREAT.....	9
1.2 KINDS OF ICE .....	9
1.2.1 Clear (or Glaze) Ice .....	10
1.2.2 Rime Ice .....	11
1.2.3 Mixed Ice .....	12
1.3 WHY THEY FALL: EFFECT OF ICE ACCRETION ON AIRCRAFT FLIGHT DYNAMICS...	13
1.3.1 Performance Degradation.....	13
1.3.2 Aircraft Handling .....	16
1.3.3 Airfoil sensitivity .....	18
1.4 ICING RELATED ACCIDENTS.....	20
CHAPTER 2 .....	25
THE ICING WEATHER .....	25
2.1 MECHANISM AND COMPOSITION OF CLOUDS.....	25
2.2 COMPOSITION AND STRUCTURE OF THE ATMOSPHERE.....	26
2.2.1 Composition of the Atmosphere .....	27
2.2.2 Structure of the Atmosphere .....	28
2.3 WATER CYCLES IN THE ATMOSPHERE .....	30
2.4 CLOUDS FORMATION.....	32
2.5 CLOUDS CLASSIFICATION .....	32
2.5.1 High Clouds (Above 6 km, or 20,000 ft) .....	34
2.5.2 Middle Clouds (2 to 6 km, or 6,500 to 20,000 ft) .....	34
2.5.3 Low Clouds (Below 2 km, Or 6,500 ft) .....	35
2.5.4 Clouds Of Vertical Development .....	36
2.6 ICING CLOUDS .....	37
2.6.1 Stratiform Clouds .....	37
2.6.2 Cumuliform Clouds .....	39
2.7 FRONTAL ICING CONDITIONS.....	40
CHAPTER 3 .....	42
ICE ACCRETION PHISICS .....	42
3.1 FORMATION OF ICE IN THE ATMOSPHERE .....	42
3.2 SUPERCOOLED WATER DROPLETS .....	44
3.3 MECHANISM OF AIRCRAFT ICING .....	44
3.4 ICING VARIATIONS .....	46
3.5 ICE GROWTH.....	47
3.6 PRECIPITATION TYPE AND ICING .....	50
CHAPTER 4 .....	53

<b>MAIN PARAMETERS IN AIRCRAFT ICING.....</b>	<b>53</b>
4.1 PHYSICAL FACTORS AFFECTING AIRCRAFT ICING.....	53
4.2 ICING INTENSITY.....	53
4.3 LIQUID WATER CONTENT.....	55
4.4 TEMPERATURE.....	58
4.5 DROPLET DIAMETER.....	60
4.6 COLLECTION EFFICIENCY.....	64
4.7 AIRSPEED.....	65
4.8 ICING MEASUREMENT INSTRUMENTS.....	66
<b>CHAPTER 5 .....</b>	<b>67</b>
<b>ICING CERTIFICATION .....</b>	<b>67</b>
5.1 AIRCRAFT CERTIFICATION ISSUES.....	67
5.2 BASIC ASPECTS OF SAFETY .....	69
5.3 ICE PROTECTION SYSTEM BASIC ISSUES .....	71
5.4 CURRENT DESIGN ENVELOPES.....	73
<b>CHAPTER 6 .....</b>	<b>79</b>
<b>ICING SIMULATION TOOLS .....</b>	<b>79</b>
6.1 BRIEF OVERVIEW OF THE AVAILABLE TOOLS.....	79
6.2 DIFFERENT SIMULATION TECHNIQUES.....	81
6.3 GROUND FACILITIES.....	83
6.3.1 Icing Wind Tunnels.....	84
6.3.2 Engine Icing Facilities.....	85
6.3.3 Low Velocity Facilities .....	86
6.4 USE OF ICING SIMULATION TOOLS IN DESIGN AND CERTIFICATION.....	87
6.4.1 Current Simulation Capabilities .....	89
6.4.2 Limitation Of Current Simulation Methods.....	91
<b>CHAPTER 7 .....</b>	<b>95</b>
<b>CIRA – ICING WIND TUNNEL.....</b>	<b>95</b>
7.1 IWT OVERVIEW .....	95
7.2 WIND TUNNEL GENERAL DESCRIPTION.....	99
7.2.1 Cooling Systems .....	101
7.2.2 Air Plant .....	102
7.2.3 Fan System .....	103
7.2.4 Spray Bar System.....	104
7.2.5 Test Sections.....	107
7.2.6 Engine Flow Simulator.....	110
7.3 TEST EQUIPMENT.....	111
7.3.1 Turn Tables.....	111
7.3.2 Model Sting Support .....	113
7.3.3 Probe Traversing System .....	115
7.3.4 External Balance System.....	115
7.4 ICING INSTRUMENTATION.....	118
7.4.1 Droplet Sizing Measurement Methods.....	119

7.4.1.1 Phase Doppler Particle Analyser (PDPA) Technique .....	119
7.4.1.2 Forward Scattering Spectrometer Probe (FSSP).....	121
7.4.1.3 Optical Array Probe (OAP) .....	122
<b>7.4.2 Liquid Water Content Measurement Methods .....</b>	<b>122</b>
7.4.2.1 Icing Blade System .....	123
7.4.2.2 Hot-Wire LWC Probe .....	124
<b>7.4.3 Liquid Water Content Uniformity Measurement Methods .....</b>	<b>125</b>
<b>7.5 AERODYNAMIC INSTRUMENTATION .....</b>	<b>126</b>
7.5.1 Hot Wire .....	126
7.5.2 Flow Angularity Probe .....	126
7.5.3 Temperature Probe.....	126
7.5.4 Laser Doppler Velocimeter .....	127
<b>CHAPTER 8 .....</b>	<b>128</b>
<b>ICING CLOUD CHARACTERIZATION IN THE CIRA IWT .....</b>	<b>128</b>
<b>8.1 STS ICING CLOUD CHARACTERIZATION .....</b>	<b>129</b>
8.1.1 Droplet size calibration .....	132
8.1.2 SBS temperature assessment .....	140
8.1.3 Icing cloud uniformity and coverage area .....	143
8.1.4 Liquid Water Content measurements .....	149
8.1.5 Icing cloud operative envelope .....	155
<b>8.2 ATS ICING CLOUD CHARACTERIZATION .....</b>	<b>156</b>
8.2.1 Droplet size calibration .....	156
8.2.2 SBS temperature assessment .....	163
8.2.3 Icing cloud uniformity and coverage area .....	164
8.2.4 Liquid Water Content measurements .....	170
8.2.5 Icing cloud operative envelope .....	176
<b>8.3 DATA COMPARISON.....</b>	<b>177</b>
8.3.1 MVD Data Comparison: basic analysis.....	177
8.3.1 MVD Data Comparison: thermodynamic effects .....	181
8.3.2 MVD Data Comparison: Fluid Dynamic effects .....	183
8.3.3 SBS Temperature Envelope Comparison .....	186
8.3.4 Uniformity Measurements Comparison.....	187
8.3.5 LWC Data Comparison.....	191
<b>CONCLUSIONS .....</b>	<b>194</b>
<b>APPENDIX A: .....</b>	<b>196</b>
<b>DE ICING AND ANTI ICING SYSTEMS .....</b>	<b>196</b>
<b>APPENDIX B: .....</b>	<b>199</b>
<b>OTHER CERTIFICATION/QUALIFICATION ASPECTS .....</b>	<b>199</b>
<b>B 1.0 GENERAL ASPECTS OF CERTIFICATION AND QUALIFICATION .....</b>	<b>199</b>
<b>B 2.0 ARTIFICIAL SHAPES, WIND TUNNEL TESTS AND TANKERS.....</b>	<b>203</b>
<b>B 3.0 POSSIBLE FAR EXTENSION.....</b>	<b>205</b>
<b>B 4.0 CERTIFICATION/QUALIFICATION RULES .....</b>	<b>206</b>
<b>B 5.0 THE CASE OF THE ATR 72 .....</b>	<b>212</b>
<b>APPENDIX C: .....</b>	<b>215</b>



NOTES ON SCALING METHODS .....	215
<i>C 1.0 REVIEW OF SIMILARITY REQUIREMENTS</i> .....	215
<i>C 1.1 SIMILARITY CONSIDERATIONS: A BRIEF OVERVIEW</i> .....	215
APPENDIX D.....	218
DROPLET SIZE MEASUREMENTS ANALYSIS: THE CASE OF THE ATS.....	218
APPENDIX E.....	226
SBS TEMPERATURES ANALYSIS: THE CASE OF THE STS .....	226
BIBLIOGRAPHY .....	237
LIST OF ACRONYMS AND ABBREVIATIONS.....	240
RINGRAZIAMENTI .....	243

## INTRODUCTION

“Strange as it may seem, a very light coating of snow or ice, light enough to be hardly visible, will have a tremendous effect on reducing the performance of a modern airplane.” These words are as true today as they were about 60 years ago when Flight Safety Foundation (FSF) founder Jerome “Jerry” F. Lederer said them during a lecture on aviation safety. And despite new technology, training and procedures developed since then to address the problem, accidents related to icing conditions continue to occur.

In the past 50 years, ice has played a role in numerous accidents that have killed crews and passengers and destroyed aircraft. No phase of operations is immune to the threat. U.S. examples of icing encounters with fatal consequences include the following [16]:

(a) A commuter flight impacted terrain during landing in December 1989, in Pasco, Washington, U.S., killing both crewmembers and all four passengers. The aircraft had been in icing conditions for about 10 minutes on approach.

(b) An air transport stalled on takeoff in March 1992, in Flushing, New York, U.S., killing two crew members and 25 passengers; 24 persons survived. The aircraft had been de-iced twice before leaving the gate.

(c) A commuter flight went out of control in icing conditions and dived into a soybean field en route to Chicago, Illinois, U.S., in October 1994, killing all 68 aboard.

Finally, an US National Transportation Safety Board study, on icing related accidents between 1982 and 2000, found that 819 people were killed on 583 airframe icing accidents during the same period. The accidents included in the NTSB study, were all

related to both FAR Part 23 and FAR PART 25 aircraft, although smaller personal and corporate planes have shown to be particularly vulnerable to ice.

It turns obvious that icing-related accidents have captured the airworthiness authorities' as well as aircraft industry, and that the problem is international. Several research centers such as NASA (National Aeronautics and Space Administration), NRC (National Research Council of Canada), CIRA (Italian Aerospace Research Center), as well as several Universities and major aerospace industries worldwide, have expressed the need for continuing research and development of new technological improvements on basic and applied research i.e. for new anti-icing systems developments, as well as flight in icing conditions and ground testing facilities simulation.

Specifically, small scale icing facilities have been widely used for developing new instrumentation and for carrying out basic research on small droplets as well as on SLD (Supercooled Large Droplets). Large scale Icing Wind Tunnels have been a very useful tool for validating computer codes dedicated to icing simulations but have mainly supported the demonstration of compliance to the current airworthiness regulation in industrial programs such as NH90, A380, Falcon 7X, A400M, B777 just to name few among the latest. Finally, it can be stated without doubts, that large scale icing facilities have been used by engine, airframe, ice detection and ice protection systems manufacturers, with satisfaction from airworthiness authority as well.

What here above mentioned, has been possible thanks to the shown icing wind tunnels capability to simulate the current Appendix C certification envelope in terms of pressure altitude, temperature, liquid water content and mean volume diameter.

However, despite their importance, only very few countries have large scale tunnels available for research/industrial activities. Italy, through CIRA (Italian Aerospace Research Center), owns the Icing Wind Tunnel (IWT), the world's largest and most advanced icing facility able to reproduce simultaneously those conditions of real altitude, temperature, humidity and velocity normally encountered in flight. The IWT facility is a closed loop circuit, refrigerated wind tunnel, with three interchangeable test sections (Secondary, Main, and Additional) and one Open Jet configuration. As many conventional wind tunnels, the IWT is fan driven, but, a twin row heat exchanger, coupled with a Spray Bar System (SBS), installed in the circuit can provide up to date low temperature operation capabilities, and utmost cloud generation features.

Objective of this doctoral investigation, is to characterize cloud reproduction capability for the smallest test section (STS) and the largest one (ATS) and firstly looking for FAR 25 Appendix C envelope coverage. The data acquired during the icing characterization shall enable a full investigation of the cloud characteristics over the entire spray bar pressures ranges. Thanks to the tests performed, equations describing the droplets Mean Volume Diameter (MVD) and cloud Liquid Water Content (LWC) as function of SBS feeding water and air pressures shall be determined for both test sections. Also cloud uniformity measurements and SBS supply temperature for both air and water have to be investigated for checking droplets super cooled status. Finally, the data obtained for STS and ATS will be compared, whenever possible, with some data previously obtained for the MTS calibration, enabling an evaluation of possible commonalities in terms of icing performance.

# CHAPTER 1

## WHY AIRCRAFT ICING IS DANGEROUS

### ***1.1 ICING THREAT***

In-flight icing is a serious hazard. It destroys the smooth flow of air, increasing drag, degrading control authority and decreasing the ability of an airfoil to lift. The actual weight of the ice on the airplane is secondary to the airflow disruption it causes. As power is added to compensate for the additional drag and the nose is lifted to maintain altitude, the angle of attack increases, allowing the underside of the wings and fuselage to accumulate additional ice. Ice accumulates on every exposed frontal surface of the airplane – not just on the wings, propeller, and windshield, but also on the antennas, vents, intakes, and cowlings. It accretes in flight where no heat or boots can reach it. It can cause antennas to vibrate so severely that they can break. In moderate to severe conditions, a light aircraft can become so iced up that continued flight is impossible. The airplane may stall at much higher speeds and lower angles of attack than normal. It can roll or pitch uncontrollably, and recovery may be impossible.

### ***1.2 KINDS OF ICE***

Ice adheres to the external surfaces of the airplane. It is described as clear (or glaze), rime, or mixed:

- Clear or glaze ice;
- Rime ice;
- Mixed ice (is only a combination of rime and clear ice).

### ***1.2.1 Clear (or Glaze) Ice***

Clear ice is most likely to form in freezing rain, a phenomena comprising raindrops that spread out and freeze on contact with the cold airframe. It is possible for liquid water drops to exist in the atmosphere at temperatures well below the normal freezing point of water. These are known as super-cooled drops. This situation can occur below a warm front. Super-cooled drops are unstable, and will freeze on contact with a surface that is below zero degrees — the skin of an airplane, or the propeller blades, for example. Freezing of each drop will be relatively gradual, due to the latent heat released in the freezing process, allowing part of the water drop to flow rearwards before it solidifies. The slower the freezing process, the greater the flow-back of the water before it freezes. The flow-back is greatest at temperatures around the 0°C. The result is a sheet of solid, clear, glazed ice with very little air enclosed (see figure 1.1).

The surface of clear ice is smooth, usually with undulations and lumps (see figure 1.2). Clear ice can alter the aerodynamic shape of airfoils quite dramatically and reduce or destroy their effectiveness. Clear ice is tenacious and, if it does break off, large chunks may damage the airframe.



**Fig. 1.1:** Clear or glaze ice

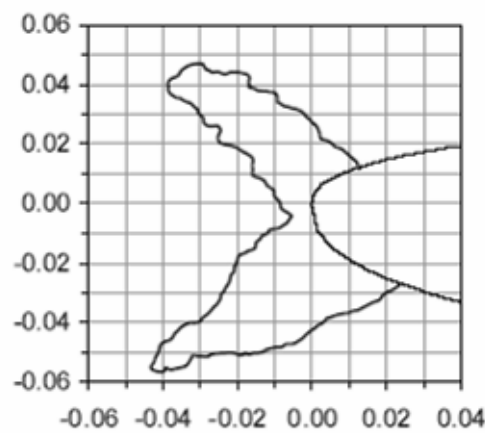


**Fig. 1.2:** Clear or glaze ice on a wing section

### **1.2.2 Rime Ice**

Rime ice occurs when tiny, super-cooled liquid water droplets freeze on contact with a surface whose temperature is below freezing. Because the droplets are small, the amount of water remaining after the initial freezing is insufficient to coalesce into a continuous sheet before freezing. The result is a mixture of tiny ice particles and trapped air, giving a rough, opaque, crystalline deposit that is fairly brittle (see figure 1.3 and 1.4). Rime ice often forms on leading edges and can affect the aerodynamic

qualities of an airfoil or the airflow into the engine intake. Due entrapped air, and slow accumulation rate, rime usually does not cause a significant increase in weight. Also depending upon the Liquid Water Content, the temperature range for the formation of rime ice can be between  $0^{\circ}\text{C}$  and  $-40^{\circ}\text{C}$ , but is most commonly encountered in the range from  $-15^{\circ}$  to  $-40^{\circ}\text{C}$ .

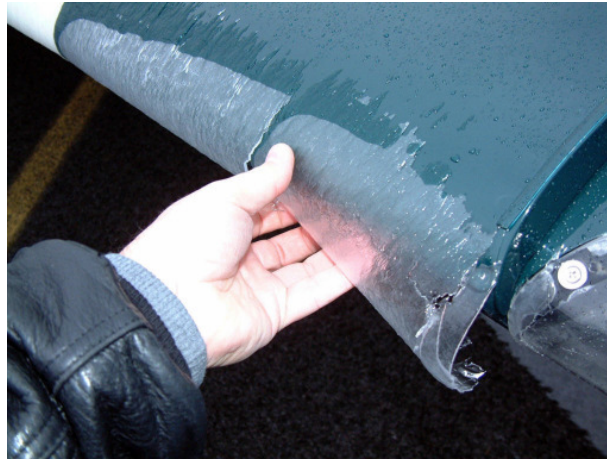


**Fig. 1.3:** Rime ice

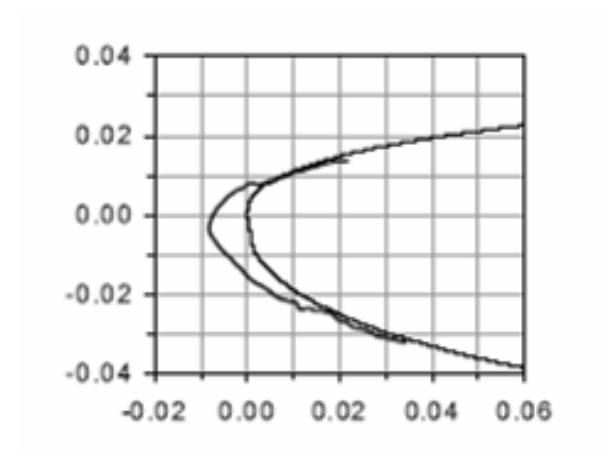


**Fig. 1.4:** Rime ice section

### **1.2.3 Mixed Ice**

Different moisture droplet sizes are commonly encountered in cloud, this variation produces a mixture of clear ice (from large drops) and rime (from small droplets.)



Known as mixed ice, or in some countries as cloudy ice, most ice encounters take this form. Pure rime ice is usually confined to high altostratus or altocumulus, while pure clear ice is confined to freezing rain (below nimbostratus).

### ***1.3 WHY THEY FALL: EFFECT OF ICE ACCRETION ON AIRCRAFT FLIGHT DYNAMICS***

Ice distorts the flow of air over the wing, diminishing the wing's maximum lift, reducing the angle of attack for maximum lift, adversely affecting airplane handling qualities, and significantly increasing drag. As already stated, wind tunnel and flight tests have shown that frost, snow, and ice accumulations (on the leading edge or upper surface of the wing) no thicker or rougher than a piece of coarse sandpaper can reduce lift by 30 percent and increase drag up to 40 percent. Larger accretions can reduce lift even further and increase drag by 80 percent or more [1]. Even aircraft equipped for flight into icing conditions are significantly affected by ice accumulation on the unprotected areas. A NASA study (NASA TM83564) revealed close to 50 percent of the total drag associated with an ice encounter remained after all the protected surfaces were cleared. Unprotected surfaces include antennas, flap hinges, control horns, fuselage frontal area, windshields, windshield wipers, wing struts, fixed landing gear, etc. Ice forms on aircraft surfaces at around 0°C or colder when liquid water is present.

#### ***1.3.1 Performance Degradation***

Flight safety of aircraft operating under natural icing conditions is one of the major concerns of the certification authorities and aircraft manufacturers. As the number of

commercial flights increase, the probability of encountering severe icing conditions also increases. Today, despite the existence of a considerable amount of expertise in the area of aircraft design and the related support equipment and of extensive flight regulations, there are icing-related accidents still to face.

According to the Federal Aviation Administration (FAA) icing is defined as the condition where we have visible moisture and temperature of the surface below freezing. The formation of ice on aircraft components such as wings, control surfaces and engine intakes, occurs when the aircraft flies at a level where the temperature is at, or below freezing point and hits supercooled water droplets. The rate of heat loss from the aircraft surfaces is such that some or all of the droplets are frozen before they can run off the body. As it has been explained before, droplets freeze upon impact by forming a rime ice deposit, if all the impinging water freezes, or glaze ice deposit if only a fraction of the water droplets freeze while the remaining run back along the surface or along existing ice and freeze downstream. The amount and the shape of ice collected depend mainly on liquid water content, temperature, airspeed, droplet size, and surface roughness [1 - 5].

The presence of ice accretion on unprotected aircraft components can lead to a number of aerodynamic penalties and consequently causes a serious safety problem [1, 3]. The most severe penalties encountered deal with decreased lift, increased drag, decreased stall angle, changes in the pressure distribution, vibration, early boundary layer transition, and reduced controllability. In fact, as briefly anticipated before, test data on ice effects indicate that the presence of ice on unprotected wing may increase drag by as much as 40% and reduce lift by 30% [6, 7, 8] (see figure 1.5). To overcome these penalties, various practical methods have been used to remove or prevent accumulation

of ice on aircraft surfaces by applying de-icing/anti-icing procedures [3]. However, failure of protection systems and the presence of residual ice still produce a loss in the aircraft efficiency. In addition, modern airfoils using new materials have been developed and have demonstrated a high aerodynamic efficiency. But, at the same time, these new types of airfoils need specific ice protection systems to maintain their aerodynamic efficiency and safety margin [1, 3]. The design of such system will require efficient optimization of ice protection systems, accurate modeling of ice accretion and its removal from critical surfaces. Today, research is being pursued in both numerical and experimental fields for a better understanding of atmospheric icing and its effects on aircraft performance. These researches encompass a wide spectrum of technology which ranges from meteorological criteria to methodologies used for certification [1, 3]. Many and interesting would be the pages that could be written on this topic, but this is not the objective of this work, therefore the reader interested on these issues is kindly asked to refer to the bibliography here reported.

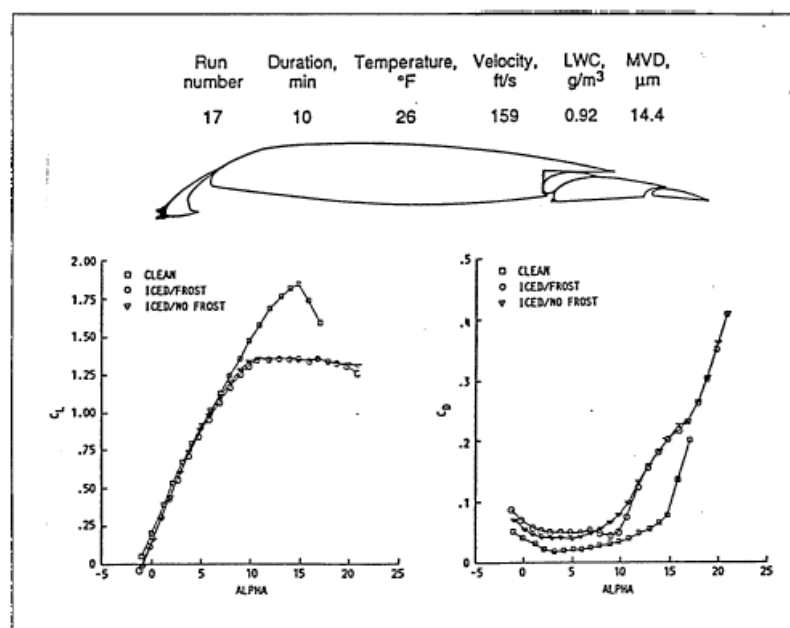


Fig. 1.5: Performance degradation due to glaze ice accretion on a wing model

### ***1.3.2 Aircraft Handling***

Another possible hazard of icing is the un-commanded and uncontrolled roll phenomenon referred to as roll upset that is associated with severe in-flight icing [16]. Pilots flying airplanes certificated for flight in known icing conditions should be aware that severe icing is a condition that is outside of the airplane's certification icing envelope. Roll upset may be caused by airflow separation inducing self-deflection of the ailerons and loss of or degraded roll handling characteristics. This phenomenon can result from severe icing conditions without the usual symptoms of ice accumulation or a perceived aerodynamic stall. The term "severe icing" is associated with the rapid growth rate of visible ice shapes most often produced in conditions of high liquid water content and combinations of other environmental and flight conditions. Severe icing is often accompanied by aerodynamic performance degradation such as high drag, aerodynamic buffet, and premature stall.

In addition, ice associated with freezing rain or freezing drizzle can accumulate on and beyond the limits of an ice protection system. This kind of ice may not produce the familiar performance degradation; however, it may be potentially hazardous. Freezing rain and freezing drizzle contain droplets larger than the criteria specified by certification requirements.

Another hazard of structural icing is the tail-plane (empennage) stall. Sharp-edged surfaces are more susceptible to collecting ice than large blunt surfaces. For this reason, the tail-plane may begin accumulating ice before the wings. The tail-plane will also accumulate ice faster. Because the pilot cannot readily see the tail-plane, the pilot may be unaware of the situation until the stall occurs. A tail-plane stall occurs when the

critical angle of attack is exceeded. Since the horizontal stabilizer counters the natural nose down tendency caused by the centre of lift of the main wing, the airplane will react by pitching nose down, sometimes uncontrollably, when the tail-plane is stalled. Application of flaps can aggravate or initiate the stall. The pilot should use caution when applying flaps during an approach if there is the possibility of icing on the tail-plane.

Perhaps the most important characteristic of a tail-plane stall is the relatively high airspeed at the onset and, if it occurs, the suddenness and magnitude of the nose down pitch. A stall is more likely to occur when the flaps are approaching the fully extended position or during flight through wind gusts.

Ice detection is very important in dealing with icing in a timely manner. A careful pre-flight of the aircraft should be conducted to ensure that all ice or frost is removed before takeoff. Pilots operating in icing conditions must check for ice formation. At night, aircraft can be equipped with ice detection lights to assist in detecting ice. Being familiar with the airplane's performance and flight characteristics will also help in recognizing the possibility of ice. Ice build-up will require more power to maintain cruise airspeed. Ice on the tail-plane can cause diminished nose up pitch control and heavy elevator forces, and the aircraft may buffet if flaps are extended. Ice on the rudder or ailerons can cause control oscillations or vibrations.

De-icing is a procedure in which frost, ice, or snow is removed from the aircraft in order to provide clean surfaces. Anti-icing is a process that provides some protection against the formation of frost or ice for a limited period of time. There are various methods and systems that are used for de-icing and anti-icing. Pneumatic boots are commonly used on smaller aircraft and usually provide ice removal for the wing and tail section by inflating a rubber boot. Ice can also be removed by a heat system or by a chemical fluid.

De-icing the propeller is usually done by electrical heat; however, it can also be done with a chemical fluid. Anti-icing can be accomplished by using chemical fluid or a heat source. Anti-ice systems are activated before entering icing conditions to help prevent the ice from adhering to the surface. These methods provide protection for the wings, tail, propeller, windshield, and other sections of the aircraft that need protection. For an airplane to be approved for flight into icing conditions, the airplane must be equipped with systems that will adequately protect various components. There are two regulatory references to ice protection: The Application to Airplane Type Certification in FAR Parts 23 and 25 (see chapter 5).

### ***1.3.3 Airfoil sensitivity***

Although ice can accrete on many airplane surfaces, concern is focused on wing-airfoil icing. Some airfoil designs tend to be less sensitive to lift loss with contamination than other, more efficient airfoils from this point of view [16]. Traditionally, the industry has relied on the infrequency of occurrence, limited extent of coverage, forecasting and reporting to avoid freezing rain and freezing drizzle, and recognition to exit the conditions.

An infinite variety of shapes, thickness and textures of ice can accrete at various locations on the airfoil. Each ice shape essentially produces a new airfoil with unique lift, drag, stall angle and pitching moment characteristics that are different from the wing's own airfoil, and from other ice shapes. These shapes create a range of effects. Some effects are relatively benign and are almost indistinguishable from the wing's airfoil. Others may alter the aerodynamic characteristics so drastically that all, or part of the

airfoil, stalls suddenly and without warning. Sometimes the difference in ice accretion between a benign shape and a more hazardous shape appears insignificant. The effects of severe icing are often exclusively associated with ice thickness. For example, it is reasonable, in a given set of conditions, to believe that a specific 3 in (about 7.6 cm) shape would be more adverse than a similar 1.5 in (3.8 cm) shape in the same place. Contrary to that criterion, however, a 5 in (12.7 cm) ice shape on one specific airfoil is not as adverse as a 1 in (2.54 cm) ice ridge located farther aft on the chord. In another example, a layer of ice having substantial chord wise extent is more adverse than a 3 in ice accretion having upper and lower horn-shaped ridges (double horn). Ice can contribute to partial or total wing stall followed by roll, aileron snatch or reduced aileron effectiveness.

Wing stall is a common consequence of ice accretion. Ice from freezing drizzle can form sharp-edged roughness elements approximately 0.5 cm to 1 cm (0.2 in to 0.4 in) high over a large chord wise expanse of the wing's lower surfaces (perhaps covering 30 percent to 50 percent) and fuselage, increasing drag dramatically, thereby reducing speed. Therefore is required to the pilot to increase power, increase the angle-of-attack (AOA) or both to maintain altitude. Ultimately, such unmitigated adjustments lead to exceed the stall angle with a conventional stall, likely followed by a roll, as a consequence.

Another issue is that the ailerons may be substantially ineffective when they are deflected. Degradation of roll control effectiveness results from flow disruption over the wing ahead of the ailerons, and the controls do not produce the rolling moments associated with a given deflection and airspeed. Degradation of aileron control caused by ice may or may not be accompanied by abnormal control forces. If, for example, the

airplane is displaced in roll attitude, through partial stall caused by ice, the pilot's efforts to correct the attitude by aileron deflection are defeated by the aileron's lack of effectiveness.

Ice tends to accrete on airfoils in different ways, depending on the airfoil, the AOA and other aircraft variables. Ice accretion at the wing tip may be thicker, extend farther aft and have a greater adverse effect than ice at the root. The airfoil at the tip is in all probability a different airfoil than at the root. It is probably thinner, may have a different camber, be of shorter chord, and probably two or three degrees of washout relative to the root section.

#### **1.4 ICING RELATED ACCIDENTS**

While research is carried out however, the phenomenon "in-flight icing" has affected all types of aircrafts ranging from small turbojet with conventional airfoils, like the Learjet, to large turbojet such as the DC-9 and B737. All the new aircrafts such as the A380, or the B787, will have to be certified in icing conditions.

Few example of icing related accidents taking into account the period 1974-1994, are given in Table 1 [1]. Probably the most famous icing related accident occurred on October 31st, 1994, where an ATR 72 from the American Eagle Airline, a subsidiary company of American Airlines, has crashed in Roselawn, Indiana. Indeed the probable cause of accident is believed to be the presence of supercooled large droplets, exceeding the maximum limit diameter of 50  $\mu\text{m}$ , which may have affected the controllability of the aircraft.



Date	Location, Airline and Aircraft Type	Precipitation/Observations
26 Jan. 74	Cumaovas THY F28	Frost accretion on the wings
03 Jan. 77	Anchorage JAL DC-8-62	Fog
04 Jan. 77	Frankfurt ? B737	Light snow, rime ice
27 Nov. 78	Newark TWA DC-9-10	Blowing rain and snow
20 Dec. 78	Mineapolis N4OSN Learjet	Probable cause: snow and ice on wing
19 Jan. 79	Detroit N73161 Learjet	Premature stall, ice on wing
12 Feb. 79	Clarksburgh ALLEGHENY Nord 262	Light snow, frozen snow on empennage
18 Feb. 80	Boston REDCOTE Bristol 253	Light snow
13 Jan. 82	Wash. D.C. AIR FLORIDA B737	Moderate to heavy snowfall
05 Feb. 85	Philadelphia AIRBORNE DC-9-10	Light freezing rain, ice & snow pellets fog
12 Dec. 85	Gander ARROW AIR DC-8-63	Light freezing drizzle, snow grains
15 Nov. 87	Denver CONTINENTAL DC-9-10	Moderate snow, fog
18 Jan. 88	New Mexico N2614U Cessna 402	Prob. cause: Ice/Frost removal inadequate
06 Feb. 88	California N2832J Cessna	Ice/Frost removal inadequate
23 Dec. 88	Montana N5570H Piper	Probable cause: Wing ice
10 Mar. 89	Dryden AIR ONTARIO F28	Heavy snow
25 Nov. 89	Kimpo KOREAN AIR F28	Dense fog, ice on the wing
16 Feb. 91	Cleveland RYAN DC-9-10	light snow
Dec. 91	Stockholm SAS MD-80	Freezing precipitation, ice on wing
22 Mar. 92	LaGuardia, NY USAIR F28	Heavy snow
31 Oct. 94	Roselawn, IN American Eagle ATR72	Probable cause, ice due to freezing rain

**Table 1.1:** Date and location of some icing related accidents

More recent US statistical data [9] clearly show that General Aviation (GA) accidents dominate the total number of accidents during the period 1982-2000 (see figure 1.6). GA accidents were responsible for 80.6% of all airframe icing accidents, while Part 135 (Taxi e Commuter) and Part 121 (air carrier) accounted for 17.6% and 1.7%, respectively. However, the annual GA accident rate significantly declined during the same period. The number of general aviation accidents dropped from a high of 49 in 1982 to 17 in 2000.

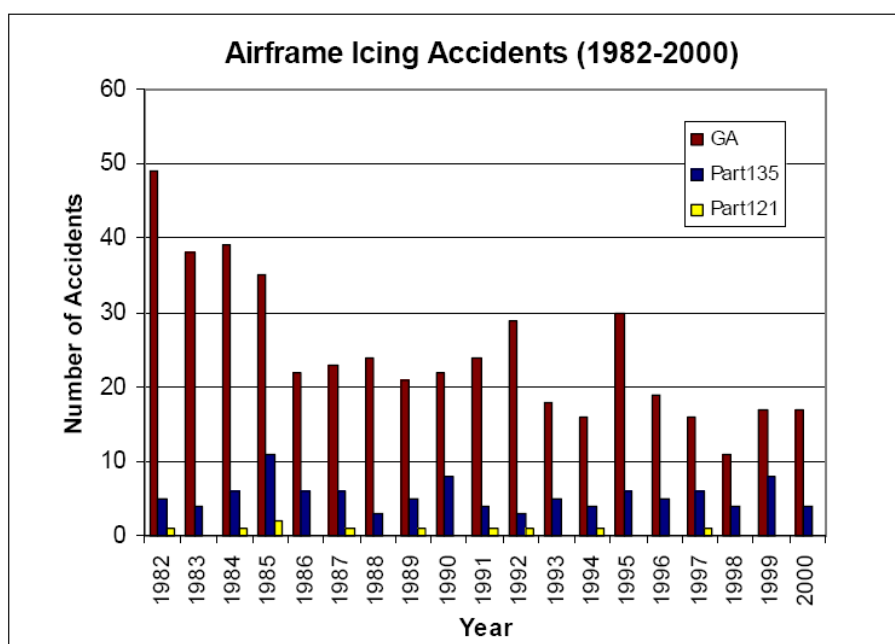


**Fig. 1.6:** Aviation accidents associated with airframe icing for the period 1982-2000

A graph depicting the number of fatal airframe icing accidents is provided in figure 1.7. There were one or more fatalities in 47% of the GA accidents, while only 26% of Part 135 accidents were fatal. Six out of the ten Part 121 accidents during the period were fatal accidents.

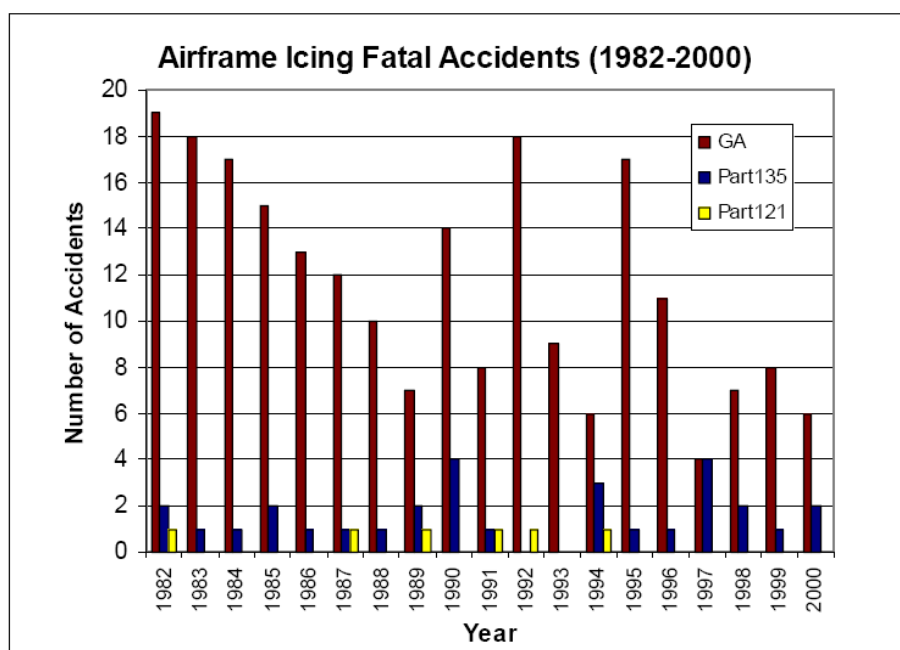


**Fig. 1.7:** Aviation accidents associated with airframe icing for the period 1982-2000.

Airframe icing accidents led to 819 deaths spanning the 19-year period reviewed in this study. As one might anticipate, GA accidents were responsible for the largest number of fatalities (522). The observed annual decrease in fatalities within the GA segment of operation is directly correlated with the decline in the overall number of GA accidents. Peaks in the number of fatalities linked to Part 135 and 121 operations are related to some very notable U.S. icing accidents (figure 1.8), including Air Florida flight 90 (Washington, DC 1982), USAir flight 405 (Flushing, NY 1992), Comair flight 3272 (Monroe, MI 1997), and American Eagle flight 4184 (Roselawn, IN 1994).

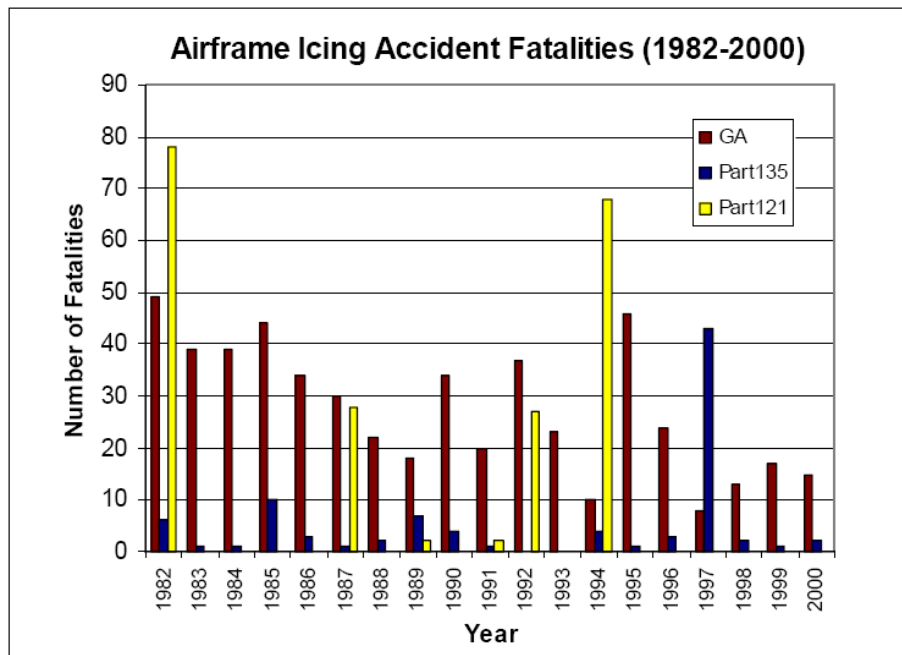


**Fig. 1.8:** Aviation accidents associated with airframe icing for the period 1982-2000.

# CHAPTER 2

## THE ICING WEATHER

### ***2.1 MECHANISM AND COMPOSITION OF CLOUDS***

Since the first days, the Federal Aviation Administration (FAA) has recognized the danger of icing and contamination of aircraft surfaces and has written regulations for aircraft operating in icing conditions [1] based on the flight investigation of the meteorological conditions which begun in 1944 by the US Army and the National Advisory Committee of Aeronautics (NACA). The design, analysis, and certification of ice protection systems depend mainly on the knowledge of icing characteristics. Statistical icing data used by most U.S., Canadian, and British commercial and military design criteria are cited by reference [10]. To understand how aircraft icing occurs, it is necessarily to understand the mechanism and the composition of cloud, and the characteristics of water vapor. Indeed, although water vapor is found only in the lower levels of the atmosphere it is considered as the most important gas from the standpoint of weather since it can change into water droplets (liquid) or ice crystals (solid) under different atmospheric condition of temperature and pressure and becomes a serious hazards for aircraft [11, 12].

The four basic factors that should be considered to study in-flight aircraft icing are:

1. the temperature, which influences the type and intensity of ice,

2. the liquid water content, which indicates the severity of icing and to some extent its type and shape,
3. the droplet size which influences the type and the rate of icing through the increase of collection efficiency, and
4. the type of aircraft.

In this chapter icing atmosphere characteristics are shown together with, concentrations and size of particles in the atmosphere, water phases, cloud formation, and characteristics of high clouds, middle clouds, low clouds, and clouds of vertical development along with their vertical and horizontal extends. Then, it is discussed the properties of icing clouds, frontal zone icing and continuous and intermittent icing envelopes for the certification of aircraft as required by the Federal Aviation Regulation (FAR), Part 25, Appendix C.

## ***2.2 COMPOSITION AND STRUCTURE OF THE ATMOSPHERE***

The performance characteristics of aircraft depend on the properties of the atmosphere where they fly. To reduce the hazards of air navigation, meteorological organizations collect, analyze and broadcast information regarding weather and any change in the atmosphere. The following sections present the most important characteristics of the atmosphere where ice finds its way to form.

### ***2.2.1 Composition of the Atmosphere***

The atmosphere is composed of a mixture of many gases, mainly nitrogen, oxygen, argon and carbon dioxide in which are suspended, in a variable amounts, particles of liquid or solid matter. Unlike the most abundant gases which remain in the gaseous state water vapor is the only substance that can be found in the atmosphere in all three forms: gas, liquid or solid depending on the temperature and pressure conditions. Various parts of the upper atmosphere contain ions and electronically excited species. Composition of the atmosphere is approximately 78% nitrogen, 20,946% oxygen, 0.934% of argon and 0.03% of carbon dioxide [12, 13]. These portions vary with location and time. At some places the atmosphere may contain up to 4% of moist air volume. In addition, 99% of the water vapor is located in the lowest atmosphere and decreases with height above the ground. The atmosphere may also contain other types of materials such as salt crystal, dust, and smoke particles swept up by the wind. Many of these small particles in the atmosphere serve as nuclei around which water droplet or ice crystals form [1, 12]. These microscopic impurities are important for aviation since they act in the condensation process. The water vapor present in the atmosphere condenses on particles present in the atmosphere, the process is called condensation nuclei. Salt represents good nuclei since it absorbs water; particle having this property are termed hygroscopic nuclei. Table 2.1 resumes sizes and concentration of these nuclei compared to cloud droplets. The table shows also the approximate value of terminal velocity defined as the falling speed reached by a drop such that its drag force is equal to the difference between the force of gravity and the buoyant force.

Type	Diameter range (mm)	Concentration range (no./cm <sup>3</sup> )	Approx. terminal velocity (cm/sec)
Small ions	$(0.15-1) \times 10^{-5}$	$(1-7) \times 10^2$	
Large ions	$(1-20) \times 10^{-5}$	$(2-20) \times 10^3$	
Small Aitken	$(0.1-4) \times 10^{-4}$	$10-10^5$	$10^{-5}-10^{-3}$
Large nuclei	$(4-20) \times 10^{-4}$	$1-10^3$	$10^{-3}-0.07$
Giant nuclei	$(20-1000) \times 10^{-4}$	$10^{-4}-10$	$0.07-0.7$
Fog & cloud droplets	$(1-200) \times 10^{-3}$	$25-600$	$0.01-70$
Drizzle	$(2-40) \times 10^{-2}$	$1-10$	$1-170$
Raindrops	$0.4-4$	$10^{-3}-1$	$170-900$
Snow crystals	$0.5-5$	$<10$	$30-100$
Snow flakes	$4-20$	$10^{-3}-1$	$80-200$
Hail	$5-75+$ (largest: 140)	$10^{-6}-10^{-1}$	$800-3500+$

**Table 2.1:** Different types of nuclei

### 2.2.2 Structure of the Atmosphere

According to the change of temperature with the height, the atmosphere is divided into four distinct layers surrounding the earth: the troposphere (negative temperature gradient), the stratosphere (zero temperature gradient), the mesosphere (negative temperature gradient), and the thermosphere (positive temperature gradient) [1].

The top of each layer, except the thermosphere, is named tropopause, stratopause, and mesopause. Due to the presence of water vapor and large vertical currents, the most important atmospheric layer from the standpoint of weather is the troposphere. Figure 2.1 shows the vertical distribution of atmospheric properties. In the troposphere, the lowest layer of the atmosphere, the pressure, temperature and density decrease rapidly with height. The temperature average rate decrease is around  $6.5^\circ\text{C}/\text{km}$ . All clouds and weather, and most of the dust and water vapor are found in the troposphere.



In the tropopause, the temperature remain constant, at about  $-56^{\circ}\text{C}$ , but in the mesosphere the temperature increases, may reach around  $10^{\circ}\text{C}$ , due the existence of the ozone's layer. In the thermosphere, the temperature reaches high values.

In aeronautical applications, detailed tables of average conditions within the troposphere are available and organized into U.S. Standard Atmosphere [1]. These tables provide a basis for comparing aircraft performance.

From the aeronautical stand point, the temperature decreases linearly from sea level to 11 km. Above 11 km in the isothermal region (stratosphere), the temperature is constant. At 25.1 km, the temperature increases till 47 km.

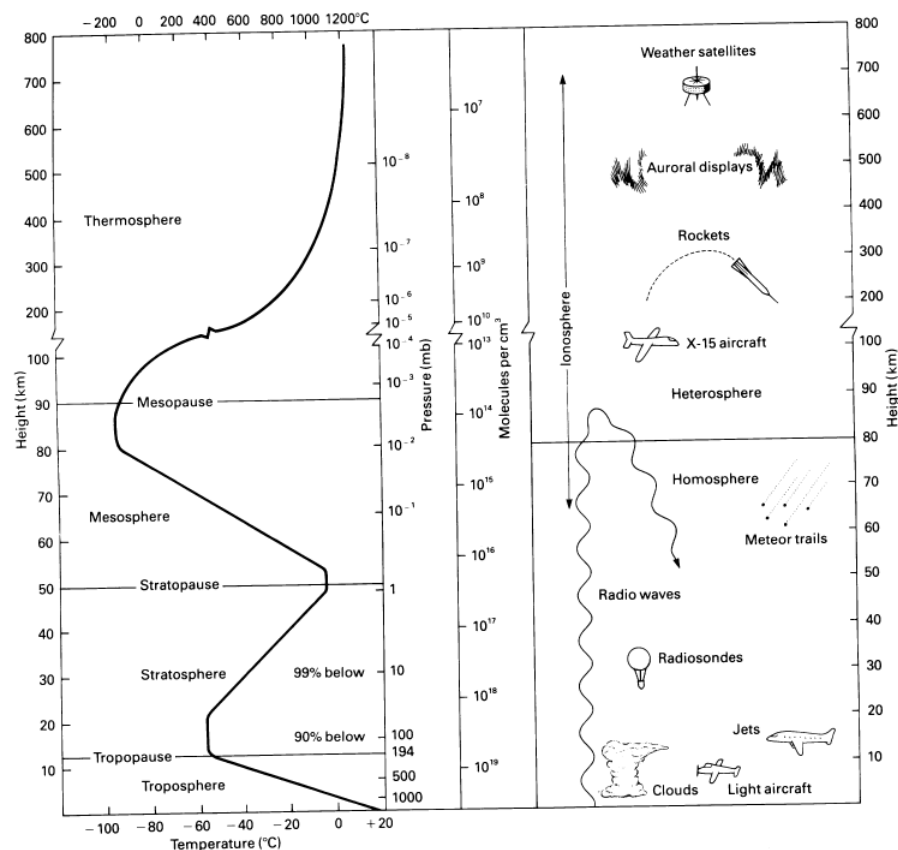


**Fig. 2.1:** Vertical distribution of atmospheric properties

## **2.3 WATER CYCLES IN THE ATMOSPHERE**

From standpoint of icing and weather, water vapor may change into water droplet or ice crystals and causes major problems for aircraft. In the homosphere, defined as the layer where relative concentration of the most abundant gases are uniform for an average distance of 80 km, water vapor is the most variable gases (from 0% to 4%) which decreases with height. The quantity of water vapor present in the atmosphere is important to determine the region of cloud formation and atmospheric drying conditions.

Under different circumstances, water vapor in the atmosphere may be disturbed and its state changes by evaporation-condensation, melting-freezing or sublimation deposition [1]. These characteristics are important to understand the presence of liquid and solid cloud particles that grow in size and fall as precipitation, and the existence of large amounts of latent heat in the atmosphere which is considered as an important source of atmosphere energy, especially for storms and hurricanes.

The main process of droplet changes is summarized in figure 2.2 with the energy required or released during water phase changes.

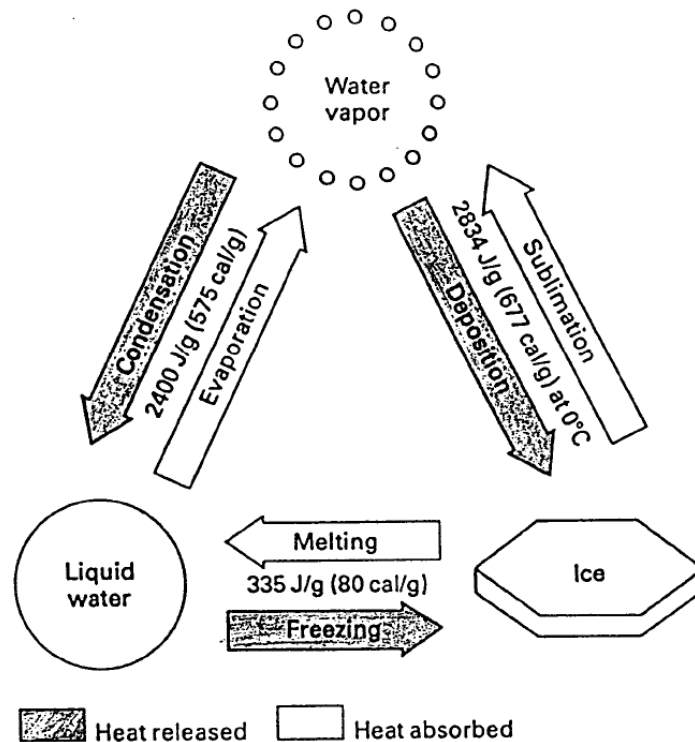


Fig. 2.2: Vertical distribution of atmospheric properties

When cloud droplets form water vapor (condensation), the atmosphere receives a heat of 2400 J/g (575 cal/g) and when snowflakes form (deposition) the heat released is 2834 J/g (677 cal/g) [1]. These heat quantities (latent heat) are also supplied to transform liquid water and ice to water vapor by evaporation and sublimation respectively. Thus, heat consumed in one place in the atmosphere during evaporation or sublimation may be released in different places during condensation or deposition. This is considered as an effective way of transporting heat over great distances. When winds transport moist air to other region it forms clouds by condensation producing rain and snow. This cycle of moving and transforming water is called hydrologic cycle.

When the amount of water vapor is increased sufficiently, the air reaches the state of saturation which represents the maximum amount of water vapor that can exist in the

atmosphere. When the amount of water vapor is increased or the air is cooled, the water vapor in excess condensates or transforms into ice crystal by deposition.

## ***2.4 CLOUDS FORMATION***

Clouds are formed by condensation of the invisible water vapor into visible water droplets, snow, or ice crystals. This formation requires a sufficient water vapor, a cooling process and the presence of nuclei in the atmosphere. The cooling process of the air in the atmosphere is initiated by convection due to the upward or downward movement of the air, by orographic lifting resulting from topographical features such as hills or mountains, by frontal lifting where a mass of warm air is advancing a mass of cold air, and by lifting associated with turbulence caused by friction between air and earth [1].

## ***2.5 CLOUDS CLASSIFICATION***

Clouds are composed of liquid water droplets where temperature is above freezing, Supercooled droplets where temperature is below freezing, and solid particles (ice crystals). The observation of such clouds is an important part of atmospheric study since the type and the amount of clouds formation indicate the weather conditions that can be expected in the troposphere. Tables 2.2 to 2.5 summaries types and characteristics of clouds in the atmosphere. According to the International Cloud Atlas published in 1957 by the World Meteorological Organization [11], clouds are classified according to appearance, form and height of their bases. There are three levels, ten genera, fourteen species, nine varieties and nine supplementary features which

characterized clouds [13]. However, the most important characteristics for pilots are the ten genera. The clouds may be divided as high clouds (above 6 km), middle clouds (2 km to 6 km), low clouds (below 2 km) and clouds of vertical development (see figure 2.3).

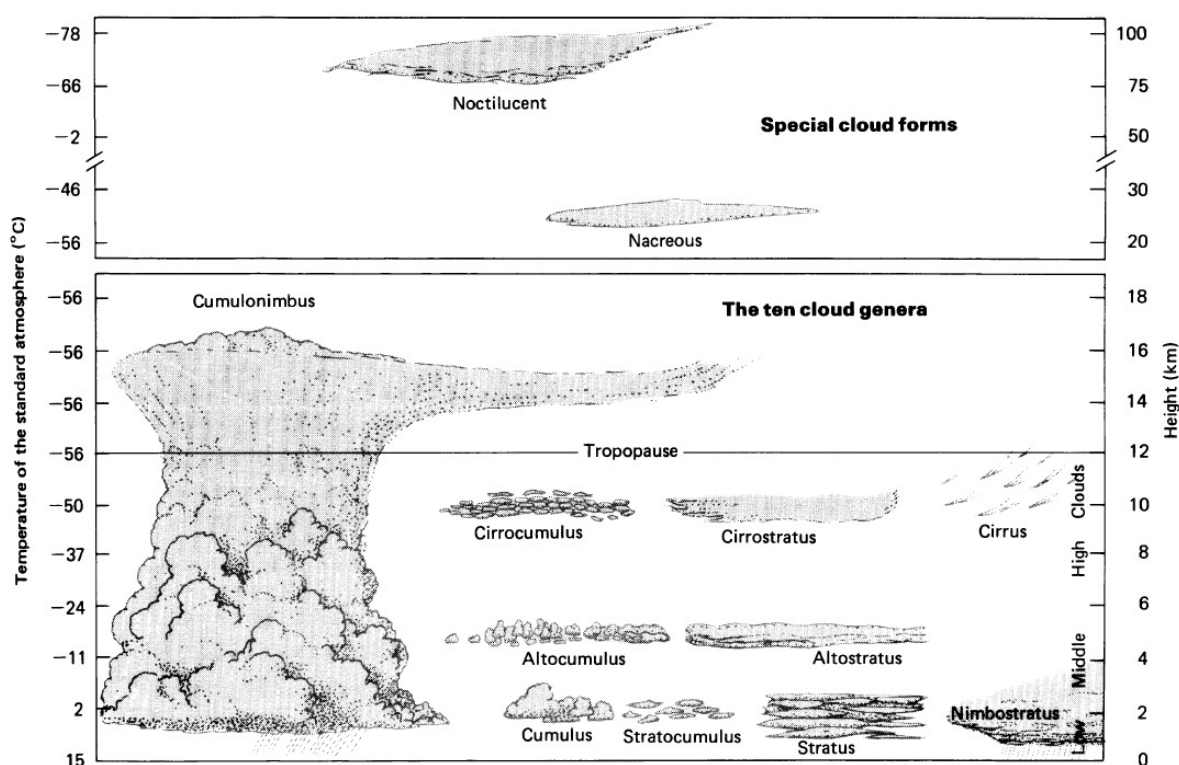
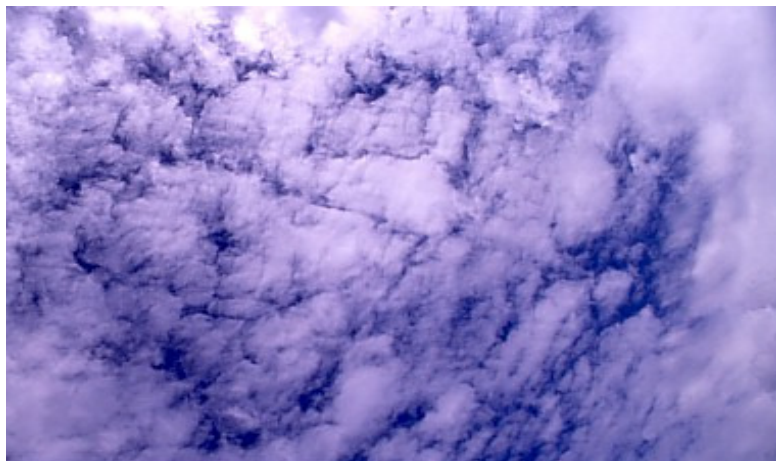


Fig. 2.3: Schematic diagram of the most common clouds

Clouds are classified into 10 main structures. Tables 2.2-2.5 and figures 1.1-1.7 [1] show the characteristics of each type of clouds along with their structure and appearance. Clouds are identified according to their form and average height above the ground level (AGL). Names of clouds are grouped in the following roots: Cirrus “feathery or fibrous,” Stratus “stratified or in layers,” Cumulus “heaped up,” and Nimbus “rain.”

### ***2.5.1 High Clouds (Above 6 km, or 20,000 ft)***

High clouds contain cirrus (CI), cirrocumulus (CC) and cirrostratus (CS) clouds. The bases of high clouds are usually above 6 km, or 20,000 ft. These types of clouds are composed of ice crystals. Table 1.2 resumes the characteristics of high clouds along with an example of their appearance as shown by figure 2.4.



**Fig. 2.4:** Characteristic of high clouds

### ***2.5.2 Middle Clouds (2 to 6 km, or 6,500 to 20,000 ft)***

Middle clouds contain altocumulus (AC) and altostratus (AS) clouds. The bases of middle clouds range from 2 km, or 6,500 ft, to 6 km, or 20,000 ft. These types of clouds are composed of water droplets and ice crystals. Table 1.3 resumes the characteristics of middle clouds along with an example of their appearance as shown in figure 2.5.



**Fig. 2.5:** Characteristic of an altocumulus (middle clouds, 2 to 6 km)

### ***2.5.3 Low Clouds (Below 2 km, Or 6,500 ft)***

Low clouds contain nimbostratus (NB), stratocumulus (SC) and stratus (ST) clouds which are below 2 km, or 6,500 ft and composed of supercooled water droplets and sometimes ice crystals. Table 1.4 resumes the characteristics of low clouds along with an example of their appearance as shown by figure 2.6.



**Fig. 2.6:** Characteristic of a Stratocumulus stratiformis (low clouds, below 2 km)

#### 2.5.4 Clouds Of Vertical Development

Clouds of vertical development contain cumulus (CU) and cumulonimbus (CB) clouds. The bases of these clouds is below 2 km, or 6,500 ft, but the top of the clouds Can extend to great heights. This type of cloud is composed of water droplets and ice crystals. Table 1.5 resumes the characteristics of this type of clouds along with an example of their appearance as shown by figure 2.7.

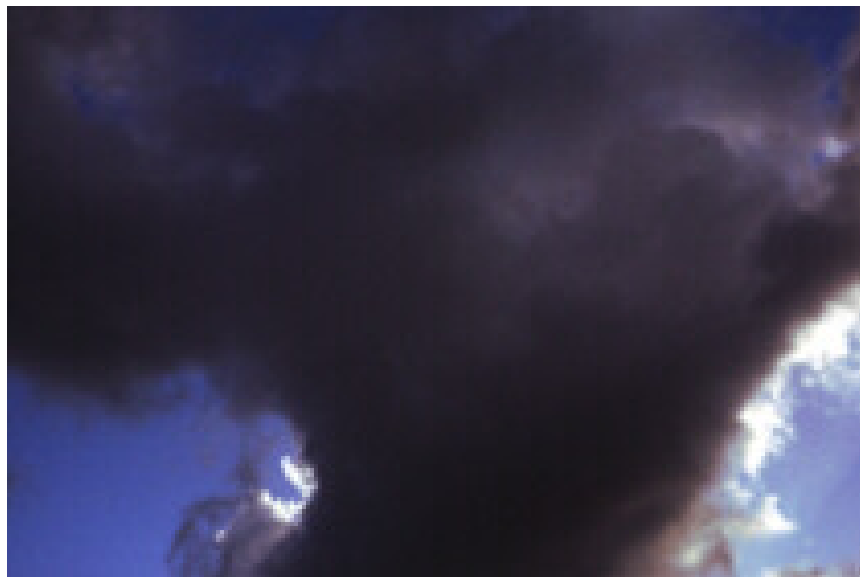


**Fig. 2.7:** Characteristic of a cumulonimbus (clouds of vertical development)

Cloud type	Composition	Appearance
Cirrus (CI)	Ice crystals	Thin, detached cloud with fibrous texture and white color usually without shading
Cirrocumulus (CC)	Ice crystals	This white cloud in the form of small globular masses or white flakes. Often arranged in rows without dark bases
Cirrostratus (CS)	Ice crystals	A thin, transparent white sheet with indefinite borders. Sometimes slightly fibrous.

**Table 2.2:** Characteristic of high clouds above 6 km



Cloud type	Composition	Appearance
Alto cumulus (AC)	Mostly small droplets (rarely some ice crystals)	White to gray clouds composed of fairly large, flattened globules separated by patches of sky. Often arranged in lines or rows.
Altostratus (AS)	Mixture of ice crystals and water droplets	More dense than CS but partially translucent, gray sheet. Usually precedes a general rain by few hours.

**Table 2.3:** Characteristic of middle clouds between 2 and 6 km

## **2.6 ICING CLOUDS**

There are two types of clouds where aircraft icing can occur:

1. stratiform clouds and
2. cumuliform clouds.

### **2.6.1 Stratiform Clouds**

Stratiform clouds form in horizontal layers. Icing conditions are less severe than in cumuliform clouds, however, exposure to the icing can be prolonged due to the great horizontal extend. Icing in the stratiform clouds is light to moderate with maximum in the upper layer. The liquid water contents range from 0.1 to 0.8 g/m<sup>3</sup> and the water droplet diameter from 5 to 50 µm [1]. The most frequently icing in stratiform clouds is rime ice.

Cloud type	Composition	Appearance
Stratocumulus (SC)	Water droplets (rarely some ice crystals)	Soft gray clouds in the form of large globules patches. May resemble puffs of cotton. When overcast, they produce an irregular pattern of light and dark patches larger than AC.
Nimbostratus (NB)	Mixture of ice crystals and water droplets, snowflakes or raindrops near base	Gray or dark layer with no distinct cloud element. Thick enough to obscure the sun. Produces precipitation and may be obscured by lower stratus clouds.
Stratus (ST)	Water droplets (rarely some ice crystals)	Low uniform layer resembling fog but not resting on the ground. Sun and moon are not visible through it except when layer is very thin.

**Table 2.4:** Characteristics of low clouds, below 2 km (6,500 ft)

Cloud type	Composition	Appearance
Cumulus (CU)	Water droplets	Detached dense vertically developed clouds often characterized by flat bases. Horizontal base is usually dark.
Cumulonimbus (CB)	Mixture of ice crystals and water droplets	White dense clouds with great vertical development, associate with heavy rainfall, thunder, hail and tornados.

**Table 2.5:** Characteristics of clouds of vertical developments

The stratiform clouds are composed of high, middle and low level clouds (see Tables 2.2-2.4). In the high level, above 6 km (20,000 ft), there are only ice crystals which offer no icing problems, since they do not stick to the aircraft upon impact, but icing should be considered in air compressor systems, total pressure probes and engines. The middle and low level stratiform clouds are important for icing since both ice crystals and liquid water droplet are present. Below 2 km (6,500 ft) icing is very important because the

liquid water content is high. Turbulence, on the other hand increases the severity of icing, particularly when cumuliform clouds are embedded in the stratiform clouds. Aircraft should avoid stratiform clouds by flying under the icing zones where the temperature is above freezing, or above the icing zones where only ice crystals are present. The stratiform clouds are a continuous icing conditions as designated in the FAA envelope of the Appendix C part 25 (see chapter 5).

### ***2.6.2 Cumuliform Clouds***

In cumuliform clouds air contains great quantities of water droplets. Liquid water contents range from 0.1 to 3.0 g/m<sup>3</sup> and, in some occasions, may reach 3.9 g/m<sup>3</sup> for a short distance [1, 10]. The vertical turbulence may support supercooled large droplets which may form a glaze ice on the exposed surface of an aircraft and become a serious hazard in a short time. The cumuliform clouds are composed of cumulus (CU) and cumulonimbus (CB) (see Table 2.5). These clouds cover less area horizontally (3.7 to 11 km) [10] but have a large vertical development where intermittent icing is found.

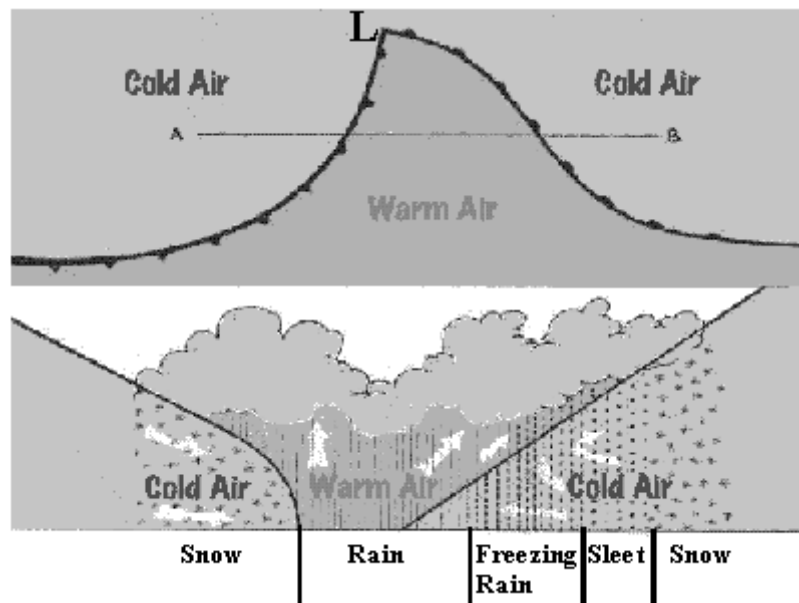


Fig. 2.8: Conditions of icing due to freezing rain

## 2.7 FRONTAL ICING CONDITIONS

Representing frontal icing regions by an ideal model is a difficult task since the structure and characteristics of these regions are very complex [1]. Thus, we would rather give an overview of the icing conditions that might exist in frontal zones. First, frontal zones are defined as the transition area which marks the boundary between different air masses. A sharp contrast of temperature and humidity may exist across the front that separates the two air masses. The horizontal extend of icing is usually associated with warm fronts, while severe icing is associated with cold fronts (see figure 2.8 and 2.9). Icing associated with warm front may occur either above the frontal surface or below. Rain falling from the warm air where temperature is above freezing encounters the cold air zone and freezes on contact with cold object.

This process is called freezing rain which is considered as one of the most dangerous icing encountered by aircraft. The droplets are so large that the impingement limits

move further downstream of an aircraft wing and ice forms beyond icing protection systems. In the cold front, where a warm air mass is lifted by an advancing wedge of cold air, the horizontal extend is less than warm front. Icing may be severe and rapid due to the heavy precipitation even though its time duration is short. Figures 2.9 and 2.10 show the characteristics of warm and cold front zones.

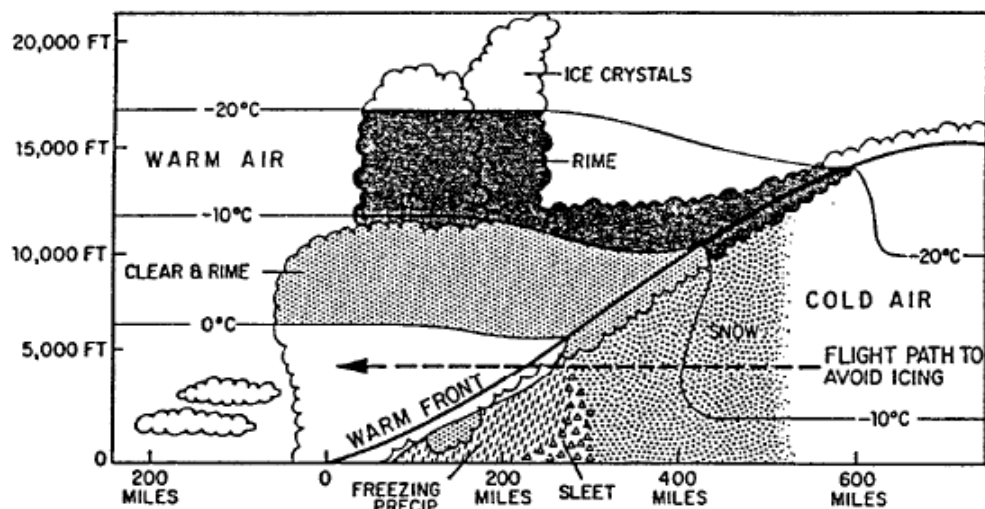


Fig. 2.9: Characteristics of icing conditions in an area of a warm front

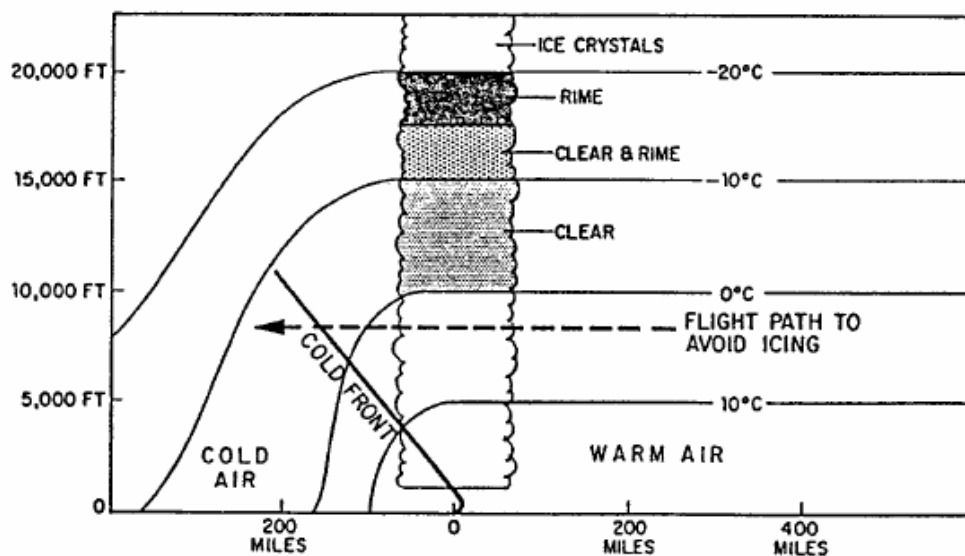


Fig. 2.10: Characteristics of icing conditions in an area of a cold front

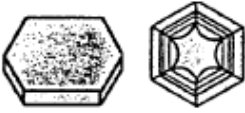
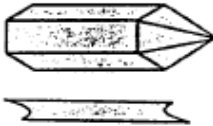


## CHAPTER 3

### ICE ACCRETION PHISICS

#### ***3.1 FORMATION OF ICE IN THE ATMOSPHERE***

In the previous chapters it has been established the fact that unlike the most abundant gases in the atmosphere, which remain in the gaseous state, water vapor is the only substance that can be found in the atmosphere in all three forms: gas, liquid or solid depending on temperature and pressure conditions. The fact that water vapor commonly exists is of direct importance to understand the presence of water droplet and ice crystal in different type of clouds. One of the most important processes is the condensation of water vapor into liquid. The concentration of water vapor may range from near zero in desert regions to as high as 4% in tropical regions. Saturation occurs when water vapor is added to the air or, when the air is cooled. Water droplet start initially with the microscopic particles present in the atmosphere, such as salt crystal, dust, and smoke particles swept up by the wind [1]. This process is called condensation nuclei and particles which contribute to transform the water vapor are known as hygroscopic particle. Thus, water vapor condenses around hygroscopic particles and a newborn cloud droplet begins. When condensation occurs on active salt nuclei of 1  $\mu\text{m}$ , for example, a droplet of 10  $\mu\text{m}$  is born after 1 second, it would then take 500 seconds for the droplet to get 100  $\mu\text{m}$  in diameter and 3 hours to become rain drop. For large droplets however, as rain drops, collision-coalescence is necessary to explain the process of ice growth (see section 3.5 for more details).

When temperature in the cloud is below freezing water droplets transform to ice crystal by deposition process. Clouds that form in the upper atmosphere are composed entirely of ice crystals as indicated in chapter 2. The presence of ice crystals alone does not offer icing problems, since they do not stick to cold aircraft surfaces, though it has been reported that ice crystals should be considered for engines.

Crystallization temperature	Structure	Shape
0 to $-3^{\circ}\text{C}$ and $-8$ to $-25^{\circ}\text{C}$	Hexagonal plates	
$-3$ to $-8^{\circ}\text{C}$	Prisms and needles	
$-12$ to $-16^{\circ}\text{C}$	Dendrites	
$-25$ to $-50^{\circ}\text{C}$	Prisms	

**Fig. 3.1:** Different forms of ice crystals and their crystallization temperature

Study of ice-crystals forms show that a various shapes may exist. The typical one has a hexagonal shape due to the way water molecules are arranged. Figure 3.1 shows the different shapes of ice crystals with corresponding crystallization temperatures.

### ***3.2 SUPERCOOLED WATER DROPLETS***

As a result of upward currents, clouds of lower atmosphere may have both ice crystals and water droplets. Most clouds have a lower region of water droplets, a middle region where both ice crystals and water droplets exist together, and a high region where water droplets are frozen into ice crystals [1]. When the air is cooled by expansion, the relative humidity increases and droplets begin to form clouds in the manner as described by sections 2.4, 2.5 and 2.6. Observation shows that cloud droplets do not freeze until they reach temperatures far below the melting point (0°C or 32°F). When temperature approaches -40°C the droplets freeze rapidly and transform to ice crystals. The droplets that stay liquid at temperature below freezing are called supercooled droplets. It is reported that small droplets do not freeze at 0°C because their molecules do not line up in the proper order to form ice crystal. Supercooled droplets are unstable and may rapidly change from liquid to ice whenever their stability is perturbed. These droplets are common occurrence in the atmosphere and present the most hazards to aircraft, particularly when they become large.

### ***3.3 MECHANISM OF AIRCRAFT ICING***

Two basic conditions must be met for aircraft ice to be formed: the ambient temperature must be below freezing and supercooled water droplets must be present. Icing on aircraft occurs when the aircraft flies at a level where the temperature is at, or slightly below the freezing point and the atmosphere contains supercooled water droplets. When these droplets are hit by the aircraft they begin to freeze immediately. As the water droplets freeze, however, heat is released so that their temperature rises until 0°C



is reached. As this temperature is reached, freezing stops while the remaining liquid fraction of the droplets starts to run back along the surface of the aircraft or along existing ice and freezes downstream. The freezing fraction depends mainly on the temperature. At colder temperature a large part of a droplet freezes by impact while at higher temperature only a small part freezes while the remaining part freezes slowly. The more dangerous types of ice are encountered in dense clouds, composed of heavy accumulations of large water droplets.

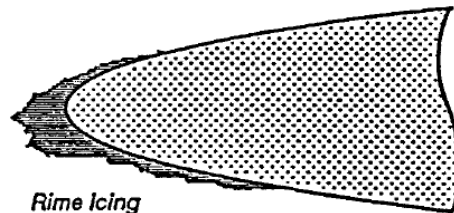
Upon impinging on aircraft surfaces, the shape of the ice accretion which will be formed depends mainly on the liquid water content (LWC), the droplet diameter, the ambient temperature, the airspeed, the surface roughness and the shape of the accreting components which pick up the droplets. There are principally two different types of ice deposit which form on aircraft during flight through clouds, containing supercooled droplets, or precipitation. Icing is referred to as rime and glaze ice and they have been already described in chapter one. Here below however, a brief description is reported again for reader convenience:

**Glaze ice:** is a wet growth ice formed at a temperature around 0 °C and high liquid water content. It has a density closer to that of the cloud water indicating the wet nature of this icing type. It occurs when only a fraction of the water droplets freezes upon impact while the remainder droplets run back along the surface or along and freeze downstream. This ice accretion process produces different ice shape deposit: such as double horned, beak or a rounded glaze ice as illustrated by figure 3.2. As already stated in section 1.2.1 glaze ice accretion dangerously affects and alters the shape of the original surface body producing aerodynamic penalties much more severe than rime ice accretion can cause.

**Rime ice:** is a dry, milky and opaque ice deposit which usually occurs at low airspeed, low temperature and low liquid water content. It is characterized by the instantaneous freezing of the incoming supercooled water droplets as soon as they hit the surface of the body trapping the air inside. More details have been already given in section 1.2.2. Another example of rime ice shape is given by figure 3.2.

#### Rime ice conditions

- Air temperature: Low
- Airspeed: Low
- Liquid Water Content: Low
- Water droplets: Freeze on impact



#### Glaze ice conditions

- Air temperature: High
- Airspeed: high
- Liquid Water Content: High
- Water droplets: Only a fraction freezes on impact, some flow on surface

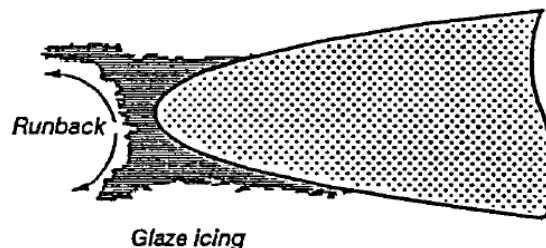


Fig. 3.2: Typical rime and glaze growth on an airfoil

### 3.4 ICING VARIATIONS

In chapter 2 it has been studied the different types of clouds that may produce icing. It has been shown that icing intensity may be severe in some regions and light in some other regions depending on the structure, horizontal and vertical extents, and the contents of the clouds. Many investigations of flight data have indicated that icing

conditions varies with altitude, season and geographical regions [1]. It was reported that icing is more serious in winter season at altitudes of 7000 to 9000 ft above ground level. In high altitude, above 20,000 ft (6 km) icing is rare and has light intensity. The minimum low temperature for icing is  $-40^{\circ}\text{C}$ , for low temperature all water droplets transform to ice crystals. Icing may also vary with horizontal extent of clouds due to the variation of liquid water, which is lower. This characteristic is shown by figure 3.3.

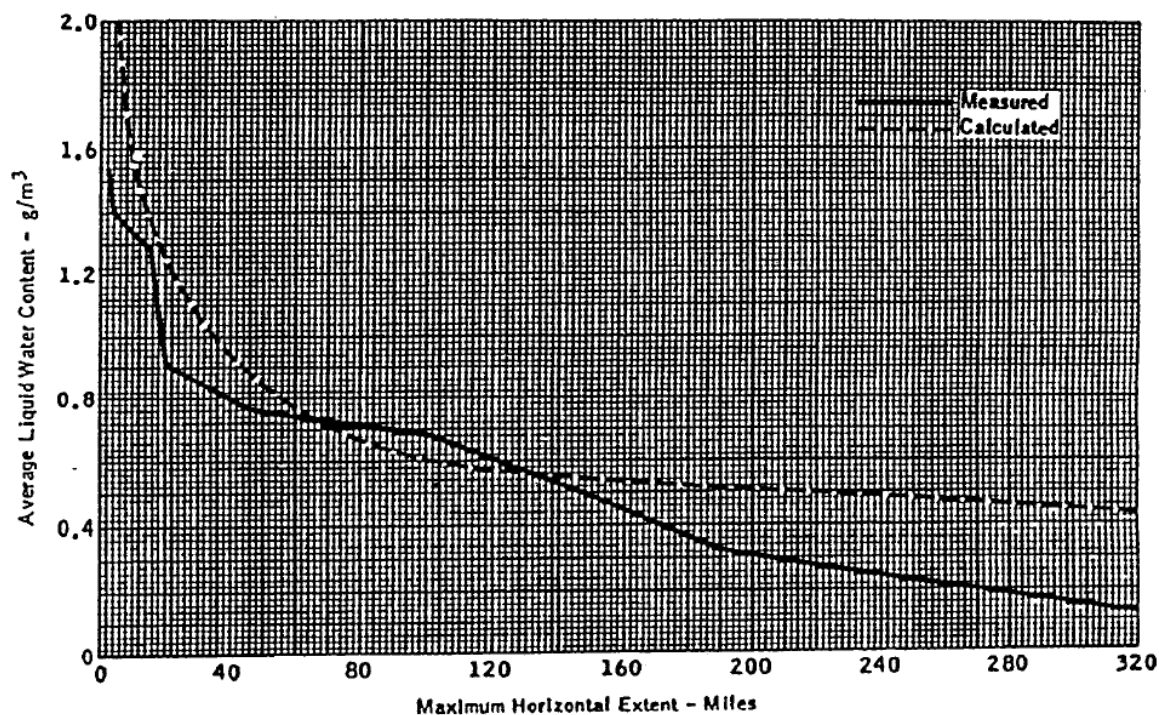


Fig. 3.3: Variation of liquid water content as a function of horizontal extent

### 3.5 ICE GROWTH

In section 3.1 it has been seen that water droplet starts with the process of condensation nuclei. Water vapor condenses around hygroscopic particles and forms water droplet. The particles may grow up to  $50\text{ }\mu\text{m}$  or more. For larger droplets, such as

rain drops which may exceed 1000  $\mu\text{m}$ , collision-coalescence and ice crystal theory must be included to explain growth process. Under different circumstances, water droplets present in the atmosphere may be disturbed and their state change by evaporation, condensation, melting, freezing, sublimation, or deposition. In the clouds, precipitation is developed when cloud droplet population becomes unstable and some droplets grow to the expense of others. This growth influences the rate of aircraft icing through the increase of collection efficiency. There are two mechanisms by which cloud droplets grow (see figure 3.4): coalescence process which occurs because of the different fall velocities of the cloud droplets, and growth of ice crystals (Bergeron process) due to the coexistence side by side of both ice crystals and cloud droplets [1].

In the first process, which is the most important, the presence of cloud droplets with different size and different velocity induce large droplets having more inertia than the small ones and tend not to follow the airflow. Therefore, they collide and coalesce with small droplets and become larger producing raindrop growth. In a still air, large droplet takes less time to capture the small droplets lying in its path. With a vertical air current, as in most clouds, large droplets, while having the same process of sweeping up, take more time to fall. As a result, the growth process is extended and droplets size becomes greater with a maximum value depending on the time spent by the larger droplets in the cloud and the number of small droplets captured. Since droplets require strong vertical air current to support them, thicker cloud and greater updraft will favore the growth of larger droplets. These droplets are likely to be created in cloud formed over mountains and hilly terrains.

In the second process of cloud droplet growth, ice crystals are present in a cloud containing a number of supercooled water droplets. In this case, since at freezing

temperature the saturation vapor pressure over ice surface is less than that over liquid surface, there is a pressure force driving water molecules from water to ice and ice crystals tend to grow at the expense of small droplets. Once ice crystals have grown large enough to begin falling they will collide or pick up other water droplets lying in their path or break up into small ice crystals which may serve as freezing nuclei. If the temperature below the region of formation, is below freezing ice crystals produce snowflakes. For temperature above freezing, snowflakes melt and rain occurs. Most serious aircraft icing occur when an aircraft is flying near the top of cold air mass under a layer of warm air. The precipitation in this case is freezing rain (see section 3.6).

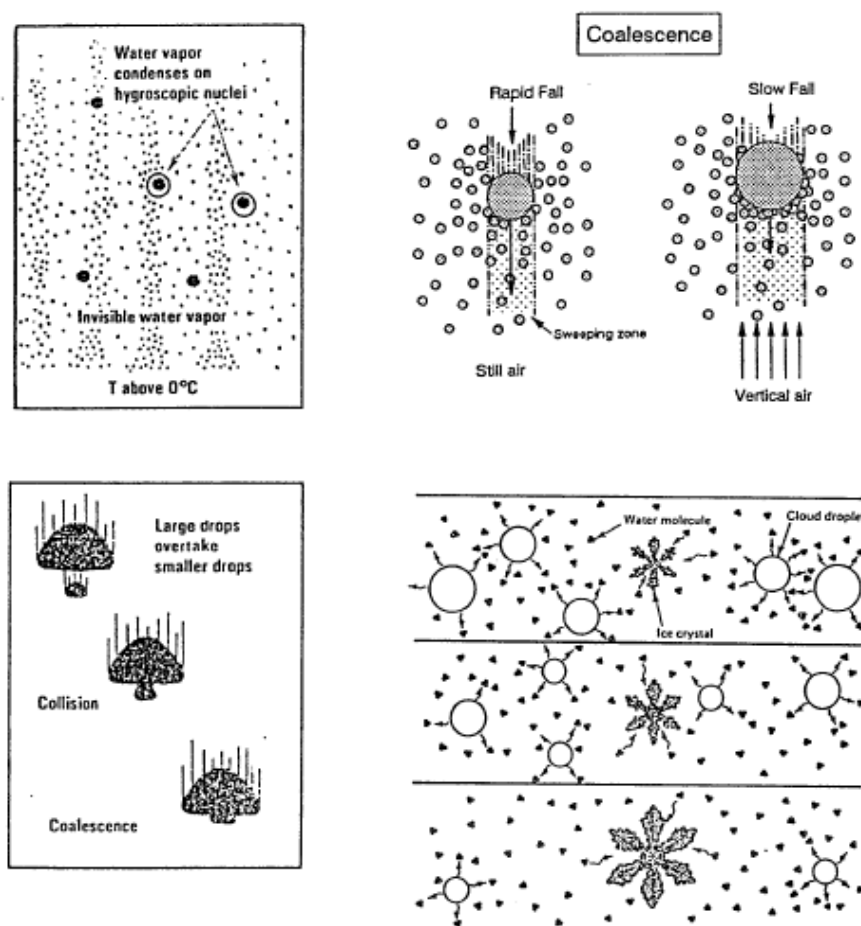


Fig. 3.4: Ice growth by coalescence and Bergeron process

### **3.6 PRECIPITATION TYPE AND ICING**

Precipitation is a general term given to water droplets that grow sufficiently in size and weight by the process described before and fall due to their gravity. Precipitation includes rain, freezing rain, drizzle, snow, snow pellets, ice pellets, and hail:

- Rain: precipitation of water droplets with diameter ranging from 0.4 to 4.0 millimeters. The only difference between rain and drizzle is the size of water droplet. Rain drops are much larger than cloud droplets and therefore give a very high rate of catch.
- Freezing rain: is composed of supercooled water droplets that freeze on impact with an object, such as aircraft surfaces, which is itself at a temperature below freezing. This is common ahead of warm front in winter. Serious icing occurs when the aircraft is flying near the top of the cold air mass beneath a deep layer of warm air.
- Drizzle: precipitation in the form of very small water droplets which appear to float. At temperatures at or below the freezing level, drizzle will freeze on impact with objects and is known as freezing drizzle. Drizzle falls from stratus cloud with a high water content. Icing in freezing drizzle is usually maximum, just below the cloud base where the drops are largest.
- Snow: Precipitation of ice crystals. The water vapor in the air sublimates directly into ice crystals, without passing through any intermediate water stage. Snow flakes are formed of an agglomeration of ice crystals and are usually of a hexagonal or star like shape. Snow and ice crystals do not adhere to cold aircraft

and do not usually constitute an icing problem. However, if the aircraft is warm, the snow may melt as it strikes the warm surface and ice accretion may result. If supercooled water droplets are also present with the snow, a rapid build up of rough ice can occur.

- Snow pellets: precipitation of white, opaque, and spherical or conical grains of ice with diameter about 2-5 mm.
- Ice pellets: precipitation of transparent ice pellet, which are spherical or irregular with a diameter of 5 mm or less. The pellets of ice usually bounce when they hit hard ground.
- Hail: precipitation in the form of balls or lumps of ice with a diameter of 5 mm or more. Anything smaller than this, it is called ice pellets, snow pellets, or grapple.

Usually meteorologists use a diameter of 200  $\mu\text{m}$  as a demarcation between cloud droplets and raindrops. Table 3.1 shows an example of cloud droplets diameter, drizzle drops diameter and raindrops diameter [14]. Water drops with diameter between 200  $\mu\text{m}$  and 500  $\mu\text{m}$  are called drizzle drops, but usually drops higher than 200  $\mu\text{m}$  are simply called raindrops. Table 3.2 describes the several possible kinds of precipitations as a function of the different clouds.

Droplet type	Diameter ( $\mu\text{m}$ )	Terminal Velocity (cm/s)
Cloud droplets	10	0.3
	50	7.6
Drizzle drops	200	72
	500	206
Raindrops	2000	649
	3000	806

**Table 3.1:** Example of water drops diameter and terminal velocity

Cloud Type $\Rightarrow$	AS	NB	SC	ST	CU	CB
Precipitation $\Downarrow$	Middle clouds (2 to 7 km)		Low clouds (below 2 km)			Vertical development
Rain	✓	✓	✓		✓	✓
Drizzle				✓		
Freezing drizzle			✓			
Snow	✓	✓	✓			✓
Snow pellets			✓			
Ice pellets	✓	✓				✓
Ice prisms				✓		
Hail						✓

**Table 3.2:** Precipitation as a function of cloud types



## **CHAPTER 4**

### **MAIN PARAMETERS IN AIRCRAFT ICING**

#### ***4.1 PHYSICAL FACTORS AFFECTING AIRCRAFT ICING***

The amount and the rate of icing depend on a number of meteorological and aerodynamic conditions, such as liquid water content, temperature, droplet diameter, and rate of catch (see chapter 3). The objective of this chapter is to study the important parameters qualitative affecting aircraft icing. However, before discussing meteorological (MVD, LWC, static pressure, and temperature) and aerodynamic icing parameters (airspeed total temperature wing profile), it will be helpful to define the icing intensity.

#### ***4.2 ICING INTENSITY***

Icing may be described as trace, light, moderate and severe. The definition of icing intensities have been established in 1964 based on meteorological and operational conditions and updated in 1968 [1].

Tables 4.1 and 4.2 summarize types of icing intensities, and relationship with liquid water content in cumuliform and stratiform clouds. The intensity of an icing condition depends mainly on the aircraft type and the weather situation. This, in turn, will depend on the amount of ice catch rate and aircraft performance degradation. The variation of icing intensity as a function of cloud types is given by Table 4.2 where the assumed

droplet diameter for cumuliform clouds is 17  $\mu\text{m}$  and 14  $\mu\text{m}$  for stratiform clouds. The corresponding average liquid water content (LWC) (statistical averaging) for icing intensity are less than 0.07  $\text{g/m}^3$  in trace icing, 0.3  $\text{g/m}^3$  in light icing, 0.88  $\text{g/m}^3$  in moderate icing and more than 1.0  $\text{g/m}^3$  in severe icing conditions.

Ice Intensity	Description
Trace	Ice becomes perceptible. Rate of accumulation slightly greater than rate of sublimation. It is not a hazard even though except when deicing/anti-icing equipment is not utilized, unless encountered for an extended period of time (over one hour).
Light	The rate of accumulation may create a problem if flight is prolonged in this environment (over one hour). Occasional use of deicing/anti-icing equipment removes/prevents accumulation. It does not present a problem if deicing/anti-icing equipment is used.
Moderate	The rate of accumulation is such that even short encounters become potentially hazardous and use of deicing/anti-icing equipment or diversion is necessary.
Severe	The rate of accumulation is such that deicing/anti-icing equipment fails to reduce or control the hazard. Immediate diversion is necessary.

**Table 4.1:** Classification of airframe icing

Cumuliform Clouds LWC ( $\text{g/m}^3$ ) (Assumed droplet diameter is 17 $\mu\text{m}$ )	Icing Intensity	Stratiform Clouds LWC ( $\text{g/m}^3$ ) (Assumed droplet diameter is 14 $\mu\text{m}$ )
$\leq 0.07$	Trace	$> 0.11$
0.08 to 0.49	Light	0.12 to 0.68
0.50 to 1.00	Moderate	0.69 to 1.33
$> 1.00$	Severe	$> 1.33$

**Table 4.2:** Relationship between icing intensity and liquid water content

### **4.3 LIQUID WATER CONTENT**

Liquid Water Content (LWC) is defined as the amount or total mass of water contained in a given unit volume of cloud. Units of LWC are usually given as grams of water per cubic meter of air ( $\text{g/m}^3$ ). From the different parameters affecting aircraft icing, the liquid water content is considered as the most important one. It was reported by Hansmann [19] that for a given temperature and droplet size an increase in LWC may cause transition from rime ice to glaze ice. In addition, when LWC is high, supercooled water droplets will more likely impact and run back downstream of an object as in the case of ice accretion on an aircraft wing.

When LWC is high, then there is a great potential of icing. The variation of LWC depends mainly on the temperature. As it has been discussed in Chapter 3, when temperature is very low the water vapor present in the cloud will sublime onto ice crystals which grow at the expense of supercooled water droplet. As ice crystals grow the number of supercooled water droplets decreases, hence the LWC decreases. When the cloud is warmer, however, the mixing ratio (mass of vapor over mass of air) becomes higher and the LWC increases.

LWC decreases with precipitation since available water droplets are swept out, or when there is evaporation as in the case of dry air mixing with cloud. The liquid water content of clouds usually increases with height for temperatures not far below melting, but decreases when temperatures are well below melting due to the high amount of ice crystals. Variations of liquid water content as a function of icing intensity and cloud types is presented in Table 4.2.

Observations of LWC in non-precipitating clouds and study of its spatial distribution have found that LWC increases with height above cloud base [1]. Figures 4.1 and 4.2 show example of the variation of LWC as a function of temperature in a typical cumulus and stratus clouds.

To investigate qualitative effects of LWC on ice accretion an airfoil some simulation as well as wind tunnel testing have been performed on a NACA 0012 with the following conditions: angle of attack 0 deg, free stream velocity 129 m/s, temperature -12.6°C, liquid water content 1.0 g/m<sup>3</sup> and 0.25 g/m<sup>3</sup>, accretion time 20 seconds, and airfoil chord 0.3 m. As can be seen from Fig. 4.3, when LWC is increased from 0.25 g/m<sup>3</sup> to 1.00 g/m<sup>3</sup> the amount of ice collected also increases. However, the impingement limits, which determine the local and global collection efficiencies, are not affected. Figure 4.4 [15] shows the effect of LWC on ice shapes over NACA 0012 airfoil (0.53 m-chord), with an airspeed of 58 m/s, droplet diameter of 20 µm at an angle of attack of 4 deg. and an accretion time of 8 minutes. The distribution of drag coefficient as a function of LWC is also presented in the same figure. The LWC effect is greatest when temperature effect is greatest.

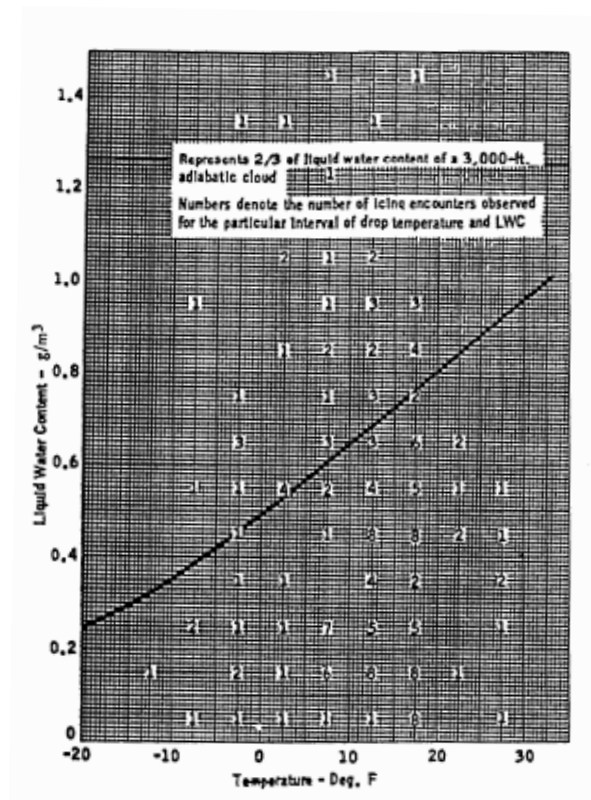


Fig 4.1: LWC as a function of temperature in cumulus clouds

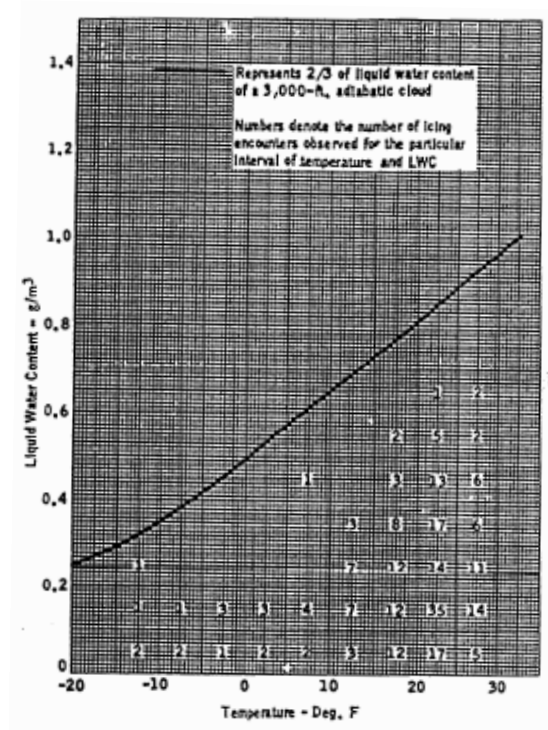


Fig. 4.2: LWC as a function of temperature in stratus clouds

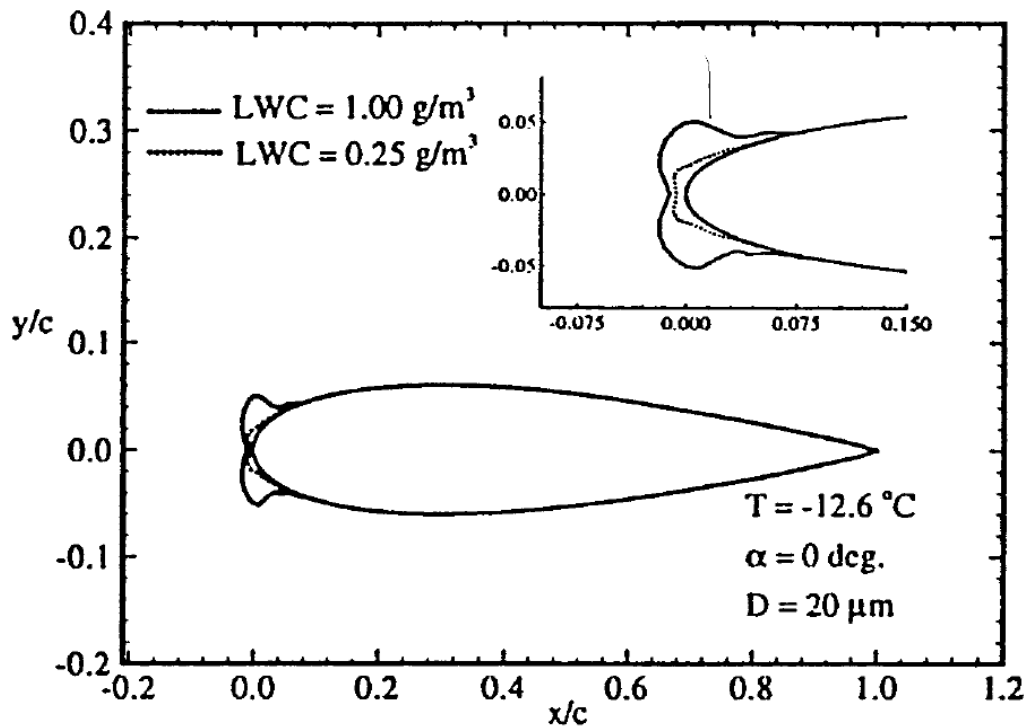


Fig. 4.3: Qualitative effect of liquid water content (LWC) on ice shapes

#### 4.4 TEMPERATURE

As we discussed in chapter 3, one of the two basic conditions that must be met for ice to be formed is that ambient temperature must be below freezing temperature in a cloud which contains supercooled water droplets. The temperature has a great effect on the fraction of water that freezes on impact consequently it will have an effect on the type of ice which will accumulate. When surface temperature is not far from freezing and droplet are large, then only a small fraction of the impacting droplets will freeze, while the remaining will freeze downstream. This process forms double-horns ice shapes. It is also reported that frequency of icing occurs in the range of  $-5$  to  $-7^{\circ}\text{C}$  since the moisture is higher and ice crystal is low. Variation of temperature as a function of LWC is given by Figs. 4.1 and 4.2. Ice shapes will also vary depending on the time the aircraft is

exposed to icing. Figure 4.4 shows the effect of ice accretion time on ice shapes for two different temperatures,  $-8^{\circ}\text{C}$  and  $-18^{\circ}\text{C}$ , for NACA 0012 with a 0.53 m-chord and different angle of attacks [15]. It can be observed that at colder temperature rime ice occurs while at higher temperature glaze ice is most likely.

Finally figure 4.5 shows the effect of temperature on ice shapes as well as on the drag wing profile.

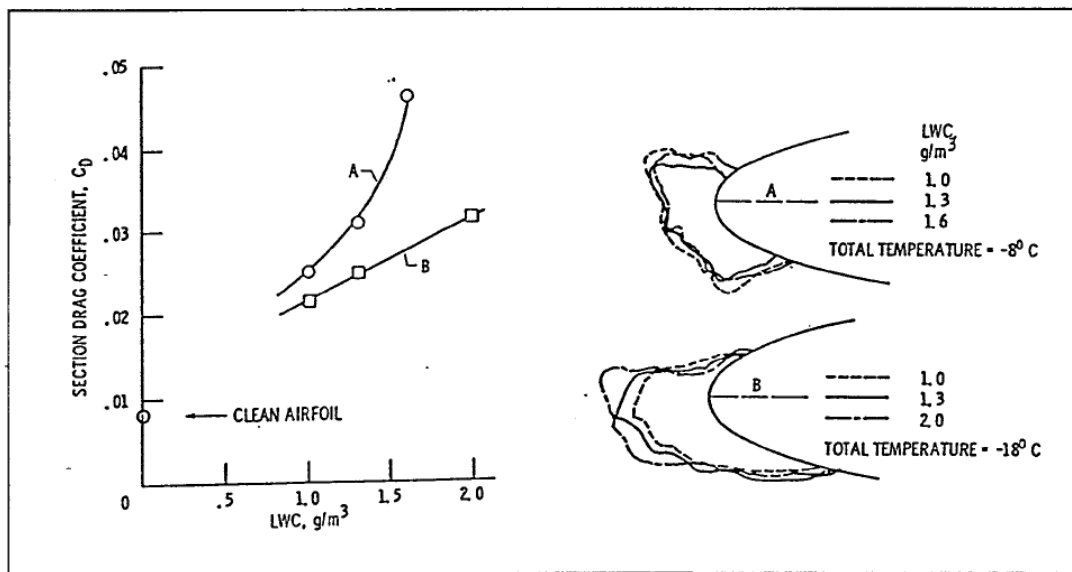


**Fig. 4.4:** Qualitative effect of liquid water content (LWC) on ice shapes

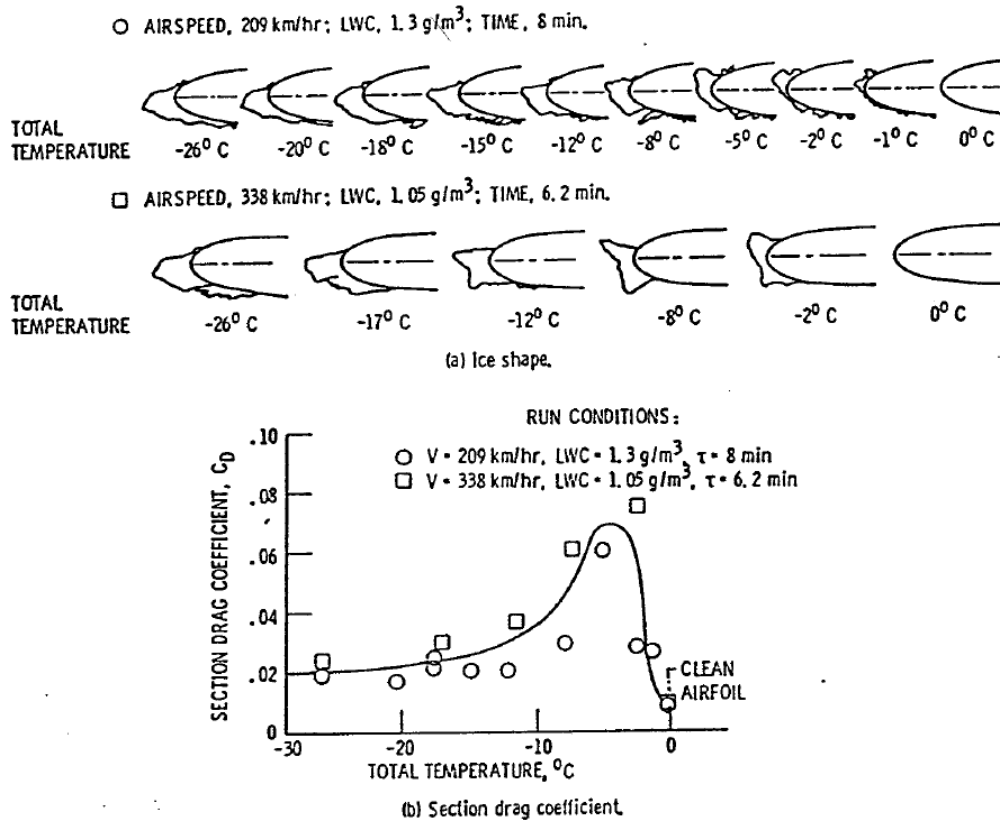


Fig. 4.5: Effect of temperature on ice shapes and on drag

#### 4.5 DROPLET DIAMETER

Droplets present in the atmosphere have different diameters. A photograph of cloud droplets as captured on an oil-coated microscope while flying through a cloud is given by figure 4.6 [1]. The largest droplet was  $40 \mu\text{m}$  in diameter. In icing calculation it is usually used the Median Volume droplet Diameter (MVD) defined as the diameter dividing the total water volume in half, where half the volume is in larger droplets and half the volume in smaller droplets.

Droplets sizes tend to increase with cloud height (figure 4.7). Variation of ice shapes as a function of droplet diameter is shown by figure 4.8 for NACA 0012 with droplet



diameters of 14, 20, 26 and 36  $\mu\text{m}$  [15]. Large droplets are more likely to impact on the airfoil while small droplets are deviated. Thus, ice may form beyond ice protection systems. This is further illustrated by figure 4.9 which shows the effect of large droplets on particle release position. Since large droplets have higher inertial force and non negligible terminal velocity compared to small droplets, they impinge directly on the airfoil while the small droplets are deflected.

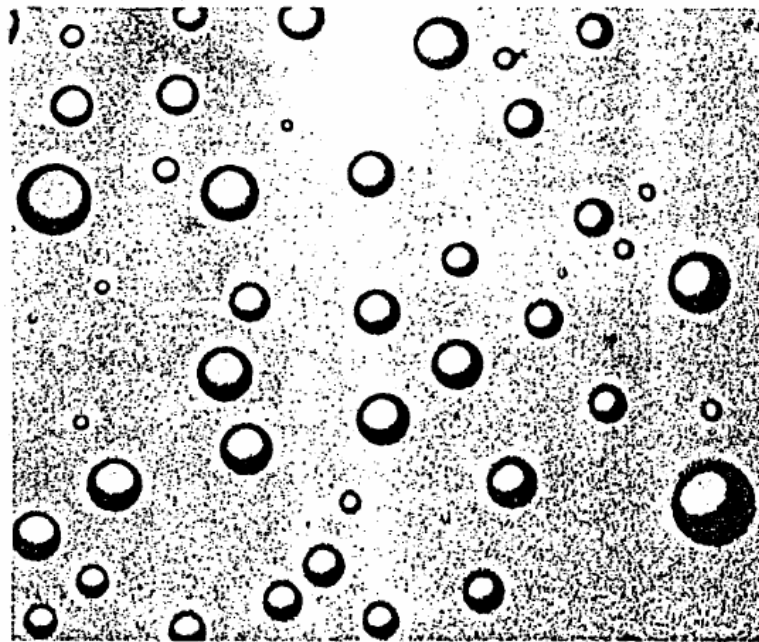


**Fig. 4.6:** Photograph of droplets present in a cloud

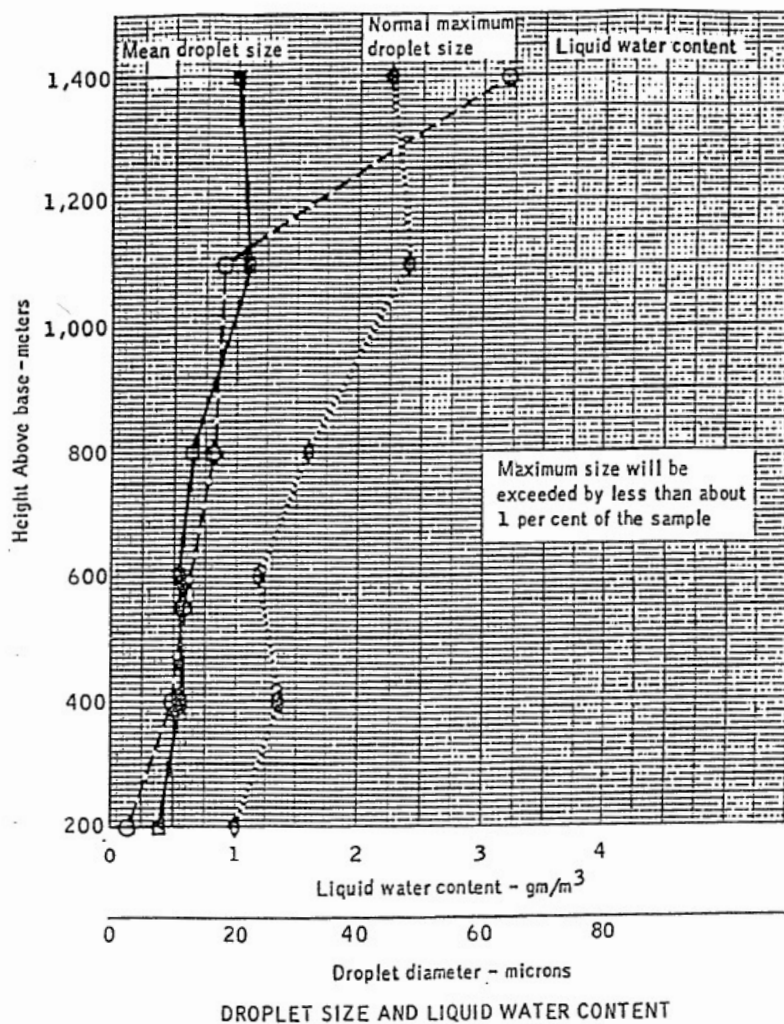


**Fig. 4.7:** Properties of typical cumulus congests clouds - LWC and droplet size

To impact on the airfoil, large droplets are released at higher coordinate compared to small droplets. Figure 4.9 shows also the effect of droplet diameter on collection efficiency. As expected, the droplet size influences the rate of icing through the increase of collection efficiency and the change of the upper and lower impingements limits which move further downstream. Characteristics of ice as a function of droplet diameter are summarized in Table 4.3.

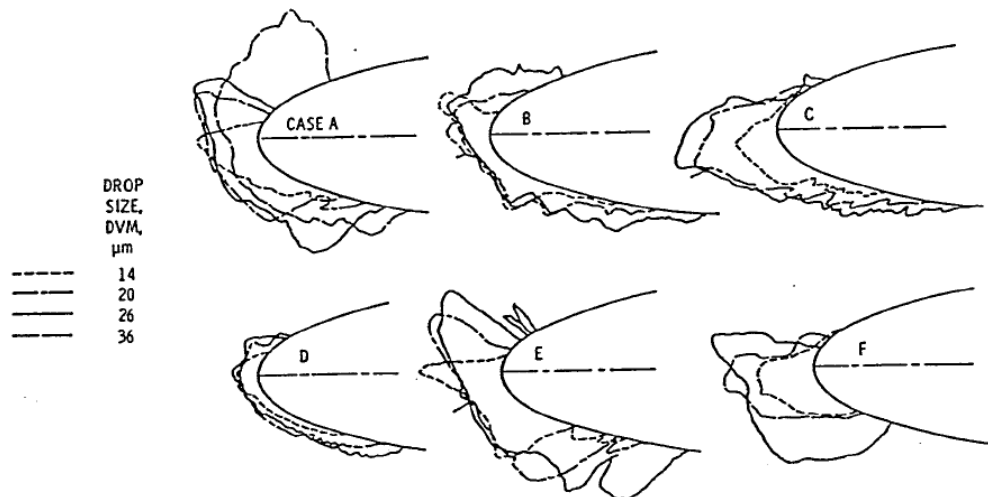


Fig. 4.8: Variation of ice shapes as a function of droplet diameter

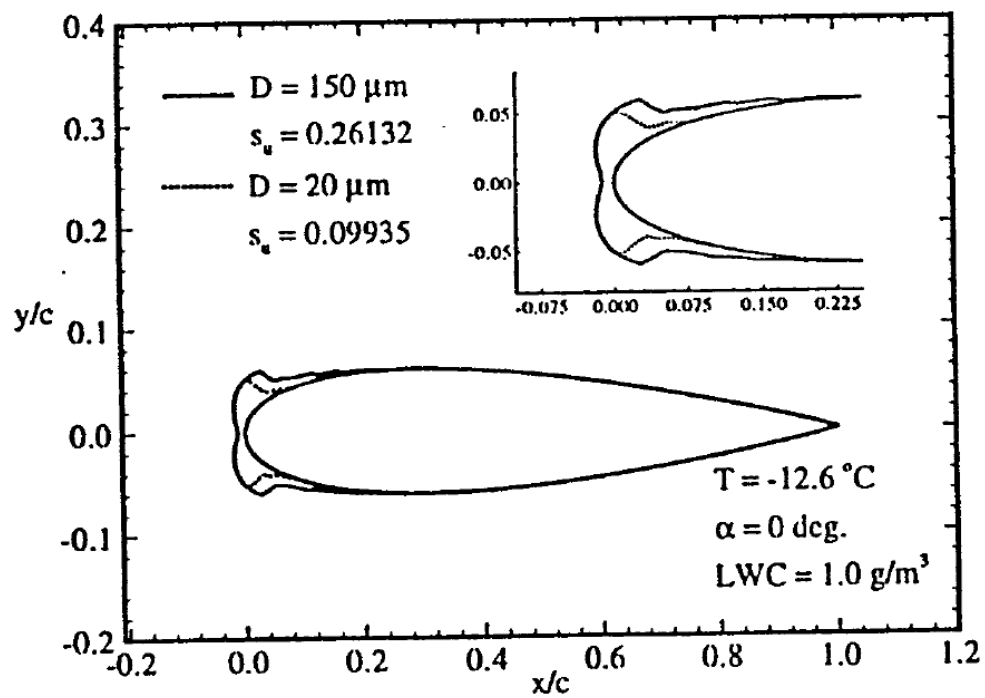


Fig. 4.9: Effect of large droplet on ice shapes

Category	Droplet Diameter	Observation Criteria
Small	<10 m	Ice accretion is limited to the leading edge of large component.
Medium	10 to 30 m	Ice accretion occurs aft of the leading edge but do not exceed the zones where ice protection systems are active.
Large	30 to 100 m	Ice accretion exceeds the zones where ice protection systems are active.
Freezing Rain or Drizzle	100 to 1000 m	Ice accretion has an important extend downstream.

**Table 4.3:** Ice observation as a function of droplet diameter

## 4.6 COLLECTION EFFICIENCY

Collection efficiency is defined as the ratio of the mass of droplets impinging on an obstacle, such as wing or airfoil, in unit time to the mass of droplets which would impinges if the droplets were following a straight line trajectories. The icing rate depends to a large degree upon the collection efficiency of the aircraft. This parameter is important since it is needed to measure the rate of supercooled water droplet impingement, in kg/hour/meter of span, for an airfoil [1]. There are two collection efficiencies (figure 4.10): the global one “E,” and local one “ $\beta$ ” defined as below.

$$\beta = \frac{dy}{ds} \quad \text{and} \quad E = \frac{\Delta y}{H}$$

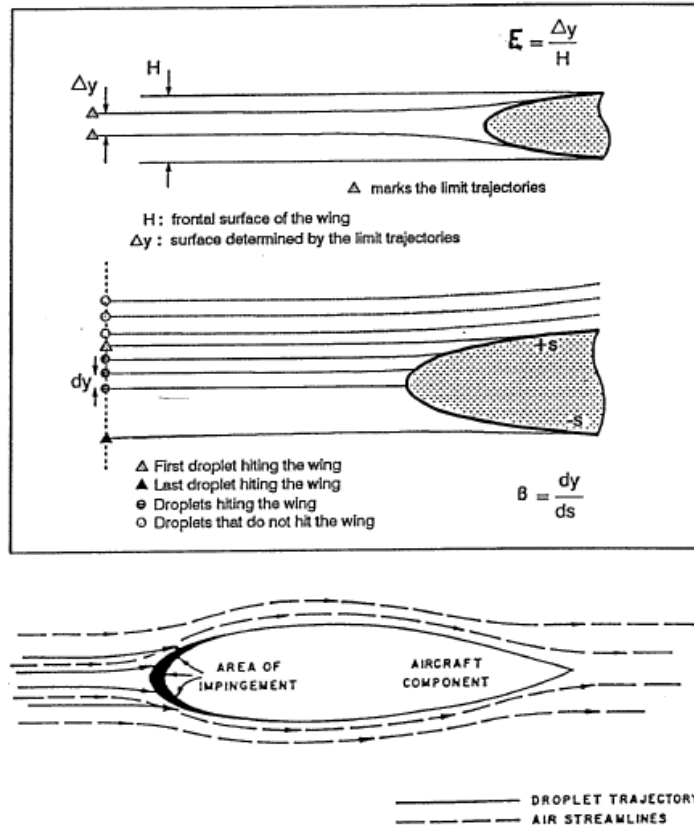


Fig. 4.10: Collection efficiencies and area of water droplet impingement on an airfoil

The local collection efficiency is needed in the prediction of ice shapes. Large leading edge curvature radius collects less water droplet than smaller one, particularly when small droplets are involved. This is due to the fact that water droplets deviate more when radius of curvature is large, thus ice collected will be small.

#### 4.7 AIRSPEED

Airspeed has an effect on the ice shapes. When the airspeed is high water droplets do not have enough time to deviate from the airfoil, thus more droplets impact on the airfoil.

As a consequence, the collection efficiency will be higher and the icing will be greater than the case where the airspeed is low. In addition, the velocity has an effect on the type of icing. For high velocity we usually have a glaze ice with horns which may cause separation over the airfoil.

#### **4.8 ICING MEASUREMENT INSTRUMENTS**

As was discussed previously, the most important parameters in icing are the liquid water content (LWC) and the median volumetric diameter (MVD) defined as the droplet diameter where half of the volume is in larger droplets and half of the volume is in smaller droplets, with the diameter obtained by calculation assuming a droplet size distribution.

There are many instruments used for the measure of LWC and droplet sizes. To measure the icing cloud liquid water content usually the following instrumentation is used: hot wire probes, such as Johnson-Williams (J-W) type, vibrating probes, light beam interruption instrument, rotating multi-cylinders. However the standard instrumentation is the icing blade, later on better described. For droplet sizes, usually is used optical means such as the optical array probe (OAP), or axial scattering spectroscopy as in forward scattering spectroscopy probe (FSSP). However new technologies are allowing to better characterize the MVD. New instrumentation based on the PDPA technique, such as the ADA system, is for time being, considered the new standard. Chapter 7 will provide more details on these topics.

## **CHAPTER 5**

### **ICING CERTIFICATION**

#### ***5.1 AIRCRAFT CERTIFICATION ISSUES***

Civil transport aircraft are either fast and jet powered, or slower, usually smaller and turbine/propeller (turboprop) powered. The turboprops have almost straight wings and fly more often at lower altitudes, especially during hold. Both factors increase the danger of icing and of corresponding performance degradation compared with swept wing jets cruising at higher altitudes. Both types of aircraft are also in military use and their qualification usually adapts the same rules as prescribed for civil certification. Fighter aircrafts fly only for short times in icing conditions and as a consequence of their high speeds with corresponding surface heating, larger wing sweep, and sharp leading edges, the danger of ice accretion and the respective attention to it concentrates mainly on the engine inlet. Helicopters are equally in use for military and civil purposes but the development of full ice protection systems still poses difficult problems to manufacturers [17].

From the aerodynamic point of view the problems of the certification or qualification procedure are characterized by the performance degradation of various components of an aircraft due to ice accretion. It is not however easy to identify and locate the most critical cloud conditions, as prescribed by qualification/certification authorities, in the natural environment. Therefore, qualification and certification are extremely time consuming and very costly.

With regard to ice protection, airplane type certification is currently accomplished by meeting either the requirement of FAR 23.1419 or FAR 25.1419 (see paragraph 5.4). These rules require an analysis to establish the adequacy of the ice protection system for the various components of the airplane based on the operational needs of that particular aircraft. In addition, tests of the ice protection system must be conducted to demonstrate that the airplane is capable of operating safely in the continuous maximum and intermittent maximum icing conditions. These conditions are described in Part 25, Appendix C and are detailed in the next sections. The Type Certificate Data Sheet (TCDS) gives the certification basis for the airplane and lists the regulations with which the airplane has demonstrated compliance. Therefore, when an airplane complies with one of the regulations which refer to Part 25, Appendix C, the icing certification is indicated on the TCDS and in the Aircraft Flight Manual (AFM). The AFM lists the equipment required to be installed and operable. The AFM or other approved material will also show recommended procedures for the use of the equipment. The FAA operating rules also permit flight into specified icing conditions provided that the aircraft has functioning de-ice and/or anti-ice equipment protecting specified areas of the aircraft. There are aircraft with partial installations of de-icing and/or anti-icing equipment that do not meet the certification or the operating regulatory requirements for flight into icing conditions. Those installations are approved because it has been demonstrated that the equipment does not adversely affect the aircraft's structure, systems, flight characteristics, or performance. In such cases, the AFM or other approved material must explain the appropriate operating procedures for the partial de-icing and/or anti-icing equipment and contain a clear statement that the aircraft is not approved for flight into known icing condition.



It is important for pilots to understand that an airplane equipped with some types of de-ice and/or anti-ice systems may not be approved for flight into known icing conditions. To be approved for such flight, the airplane must be specifically certificated to operate in known icing conditions. Also, it is important to remember that the certification standards provide protection for the majority of atmospheric conditions encountered, but not for freezing rain or freezing drizzle or for conditions with a mixture of supercooled droplets and snow or ice particles.

## ***5.2 BASIC ASPECTS OF SAFETY***

As it has been seen, ice accretion is a consequence of certain meteorological conditions - usually connected with the occurrence of supercooled droplets in clouds - and can cause very critical situations with respect to the flight safety of an aircraft. Once ice has accumulated on the aircraft surface, it essentially affects the aerodynamic performance of all types of lifting components. These are the wings, the horizontal tail, the vertical tail, and any rotary wings including propellers. As already explained in previous chapters, not only the aircraft flight performance can become drastically reduced but also the handling qualities can be deadly affected. The stability and control properties, in longitudinal as well as in lateral movements, can diminish remarkably, and the flight can become quite dangerous as the mission may not be completed (e.g. the flight range may be cut, or ceiling heights needed for crossing mountains may not be reached), or the safe control might be lost (e.g. tail stall effects may occur earlier). Also, engines can become adversely affected, eventually even leading to flame-outs. This could result from ice accretion directly on the air inlets, which may cause inflow problems, or from ice shedding into the inlet. Ice shed from other aircraft surfaces may also fall into the

inlet and damage fan or compressor blades. The hazards resulting from ice accretion are underlined by cases reported in several studies some of which have also been reported in chapter 1. However it can be reminded that more than one half of all related accidents are due to carburetor icing of general aviation aircraft, mostly not fatal. More than one quarter are due to take-off icing – which should not happen at all because of the “clean wing concept” (the act of cleaning the wing when the aircraft is on the ground). It is demonstrated also that roughly one third of the accidents happen in each of the three basic flight phases: take-off, in-flight, and landing [18].

Of course, in present days all aircraft used by commercial airlines have to be equipped with an effective de-icing (in-flight removal of ice) or anti-icing (prevention of ice accretion) system in order to maintain acceptable aerodynamic performance and safety of the aircraft in flight under icing conditions. A lot of efforts are presently spent to improve ice protection systems in the directions of enhanced safety or of avoiding performance disadvantages of classical de-icing devices. Inflatable rubber boots, for example, are not compatible with maintaining laminar flow on the surface. The ice protection problem does not only concern the wings but also the tail surfaces, engine inlets, ducts, and Pitot probes. For example, ice contaminated tail plane stall (ICTS) is one of the most dangerous icing effects and must be considered thoroughly with respect to tail ice protection. Ice plugged Pitot-probes which can give false airspeed readings as well as possible engine flame-outs due to icing, must be prevented by a suitable ice protection.

### **5.3 ICE PROTECTION SYSTEM BASIC ISSUES**

Federal Aviation Regulations for equipment in icing conditions, sec. 121.341, lay down that nobody may operate an aircraft in icing conditions unless it is equipped with means for prevention or removal of ice on windshields, wings, empennage, propellers and other parts where ice formation will adversely affect the safety of the aircraft. Of course these anti-icing or de-icing systems must be certified under transport category airworthiness requirements relating to ice protection.

While in these times of extensive air traffic ground icing is routinely removed and subsequently prevented by application of de-icing fluids (clean wing concept), ice protection systems of any kind are extensively investigated and taken into account during the design phase.

As already explained ice may build up on all forward facing surfaces. Aircraft components that therefore may need some consideration and possibly ice protection are:

- Leading edges, lifting and control surfaces
- Rotor blades
- Propellers and spinners
- Engine inlets
- Windshields and radomes
- Flight sensors
- Antennas.

The classical ice protection systems are as follows:

- On medium sized and large jet aircraft, typically heating is applied in the region of the leading edge using bleed air from the engine compressors, either to evaporate all impinging water droplets (anti-icing) or to melt accreted ice at the surface and thus to cause it to move downstream. In the latter case there is a potential that the ice-water mixture can refreeze forming further downstream, the so-called runback ice. For modern high bypass turbofans the amount of available bleed air is rather limited and therefore the manufacturers try to reduce the extent of the protected regions as far as possible and research on alternate systems is to be encouraged.
- For turboprop aircraft, the most usual de-icing devices are pneumatic boots. These are inflated cyclically and require a very small amount of energy. These systems fracture, de-bond and expel the ice accretion from the surface. For effective ice removal the ice shapes must have a minimum thickness of about one quarter to one half of an inch and this thickness must be tolerable for safe flight of the aircraft. In extreme icing conditions some residual ice may remain behind the boots and form a nucleus for the growth of possibly dangerous ice ridges.
- On some aircraft anti-icing is done by forcing a freezing point depressant fluid (normally mixture of glycol and water) out of a porous panel at the leading edge, thus either preventing ice accretion or releasing ice already accreted and moving it downstream on a liquid film on the airfoil surface. Such systems can in principal be extended to become, in addition, anti-

contamination systems for wings designed to maintain a long laminar flow range.

- Engine inlets for the jet aircraft are usually anti-iced to evaporate all the water impinged on the inlet lip. This prevents any runback ice which can potentially damage the fan blades.
- Helicopter rotors and propellers are mainly protected by electric heating of the leading edge region of the blades. Also, electric heating is sometimes applied for parts of fixed-wing aircraft, usually for smaller, critical components.

An overview of ice protection systems including those presently under development are listed in Appendix A.

Finally, certification and qualification procedures for the ice protection system and for the aircraft itself in icing conditions are very time-consuming and costly. Besides the normal flight situations when the ice protection system is in action, a failure of the ice protection system under special circumstances must also be taken into account. Safe flight must be demonstrated during extreme flight situations that may not be encountered intentionally (e.g. maximum rudder deflection with ice accretion, although this is normally used only during one engine failure).

#### **5.4 CURRENT DESIGN ENVELOPES**

Because of the danger of flight in icing conditions the civil certification authorities FAA (Federal Aviation Administration in the United States) and EASA (European Aviation

Safety Agency) have established some important rules for so-called “ice-certification”. These are laid down for transport aircraft in JAR/FAR 25.1419 (Joint Airworthiness Requirements/Federal Aviation Regulations, part 25). Smaller general aviation aircraft have to follow the rules of JAR part 23 that are similar to part 25 with respect to ice certification. For helicopters the JAR parts 27 (small rotorcraft) and 29 (transport rotorcraft) are applicable. The military authorities, which of course possess national sovereignty, also have established rules for the ice qualification of their aircraft which usually follow the civilian regulations in many aspects. The basic demand of all these regulations is that safe flight must be maintained in all permitted icing conditions.

More serious icing conditions must be avoided or immediately left; examples are:

- Take-off is not permitted if any ice contamination on the aircraft's surfaces exists (clean wing concept).
- Freezing rain must be avoided (conditions which exhibit much larger freezing water droplets than other, more frequent icing environments and contaminate all aircraft surfaces completely).

FAR 25 Appendix C are summarized in figures 5.1 through 5.4. They show the main civil design criteria for in-flight icing conditions. These design envelopes have been in use since the mid 1950's. Figures 5.1 and 5.2 apply to the more or less horizontally continuous icing conditions associated with stratiform-like clouds and overcast. Figures 5.3 and 5.4 apply to the more intermittent icing conditions associated with convective and vertically taller cumuliform clouds. All of the figures are based on an extensive set of cloud physics research flights conducted by researchers from the US Weather Bureau and the National Advisory Committee for Aeronautics (NACA) during the winters

of 1946 to 1950 [10, 11, 17]. These flights were dedicated to characterizing the icing environment for the rapidly expanding, post war, commercial airline industry. The basic envelopes (figures 5.1 and 5.3) simply give the "probable maximum" value of LWC to be expected over a specific averaging distance, for a given temperature and cloud droplet size distribution represented by the median volume diameter (MVD) of the droplets. The presented figures actually use the older concept of mean effective diameter, MED; but for all practical purposes MED and MVD are the same [17]. Thus, if one wants to simulate the approximate extreme values of LWC for an MVD and temperature of interest, figures 5.1 and 5.3 will give the values of LWC to be used. For example, figure 5.1 indicates that  $0.8 \text{ g/m}^3$  is the largest value of LWC to be expected in supercooled stratiform clouds as an average over 17.4 nautical miles (nm) when the cloud droplets have an MVD of  $15 \text{ }\mu\text{m}$  and the in-cloud, flight-level temperature is  $0^\circ\text{C}$ . "Probable maximum" is understood to mean the 99<sup>th</sup> percentile value of LWC, as well as the 0.1% probability that all three variables (LWC, MVD, and temperature) represented by a point on the envelopes will be exceeded simultaneously in natural icing conditions [17]. Except for the selection of overall maximum values of LWC, these envelopes are otherwise of no help for icing simulation purposes. For example, they do not indicate which MVD's are more probable, and in fact they do not even show any MVD's smaller than  $15 \text{ }\mu\text{m}$ . A major difficulty is that the envelopes, as shown, are valid only for fixed averaging distances of 3 statute miles (2.6 nm) for convective (intermittent) clouds, and 20 statute miles (17.4 nm) for stratiform (continuous) clouds. These are arbitrary reference distances but were convenient for the original NACA researchers because most of their measurements were averaged over about 3 and 10 miles. It is known, however, that for both types of clouds, longer averaging distances will result in lower maximum values of LWC as an average over the total exposure distance. To account

for this behaviour, additional curves (Figs. 5.2 and 5.4) had to be developed so the envelopes could be adapted to other averaging distances. For example, to find the maximum probable LWC to be expected as an average during flight through a 100 nm - wide expanse of stratiform icing clouds, the appropriate multiplying factor (0.46 in this example) is taken from figure 5.2. Thus, for stratiform clouds in which the MVD is 25  $\mu\text{m}$  and the temperature is  $-10^{\circ}\text{C}$ , the maximum average LWC over 100 nm is  $0.46 \times 0.3 \text{ g/m}^3 = 0.14 \text{ g/m}^3$ .

More information about the FAR certification envelopes i.e. their possible future extension can be found in Appendix B.



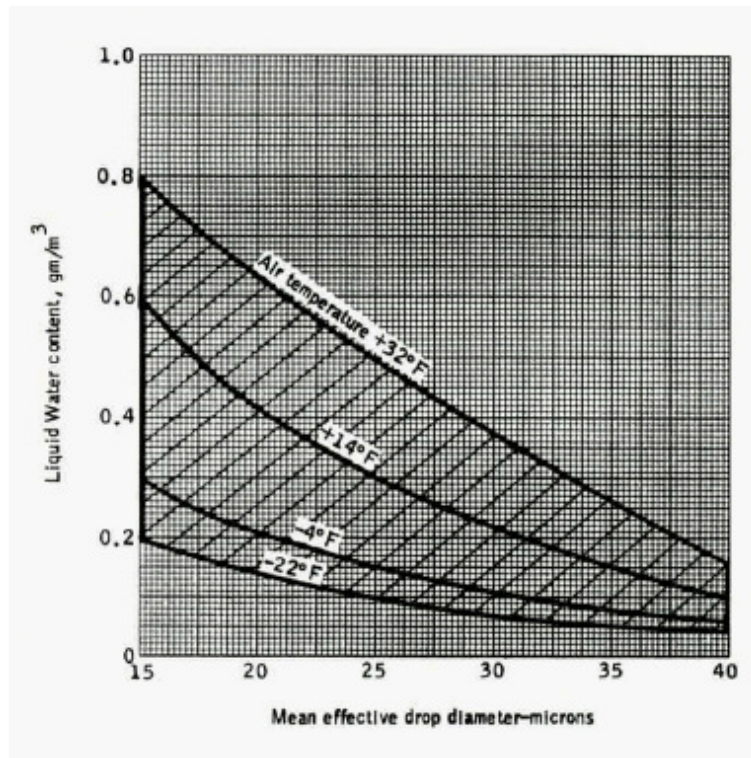


Fig. 5.1: Conventional LWC vs. MVD Envelopes for Stratiform Icing Clouds

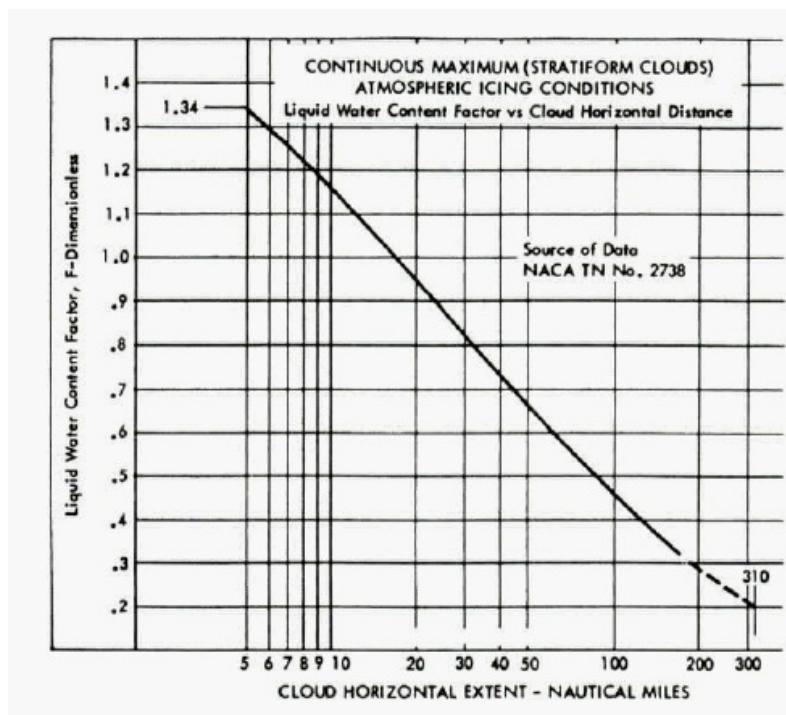


Fig. 5.2: LWC Scale-Adjustment Factor for use with Fig. 5.1

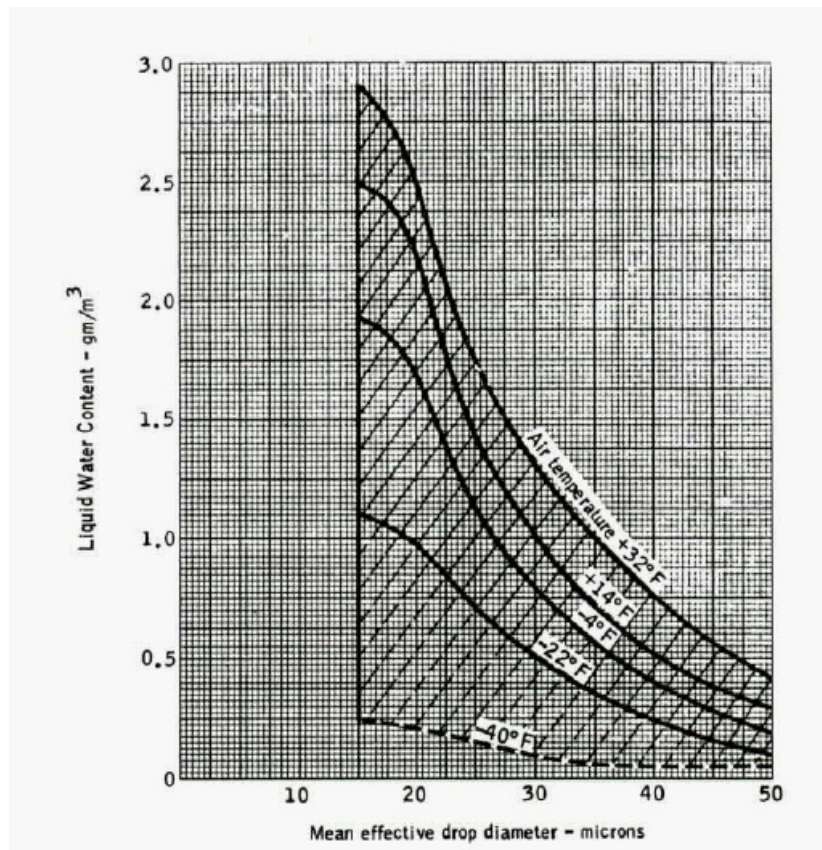


Fig 5.3: Conventional LWC vs. MVD Envelopes for Cumuliform Icing Clouds

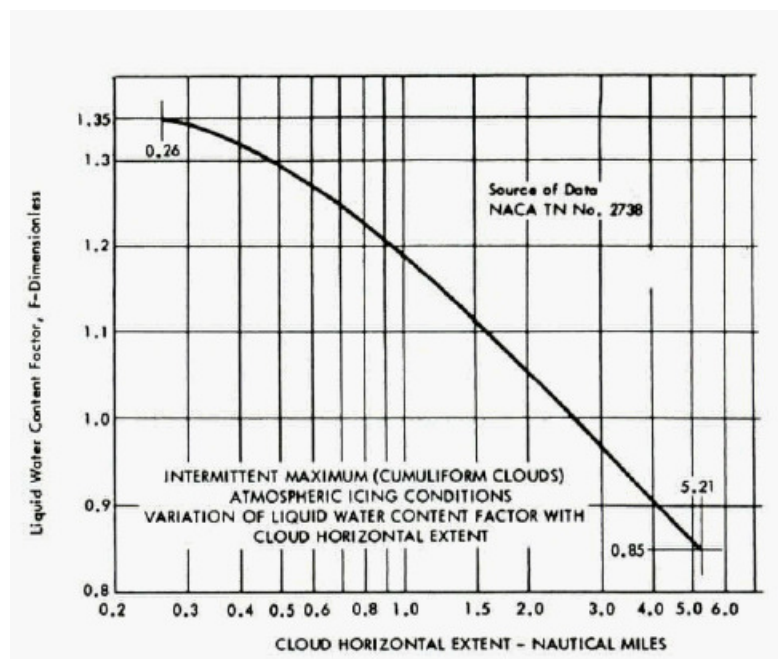


Fig. 5.4: LWC Scale-Adjustment Factor for use with Fig. 5.3

## CHAPTER 6

# ICING SIMULATION TOOLS

### ***6.1 BRIEF OVERVIEW OF THE AVAILABLE TOOLS***

In-flight testing in natural icing conditions is the most realistic means for checking effects of icing on aircraft. However, in-flight testing is costly, potentially hazardous and it is usually difficult to find in nature the specific performance and handling critical atmospheric conditions needed to demonstrate the adequacy of the systems. Even finding a reasonable encounter for a short time period, can require many flight hours. As much as ten percent of the total certification flight program hours are often spent in looking for the proper icing conditions. The elapsed time to certify single engine airplanes and rotorcraft has taken up to 5 years [17]. This perhaps reflects the difficulty that certain types of aircraft, particularly single engine airplanes and rotorcraft, have in finding natural icing conditions. Also, the varying compliance procedures could be a contributing factor in certification efforts. Nevertheless, in-flight testing in real icing conditions is necessary to some extent in order to demonstrate the ice protection system effectiveness and verify the ice forms for simulations using artificial ice shapes. In addition, the degradation of performance and handling characteristics must be checked for natural ice accretion by investigating some reference cases.

However, if the critical ice shapes are determined using ground facilities such as icing tunnels or outdoor spray rigs or prediction codes (those accepted by the authorities), the

degraded performance and handling characteristics can be investigated by flight tests in dry air using artificial ice shapes attached to the aircraft surfaces.

Another approach to in-flight testing is to make use of icing spray tankers which fly in front of the aircraft being tested and produce a cloud of water droplets of appropriate size distribution. The spray droplets will be sufficiently supercooled by the ambient air before impinging on the aircraft if a suitable ambient temperature is chosen by flying at appropriate altitude. But, because the diameter of the spray plume is always rather limited, only components of the test aircraft can be investigated. This limitation is severe for fixed wing aircraft and therefore tanker tests cannot generally become accepted by the certification authorities. However, rotorcraft and some military aircraft have successfully been tested using icing tankers for demonstration of airworthiness.

Because of the limited size capability of ground facilities a full size aircraft can not normally be accommodated and a part, component or model simulation may be necessary. This may not be adequate to show full compliance of an airplane with the design requirements concerning ice accretion. Also, the similarity rules for scaled testing are limited and many cases perhaps are inadequate to simulate conditions for realistic ice accretion.

However, ground facilities are very valuable tools to analyze aircraft full scale components with respect to icing and to generate ice shapes for defining artificial ones being used in dry air tests. Furthermore large size wind tunnel, have been successfully used in certification process and results obtained have been accepted by the certification authorities world wide. However, rather few special existing facilities are really able to generate realistic icing condition and contemporarily are large enough to accommodate full scale aircrafts components.

Experimental ice accretion simulations on the ground cover a wide range of test types. Some intend to simulate natural in-flight icing situations, and others only simulate certain aspects present in the complex ice accretion process. Compromises have to be accepted with respect to the similarity requirements as a possibility to obtain reliable data in repeatable and controlled environments.

To perform tests in prescribed conditions, complex facilities are needed. Usually, they are specifically suited for:

- Fixed-Wing Aircraft
- Rotorcraft and Propellers
- Engines

Of course, for investigating degradation of performance and handling characteristics by applying artificial ice shapes conventional wind tunnels are sufficient.

Last but not least, the area of computational prediction of ice accretion has progressed greatly during recent years and is now an important and quite reliable simulation tool, mostly in 2D. Yet, this topic is no further discussed in the present work.

## ***6.2 DIFFERENT SIMULATION TECHNIQUES***

Experimental simulations of ice accretion are understood to cover a wide range of test types. Some are intended to simulate natural in-flight icing situations, and others only to simulate certain aspects present in the complex ice accretion process. In each case some similarity requirements, as presented in Appendix C, have sometimes and

depending from model dimension, to be met, and compromises must be accepted as the only possibility to obtain reliable data in the repeatable and controlled environments of ground test facilities.

Facility types and their specific characteristics are reviewed in the next section. Once the external flow conditions are defined and depending on the objectives sought, different simulation techniques are employed.

In a case of dry air test, investigating simulated ice shapes, only dry air is needed. The ice shape should be geometrically similar and objectives are either to measure global aerodynamic coefficients or to determine the characteristics of the flow field. Studies of this type include thermal measurements, since the local heat transfer coefficient is one of the most critical values in the determination of the ice accretion process. As is well known, surface roughness is a critical feature in heat transfer evaluation. Since some of the accreted ice surfaces are characterized by large and irregular roughness elements, the measurement of the local heat transfer coefficients becomes a complicated matter.

A second type of simulations uses two-phase flows, made up of water droplets and dry air. These simulations are used to study water droplet trajectories, local impingement distributions, droplet splashing, surface runback water, thermal effects, etc. and include the presence of a liquid film that is deposited on the surface. The temperatures are above the freezing point and the experiments are aimed at understanding the role played by liquid water, and are applicable to glaze ice accretion cases.

The third type of simulations aims at a complete similarity of all existing physical phenomena, maintaining air temperature below freezing values and including clouds of supercooled droplets. In many cases, the interest is only in the shape of the accreted

ice, with its surface details and water phenomena, but there are also experiments undertaken to determine the flow field and the overall aerodynamic characteristics, as the ice accretion progresses with time. For these simulations, in which complete physical similarity is sought, direct measurements of important variables such as surface temperature distribution, droplet splashing, local convective heat transfer coefficients, etc. require specialized instrumentation and measuring techniques in addition to the proper test facility.

### **6.3 GROUND FACILITIES**

As already mentioned, experimental icing simulations are in many instances performed in specially designed ground facilities where icing conditions are to be reproduced. Such tests may be conducted with full-scale prototypes or sub-scale models. These tests are performed in cold airstreams, which contain icing clouds made up of supercooled droplets or ice particles. Three main group of facility can be found according to the kind of testing needs to be reproduced:

1. Icing wind tunnels
2. Engine test cells, specifically designed to simulate the relevant variables in engine icing tests.
3. Low velocity facilities where components or full-scale vehicles may be tested.

### **6.3.1 Icing Wind Tunnels**

These facilities have all the systems and are of similar configuration as conventional dry air wind tunnels, but they incorporate two additional features that make them special and unique.

First, they have a refrigeration system that cools the air to well below freezing temperatures and second, they have a water spray system that injects water droplets into the air stream creating a supercooled cloud. The typical configuration of a closed loop wind tunnel has the spray system located at the end of the settling chamber, before the tunnel contraction while the heat exchanger is in the leg upstream of the corner before the settling chamber. A classical example of an icing tunnel is offered by NASA's Icing Research Tunnel (IRT) shown in figure 6.1.

Test section size usually ranges from intermediate dimensions of about 2m x 2m, to small ones of about 0.15 x 0.15. The velocities usually cover only the low speed range ( $M = 0$  to 0.4), especially for the largest facilities, but there are some small icing tunnels that can reach high subsonic values ( $M = 0.8$ ). As is the case in conventional dry air wind tunnels, flow quality is of utmost importance. In addition to requirements for uniformity of velocity and limits on flow angularity in the test section, temperature and droplet-cloud variables must have spatial uniformity. Also, the spray system must be capable of reproducing a wide range of values for liquid water content, droplet mean volume diameter (MVD) and droplet size spectra, in order to simulate nature. As these facilities include a two-phase flow in the test section, specialized instrumentation is needed to measure the flow variables, in particular for the liquid phase.



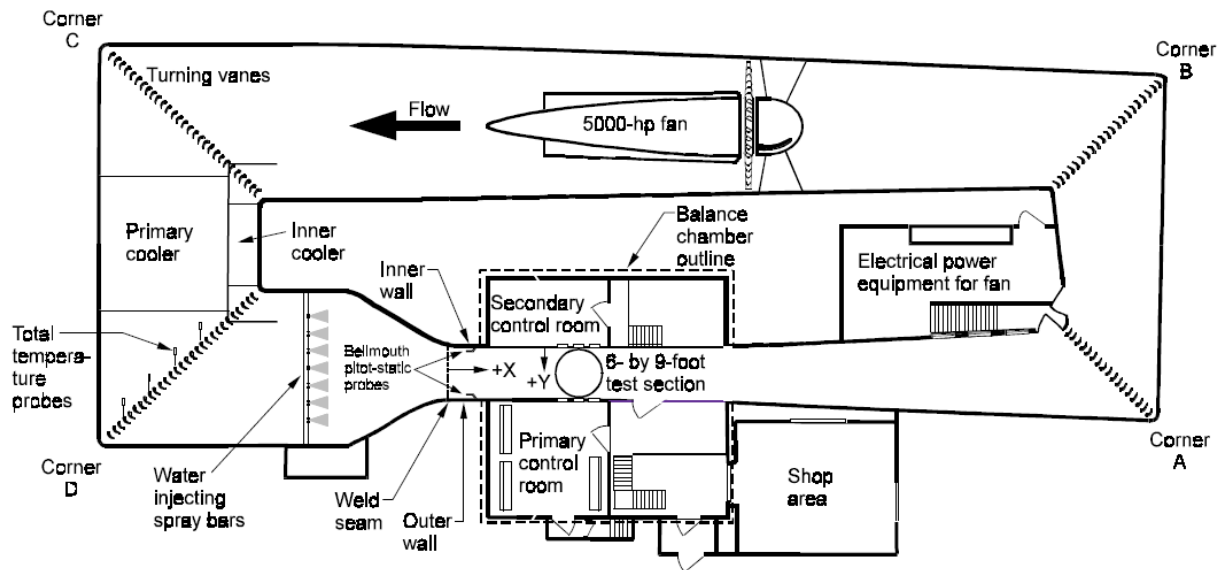
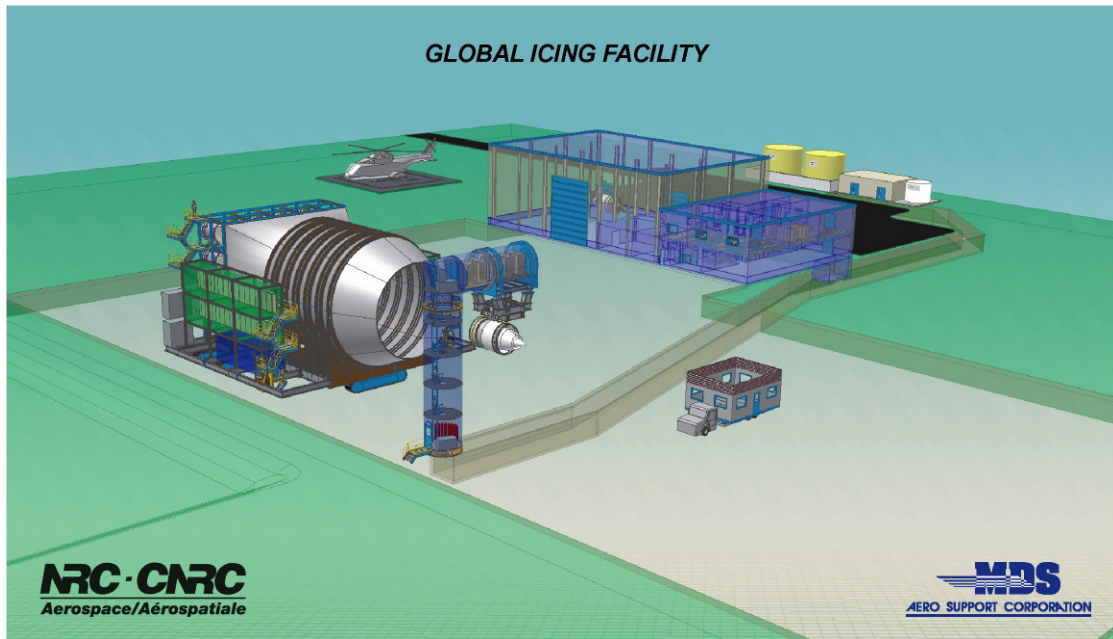


Fig. 6.1: IRT layout

### 6.3.2 Engine Icing Facilities

Engine icing test cells try to simulate, as closely as possible, natural atmospheric icing conditions, and are used to evaluate ice accretion shapes that may form on engine inlets, to measure the effects on the operation and performance of the engine and to evaluate the engine's ice protection system. These test cells are either of the "sea-level conditions" type or altitude test facilities.

The first type is of large dimensions and have, the advantage of enabling simulation of icing in crosswinds and tailwinds. This type of facility is shown schematically in figure 6.2.



**Fig. 6.2:** Engine Icing Facilities

The second type are smaller facilities, but tests can be conducted over a wide range of Mach numbers, pressures, altitude and inlet conditions and the variables defining the icing cloud can be accurately controlled and monitored during the test.

### **6.3.3 Low Velocity Facilities**

There is a group of facilities that are operated at low velocities (0-20 m/s) and generally have large dimensions. They either have refrigerated cold moms or they are operated outdoors in cold climates. The icing cloud is produced by a spray system located in front of the test vehicle, as indicated in figure 6.3. One of these facilities is capable of testing full-size hovering helicopters in a wind-blown icing cloud.

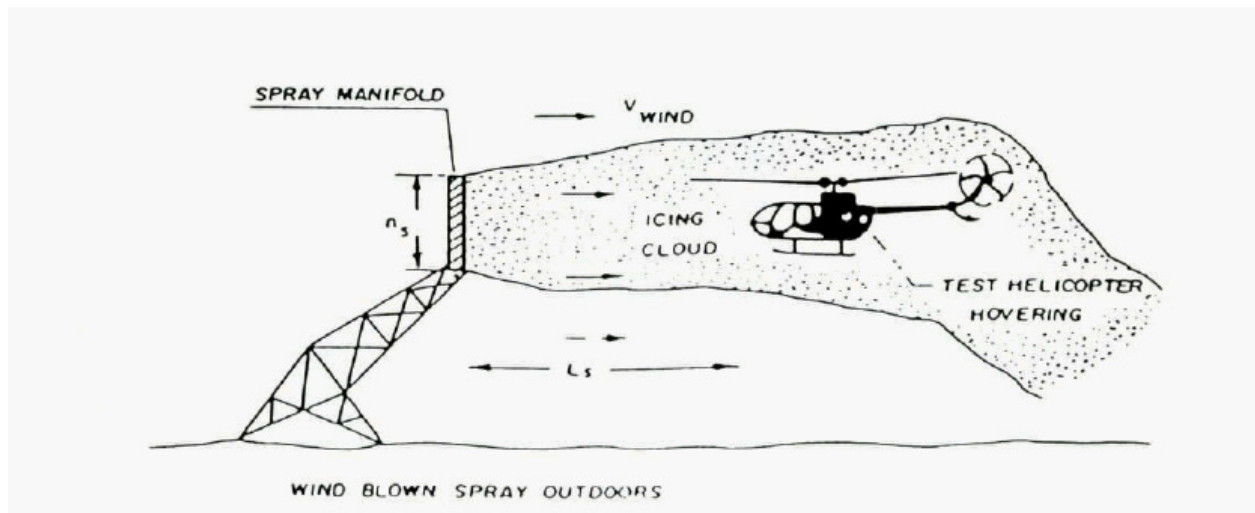


Fig. 6.3: Low Velocity Facility layout

#### 6.4 USE OF ICING SIMULATION TOOLS IN DESIGN AND CERTIFICATION

Icing simulation methods are used in both the design and certification of large commercial jet transports. These methods are part of the design and validation process which proves that

- ice protection system performs as intended;
- effects of ice accretion with a normally operating ice protection system are as predicted;
- ID systems are working properly.

The designs of thermal ice protection systems use both icing wind tunnels and computer codes. For large commercial jet transports, portions of the wing leading edge, the nacelle leading edge, and in some cases, the horizontal tail leading edge are protected with thermal systems. Icing wind tunnels and analyses with computer codes are used to design these ice protection systems. The design of these thermal systems

requires analyses of the total system's ability to provide heat energy to protect the above mentioned leading edges in the applicant's design standard typically the continuous maximum and intermittent maximum icing conditions of Federal Regulations Part 25, Appendix C. The computer codes and analyses determine heat energy required for the protected surfaces at the worst case condition of the flight and the design standard envelope. The icing tunnel tests are used to evaluate components of the design, and are valuable tools expediting redesign if the initial ice protection performance is not adequate. With respect to certification, icing simulation codes are used to define the critical ice shapes and the heat energy requirements for the protected surfaces. The simulation codes and analyses determine the critical ice shapes as a function of the flight conditions (e.g., airplane configuration, speed, angle of attack, attitude, and exposure time) and the icing conditions of Appendix C (temperature, liquid water content, and median volume diameter).

The critical ice shapes are modeled on wind tunnel models and the flight test airplane to evaluate the change in aerodynamic performance and handling characteristics. The analyses of the results of dry air wind tunnel testing of these models with artificial ice shapes are used to substantiate the predicted performance and handling characteristics. Flight testing with artificial ice shapes provides further validation of these predicted airplane performance and handling characteristics. Icing simulation methods, icing wind tunnels, and codes are used to analyze the performance of the ice protection system and to determine that the protection for the various components of the airplane is adequate for the various operational conditions within Part 25, Appendix C icing conditions. In most cases, to verify this ice protection analysis, to check for anomalies, and to demonstrate that the ice protection system and its components perform as

intended, the airplane and its components are flight tested in various operational configurations in measured natural atmospheric icing conditions.

#### **6.4.1 Current Simulation Capabilities**

Icing wind tunnels provide a controlled and repeatable icing environment for the generation of ice shapes on airfoils, wings, bodies, propulsion systems, and other components. These facilities are used to simulate Part 25, Appendix C and some “estimated” supercooled large droplet (SLD) icing conditions. In most cases, the flight operational conditions are simulations of true flight situations. Ram air turbines, air intakes, antennas, radomes, and air data sensors are evaluated for their ice accretion characteristics. Two-dimensional airfoils or truncated models are used to provide the largest possible scale, which results in only a “section cut” simulating a portion of a wing or empennage; this is done to maximize the droplet size to icing surface scale ratio, which is a powerful variable. For the evaluation of ice protections systems, wing leading edge systems are simulated on scaled or truncated airfoils, whereas for nacelle inlets, very large scale models of the nacelle leading edge ice protection systems are tested in these tunnels.

Most icing wind tunnels are atmospheric, low speed facilities with maximum velocities ranging from about 70 to 180 m/s and a temperature range of  $-35^{\circ}\text{C}$  to  $0^{\circ}\text{C}$  [17]. The water content of the air can be varied from about 0.2 to  $3.0\text{ g/m}^3$ , and with droplet size variation of 15 to  $40\text{ }\mu\text{m}$ . Data correction values are generated by calibrating each installation i.e. each test section (which is standard wind tunnel practice).

As an example, the Boeing Research Aerodynamics and Icing Tunnel (BRAIT see figure 6.4) is usually calibrated in two phases [17]. The first phase concentrates on the determination of the basic flow qualities of the clear tunnel in the dry mode without water injection. The second phase determined the calibration of the icing conditions.

The calibration is made at the center plane of the test section, and the following flow parameters are determined:

- centerline static pressure correction,
- velocity uniformity,
- turbulence intensity distribution,
- temperature uniformity,
- clear tunnel up flow and cross flow, and
- wall boundary layer thickness.

The second phase icing condition calibration is conducted by cooling the air to  $-17^{\circ}\text{C}$  and injecting water droplets into the air-stream via the spray bar system to simulate natural icing conditions encountered during flight. The calibration determines the following:

- individual nozzle calibrations,
- droplet size calibration,
- cloud uniformity, and
- liquid water content.

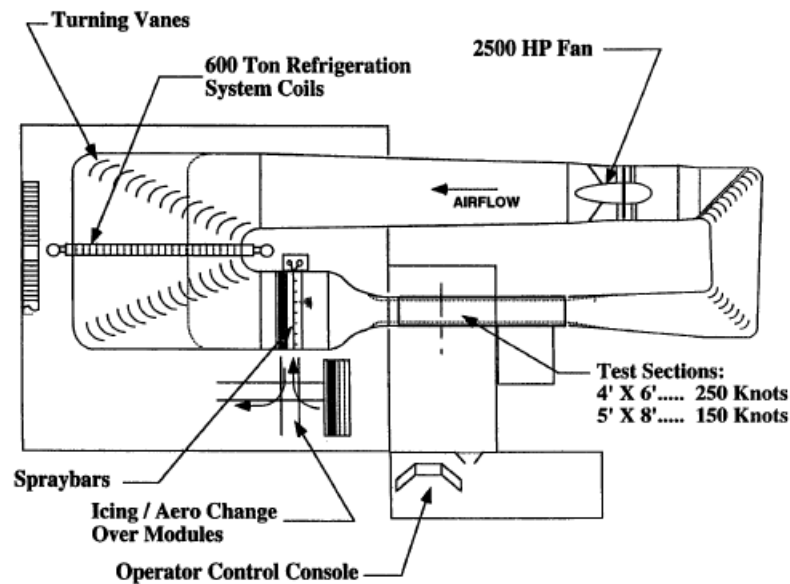


Fig 6.4: Boeing BRAIT tunnel layout.

#### **6.4.2 Limitation Of Current Simulation Methods**

The one major limitation of current simulation methods is the lack of standards or criteria to judge the acceptability of ice accretion simulation methods. This is true for simulation codes, wind tunnels, tankers, and environmental test chambers. Icing wind tunnels should be deeply calibrated according to the steps discussed in the previous section and described in [19]. The one possible missing test section characteristic is the turbulence level of the flow with the water spray on. In the past, the instrumentation and methods to measure the turbulence levels with water droplets were not available; however, very recent research has demonstrated the ability to measure this characteristic. The icing research community has not yet determined the importance of

the measurement of test section turbulence levels. Because of the presence of the water droplet spray system as well as the heat exchanger necessary to bring the air stream temperature down to levels conducive to icing, the turbulence levels in these icing simulations are generally higher (sometimes by an order of magnitude) than aerodynamic wind tunnels. Currently there is no detailed knowledge of prevailing turbulence intensities in natural icing clouds, so the proper simulation of the icing environment is in question. This issue does not appear to pose a major limitation on simulating a natural environment for simple geometries, where ice accretion is primarily a leading edge event. For complex geometries, such as multi element airfoils where ice accretion has been observed on the downstream elements as well as on the slat, the accuracy of these accretions comes into question.

Another issue that hampers the understanding of the icing wind tunnel results is the droplet scaling. Exact duplication of an aircraft in natural icing conditions cannot be always accomplished due to the various icing tunnel limitations. Typically, flight velocities are higher than the maximum tunnel velocity capability; the tunnel has a limited range of cloud liquid water content capability that does not extend as low as flight conditions; and icing tunnels are atmospheric facilities which are limited to near-sea-level pressure conditions. (This is an important factor in evaporation rates and simulating high altitude conditions.) This combination is a particularly unfortunate limitation when simulating high speed, low liquid water, high altitude cloud conditions.

To compensate for these limitations, various thermodynamic scaling and similarity laws have been developed. The methods use thermodynamic equations to determine how to vary tunnel parameters to maximize the similarity between flight and tunnel test conditions. As in aerodynamic wind tunnel testing, it is not possible to match all



parameters, and judgment is used to determine which parameters are most important. The tunnel parameters that can be set to obtain similitude with flight in icing conditions include:

1. tunnel cloud liquid water content,
2. tunnel temperature,
3. tunnel velocity,
4. tunnel cloud median volume diameter (MVD),
5. model surface temperature,
6. tunnel run time, and
7. wind tunnel model and scale.

Apart from CIRA IWT, tunnel pressure is not a parameter that can be usually controlled with the current icing tunnels, and is assumed to be fixed at the local ambient atmospheric pressure.

There have been many scaling methods developed to address this problem of testing methods in facilities with limitations in either model size or test conditions. These methods have all been based on a physical description of the ice accretion process with various assumptions and simplifications. The usual approach in developing a scaling method is to write expressions for the water droplet collection efficiency, total ice accretion on the surface, and an energy balance at the stagnation line of the airfoil. The scale and reference values of these expressions are equated to solve for the scale test conditions. Also, truncated/hybrid airfoils with full-size leading edges are used to allow

the matching of droplet trajectory and surface impingement characteristics. This is important due to the limited ability to scale droplet MVD. There are concerns that the droplet flow field in the icing wind tunnel is not being simulated adequately. The evidence for this has come from observations of ice accretion on flap lower surfaces in the icing wind tunnel. Observations from flight testing have been contradictory and have led some icing engineers to question other factors, such as the vertical velocity of droplets not being simulated properly in the icing wind tunnel.

Apart from CIRA IWT, there are no others readily available pressurized icing wind tunnels to simulate altitude effects and high-pressure icing facilities to simulate Reynolds number effects, and whether these effects play a significant part in the ice accretion process has not been yet established. Three-dimensional (3D) effects do have a significant effect on the ice accretion process however, icing wind tunnel test sections are generally too small to test complete airplane configurations.

Finally, since the droplet size in the icing process is difficult to scale down, large models are generally desired.

## CHAPTER 7

### CIRA – ICING WIND TUNNEL

#### **7.1 IWT OVERVIEW**

Officially inaugurated in September 2002, the CIRA Icing Wind Tunnel (figure 7.1) broke a number of world's records. Among these, the following ones can be reminded:

- is the largest refrigerated wind tunnel in service;
- is the highest speed icing wind tunnel ( $M=0.7$ );
- is the only facility combining altitude, humidity and temperature simulation;
- has the largest number of different test configurations (4);
- has the largest numbers of spray bar nozzles position (1000) and bars (20);
- has the widest operating range for engine flow simulation (1.5-55 kg/s mass flow).



**Fig. 7.1:** Icing Wind Tunnel

Located in the stilling chamber, the Spray Bar System (SBS) is dedicated to the generation of the icing cloud in all the conditions as prescribed in the current FAR/JAR regulations. Looking at future revisions of the airworthiness regulations, the SBS is also capable to generate Supercooled Large Droplets (SLD) within the range of freezing drizzle conditions.

Thanks to the capability of a fully remote control of the test, it is also possible a fast switching from “Max continuous” cloud conditions to “Max intermittent” cloud conditions. Other advanced systems ensure the best simulation of possible natural icing conditions, e.g. a twin row heat exchanger for temperature simulation down to  $-40^{\circ}\text{C}$ , a depressurization system for altitude simulation up to 7,000 meters (about 23,000 feet) and humidity control down to 70% RH.

The CIRA IWT is equipped with four different test section configurations in order to satisfy all the test requirements in terms of speed, model size, cloud coverage and

uniformity. Slotted walls of the test sections allows high blockage testing capabilities and extended run-time (more than 180 minutes).

The Additional Test Section (ATS) and the Main Test Section are large enough to allow the installation of scaled model (figure 7.2), or full-size airframe components, such as wing sections, tail sections and nacelles. In most cases, the test section sizes allow the use of a full scale model or even a preproduction mock-up.



**Fig. 7.2:** Scaled model installed into the ATS

Full-scale airplane (figure 7.3) and helicopter air intake mock-up have been already successfully tested in the Main Test Section, while the high speed achievable in the Secondary Test Section (STS) makes this configuration particularly suitable for helicopter blades testing (figure 7.4).



**Fig. 7.3:** Full-scale aircraft air-intake icing tests

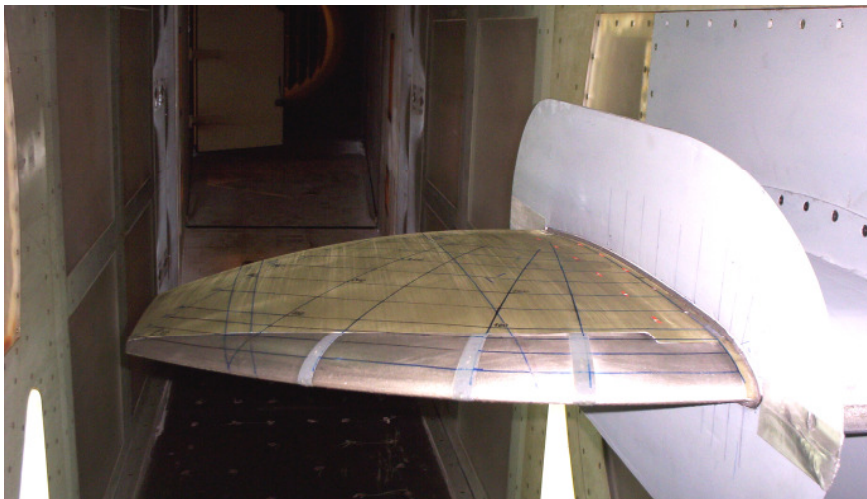


**Fig. 7.4:** Full-scale helicopter blade icing tests

Furthermore, the CIRA IWT can perform qualification and compliance tests for a variety of anti-ice and de-ice systems, including boots, hot bleed air and thermal resistance systems. Thanks to a dedicated engine flow simulation system, it is also possible to perform airplane/helicopter air intake icing qualification tests in a wide operating range.

Ice accretion tests, including the study of performance degradation effect on 2D, and 3D models are also possible, as well as qualification tests on a wide variety of instrumentation, such as ice detectors and probes.

As a further capability, CIRA IWT is able to perform high flow quality aerodynamic tests in both low and high subsonic range, at Reynolds number comparable to much larger facilities, by exploiting its low temperature operating range and pressurization capability up to 1.45 bars.

Pressure and force measurements on 2D, and 3D models, as well as Laser diagnostic measurements (PIV, LDV) can be performed in both aerodynamic and icing configuration.

## ***7.2 WIND TUNNEL GENERAL DESCRIPTION***

The IWT facility is a closed loop circuit, refrigerated wind tunnel, with three interchangeable test sections and one Open Jet configuration. A schematic of the IWT is shown in figure 7.5.

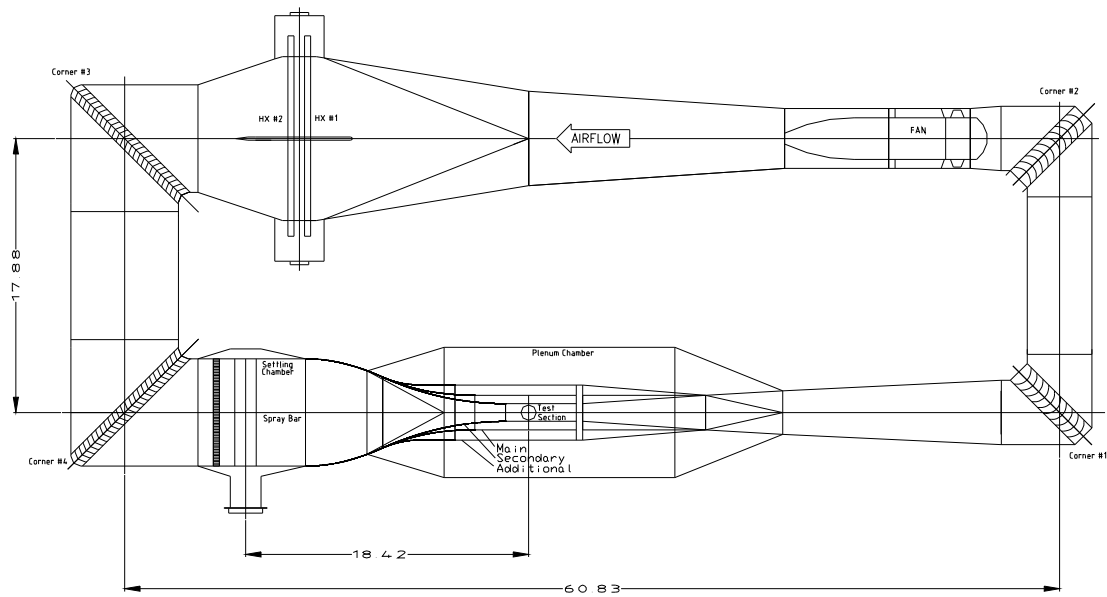


**Fig. 7.5:** Icing Wind Tunnel layout

As many conventional wind tunnels, the IWT is fan driven. The fan and the fan drive are located downstream corner 2, in the back leg. Downstream the fan diffuser, a twin row heat-exchanger is located to provide low temperature operation capability. The facility settling chamber is fitted with a honeycomb module to reduce large scale eddies thus ensuring flow straightening. Downstream the honeycomb, an interchangeable section provides the possibility to install either:

- a spray bar module generating the cloud for icing tests or
- a screen module when lower turbulence airflow is necessary for high quality aerodynamic tests.



The distance between the SBS and the model location is 18 meters. Downstream the fixed contraction, the test section leg is made up of two interchangeable components (movable contraction + test section) and a variable geometry collector diffuser.

### **7.2.1 Cooling Systems**

The function of the Cooling System is to remove the heat generated by the different heat sources and to keep constant temperature values. Air flow refrigeration is obtained via a twin row Heat Exchangers located in the back leg, upstream the third corner, and back stream the main fan.

The cooling plant is made up of 4 compressor units (1700 kW motor power each), a single evaporator and a single condenser unit, the twin row heat exchanger, connecting pipes and specific auxiliaries (e.g. pumps and valves). Compressors, evaporator and condenser units are located in a separate building just facing the heat exchanger section.

The used cooling media are the environmental compliant R507 and the Therminol Oil “brine”.

The minimum achievable temperature is  $-32^{\circ}\text{C}$  in the Main Test Section and in the Additional Test Section, whereas the Secondary Test Section can reach down to  $-40^{\circ}\text{C}$ .

Temperature is controlled via the Facility Management System, and the accuracy on the set-point is about  $\pm 0.1^{\circ}\text{C}$ . Temperature descent rate is up to  $1^{\circ}\text{C}/\text{min}$ . The Heat Exchanger is also capable to control the air Relative Humidity (RH) before the spray bar, by means of a hot air compressor and steam injection. Controlled humidity ranges

between 70% and 100% for temperatures between  $-15^{\circ}\text{C}$  and  $-20^{\circ}\text{C}$ . 100% humidity value can be set between  $-20^{\circ}\text{C}$  and  $-40^{\circ}\text{C}$ . Control accuracy is within  $\pm 5\%$  RH.

Finally, by circulation of hot brine in the same heat exchanger, the cooling system is capable to de-ice the heat exchanger itself after an icing test and to make available the “Tunnel De-icing” operation mode.

### **7.2.2 Air Plant**

An air plant is fully dedicated to the IWT in order to provide facility operation support.

A 0.7 MW centrifugal compressor unit allows the pressure to be regulated between 0.39 bars (corresponding to an altitude of 7000 meters) and 1.45 bars. Safety valves allow a fast tunnel evacuation and pressurization.

Altitude is controlled through pressure, velocity and temperature control. Accuracy on altitude set-point is about 10 meters.

Controlled depressurization ramp from sea level for altitude simulation is 200 m/min, whereas altitude descent up to sea level can be performed at a rate of 150 m/min in controlled mode or 400 m/min in “fast evaporation” mode.

A 1.2 MW axial compressor unit supplies the SBS.

Hot air and pneumatic boot de-icing systems are supplied by the hot air de-icing compressor (0.4 MW power).

A dedicated compressor supplies the pneumatic boot impulse de-icing system.

Finally, instrument air is provided by a screw compressor, at a nominal pressure of 7.5 bars. Instrument air is available at several positions in the building, the parking hall and inside the plenum chamber.

### **7.2.3 Fan System**

The facility is driven at the desired airspeed by a 24 blades, variable blade pitch angle 3.9 meters.

The wind tunnel speed is automatically controlled via the Facility Management System (FMS). Fan motor speed is electronically controlled by an inverter, up to a maximum fan rpm of 750.

Accuracy on Mach target is 0.1% in the range between  $0.6V_{\max} \leq V \leq V_{\max}$  and 0.2% in the range  $0.2V_{\max} \leq V \leq 0.6V_{\max}$ .

The fan is located in the return circuit. The fan motor is located inside the fan nacelle. The motor is cooled through a dedicated air cooling system.

Upstream the fan, a grid avoids that major ice blocks could impinge on the blades.

The fan power is 4 MW, however, a 35% power margin is available to compensate pressure losses increase due to ice build up inside the wind tunnel.

Variable blade pitch angle allows an optimal setting for different aerodynamic load conditions. Fan blades have provisions for heating system.

#### **7.2.4 Spray Bar System**

The IWT Spray Bar System is able to generate water droplets with diameters (MVD) and Liquid Water Content (LWC) covering the overall envelope prescribed by the FAR 25/29 Appendix C for both continuous and intermittent cloud conditions. Furthermore, the system is capable to generate Super-Cooled Large droplets (SLD), within the range of freezing drizzle conditions. The SBS is located in the IWT stilling chamber (figure 7.6), about 18 meters upstream the centre of test section, thus assuring a droplet residence time long enough to achieve super-cooling conditions even for large droplet sizes.



**Fig. 7.6:** SBS installed in the wind tunnel

Upstream the SBS section, a honeycomb section assures straight flow conditions at the cloud generation section. The SBS has 20 bars having a low drag aerodynamic shaped section, whose main feature is a low sensitivity to flow separation. Each bar is removable and may be vertically adjusted for optimizing cloud coverage and uniformity, if necessary, during the calibration phase. Each bar is equipped with 50 spraying nozzle

positions, for a maximum total of 1000 possible spraying positions over 20 bars. Normally, the system is equipped with 500 active spraying nozzles, whereas the remaining 500 nozzle positions are plugged (figure 7.7).

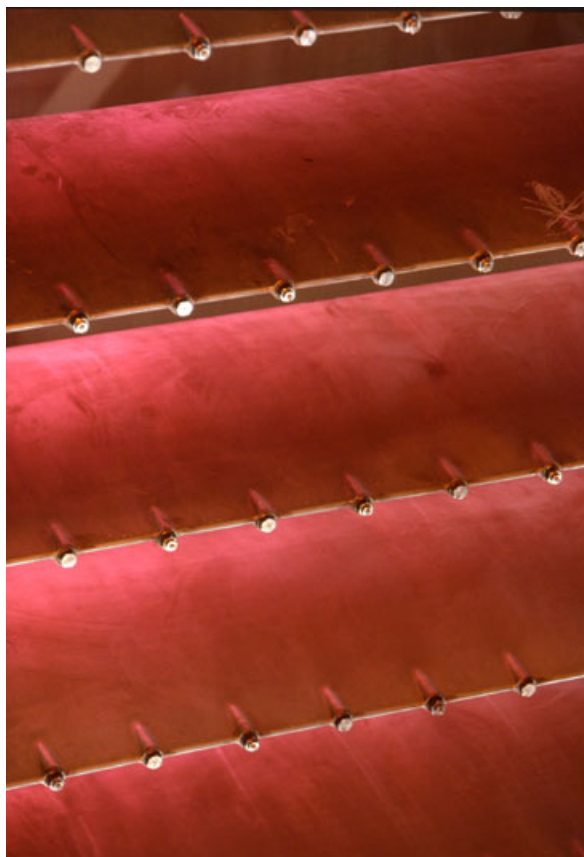


**Fig. 7.7:** SBS bars detail

Each nozzle water supply line is equipped with a solenoid valve that can be remotely switched on and off.

The number of operating nozzles may be changed during a run by using the Facility Management System Software.

The SBS is equipped with nozzle holders which may easily allow the installation of NASA STD nozzles. However, the SBS configuration with NASA STD nozzle is not considered as a standard installation in the CIRA IWT. The SBS is fed by:

- pressurized, dematerialized and conductivity-controlled water. The temperature  $T_{\text{water}}$  can be controlled up to 100 °C whereas the supply pressure can be set between  $0.01 < p_w < 10$  bar (abs);
- dry compressed hot air at temperature  $T_{\text{air}}$  controlled up to 150 °C, dew point –40 °C. The air pressure can be set between  $0.01 < p_{\text{air}} < 11.5$  bar (abs).

All the parts of the Spray Bar System in contact with pressurized air and dematerialized water (e.g. pipes, boxes, and SBS airfoil), are made of stainless steel.

A closed loop control system managed by the Facility Management System allows both keeping constant SBS air and water supply pressures and temperatures (and, as a consequence, MVD and LWC values), and fast switching from Maximum Continuous to Intermittent Continuous conditions (figure 7.8).

Finally, once started the spraying, set point conditions can be reached within few seconds.

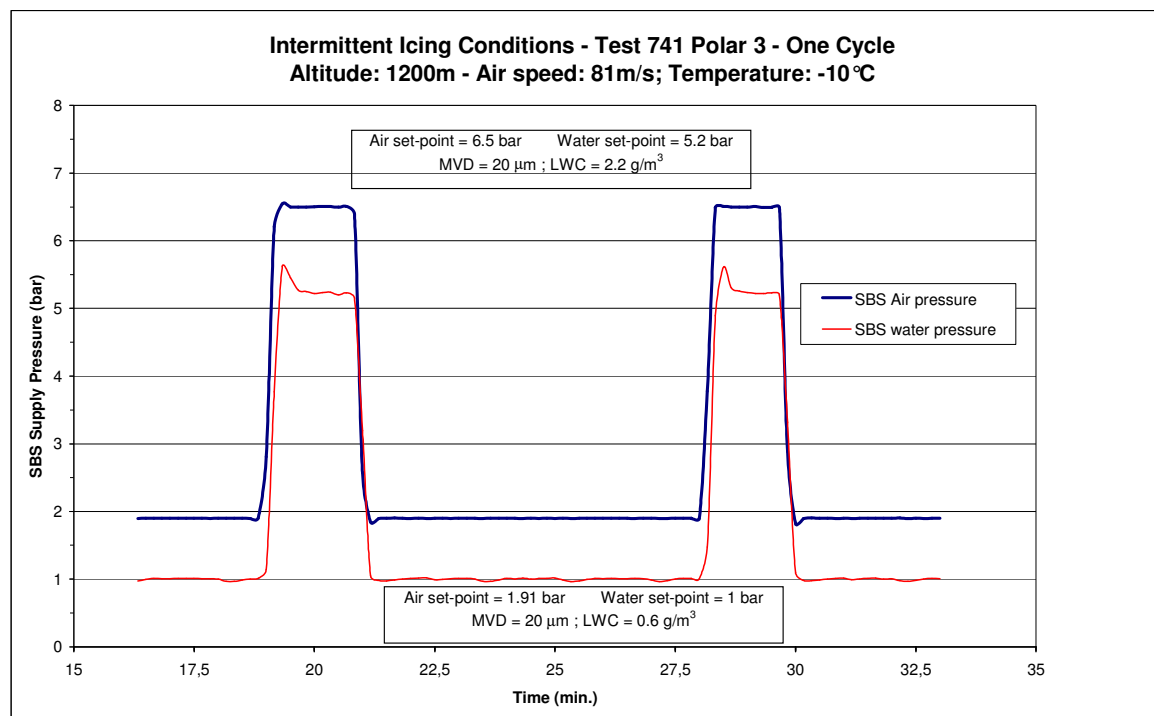


**Fig. 7.8:** SBS intermittent pressure conditions

### 7.2.5 Test Sections

As already stated CIRA IWT can be equipped with four different configurations. Each test section has synchronized turntables. The three test sections have 7% porosity slotted walls in order to allow larger than usual blockage models. Each slot has its own anti-icing system to protect its lips from ice build up and clogging. Slotted wall test sections have 80% optical access to the test model. The fourth configuration is an open-jet test section.

Every test section configuration requires a specific contraction module, whereas the collector diffuser downstream is the same one for all test section configurations, since its two-hinge angles are adjustable to fit the specific test section size.

Contraction ratio is 6:1 for the ATS, 10:1 for the MTS and 20:1 for the STS respectively.

Figure 7.9 shows the Main Test Section. A detail of the Secondary Test Section wall slot configuration is shown in figure 7.10 whereas figure 7.11 shows the ATS.

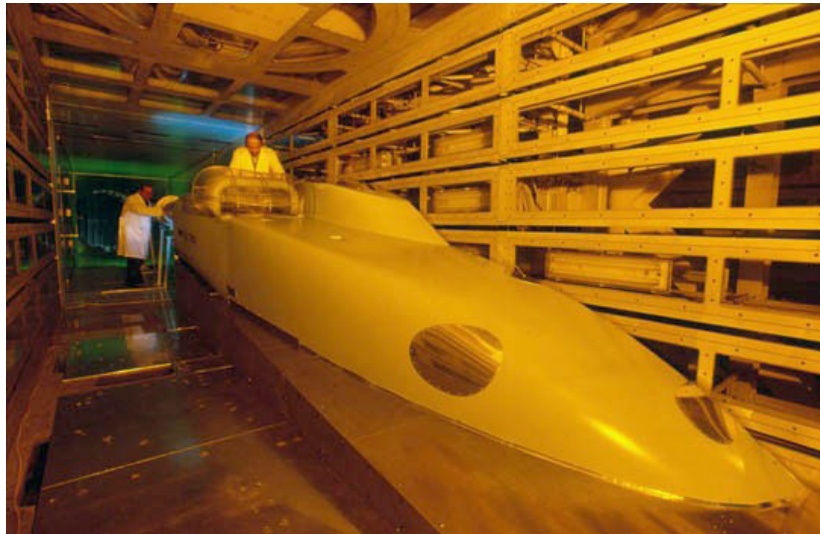


**Fig. 7.9:** Full-scale helicopter air-intake installation in the MTS



**Fig. 7.10:** Secondary Test Section





**Fig. 7.11:** Test Section in the rigging area

Tab. 7.1 shows the test sections' main features. Maximum achievable temperature, in any configuration, is +40 °C.

	Main	Secondary	Additional	Open Jet
Height (m)	2.35	2.35	2.35	2.35
Width (m)	2.25	1.15	3.60	2.25
Length (m)	7.00	5.00	8.30	7.00
Mach	0.41	0.70	0.25	< 0.4
Temp (°C)	−32°	−40°	−32°	−32°

**Table 7.1:** Test sections characteristics

Mach number indicated in the table is nominally to be intended as the maximum achievable in free stream conditions (empty test section). Nevertheless, it must be

considered that the maximum achievable Mach number strongly depends on the model blockage, the run-time and the icing conditions to be reproduced.

### **7.2.6 Engine Flow Simulator**

The Engine Flow Simulator (EFS) system can reproduce the air intake flow inside an engine nacelle. Two high pressure fans are used to extract the flow through an engine nacelle installed in the test section. The sucked air flow is re-injected back into the Wind Tunnel circuit, in the first cross leg. Maximum re-injection speed in the Wind tunnel is of about 100 m/sec.



**Fig. 7.12:** EFS Housing

A flange connection between the test article and the EFS piping is located on the floor of the wind tunnel, in the diffuser region. Several piping is available for model-to-flange connection.

Both fans (figure 7.12) can operate within the full wind tunnel temperature and pressure ranges. Nominal mass flow ranges at sea level altitude for the two EFS systems, at the floor connection flange, are:

- EFS#1: 15 to 55 kg/sec
- EFS#2: 1 to 18 kg/sec

The air mass flow is accurately metered by a twin calibrated Venturi system in order to ensure the required accuracy within the whole mass flow range. A maximum error of 1% order is thus ensured in the mass flow range between 1 and 55 kg/s.

## ***7.3 TEST EQUIPMENT***

### ***7.3.1 Turn Tables***

The function of the turntable is to allow different model installation in the different test sections. Each assembly is made-up of a square frame which includes a 2 meters diameter rotating platform (see figure 7.13).

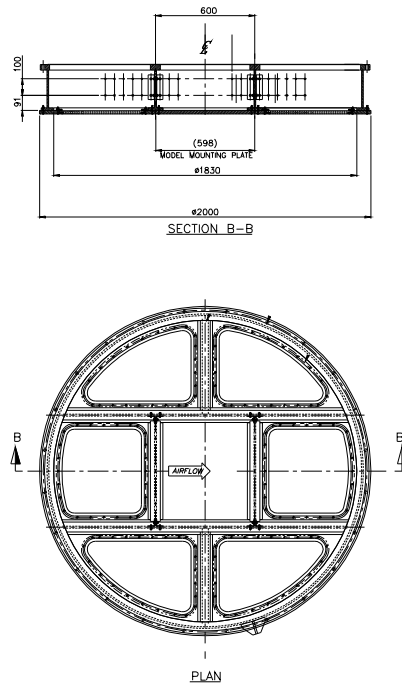


**Fig. 7.13:** Turntable assembly

Different installations are possible in the different test sections:

- the Main Test Section allows a vertical model mounting having the turntables on the floor and on the ceiling;
- the Secondary Test Section allows an horizontal model mounting having the turntables on each side-wall;
- the Additional Test Section allows a horizontal model mounting having turntables on each side-wall;
- the Open Jet configuration allows a vertical model mounting. This configuration has the turntables mounted on the plenum shell.

The turntables can be rotated within a rotation angle range from  $-100^\circ$  to  $+250^\circ$  degrees, in a synchronous mode.

The model mounting plate can be adapted for IWT user model interface or changed with a user customized interface. Maximum allowed live loads on the turntables are:

$$F_x = 14.7 \text{ kN}, \quad M_x = 21.8 \text{ kNm}$$

$$F_y = 4.9 \text{ kN}, \quad M_y = 14.1 \text{ kNm}$$

$$F_z = 86 \text{ kN}, \quad M_z = 2.25 \text{ kNm}$$

Orientation is referenced to global test section co-ordinates: x for stream-wise axis, y for lateral axis, z for vertical axis.

### ***7.3.2 Model Sting Support***

The Model Sting Support (MSS) is an arc sector type, with reference point at the test section centre. It has been designed in order to support the model weight and the aerodynamic loads generated by model aircraft, with the minimum possible flow interference (see figure 7.14).



**Fig. 7.14:** Model Support System

The MSS can be used in the MTS and in the ATS within a temperature range of  $-32^{\circ}\text{C}$  ,  $+40^{\circ}\text{C}$ , even during icing tests.

The allowable load ranges are the same as the ones of the external balances. The maximum allowable weight of the model shall be 3KN. The MSS rotations are controlled in a remote way, except for roll angle. Motion ranges, at the model center, are the following:

- Pitch angle ( $\alpha$ ):  $\Delta\alpha = -15^{\circ}, +45^{\circ}$  deg. using straight sting and  $-15^{\circ}, +90^{\circ}$  using bent sting ( $\pm 0.02^{\circ}$  accuracy);
- Yaw angle ( $\beta$ ):  $\Delta\beta = -170^{\circ}, +180^{\circ}$  deg. ( $\pm 0.04^{\circ}$  accuracy);
- Roll angle ( $\gamma$ ):  $\Delta\gamma = 0^{\circ}, 360^{\circ}$  (only manual mode).

The maximum rotation speed is 2°/min. Natural frequency is 7 Hertz. The system allows the installation of cabling from model instrumentation and other equipment needed for powered models testing.

### **7.3.3 Probe Traversing System**

The Probe Traversing System (PTS) allows three dimensional movements along x, y and z axis. It can be used either in the MTS, the STS and the ATS.

A wide variety of probes can be fitted at the PTS far end. The PTS is able to cover about the 90% of the test section height and width and can be used during icing tests too.

Longitudinal positioning along stream direction (X axis) can be achieved by installing boom extensions (spool sections). A fine positioning is achieved by means of remote telescopic extension up to a 400 mm longitudinal traversing.

Y and Z traversing are achieved in a remote way. Positioning accuracy in all the directions is lower than 0.2 mm.

Maximum carrying weight of PTS is 30 Kg.

The frame hosting the PTS is installed at the very end of the test sections. A dummy frame is fitted downstream the test section when the PTS is not installed.

### **7.3.4 External Balance System**

The IWT is equipped with a high accuracy virtual pyramidal type External Balance System (EBS), allowing both step pause and sweep mode motions with positioning accuracy of 0.005 deg. The EBS can be used both in the MTS and in the ATS, with the wind tunnel operating in aerodynamic mode (water off).

The EBS is capable to operate at low temperatures, down to  $-32^{\circ}\text{C}$ , for high Reynolds measurements, since it is thermally insulated and temperature controlled.

When using the external balance, the test section floor used for icing tests is replaced by another floor having a turntable (figure 7.15). This turntable is slaved to the balance rotation system. The system allows the passage of cabling from model instrumentation and other equipment needed for powered model testing.

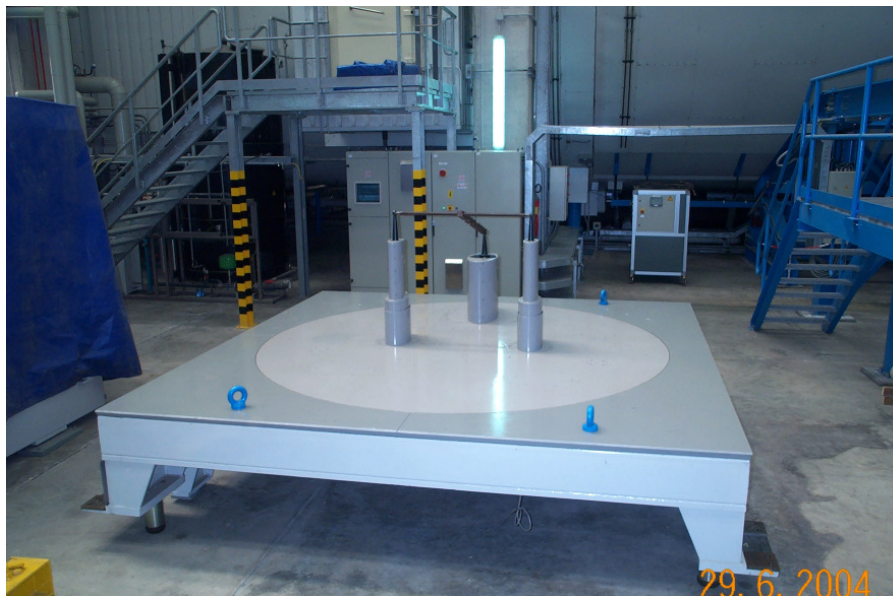


**Fig. 7.15:** Floor turntable with three pylons model Mounting

Two types of supporting frames are available:

1. three pylons model mounting;
2. half model mounting.

The first mounting assembly allows maximum model weights of 300 Kg.



It also includes a telescopic strut system which has an adjustable height in the range:

$$Z = 500 \text{ , } 1350 \text{ mm, } Dz = 5 \text{ mm}$$

Three fixation points, between the two main pylons (side) and between the front and rear struts, allow the installation of models with different size.

Model positioning ranges and accuracy (wind-off conditions) are:

Pitch angle ( $\alpha$ )	$-30^\circ \div +45^\circ$
Yaw angle ( $\beta$ )	$-170^\circ \div +180^\circ$
Accuracy ( $\alpha$ and $\beta$ )	$0.005^\circ$
Step	$0.05^\circ$
Speed	$0.1\%/s \div 2\%/s$

The maximum allowable loads of the external balance system are:

- Three pylon model mounting:

$$Z = 8150 \text{ N, } My = 1600 \text{ Nm;}$$

$$X = 2900 \text{ N, } Mx = 1200 \text{ Nm;}$$

$$Y = 1650 \text{ N, } Mz = 1550 \text{ Nm.}$$

- Half wing model:

$$Z = 11644 \text{ N, } My = 3296 \text{ Nm;}$$

$X = 2825 \text{ N}, M_x = 9810 \text{ Nm};$

$Y = 0 \text{ N}, M_z = 2158 \text{ Nm}.$

The balance accuracies are the following:

- Drag (X): 0.05% FS
- Lift (Y): 0.1% FS
- Side Force (Z): 0.1% FS
- $M_x$ : 0.2% FS
- $M_y$ : 0.1% FS
- $M_z$ : 0.05% FS

#### **7.4 ICING INSTRUMENTATION**

An important role in the calibration of simulated icing cloud conditions has been assumed by the instrumentation. An assessment of the existing microphysics instrumentation and its upgrade is continuously performed at CIRA for a best reproduction of the atmospheric super-cooling cloud characteristics in CIRA IWT.

Used measurement techniques as well as other available instrumentation are described in the following sections.

### **7.4.1 Droplet Sizing Measurement Methods**

In CIRA IWT, the phase Doppler method has been selected for size and velocity atomized water droplets characterization.

Measurement principle relies on light scattering interferometer principle, i.e. using light wavelength as the measurement scale, thus avoiding typical problems occurring in measurement techniques based upon light scattering intensity.

Nevertheless, in CIRA IWT laboratory, instrumentation for Particle Measuring Systems, such as FSSP and OAP, are also available. In the following paragraphs all available CIRA droplet size instruments are described.

#### *7.4.1.1 PHASE DOPPLER PARTICLE ANALYSER (PDPA) TECHNIQUE*

**Airborne Droplet Analyzer Probes (ADA):** This optical system is an internal probe, directly exposed to the icing cloud, which provides measurements of both super-cooled cloud water droplets diameter (MVD) and its velocity component in axial-probe direction.

The CIRA ADA system (see figure 7.16) includes two icing probes, with different measuring range, equipped with remotely controlled electro-thermal anti-icing system, in order to avoid icing formations on probe's arms during the measurements.

The measurable droplet diameter ranges from 0.5  $\mu\text{m}$  to about 170  $\mu\text{m}$  for standard probe (AEROMETRICS/TSI ADA100F) with 100mm of transmitting optical focal length, and from 1  $\mu\text{m}$  to 700  $\mu\text{m}$  for the probe equipped with larger transmitted optical focal length (AEROMETRICS/TSI ADA100LR).

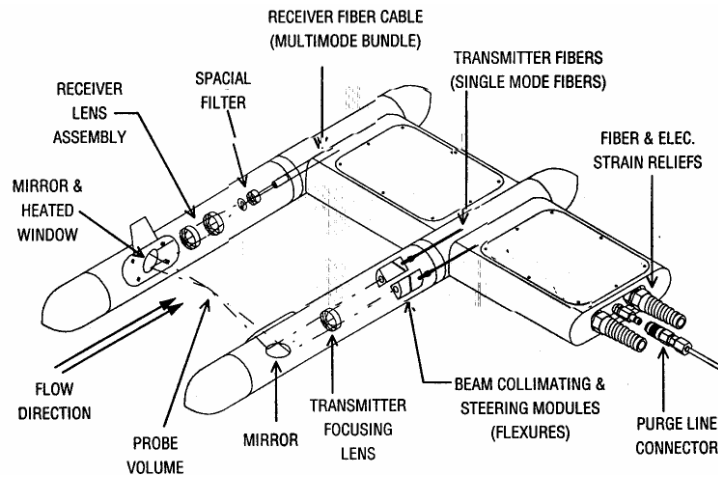


**Fig. 7.16:** ADA standard system

## External 2D PDPA System

Thanks to the available optical access on each IWT tests section, it is possible to use an external PDPA system, by installing both the transmitter (TSI TR-260-Pr-0.3) and receiver (TSI RV2200) probes externally to the test section, in the plenum chamber (see figure 7.17).

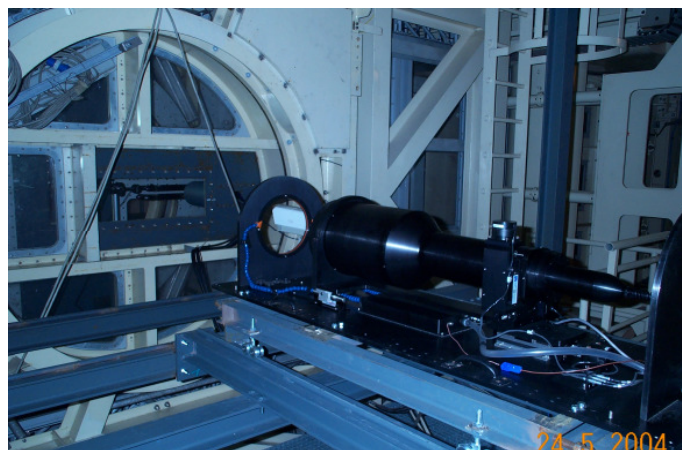


**Fig. 7.17:** PDPA system installed in the plenum chamber

Special optical design is used for these probes, due to the large optical focal lengths. During the measurement it is possible to remotely change the optical configuration to cover a wide range of spherical droplets diameters from about 0.8  $\mu\text{m}$  to 2000  $\mu\text{m}$ . The system can also provide the characterization of 2D droplet trajectory.

#### *7.4.1.2 FORWARD SCATTERING SPECTROMETER PROBE (FSSP)*

The FSSP is an optical system that calculates the diameter of a droplet by measuring the power of light scattered by the droplet as it crosses the focused laser. The size of the droplet is determined by a calibration curve, which relates scattered light (Mie theory) to droplet diameter. CIRA Icing Laboratory is equipped with a FSSP-100ER that covers a measuring range from 5 to 95  $\mu\text{m}$  (see figure 7.18).

The probe is mainly made of a 5 mW helium-neon laser, optics, and electronics, and works with a DMT M200 software system.



**Fig. 7.18:** CIRA FSSP-100ER system

#### *7.4.1.3 OPTICAL ARRAY PROBE (OAP)*

The Optical Array Probe (OAP) is an optical droplet sizing instrument used to measure the water droplet diameters larger than 100  $\mu\text{m}$  for both natural and artificial clouds. The OAP measures the diameter of particles by using an imaging technique.

CIRA has an OAP-260X (figure 7.19) covering a range between 10 and 600  $\mu\text{m}$ .

As the FSSP, the OAP is a self-contained probe, approximately 1 meter long, containing a small laser. The OAP is provided with two probe arms, both heated, one containing the laser beam transmitting optics and the other one containing the receiving optics.



**Fig. 7.19:** CIRA OAP-260X system

#### **7.4.2 Liquid Water Content Measurement Methods**

Two measurement techniques, based on different measurement principles, are available for accurate measurement of cloud liquid water content (LWC).

#### 7.4.2.1 ICING BLADE SYSTEM

A standard Icing Blade method is used as reference for LWC measurements during calibration of simulated icing cloud in CIRA IWT (figure 7.20).



**Fig. 7.20:** Icing Blade mounted in the IWT STS

The blade (300mm long, 60mm deep and 3mm thick) is made of stainless steel, mounted inside a deployable shield and attached at the end of the support.

The shield is connected to an actuator. The release of the actuator runs out the shield from the blade in 0.18 seconds.

The working principle is based on the collection of ice on the icing blade leading edge, and therefore on the measurement of the ice accreted. The LWC is then related to the thickness of ice, the airspeed, the exposure time and the collection efficiency of the blade.

The blade is used to measure the LWC at air temperature of -20°C. The exposure time is adjusted to allow approximately 3mm of ice thickness on the blade leading edge, in

order to limit the maximum width of ice and to reduce the variation of the collection efficiency during the test.

#### *7.4.2.2 HOT-WIRE LWC PROBE*

As further instrumentation for LWC measurements, a Droplet Measurement Technologies LWC-100 system is available (figure 7.21).



**Fig. 7.21:** DMT LWC-100 probe

The principle for LWC measurement is based on the amount of power required to keep the sensor at constant temperature when water droplets impinging on the probe vaporize. The LWC is linearly related to the difference between wet and convective power losses, and depends on airspeed, temperature and pressure. Typical performance ranges from LWC are  $0\div 3.0 \text{ g/m}^3$ .



### **7.4.3 Liquid Water Content Uniformity Measurement Methods**

The Icing Grid is the standard calibration system used in CIRA IWT to measure cloud uniformity and coverage area.

The Icing Grid (figure 7.22) is made of vertical and horizontal stainless steel bars equally spaced in the cross section of the test chamber. The bars are connected to an external frame, fixed to the test section internal walls. Grid mesh spacing depends upon test section dimensions and varies from 95x105 mm for the STS to 150x150 mm for the ATS. Thickness of each bar is 3 mm.

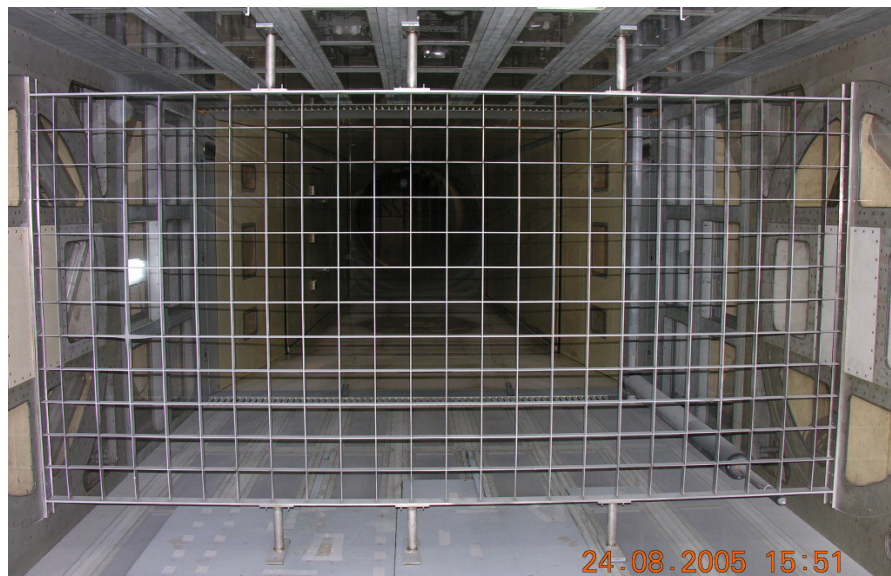


**Fig. 7.22:** Icing Grid installed in the IWT ATS

In order to get a map of the LWC distribution in the cross-section, all the measurements are converted to relative LWC normalized to the centre of the test section. The grid is exposed to the icing cloud to allow the ice to build up at -20°C air temperature. The number of measuring points changes in function of the tests section.

Digital calipers are used for fast thickness measurements.

## **7.5 AERODYNAMIC INSTRUMENTATION**

The following aerodynamic instrumentation is available for flow field characterization.

### **7.5.1 Hot Wire**

A dedicated hot wire system IFA 100 TSI system is available for turbulence measurements. A probe rotator allows angular calibrations for the 2D cylindrical probes (X probes). The system is equipped with a calibrator manufactured by Dantec, a signal recorder provided by Racal Recorder Storeplex and several probes (wedge probes, hot films and hot wires).

### **7.5.2 Flow Angularity Probe**

A customized six holes probe is available for flow angularity measurements. The central hole measures the total pressure whereas the static pressures measured on the surface of a cone of 30 deg of aperture angle are used for the flow angularity measurement.

### **7.5.3 Temperature Probe**

A model 102 AU1AF de-iced, platinum resistance type total temperature sensor is available for total temperature measurements. The sensing element consists of a platinum wire having 500 OHMS resistance at 0°C and it is insulated and hermetically

sealed within two concentric tubes. The sensing element is protected from impingement of small foreign particles. The housing can be de-iced in a static temperature range included between -10 °C and -35 °C.

Main features of the probe are:

- Temperature range: -100÷+350 °C
- Speed range: Up to Mach = 3
- Altitude range: sea level to 30 km
- Accuracy: 0.1 °C

Maximum recovery error is about 0.4% at Mach values ranging between 1 and 3.

#### ***7.5.4 Laser Doppler Velocimeter***

The CIRA Laser Doppler Velocimeter (LDV) is a special system designed by Aerometrics/TSI Inc., with long focal length operating in critical environmental conditions (low temperature, high relative humidity, low/high static pressure, etc..), for two-dimensional flow characterization. The LDV system uses the same transmitting optics as receiver optics, coupled in one probe unit (transceiver) working in backscatter mode.

## **CHAPTER 8**

### **ICING CLOUD CHARACTERIZATION IN THE CIRA IWT**

As already stated several times, icing wind tunnels are one of the most important means of compliance available supporting aircraft icing certification process, although their performance and test reproducibility must be checked through a detailed cloud characterization, in order to be sure about data reliability.

The present chapter describes CIRA IWT Secondary and Additional Test Section cloud characterization tests. Furthermore data obtained from the two calibration activities have been compared and some parametric analyses have been performed. Whenever possible, STS and ATS calibration data have been compared with MTS cloud's data to check coherence between test sections. Finally through data comparison MTS functioning envelope has been extended.

Calibration procedures for both test sections follow the here-below reported steps:

- Mean Volume droplets Diameter (MVD) measurements. Temperature, static pressure (altitude), nozzle density and velocity effect have been also estimated.
- SBS supply temperature for super cooled droplets generation.
- Cloud uniformity measurements (LWC distribution in the test section).

- Liquid Water Content (LWC) measurements have been finally carried out. Static pressure (altitude), nozzle density and velocity effect have been also estimated.

MVD and LWC (1D measurements) have been performed at the centre of the test section, while cloud uniformity (2D measurements) has been performed in the central cross section.

Thanks to all the tests performed, a set of empirical equations describing the MVD and LWC as function of water and air pressures has been determined. These equations have been settled on as final goal of the calibration and can be finally used to set the spray bar supply parameters for a given test condition, avoiding direct measurements of MVD and LWC during the test.

### ***8.1 STS ICING CLOUD CHARACTERIZATION***

Three different spraying grids, each using a different number of active nozzles, have been used to cover the largest area of FAR Part 25 App. C envelope with one type of commercialized spray nozzle (Spraying System Mod. SUJ-12). The LWC distribution was found to be at least within the ARP requirements [20], for each SBS grid configuration and several air/water pressure values.

The icing measurements have been performed in the following operating conditions:

- airspeed within the range 90 m/sec to 200 m/s;
- static air temperature between -2 °C to -37 °C;

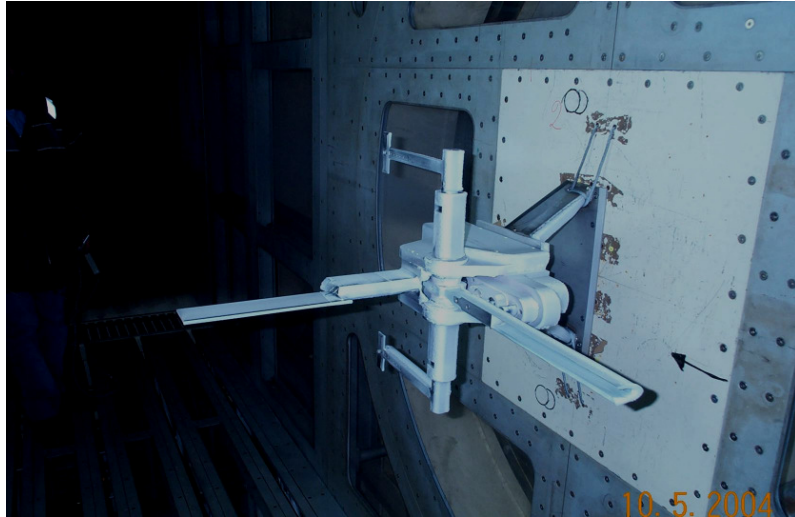
- spray bar air pressure between 75 kPa to 975 kPa;
- spray bar water pressure between 40 kPa to 700 kPa.

Four instruments were used to characterize the simulated icing cloud:

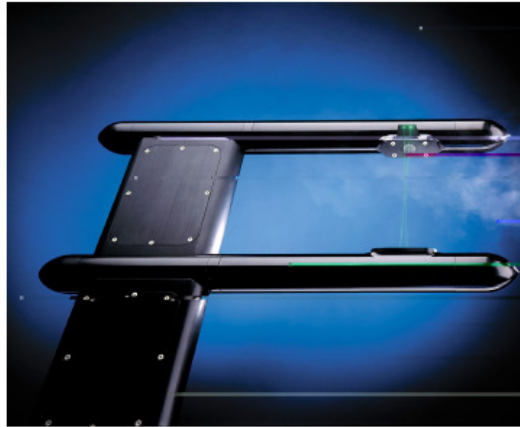
- ADA standard probe, based on PDPA technique, to measure simultaneously the droplets size and their axial velocity;
- Three cylinders to measure the droplets temperature stability;
- An icing blade system to measure the cloud concentration in terms of LWC;
- An icing grid to measure the LWC uniformity and cloud coverage.

Figure 8.1 shows as example the Icing Blade at the center of the test section, while figures 8.2 and 8.3 show the ADA probe and the Grid respectively. During the tests, the relative humidity level was only monitored. The typical value achieved at the upstream spray bar section was around 97%, which was found to be very stable during each test.

The MVD and LWC data acquired were collected in a database. The operating envelope of the spray bar system, in terms of achievable MVD and LWC as a function of water and air pressures, was then identified and represented by means of polynomial equations.



**Fig. 8.1:** Icing Blade mounted on STS vertical walls



**Fig. 8.2:** ADA system



**Fig. 8.3:** Icing Grid in the STS

### ***8.1.1 Droplet size calibration***

The particle sizing instrumentation used for the cloud calibration consists in an optical probe based on phase Doppler technique (ADA, Fig. 8.2) that is able to measure, simultaneously, both super-cooled cloud water droplets diameter and one velocity component in the axial-probe direction.

The measurement principle, upon which the Phase Doppler technique is based, is the light scattering interferometry. This technique utilizes the wavelength of coherent laser beams as the measurement scale, furthermore it is robust even with high density flows since is not based on the light intensity only, but also on the shift of the signal itself received by three different detectors. As such, the performance is not as easily degraded as it is for systems using light scattering intensity (PMS probes) for the estimation of the particle size nor does it requires frequent calibrations.



The ADA system available at CIRA, has been installed in the center of the test section and it was provided with a heating system able to avoid ice to build up upon its arms. Its droplet diameter measuring range, in the specific configuration used went from 0.5  $\mu\text{m}$  to 175  $\mu\text{m}$  and the focal length was 100 mm.

This configuration was retained able to measure all the diameter spectra generated by IWT spray bar system for the reproduction of FAR Part 25 Appendix C, as it is shown in figure 8.4 with large dynamic range ( $10^2 \div 10^{-2}$ ).

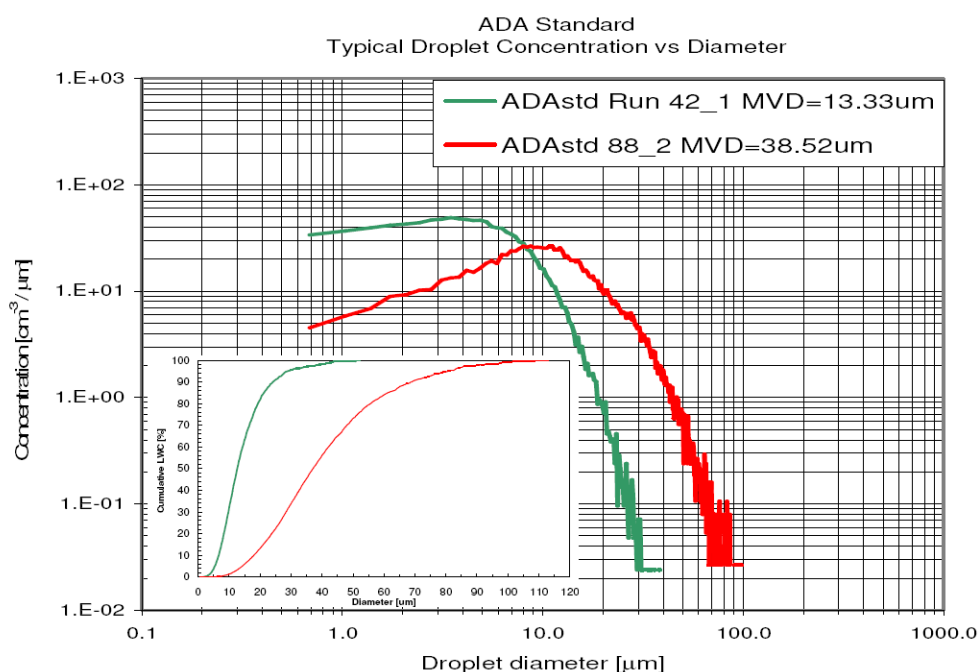


**Fig. 8.4:** Droplet diameter concentration and liquid water mass for different MVD values

After the setting of Spray Bar parameters (air pressure, water pressure and both air and water temperatures), the time to stabilize conditions had to be waited (as short as 10 sec. in average) before starting the data acquisition. For each acquisition, it has been

selected a large number of samples in order to assure that sufficient large droplets (higher than 50  $\mu\text{m}$  of diameter) were detected for reliable computation of MVD.

The number of measurements performed was 170. MVD data have been acquired during the spray bar calibration in what it has been called “basic configuration”: velocity equal to 140 m/s, 1:2 nozzle density (about 280 active nozzles), sea level and with test section air temperature set at  $-5^\circ\text{C}$ . Results are shown in figure 8.5, where curves have been parameterized with respect to the water pressure. Actually more curves than what shown in the figure 8.5 have been acquired [21], even if they are not reported in an effort to make the chart more “readable”. The difference between the air and water pressure “ $\Delta p$ ” is reported on the X axis.

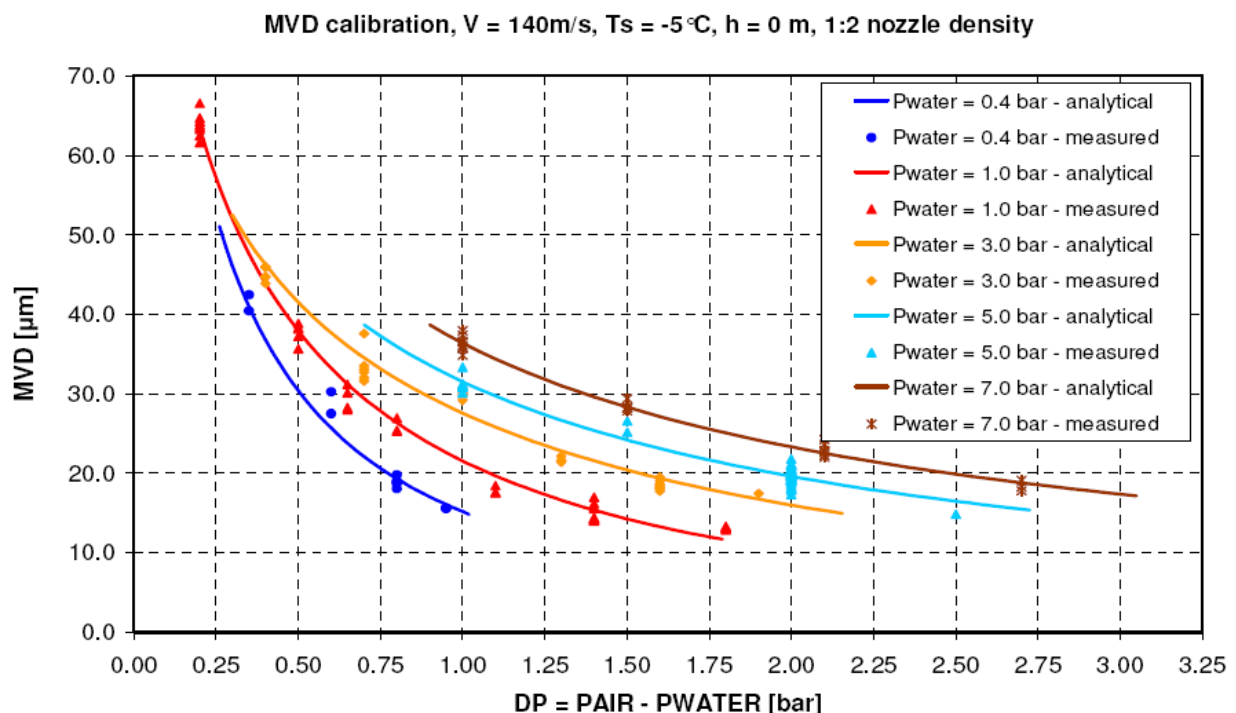


Fig. 8.5: MVD experimental values

The following expression was found to best interpolate the measured MVD values using the minimum-squared law:

$$MVD = a + b \ln p_a + c \ln p_w + d \ln^2 p_a + e \ln^2 p_w + f \ln p_a \ln p_w + g \ln^3 p_a + h \ln^3 p_w + i \ln p_a \ln^2 p_w + j \ln^2 p_a \ln p_w$$

where,  $P_a$  and  $P_w$  represents the SBS pressure in the air and water supply line respectively, both expressed in bar.

The average difference between the measured and calculated MVD corresponds to about 4% while about 90% of the values fall in the  $\pm 10\%$  boundaries. The interpolation error, decreases when droplet diameter increases.

Figure 8.6 shows both the measured points and the equation plotted, at constant MVD (from 15  $\mu\text{m}$  to 50  $\mu\text{m}$  with a 5  $\mu\text{m}$  step), as function of  $\Delta p$  ( $P_{\text{air}} - P_{\text{water}}$ ) versus  $P_{\text{water}}$ . The range of water pressure for which the above equations are applicable goes from 0.2 to 7 bar.

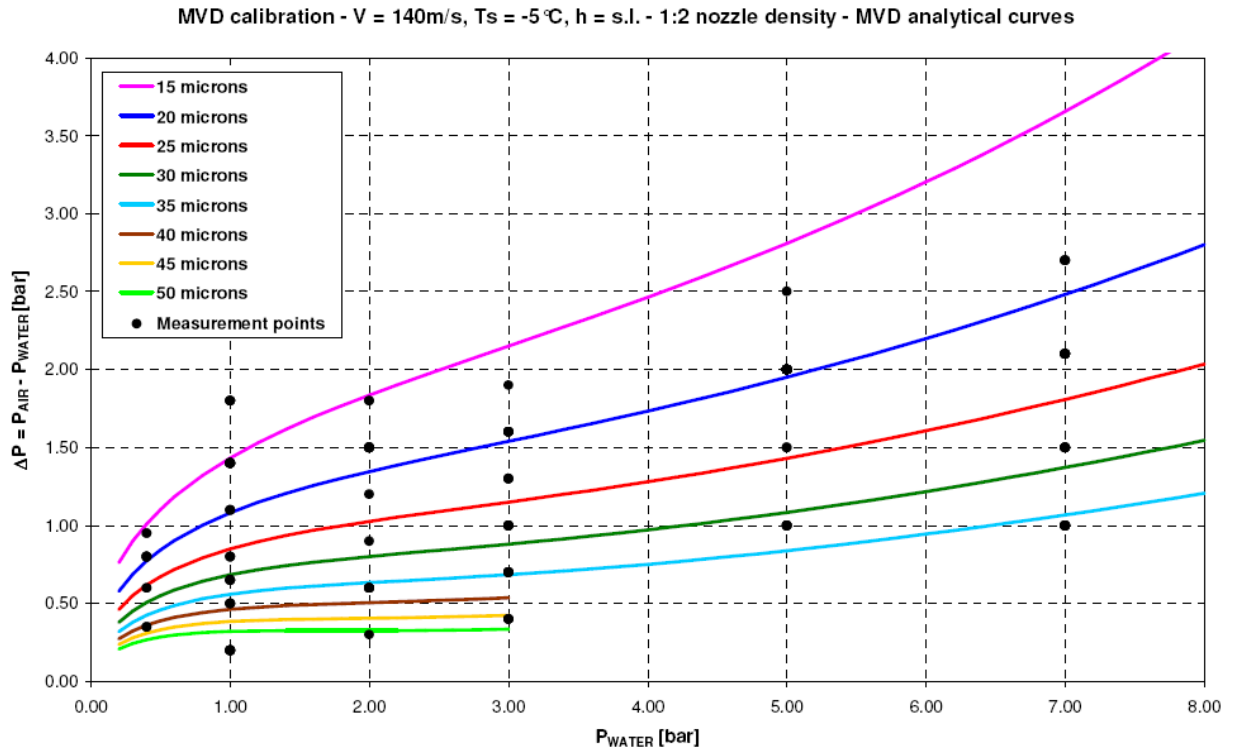
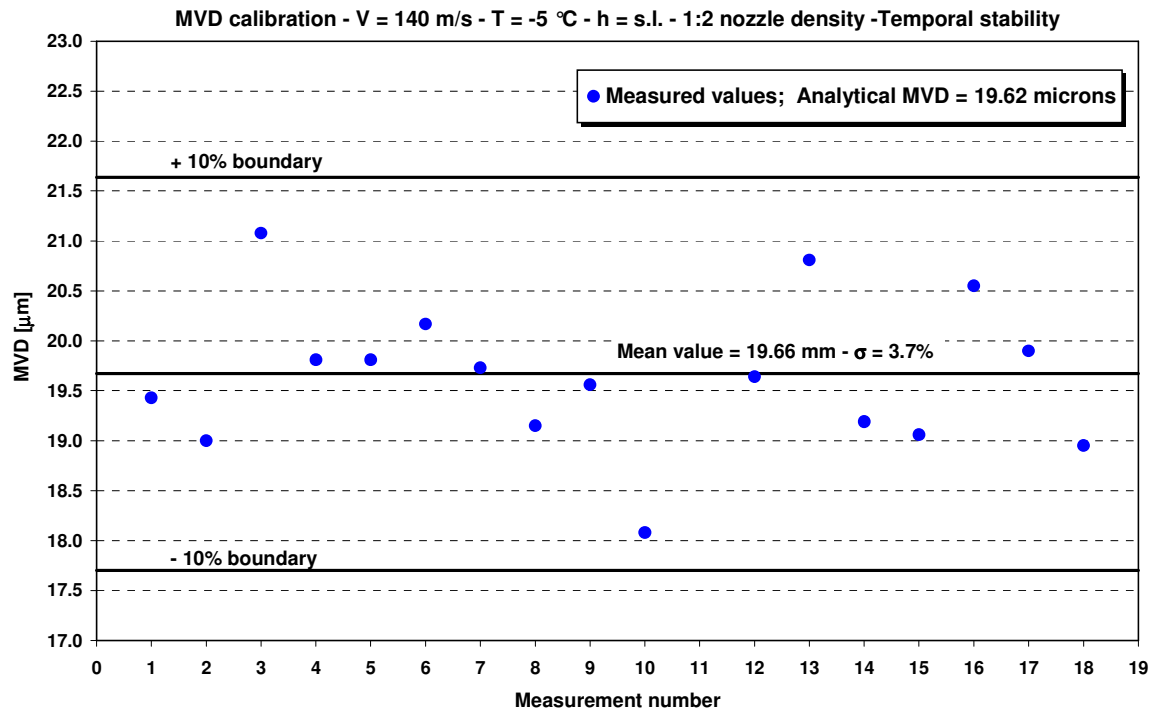


Fig. 8.6: MVD experimental values

To bring the MVD calibration to a close, also the temporal stability has been studied. Different MVD measurements were performed, without stopping the spraying, during a time interval of about 30 minutes. Acquisition time, on average, has been less than one minute per measurement. A test condition corresponding to  $\text{MVD} \approx 20\ \mu\text{m}$  was selected for this analysis. As shown in figure 8.7 it can be said that all the MVD measurements fall in the  $\pm 10\%$  boundary.



**Fig. 8.7:** MVD temporal stability

Altitude, velocity, temperature and nozzle density effect on the MVD have been analyzed: the effects have been evaluated changing only one wind tunnel condition per time (altitude, velocity, temperature or nozzle density) and repeating some of the measurements already performed in the basic calibration. Data have been compared with the theoretical basic curves. Results are shown in pictures 8.8 – 8.11: each picture shows the effect of one single parameter on the MVD. Consideration on these results are reported in section 8.3.2.

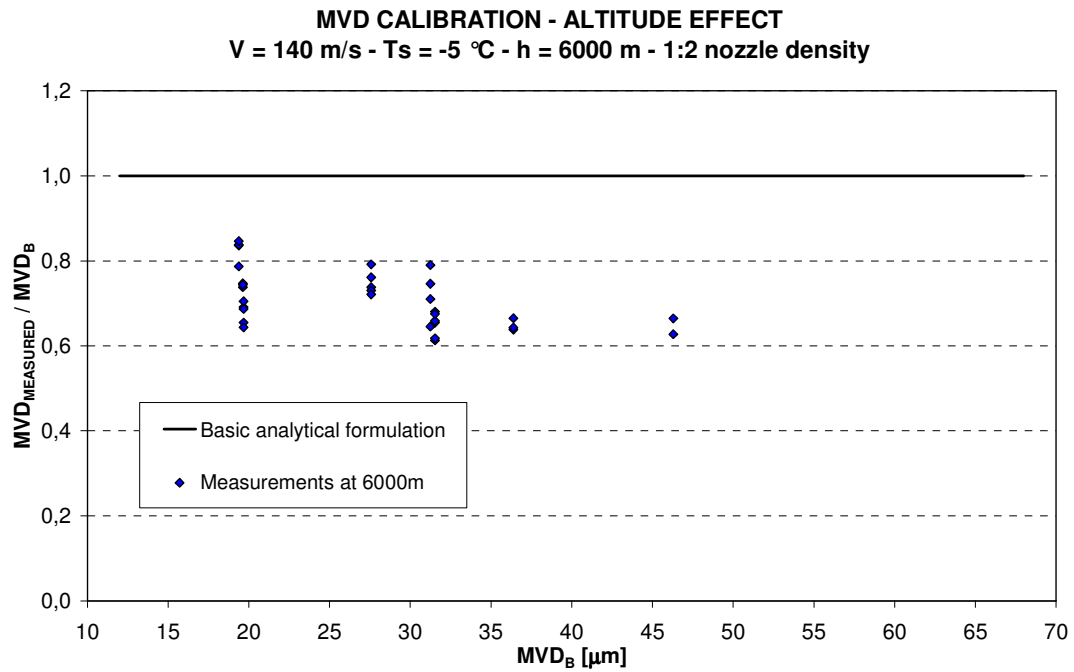


**Fig. 8.8:** Altitude (static pressure) effect on MVD

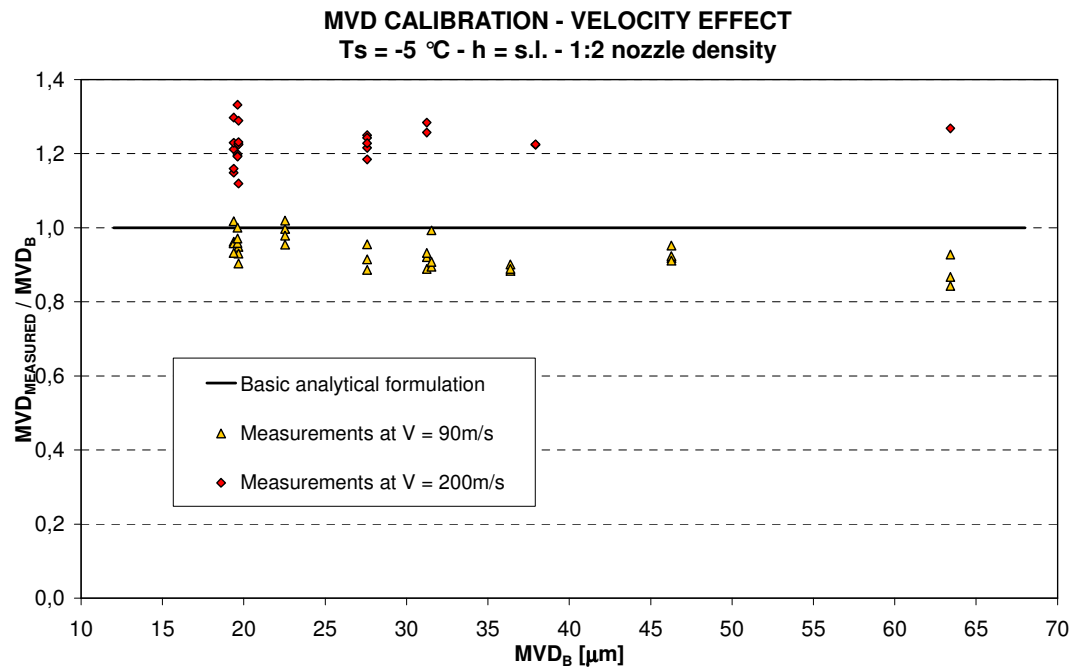


**Fig. 8.9:** Velocity effect on MVD

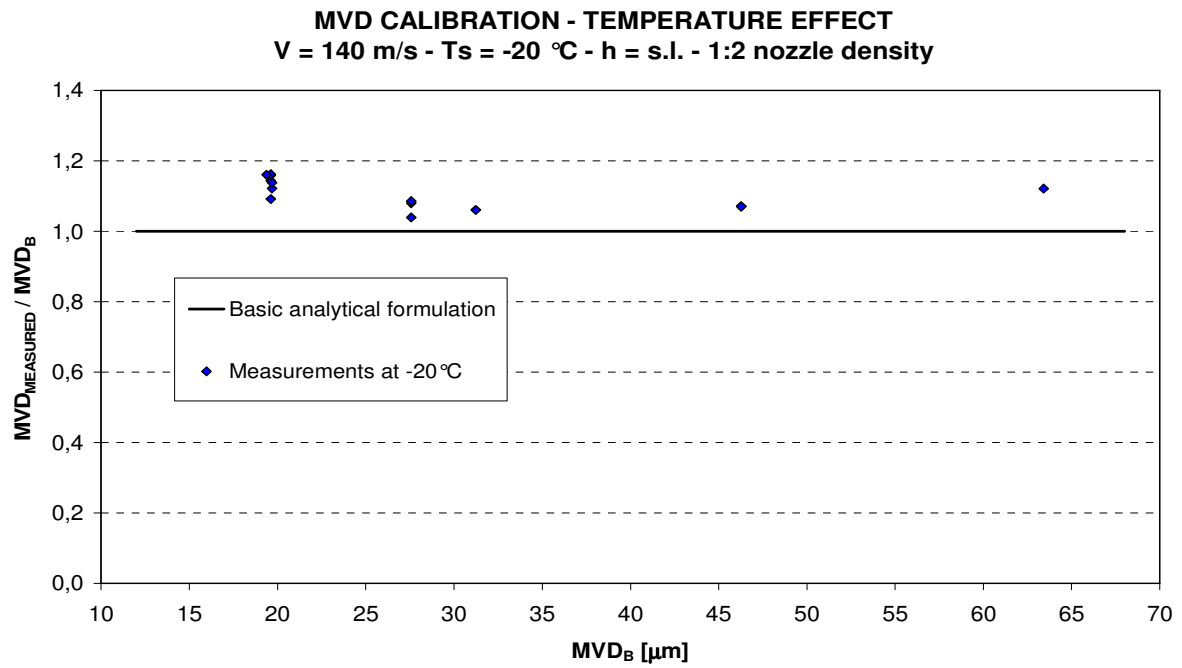


**Fig. 8.10:** Temperature effect on MVD

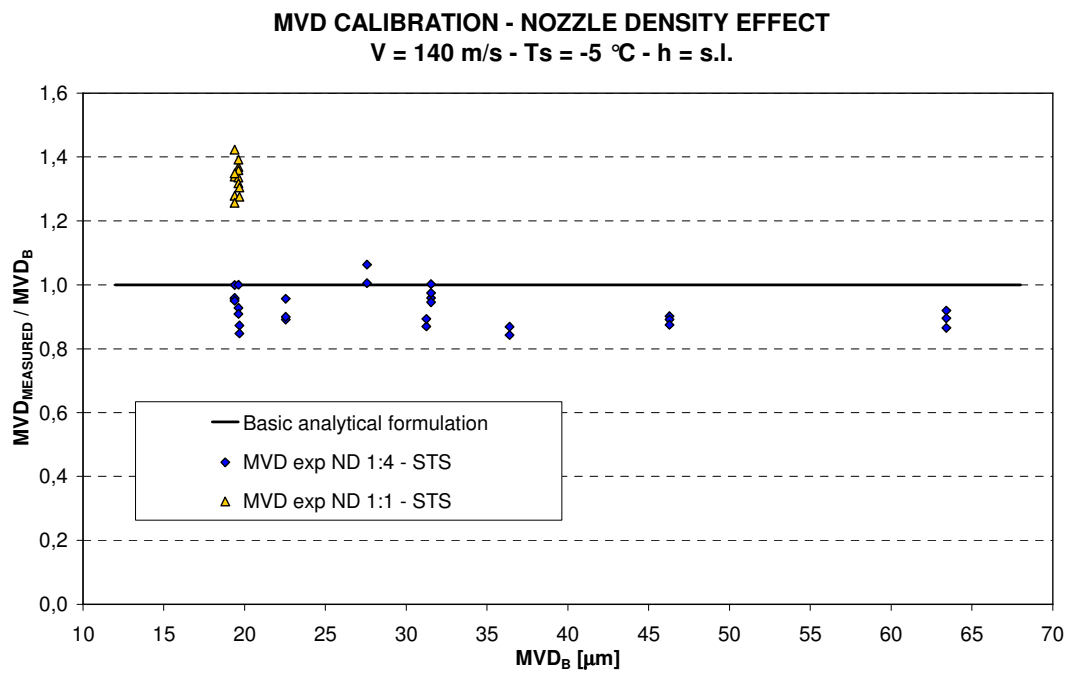


**Fig. 8.11:** SBS nozzle density effect on MVD

### **8.1.2 SBS temperature assessment**

The icing cloud is produced in the settling chamber of the IWT by means of the SBS in which spray nozzles, for certain air and water pressure, generates the requested droplets cloud. Typically the settling chamber could be in sub-zero temperature conditions. In order to avoid the droplet freeze-out phenomena, due to both the spraying conditions and the acceleration given by the tunnel contraction, both air and water temperature shall be adjusted appropriately. These temperatures should also be not too warm to prevent droplet “over-warmed” at the test article location. To check the droplet supercooling conditions in the tests section three cylindrical pipes of about 5 cm diameter and 500 mm long have been mounted, each between the test section sidewalls located along the wind axis and equal-spaced in the reference y-z test plane (see figure 8.12). Each cylinder has been equipped with two thermocouples located at about  $\pm 150\text{mm}$  respect to the centerline, in span direction. The cylinder pipe, made in stainless steel, it has received external marks from stagnation point to  $\pm 90^\circ$  step  $\pm 15^\circ$  to better control the icing build-up during the tests.



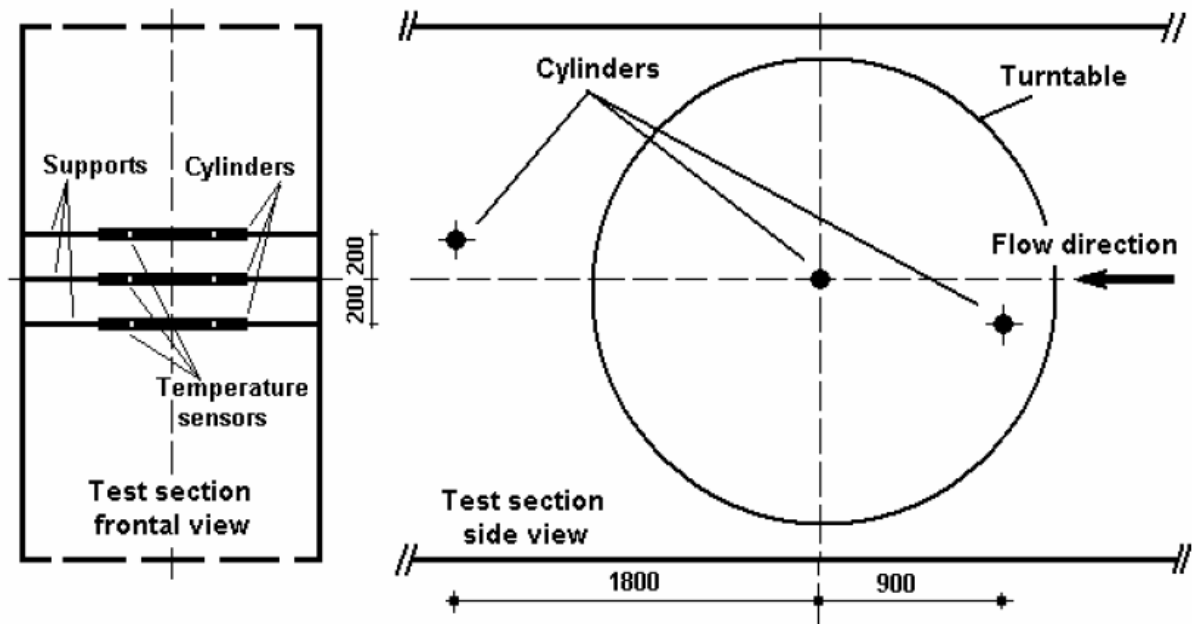
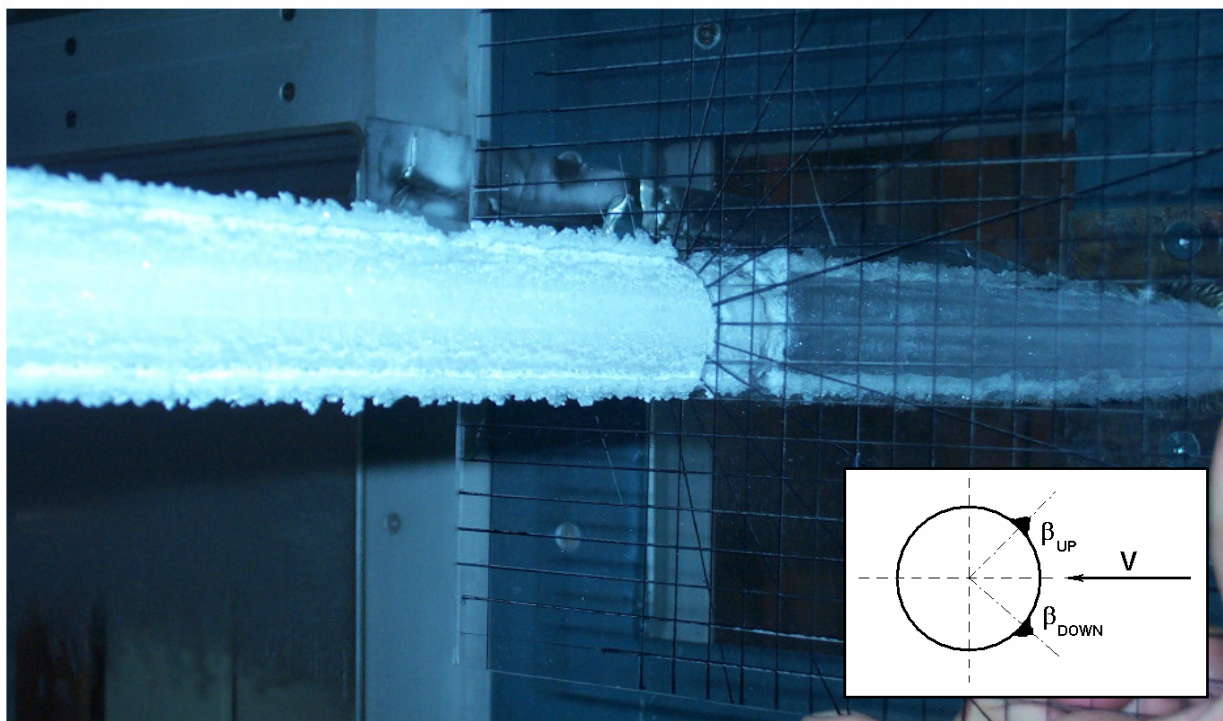


Fig. 8.12: Cylinders configuration.

This technique does not allow measuring droplets' temperature, nonetheless it does allow checking if droplets are thermally well stabilized all along the Test Section length. Indeed when ice accreted on the 3 cylinders has the same characteristics (mainly the same horn position) that means droplets maintain the same temperature all along the Test Section length, thus are stabilized.

Tests were performed at sea level and relative humidity monitored turned out to be 95-100%. Only one SBS configuration was used, with nozzle density 1:2. For each test condition (wind tunnel and cloud condition) different tests were executed varying the SBS supply temperatures ( $T_{air}$ ,  $T_{water}$ ). Tests have been analyzed measuring the horns positions with respect to the stagnation point, and taking pictures of the ice accretions on the three cylinders. Figure 8.13 shows an example of ice accreted on a

cylinder and the way horn position is estimated (more pictures and analysis are reported in Appendix E).



**Fig. 8.13:** Ice accretion on a cylinder

Results showed that, in general, the difference in the horns position among the three cylinders was not significant and difficult to evaluate, indicating that a basic good droplets thermal stabilization is present in the test section. So, the SBS supply temperatures effects have been mostly estimated looking at the quantity and quality (consistency, transparency and adherence) of the accumulated ice, rather than the horns positions. More pictures and analysis are reported in Appendix E.

From the results obtained during all the tests an envelope of suitable temperature has been obtained and it is reported in figure 8.14.

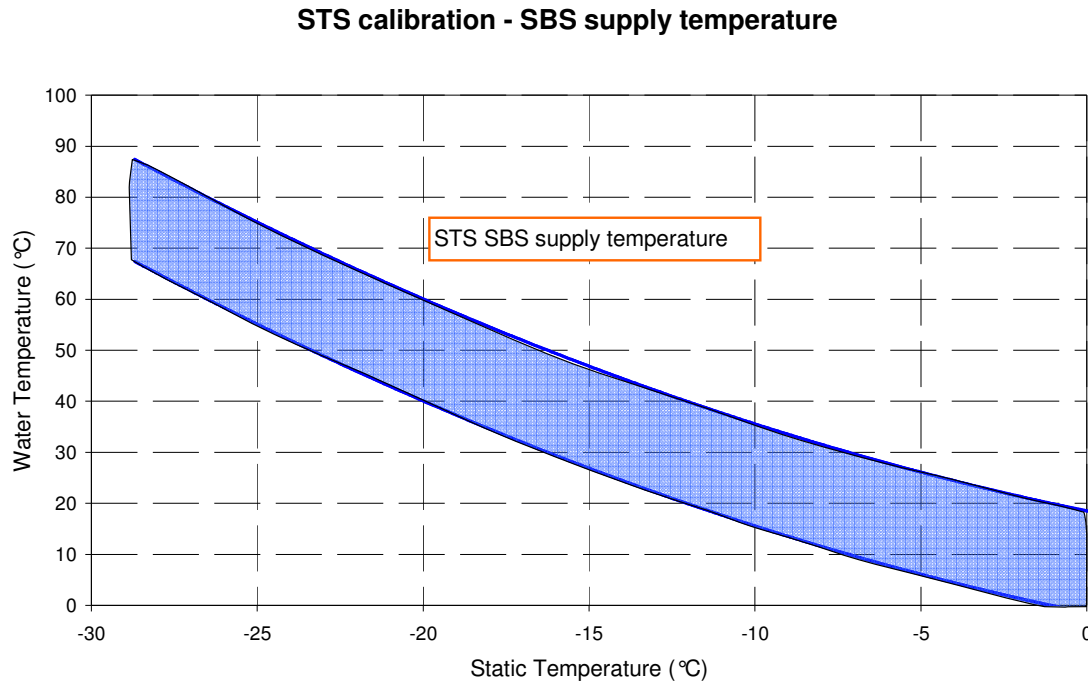


**Fig. 8.14:** SBS temperature assessment

### ***8.1.3 Icing cloud uniformity and coverage area***

The term icing cloud uniformity, refers to the degree of liquid water distribution across the tunnel test section. It is desirable that the liquid water within the cloud be uniformly distributed from wall to wall and floor to ceiling. However ice uniform distribution was checked and optimized only in the region of interest usually requested by costumers being otherwise the measurements too time consuming.

The reference area within which the uniformity has been optimized was 9 rows (–470.25mm to 365.75mm from the center) by 11 columns (from –495mm to 505mm) equivalent to 99 measurement points and about 35% of the total STS surface. The ARP

criteria for a “uniform” icing cloud is that variations in LWC of  $\pm 20\%$ , with respect to the one measured at the center, are acceptable. In the STS a  $\pm 10\%$  has been reached in many cases.

The icing cloud uniformity and coverage has been measured using an Icing Grid made of vertical and horizontal stainless steel bars, installed at the model center of rotation (figures 8.3 and. 8.15). The test section static air temperature was always cooled down to about  $-20^{\circ}\text{C}$  and, for different airspeed settings, the grid was exposed to the icing cloud to allow the ice to build up for a calculated time interval. After each test, the ice thickness measurements in all the checkpoints of the icing grid were manually performed using two cooled digital calipers to avoid ice melting during measurement. To reduce the time necessary to carry out the measurements, the ice thickness data have been directly transferred from the two chilled calipers to a Personal Computer via cable, for quick data processing.

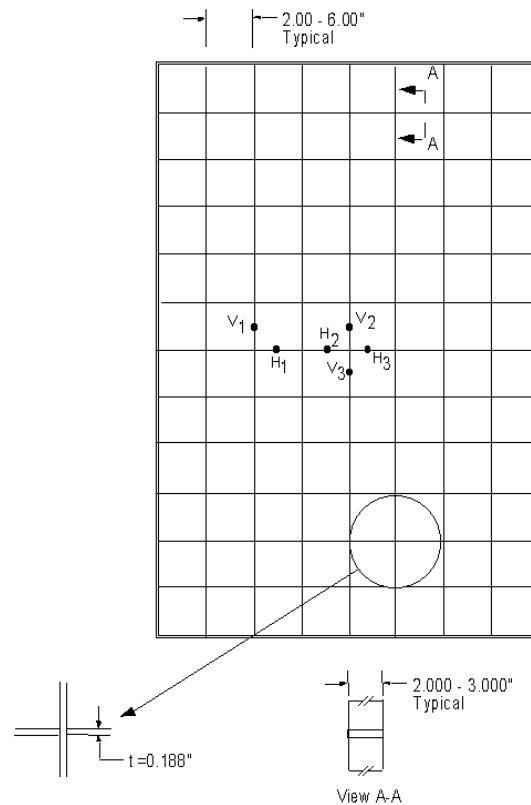


**Fig. 8.15:** Icing Grid sketch

To achieve extreme LWC values, both in the high or low ends of the FAR25 Appendix C envelope, the SBS density grid was changed to 1:1 and 1:4 respectively.

Three different SBS configurations were tested, corresponding to three different nozzle densities during the spraying:

- 1:4 nozzle density grid. A quarter of the nozzles present on the active bars are activated during the spraying (on, off, off, off, on, off, off, off, etc.).
- 1:2 nozzle density grid. Half of the nozzles present on the active bars are activated during the spraying (on, off, on, off, etc.).

- 1:1 nozzle density grid. All the nozzles present on the active bars are activated during the spraying (on, on, on, on, etc.).

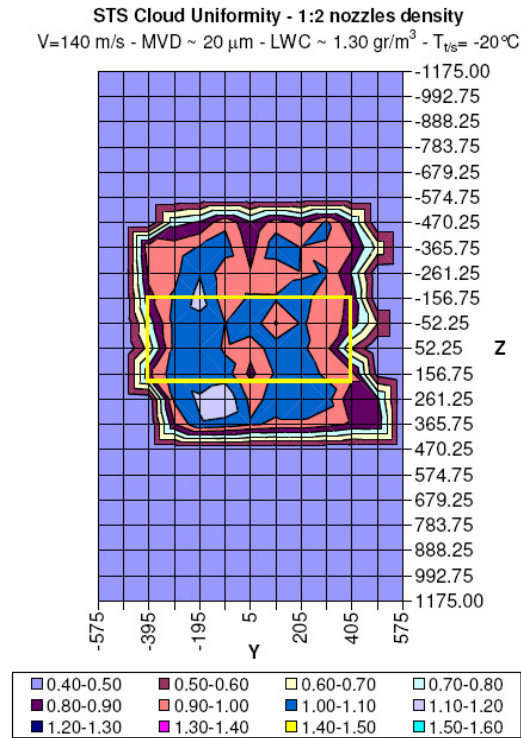
Figure 8.16 documents the cloud uniformity optimization with the following configuration:  $V = 140 \text{ m/s}$ , 1:2 nozzle density,  $T_s = -20^\circ\text{C}$ ,  $MVD \sim 20 \text{ }\mu\text{m}$ . The picture reports the relative liquid water content, normalized to the value at the centre of the test section. The yellow bounded area represents the reference area where usually a model is installed. The black grid lines in the pictures represent the icing measured points. The optimization would have been considered satisfactory already for a  $\pm 20\%$ . However for this configuration a  $\pm 10 \%$  in about all the reference area has been achieved as can be seen looking at the intervals of the contour plot.

Figure 8.17 shows the cloud uniformity at high water pressures, for the 1:4 nozzle density grid. Even in this case a  $\pm 10\%$  has been the final optimization result.

The uniformity shown in figure 8.18 results from a new optimization process performed at high water pressures and for the high density grid. The standard  $\pm 20\%$  has been reached with no difficulties on a wide area.

Finally, figure 8.19 shows an uniformity optimization obtained at  $V = 175 \text{ m/s}$  which was found to be the highest velocity achievable in the tunnel with the grid inside. The goal reached has been  $\pm 10 \%$ . The same optimization has been obtained for a velocity of  $90 \text{ m/s}$ , so that the target uniformity is maintained in the whole tested velocity range. The basic grid (1:2 nozzle density) has been used for these tests and results are reported in figure 8.20.

Although not reported in this thesis, other optimizations have also been performed in order to cover a very wide range of MVD/LWC/Velocity configurations.



**Fig. 8.16:** Uniformity at Nozzle density 1:2

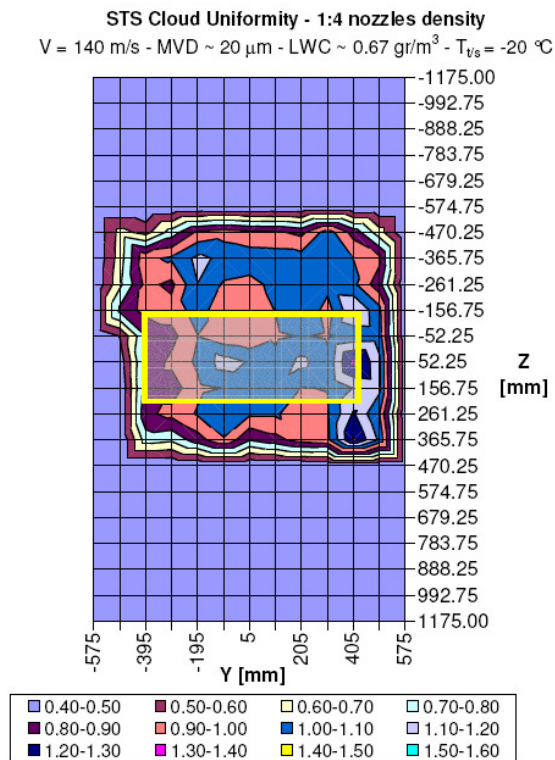


**Fig. 8.17:** Uniformity at Nozzle density 1:4

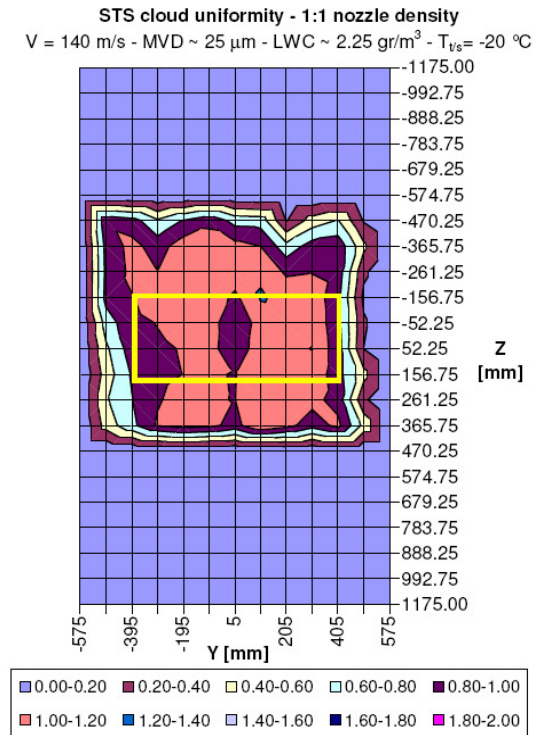


**Fig. 8.18:** Uniformity at Nozzle density 1:1

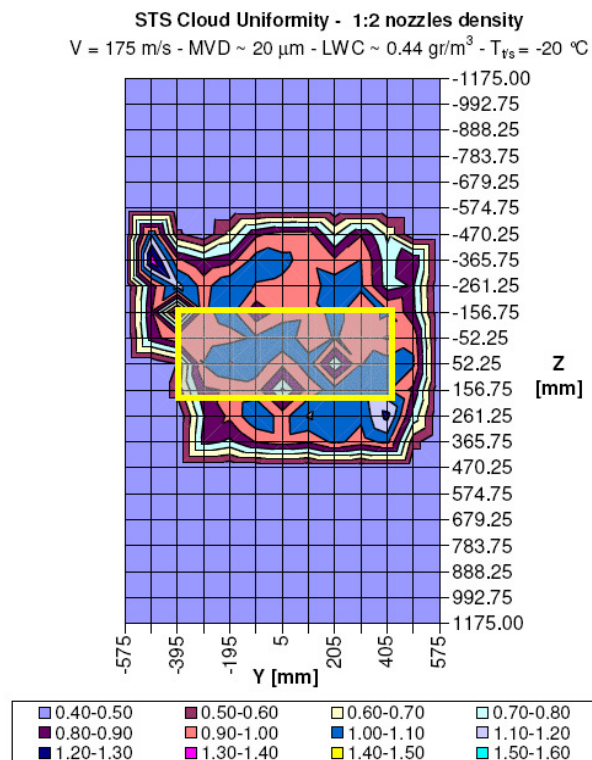


**Fig. 8.19:** Uniformity at Nozzle density 1:2 at 175 m/s



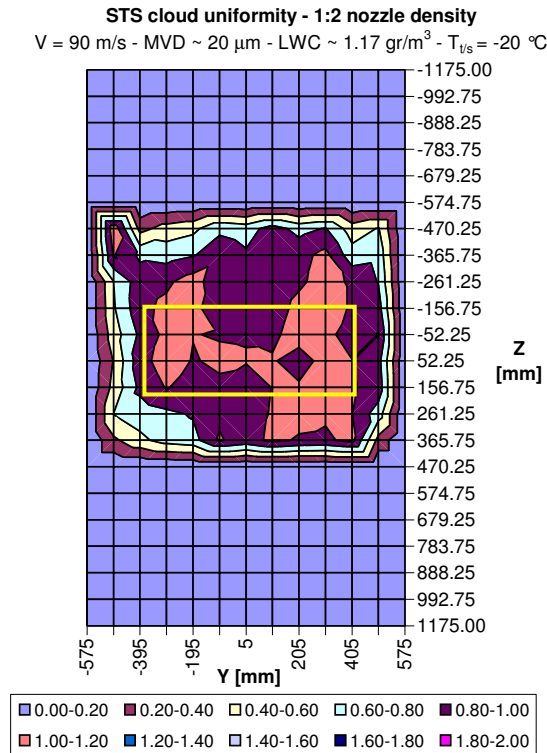


**Fig. 8.20:** Uniformity at Nozzle density 1:2 at 90 m/s

#### **8.1.4 Liquid Water Content measurements**

The liquid water content was determined using the standard Icing Blade (IB). The blade is attached at the end of the support and mounted inside a deployable shield. The shield is connected to an actuator. The release of the actuator runs out the shield from the blade in 0,18 sec. The blade is run out from its shield for a time to expose the thin edge to the icing cloud in the centre of the test section to allow the ice to build up. The icing blade is 300 mm long, 60 mm deep, and 3 mm thick (figure 8.1). The blade was used to measure the LWC over a range of airspeed, altitude, and water droplet sizes. All the tests have been run at static air temperature of  $-20^\circ\text{C}$ . The exposure time has been adjusted to allow approximately 3 mm of ice thickness on the blade leading edge to limit

the maximum width of ice and reduce the variation of collection efficiency during the test.

The thickness of ice on the icing blade was measured along three equidistant points, using chilled caliper to avoid ice melting. To calculate the LWC, has been used the equation reported below (units expressed in S.I.):

$$LWC = \frac{\rho_{ice} \cdot \Delta S}{E_b \cdot V \cdot t}$$

where,

- $\rho_{ice}$  is the ice density assumed constant (0.88 g/m<sup>3</sup>) at -20 °C;
- $\Delta S$  is the thickness of the accreted ice on the blade;
- $E_b$  is the blade collection efficiency;
- $V$  is the free-stream velocity;
- $t$  is the blade exposure time.

The blade collection efficiency was obtained, for each droplet diameter and free-stream velocity, using CIRA MULTI-ICE code which results were found in agreement with NASA's data within the 3% of average differences [21].

During the calibration 55 test points were measured at three different airspeed (90 m/s, 140 m/s and 190 m/s) and spray nozzles density configurations (1:1, 1:2, and 1:4) and two different static pressures.

Figure 8.21 shows the results of LWC measurements performed with the basic configuration and for droplet size ranging from 20  $\mu\text{m}$  to 40  $\mu\text{m}$ . The SBS water pressures were ranged from 40 kPa to 700 kPa. Using the least square error method, the following equation was found to fit the measured LWC data:

$$LWC = a + b \ln P_w + cMVD + d \ln^2 P_w + eMVD^2 + f \ln P_w MVD + g \ln^3 P_w + hMVD^3 + i \ln P_w MVD^2 + j \ln^2 P_w MVD$$

with a, b, c, d, e, f, g, h, i, j constants.

To evaluate the effect of a different nozzles density, the three different SBS configurations were taken into account. Figure 8.22 shows, for fixed wind tunnel and SBS conditions, the LWC with respect to 1:4 and 1:1 spray nozzles density. Taking the 1:2 spray nozzles configuration as the reference one, it is clear from the graph that the LWC changes roughly with a ratio of 2 doubling the nozzles density and decreases with a ratio of  $\frac{1}{2}$  with the configuration of 1:4 active nozzles.

Figure 8.23 shows the velocity effect. Now the rule of thumb is:

$$LWC_{V2} = LWC_{V1} * (V_1/V_2)^C$$

Where  $LWC_{V1}$  is the one taken as reference (in our case the LWC obtained in the basic configuration) and C is a constant.

Figure 8.24 shows that there seems to be negligible static pressure (altitude) effect upon the LWC.

Other measurements have been taken to assess MVD effects on the LWC. Data are not herein reported and are shown for the ATS only.

The results of the comparison between the IB LWC values and those calculated by the above mentioned analytical formulation can be seen in figure 8.25 where it is shown that almost all the data lie within  $\pm 10\%$  boundary.

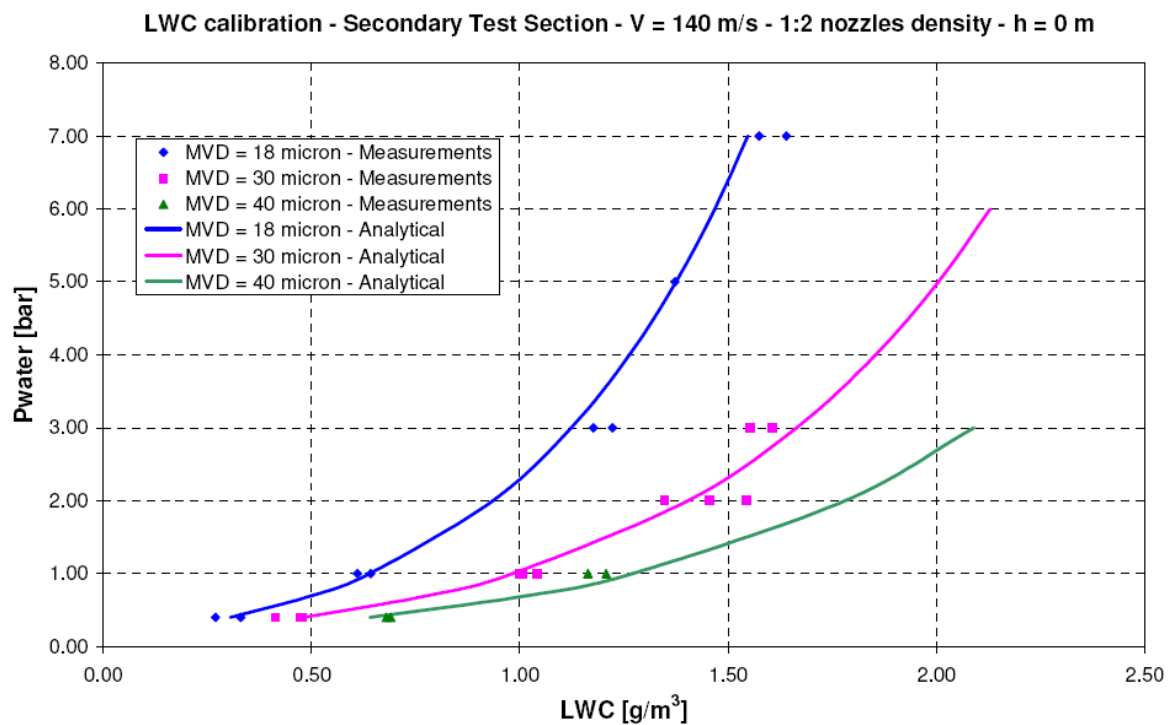


**Fig. 8.21:** LWC Basic Curves

LWC calibration - Secondary Test Section - MVD = 18 micron - V = 140 m/s - h = 0 m

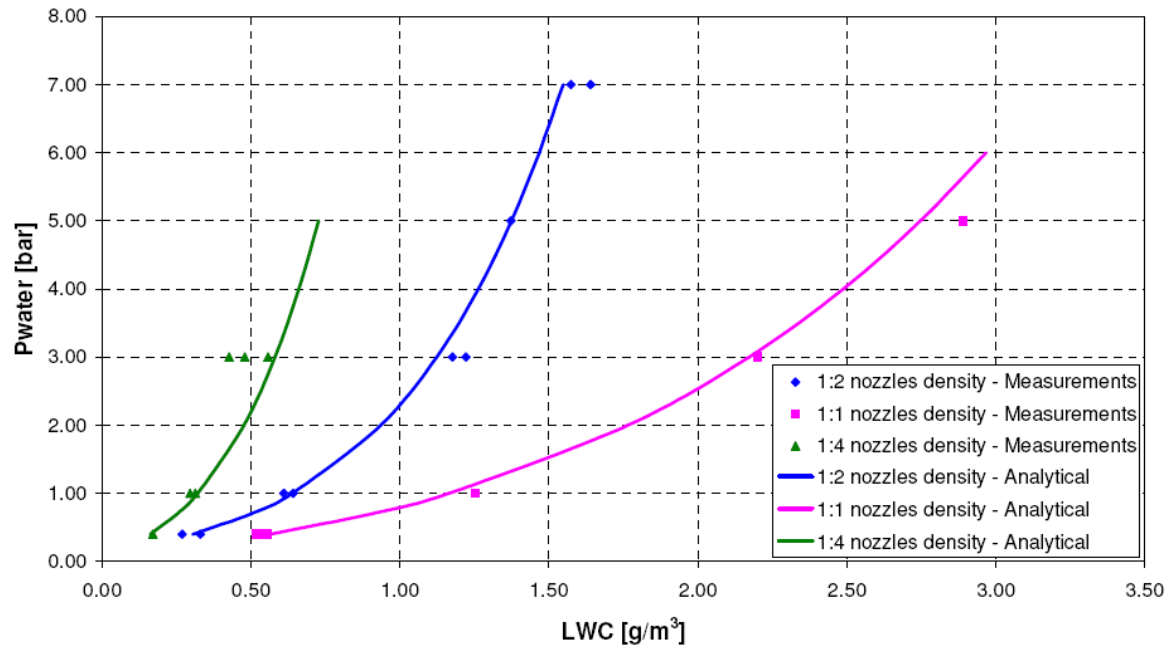


Fig. 8.22: Nozzles density effect on the LWC

LWC calibration - Secondary Test Section - MVD = 18 micron - 1:2 nozzles density - h = 0 m

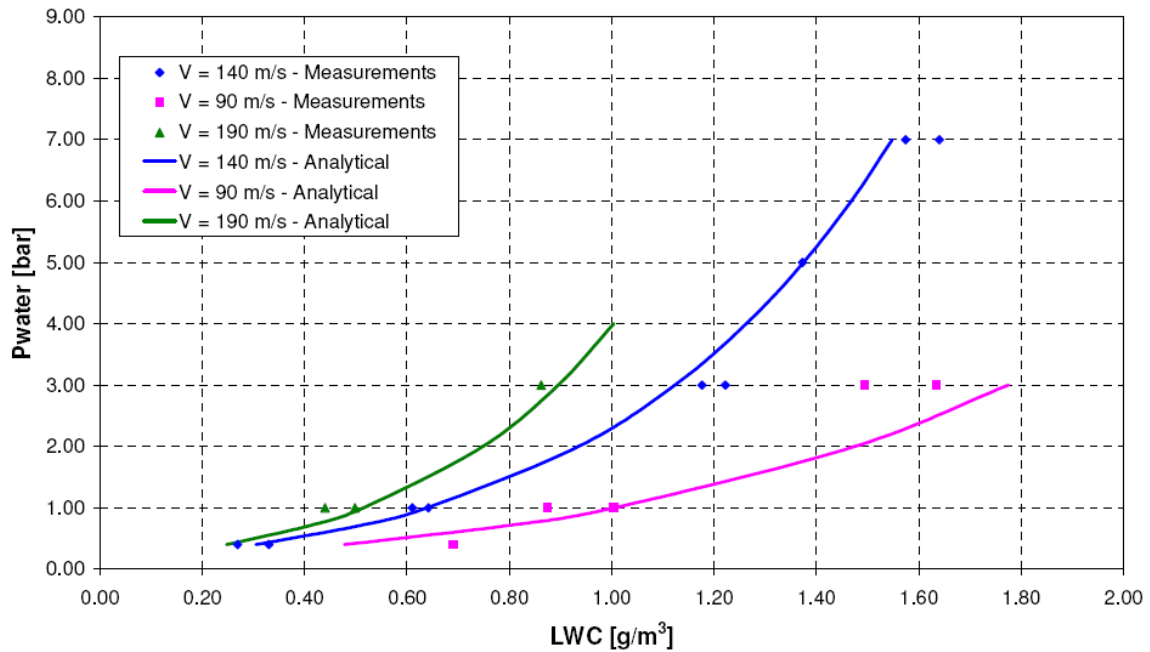
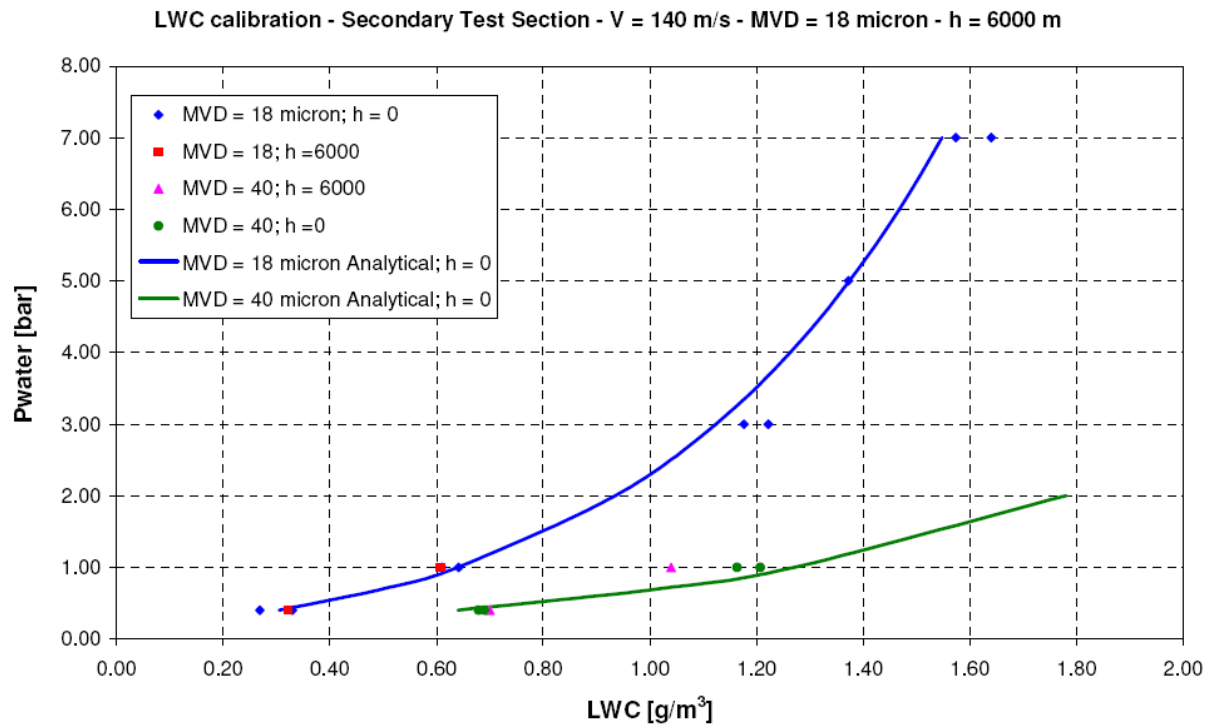
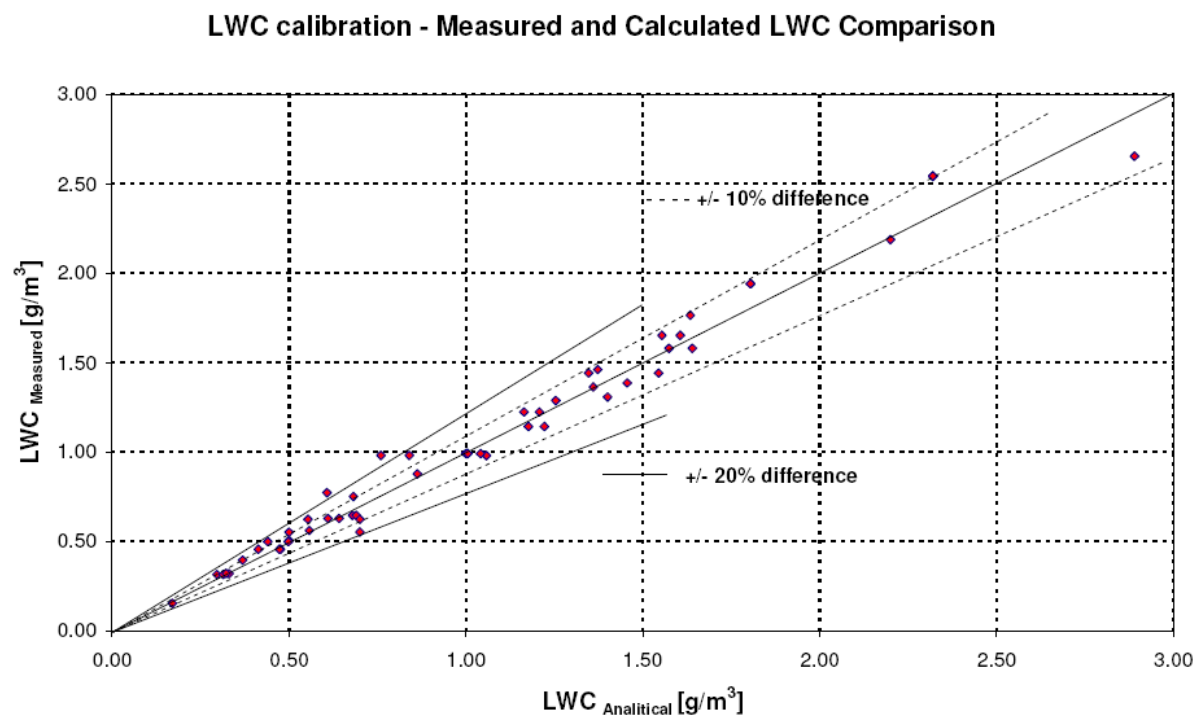


Fig. 8.23: Velocity effect on the LWC



**Fig. 8.24:** Altitude effect on the LWC



**Fig. 8.25:** Interpolation error

### 8.1.5 Icing cloud operative envelope

Figure 8.26 shows the envelope of the spray bar system taking into account the results achieved with different spray nozzles configurations at different velocities. This chart takes into account the velocity and the grid effects on MVD and LWC. In principle a new chart shall be drawn for each specific effect, however this effort is not here justified as would not add any additional information to what above already stated.

As it can be seen there is a remarkable coverage for both the intermittent and continuous cloud envelope. Of course the velocity plays the most significant role in defining the possibility to run certain defined cloud conditions given its strong influence on the LWC.

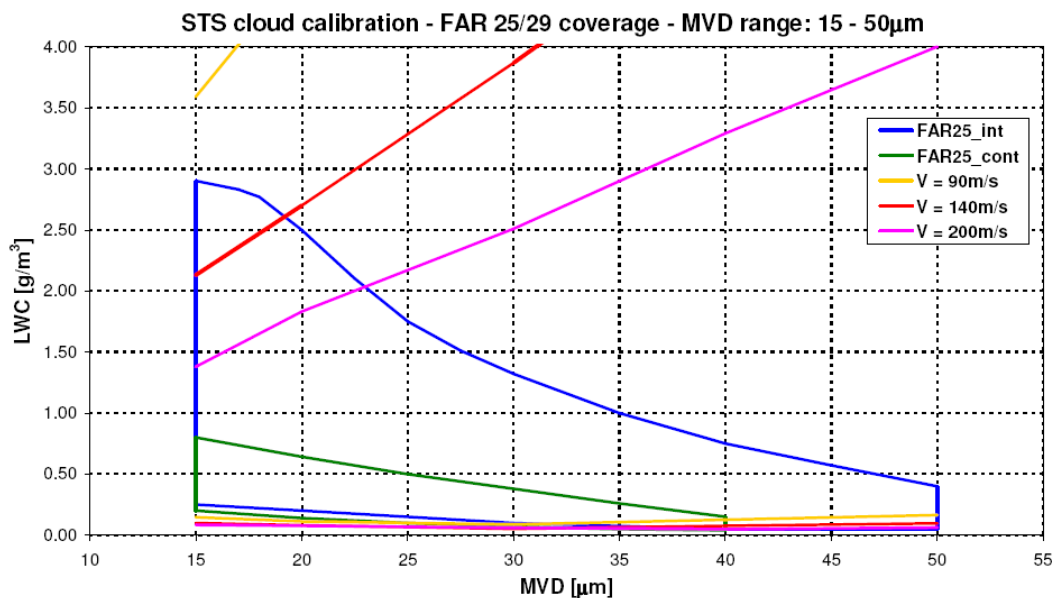


Fig. 8.26: STS MVD-LWC envelope

## **8.2 ATS ICING CLOUD CHARACTERIZATION**

Procedures, measurements and instrumentations adopted for the ATS cloud characterization are similar to the one adopted for the STS. Any exception from this general role is properly highlighted. Here below an analysis of the acquired data is given.

### **8.2.1 Droplet size calibration**

Figure 8.27 reports a picture of the instrumentation installed in the ATS. OAP and LWC probe have been installed for purposes different from the standard cloud characterization and therefore their use is not described in the present work.

Droplets sizes' have been measured via two ADA probes with different droplet size ranges [23]. They were approximately positioned at the centre of the test section, as for the STS. Other than the so-called ADA standard, also the so-called ADA large instrumentation was added, more suitable for detecting droplets with a larger diameter, with a range of  $1.9 \div 600 \mu\text{m}$ , to better account for large droplets. After the data acquisition, the analysis of the spectra obtained with the two probes allowed to identify the MVD obtained in correspondence of the SBS pressure set points.

Main difference with the STS calibration measurements is:

- Measurements have been performed utilizing not only the ADA standard probe, but also the ADA large system. More details are given in Appendix D.

Standard conditions for the tests were:



$$V = 60 \frac{m}{s}$$

$$H = 0 m$$

$$T = 0^{\circ}C$$

$$ND = 1:2$$

Figure 8.28 reports the MVD measurements versus the difference between SBS air and water pressures. The figure refers to the measurements taken in the “standard” conditions above reported: the analytical curves, obtained by interpolating the measured MVD, are also reported.

The general equation for the MVD versus  $P_{air}$  and  $P_{water}$  is:

$$\ln[MVD_B(x, y)] = a + b \cdot x + c \cdot e^{\frac{x}{j}} + d \cdot \sqrt{x} \cdot \ln x + e \cdot \sqrt{x} + f \cdot \ln x + \\ + g \cdot \sqrt{y} \cdot \ln y + e \cdot \sqrt{x} + h \cdot \sqrt{y} + i \cdot \ln y$$

Where:

$x = P_{air}$

$y = P_{water}$

$a, b, c, d, e, f, g, h, i, j = \text{constants.}$

The above equation was obtained by fitting the measurements using a least square error method.

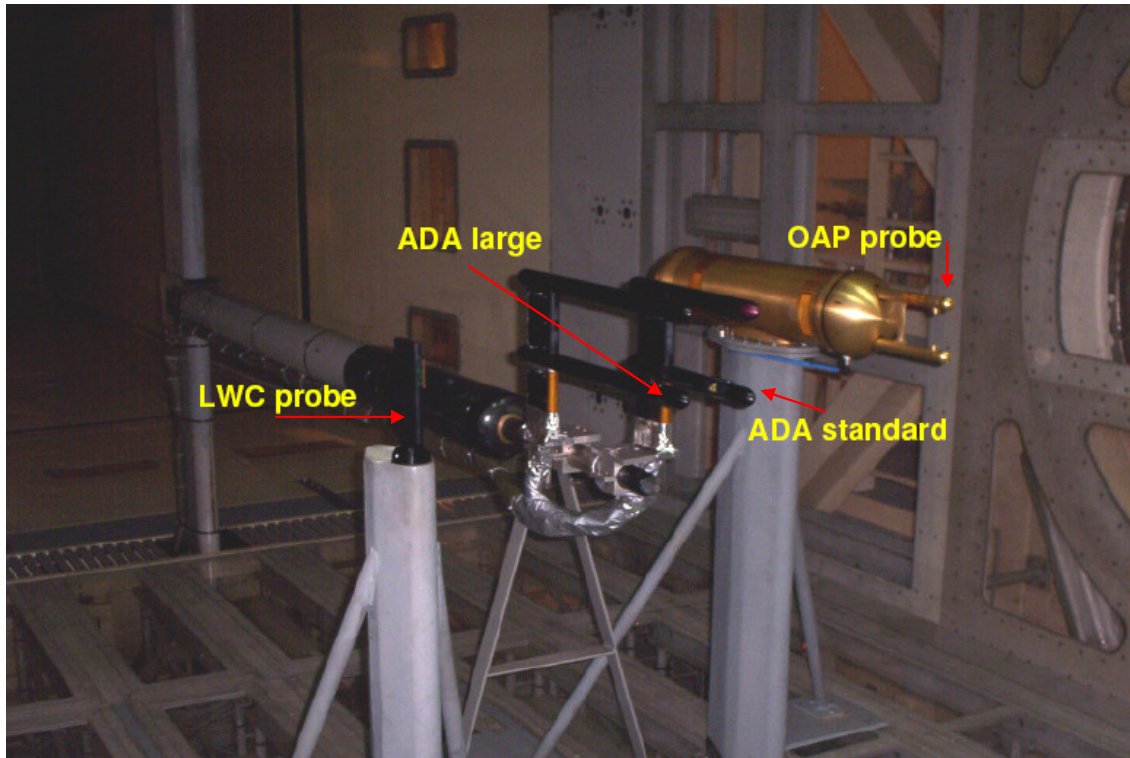


**Fig. 8.27:** Probes installed in the ATS

Using the above reported equation, the analytical envelope can be calculated as reported in figure 8.29. Black spots indicate the SBS supply pressures where the droplet size measurements were performed. Figure 8.30 reports the differences between the measured MVD values and the analytical formulation. A threshold of  $\pm 10\%$  of the basic analytical value has been added to the plot. If the range  $15\text{-}50\text{ }\mu\text{m}$  only is considered, about 93% of the data fall into these boundaries.

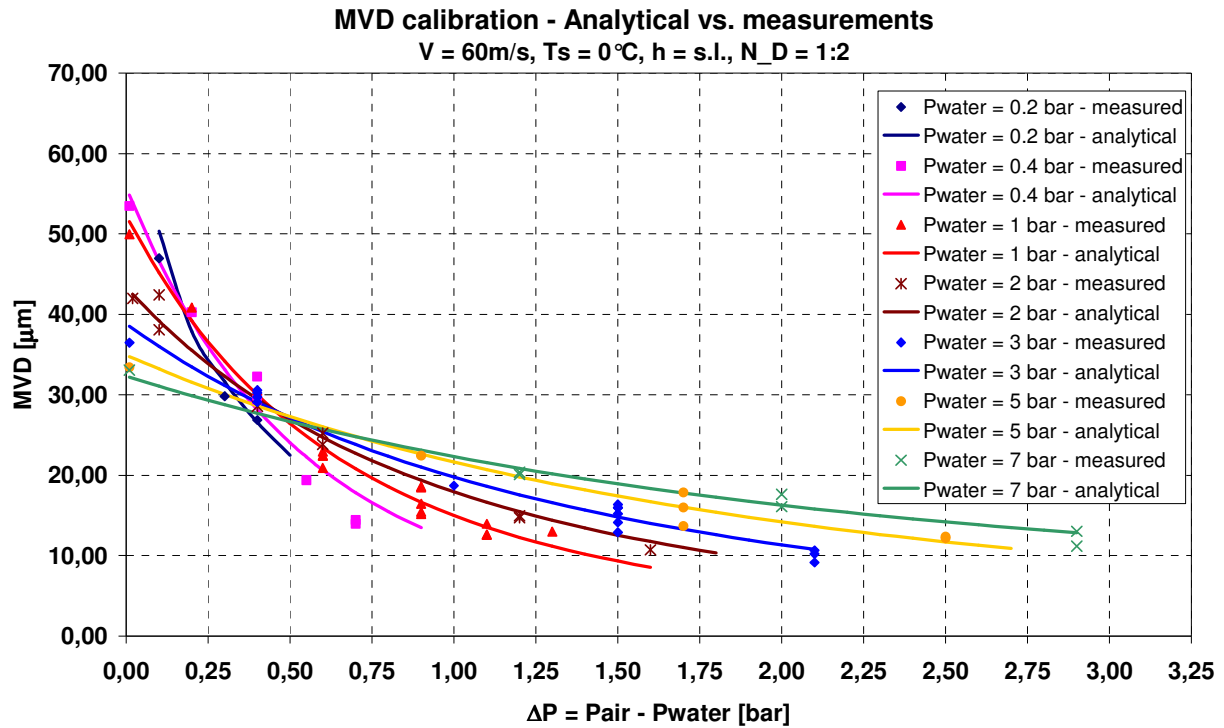


Fig. 8.28: Measured MVD and analytical curves at different SBS water pressures

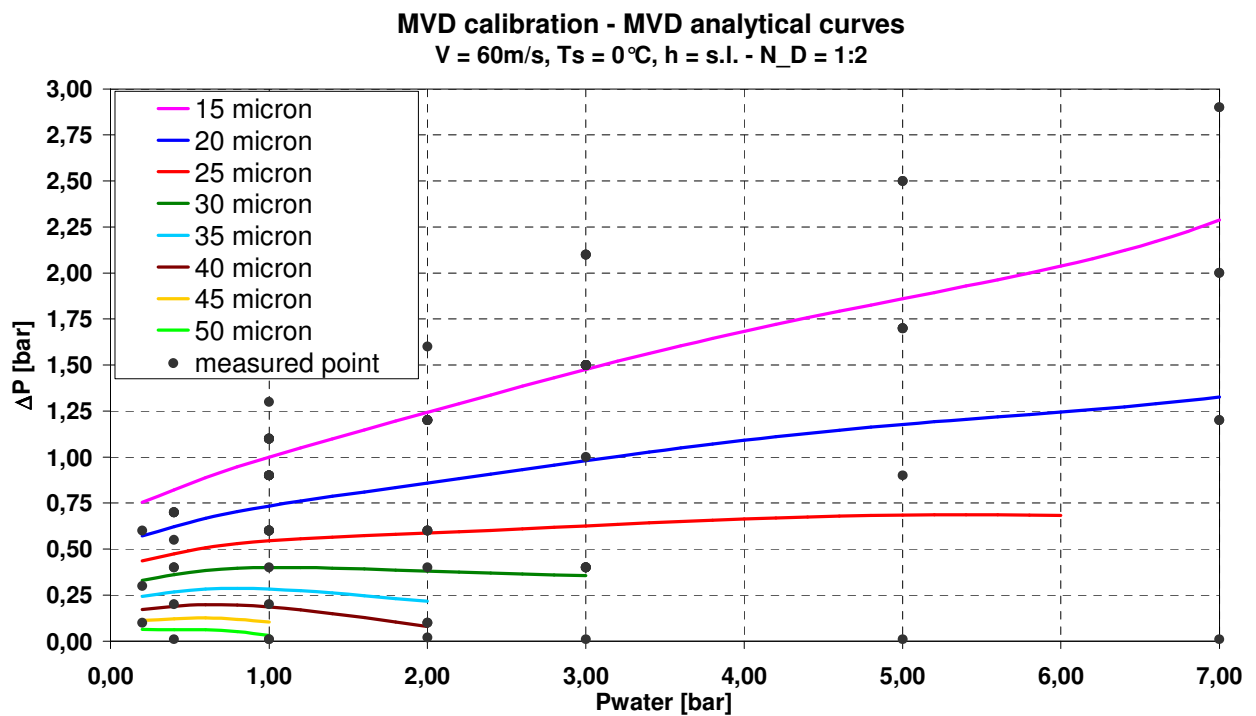
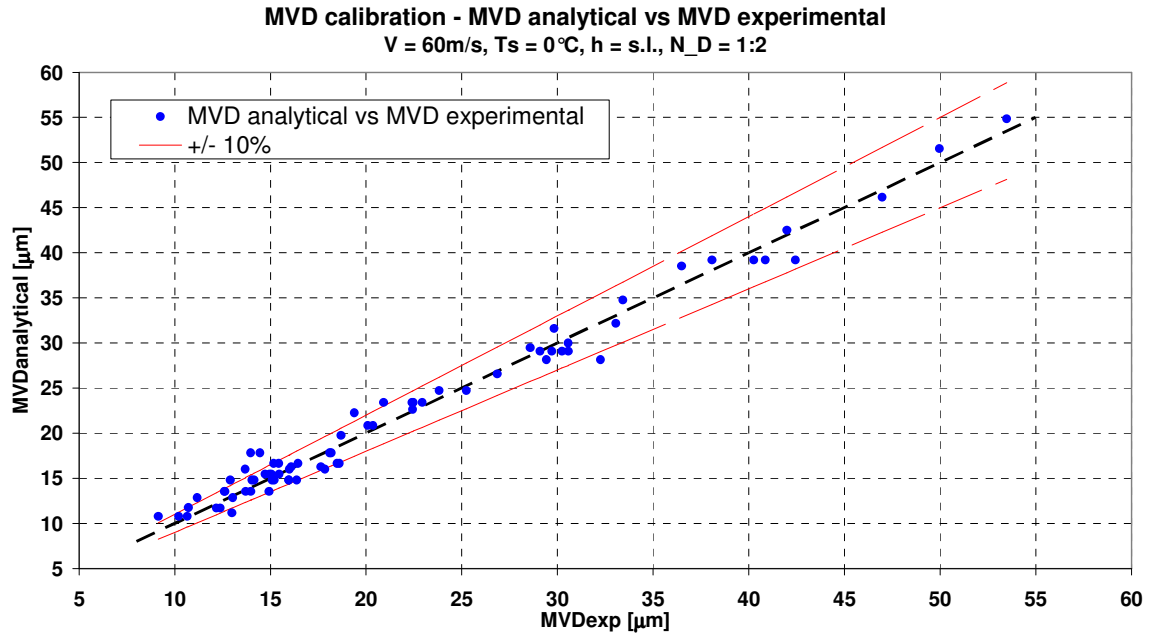


Fig. 8.29: MVD analytical curves envelope – basic formulation



**Fig. 8.30:** MVD basic calibration interpolation error

Altitude, temperature and nozzle density effects on the MVD have been also evaluated as for the STS. The effects have been evaluated changing only one parameter per time (static pressure, temperature or nozzle density) and repeating some of the measurements already performed in the basic calibration. Results are shown in figures 8.31, 8.32 and 8.33.

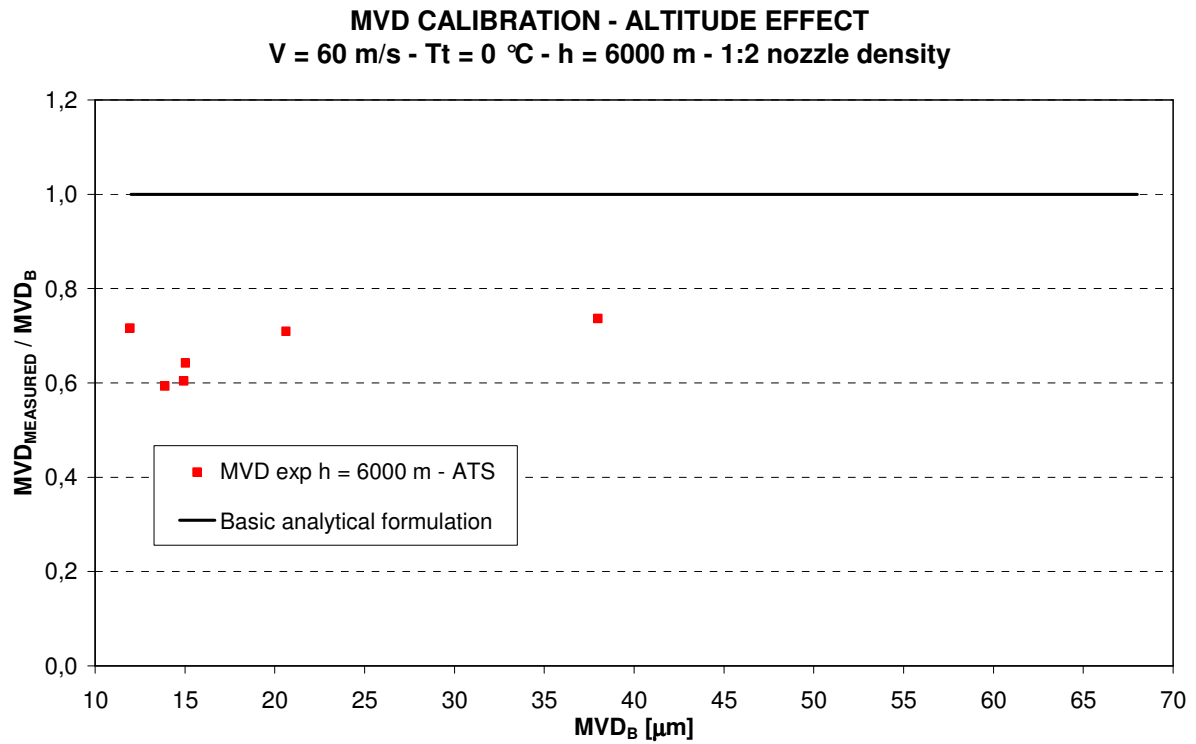


Fig. 8.31: Static pressure effect on the MVD

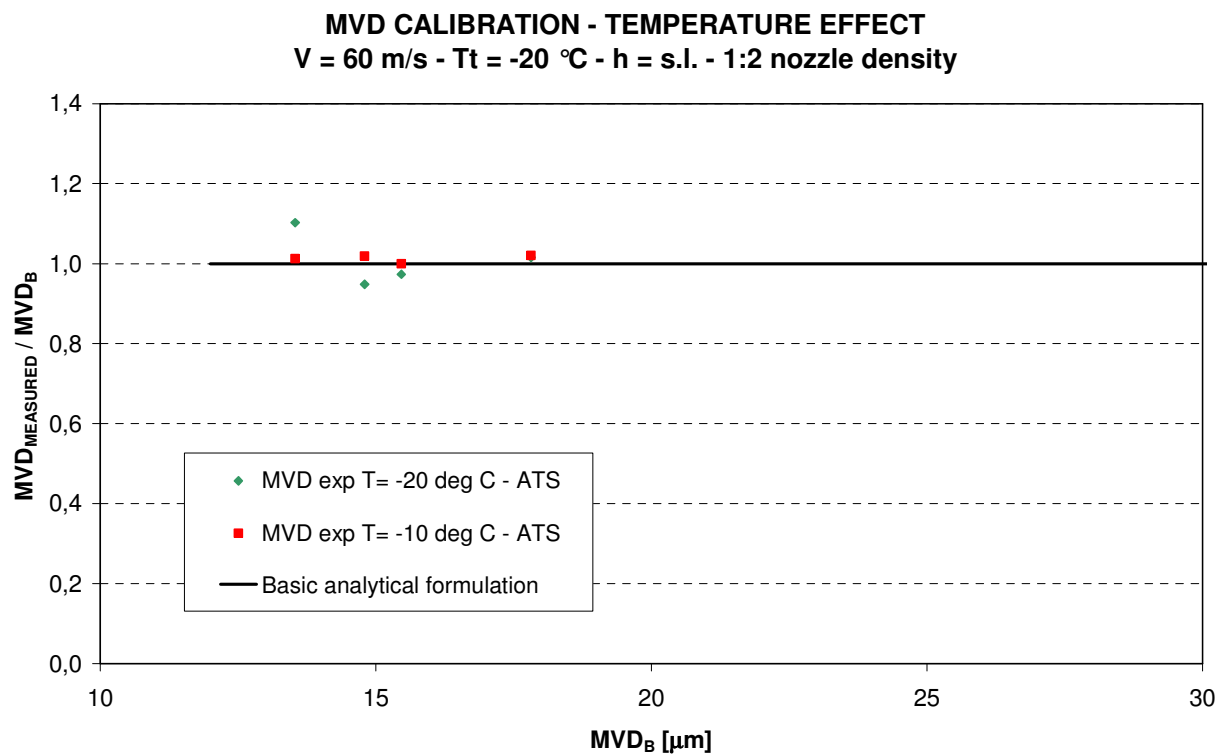
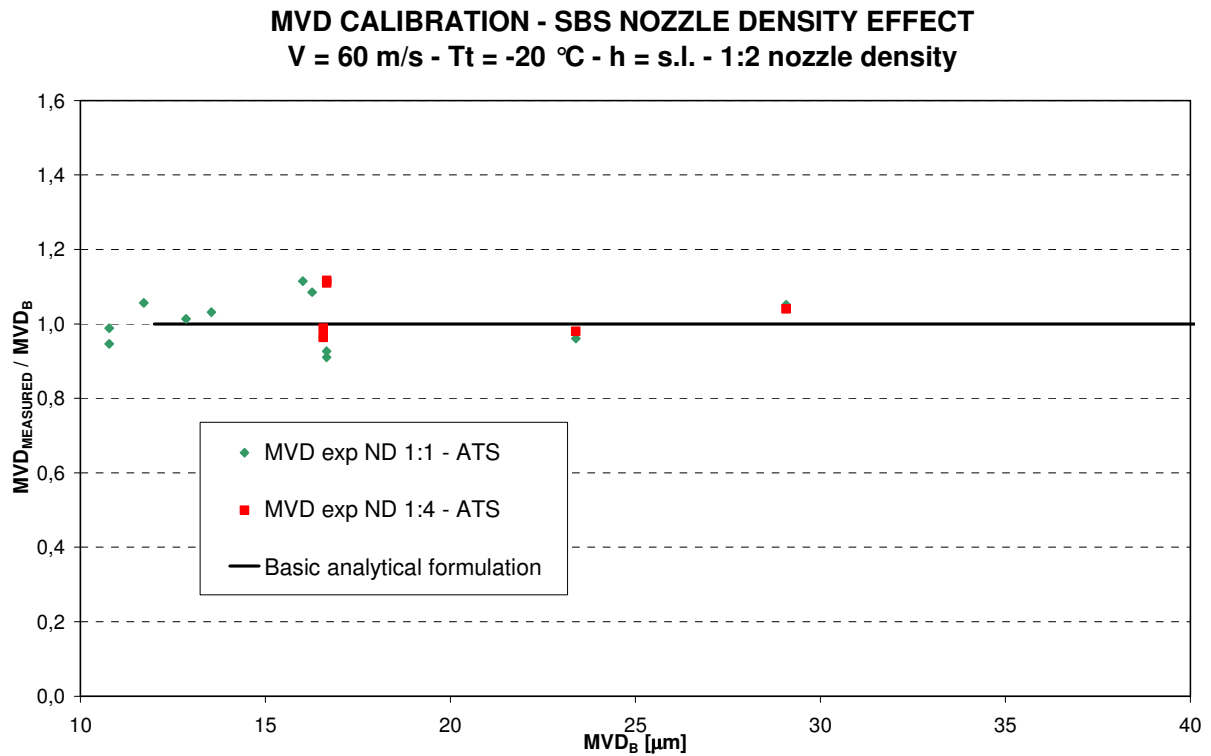


Fig. 8.32: Temperature effect on the MVD



**Fig. 8.33:** SBS nozzle density effect on the MVD

By analyzing the graphs 8.32 and 8.33, it can be said that nozzle density and temperature effect are negligible for the ATS configuration. Indeed, the ratio between the experimental MVD values in not-standard conditions and the MVD values in standard conditions is about 1. The only correction taken into account is the one related to the static pressure (figure 8.31). The correction is, as expected from STS results, on the order of 30% at 6000 meters of simulated altitude.

Finally velocity effect has not been considered for the ATS due to:

- reduced envelope of possible velocity (ranging from about 20m/s up to 90m/s)

- STS velocity effect going from 90m/s to 140m/s already turned to be quite small.

### **8.2.2 SBS temperature assessment**

Procedures followed exactly the same steps than the STS. Also in this case, tests are documented reporting the ice characteristics on the three cylinders along with their pictures.

Tests were performed at three different static temperatures. One such that the total temperature was close to 0°C, a test series at -10°C as static temperature and another at -20°C.

The velocity at which tests have been performed were 2:

- $V = 30 \text{ m/s}$
- $V = 60 \text{ m/s}$ .

The MVD was always around 20  $\mu\text{m}$ .

Also in this case results showed that, in general, a basic good droplets thermal stabilization is present in the test section (also thanks to the very long contraction see chapter 7). The SBS supply temperatures effects have been mostly estimated looking at the quantity of accumulated ice, consistency, transparency and adherence of the ice, rather than the horns positions.

Table 8.1 reports test performed whereas figure 8.34 gives the temperature envelope within which the SBS releases supercooled droplets.

RECORDING			WIND TUNNEL CONDITIONS				SPRAY BAR CONFIGURATION				CLOUD CONDITIONS		Cylinder 1		Cylinder 2		Cylinder 3	
N	Test	Pol.	V [m/s]	T [°C]	HR [%]	h [m]	Pwat [bar]	Tair [°C]	Twat [°C]	N nozz	MVD [µm]	LWC [g/m³]	beta up	beta down	beta up	beta down	beta up	beta down
1	1437	28	60	-2	100	s.l.	1,00	40	20	289	18,00	0,50	30-60	30-60	30-60	30-60	30-60	30-60
2	1437	30	30	-0,6	100	s.l.	1,00	40	20	289	18,00	1,00	15-60	15-60	15-60	15-60	15-60	15-60
3	1438	3	60	-2	100	s.l.	3,00	40	20	289	20,00	1,50	30-60	30-60	30-60	30-60	30-60	30-60
4	1438	5	60	-10	100	s.l.	1,00	40	20	289	18,00	0,50	45-60	30-60	30-45	45-60	30-60	30-60
5	1438	7	60	-10	100	s.l.	1,00	70	50	289	18,00	0,50	45-60	45-60	30-45	45-60	30-45	45-60
6	1438	14	60	-10	100	s.l.	1,00	100	75	289	20,00	0,50	60	60	60	60	60	60
7	1438	16	60	-20	100	s.l.	1,00	125	85	289	20,00	0,50	N.A.	N.A.	N.A.	N.A.	N.A.	N.A.
8	1438	18	60	-10	100	s.l.	3,00	70	50	289	20,00	1,50	60	60	60	60	60	60
9	1438	20	60	-10	100	s.l.	3,00	100	75	289	20,00	1,50	60	60	60	60	60	75
10	1438	22	60	-10	100	s.l.	3,00	40	20	289	20,00	1,50	N.A.	N.A.	N.A.	N.A.	N.A.	N.A.
11	1438	24	60	-20	100	s.l.	3,00	125	85	289	20,00	1,50	N.A.	N.A.	N.A.	N.A.	N.A.	N.A.
12	1438	26	60	-2	100	s.l.	1,00	40	20	289	20,00	0,50	45	45-60	30	30-45	30-45	30-45
13	1438	28	60	-4	100	s.l.	1,00	40	20	289	20,00	0,50	45-60	30-45	45-60	45-60	45-60	30-45
14	1438	31	30	-0,6	100	s.l.	3,00	40	20	289	20,00	1,50	30-60	30-75	30-60	30-60	30-75	30-60

**Table 8.1:** test condition for SBS temperature assessment

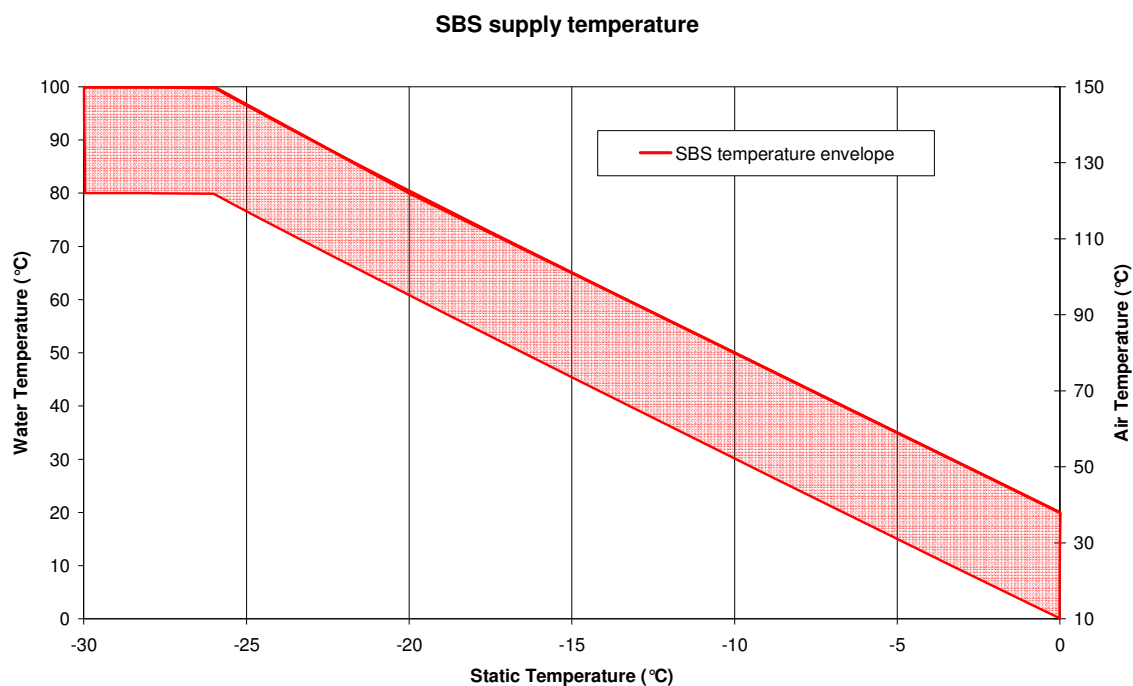


**Fig. 8.34:** SBS supply temperature

### 8.2.3 Icing cloud uniformity and coverage area

Several different SBS configurations have been tested, corresponding to three different nozzle densities during the spraying.



- 1:1 nozzle density grid;
- 1:2 nozzle density grid;
- 1:4 nozzle density grid.

Figures 8.35 to 8.40 report the relative ice thickness accreted on the grid, normalized to the value at the section -180 mm of the test section rather than the one usually taken at the very centre of the TS itself. This has been decided after it has been seen that somewhat for the ATS tunnel configuration the centre area occasionally suffers of light lack of cloud uniformity. The black grid points in the pictures are the real measurement points. Ice thicknesses were measured in a large region: 12 rows (from -655 mm to 845 mm) by 23 columns (from -1680 mm to 1620 mm) were interested by the measurements (276 measurements points). This corresponds to roughly 60% of the test section surface. The optimization is considered satisfactory when the uniformity target of  $\pm 20\%$  in the reference area is achieved.

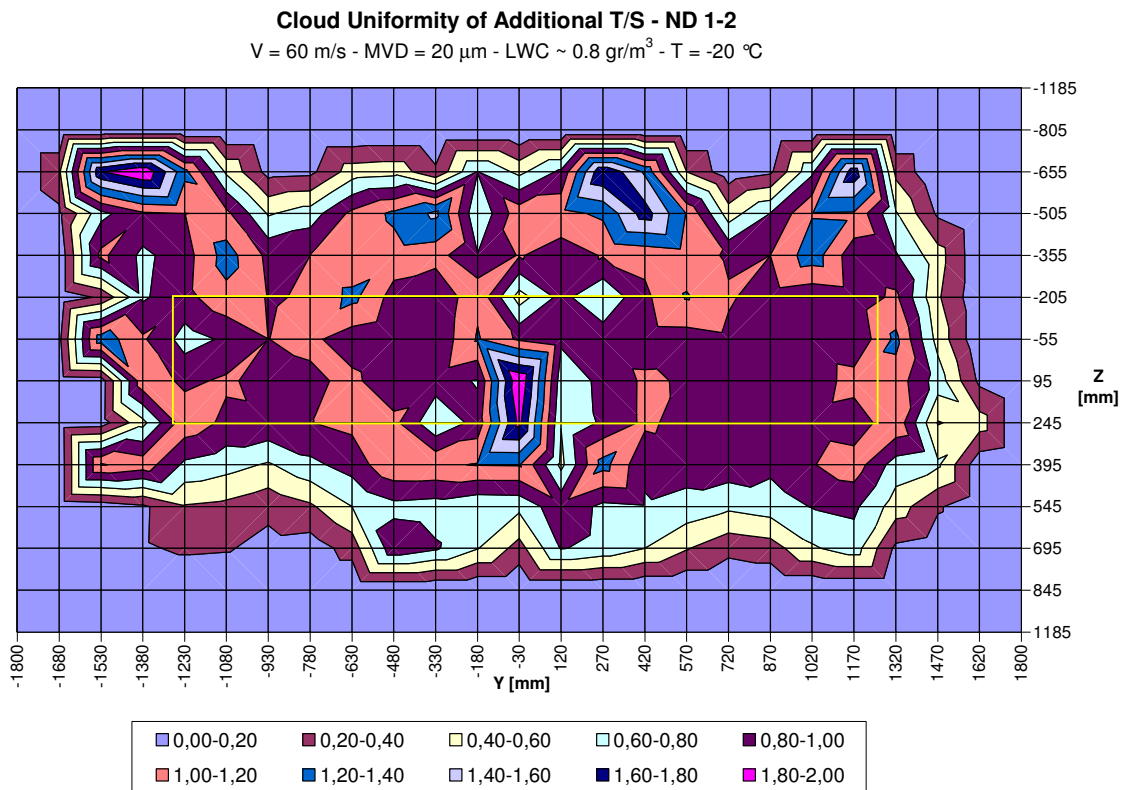
Figure 8.35 shows the optimized uniformity for a ND 1:2. This figure clearly shows that somehow at the centerline there is apparently no good uniformity while over a very large area of the test section the uniformity is remarkable. Several nozzles configuration have been tested in the central region in order to improve this result. Unfortunately none of them really turned in a better central uniformity.

Fig. 8.36 shows for the same ND 1:2 but for a higher LWC a noteworthy uniformity. Still, at the centre of the TS there is a small area where a lack of ice accretion persists, although can be definitively considered negligible. No real explanation has been found for this odd behavior of the cloud at the centre of the TS. It has to be reminded that, for this kind of tests the transient plays an important role in the final result as due to

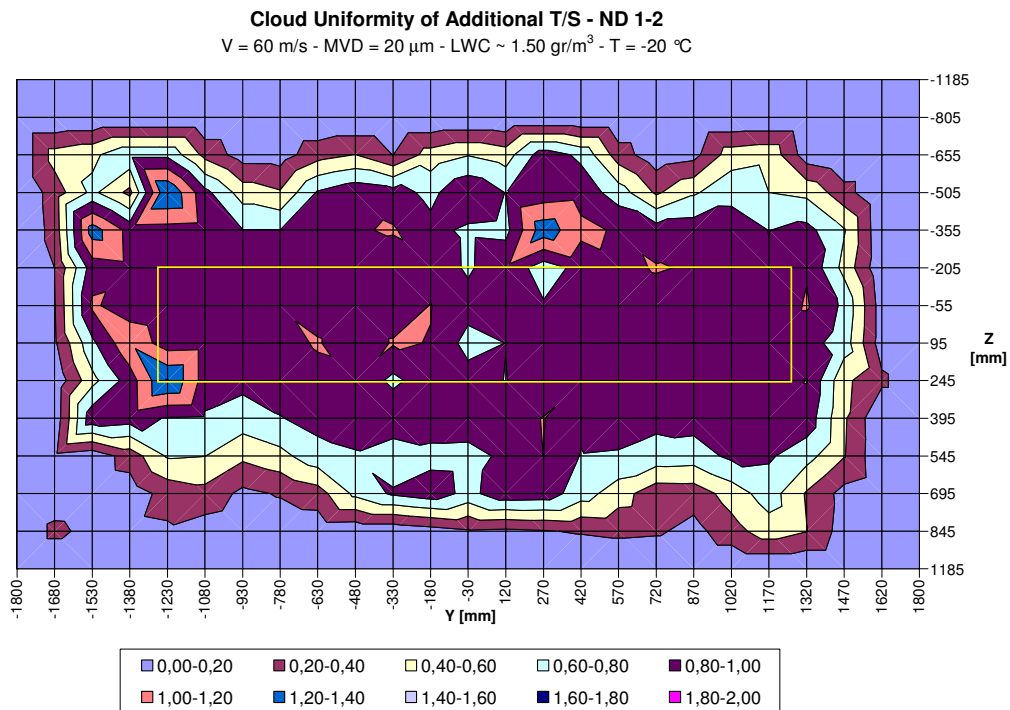
blockage problems, the test has to be short (approximately the time needed to have three mm of ice accretion on the grid). Therefore a better uniformity might be expected in a longer test being in this case the transient negligible.

Figure 8.37 shows an optimization obtained for a high value of the LWC using a ND of 1:1. Uniformity looks very good. This test has also been repeated in order to show the repeatability of the test and the obtained result shown in figure 8.38, is in a very good agreement with the previous one. Figure 8.39 shows the optimized results for a ND of 1:1 and a very high LWC (higher than 5 g/m<sup>3</sup>). In this case a lack of ice accretion is present on the left part of the picture. Even in this case a rather better result might be expected with longer testing time [23].

Figure 8.40 represents the optimized result for a ND 1:4. The shown result can be considered satisfactory in the reference area.



**Fig. 8.35:** Cloud uniformity assessment at low LWC. Nozzle density 1:2



**Fig. 8.36:** Cloud uniformity assessment at medium LWC. Nozzle density 1:2

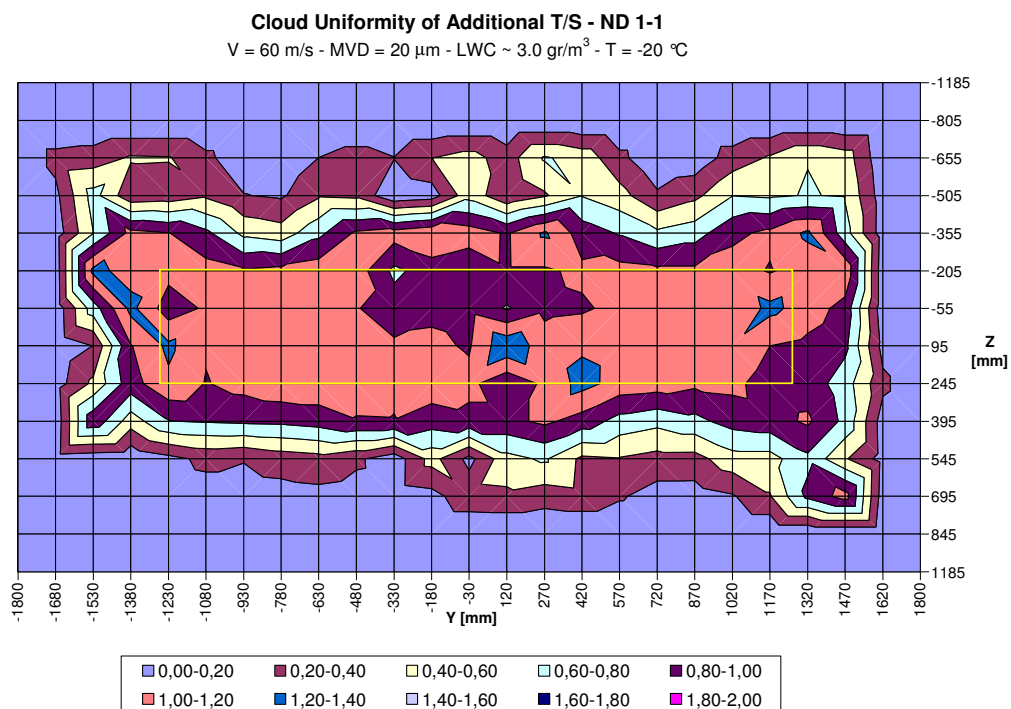


**Fig. 8.37:** Cloud uniformity assessment at high LWC. Nozzle density 1:1

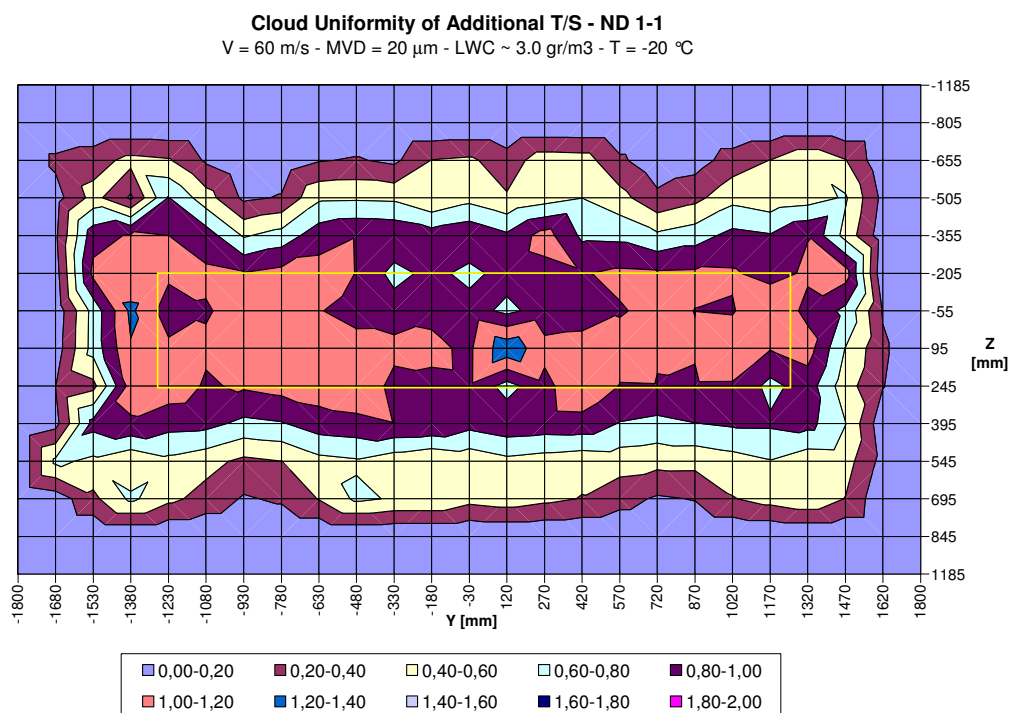


**Fig. 8.38:** Cloud uniformity repeatability at high LWC. Nozzle density 1:1

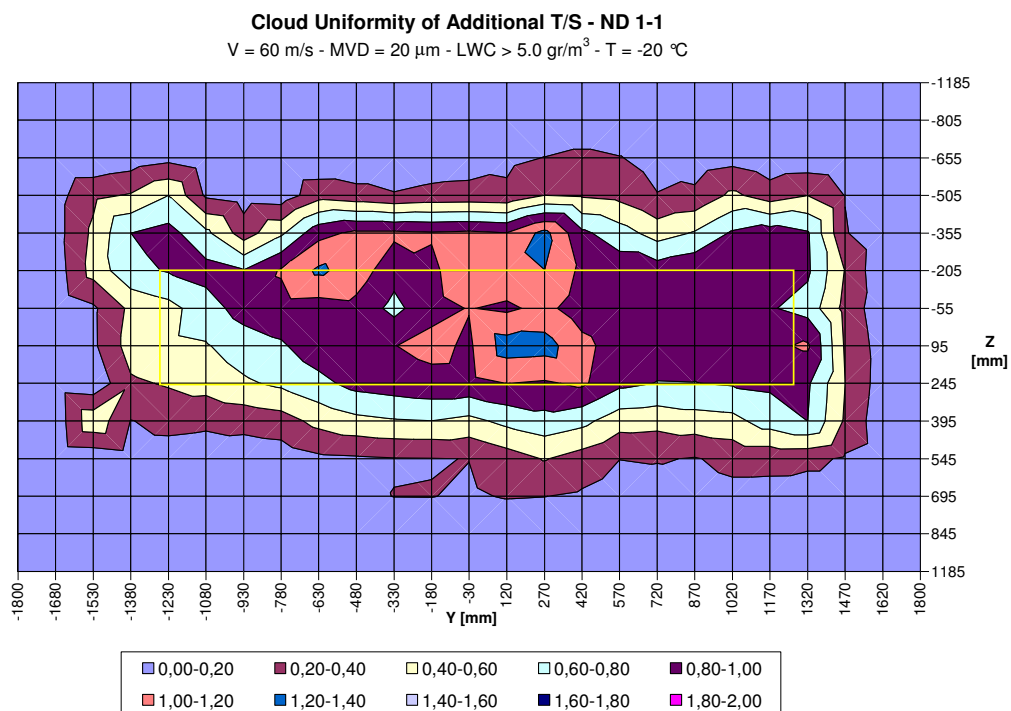


**Fig. 8.39:** Cloud uniformity assessment at very high LWC. Nozzle density 1:1

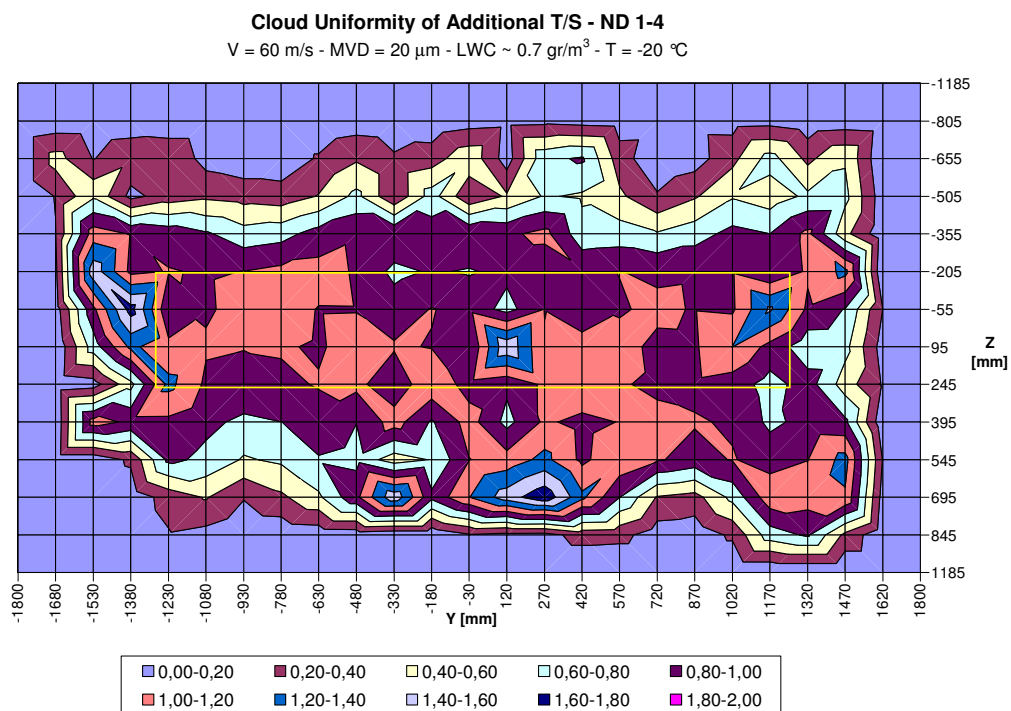


**Fig. 8.40:** Cloud uniformity assessment at medium LWC with different nozzle density (1:4)

### 8.2.4 Liquid Water Content measurements

As for the STS the standard IB technique has been used for these tests. The blade has been installed -150 mm far from the centre line toward the control room side (see fig. 8.41). This position has been chosen after the uniformity optimization phase in order to place the blade itself in a region of better uniformity (figure 8.42). Indeed the centre point of the test section in some cases showed an area of not perfect uniformity if compared to the rest of the grid as previously explained.

During the calibration 55 test points were measured at three different airspeed (30 m/s, 60 m/s and 80 m/s) and four spray nozzles density configurations (1:1, 1:2, 1:4 and 1:8). Further also the altitude effect was investigated for both 20 µm and 30 µm droplet size.

Figure 8.43 shows the result of LWC measurements performed at  $V = 60$  m/s with 1:2 spray nozzles configuration and for droplet size ranging from 20 µm to 40 µm. The SBS water pressures were ranged from 20 kPa to 500 kPa. Using the least square error method, the following equation was found to fit the measured LWC data:

$$LWC_{base} = a + b \cdot \ln(P_w) + c \cdot MVD + d \cdot \ln(P_w)^2 + e \cdot MVD^2 + f \cdot \ln(P_w) \cdot MVD$$

with a, b, c, d, e, f, constants.

To evaluate the effect of a different nozzles density, four different SBS configurations were taken into account. Figures 8.44 to 8.46 show, for fixed wind tunnel and SBS conditions, the LWC with respect to 1:8, 1:4 and 1:1 spray nozzles density.

Taking the 1:2 spray nozzles configuration as the reference one, it is clear from the graph that the LWC changes roughly with a ratio of 2 doubling the nozzles density,

decreases with a ratio of  $\frac{1}{2}$  with the configuration of 1:4 active nozzles and it goes to  $\frac{1}{4}$  with the 1:8 nozzles density configuration.

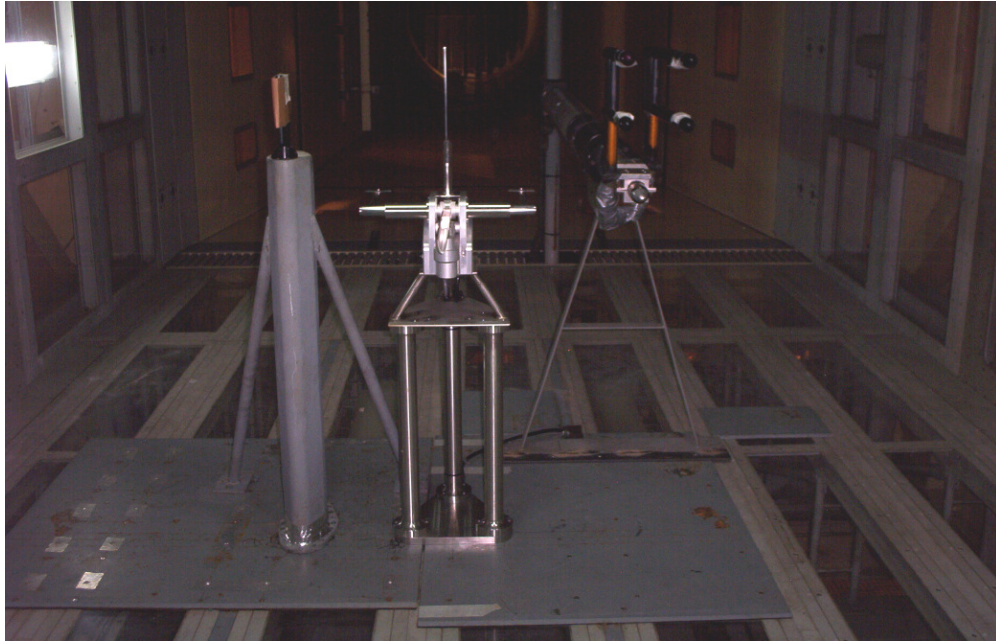
Figure 8.47 shows the velocity effect. A law that well fit the LWC behavior as function of  $V$ , has been found to be roughly:

$$LWC_{V_2} = LWC_{V_1} * \left(\frac{V_1}{V_2}\right)^c$$

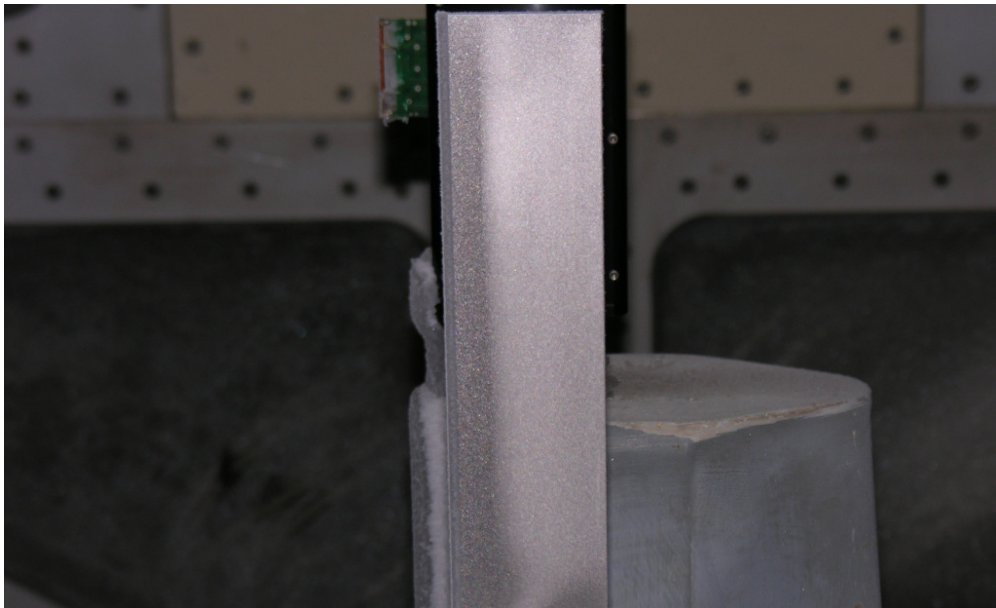
Where  $LWC_{V_1}$  is the one taken as reference (in our case LWC at  $V = 60$  m/s).

Figure 8.48 shows the altitude effect for which a different procedure has been applied: instead of keeping constant the air and water pressure, it has been decided to keep constant the water pressure and the MVD (known the effect of the altitude on the MVD itself). It was found that, unlike the STS case, an increase in LWC occurred due to the static pressure influence.

The results of the comparison between the IB LWC values and those calculated by the analytical formulation can be seen in figure 8.49, where it is shown that 69% of the data lie within  $\pm 10\%$  boundaries whereas about 97% of them lie between the  $\pm 20\%$  errors band.



**Fig. 8.41:** Icing blade location in ATS



**Fig. 8.42:** Icing blade after a test



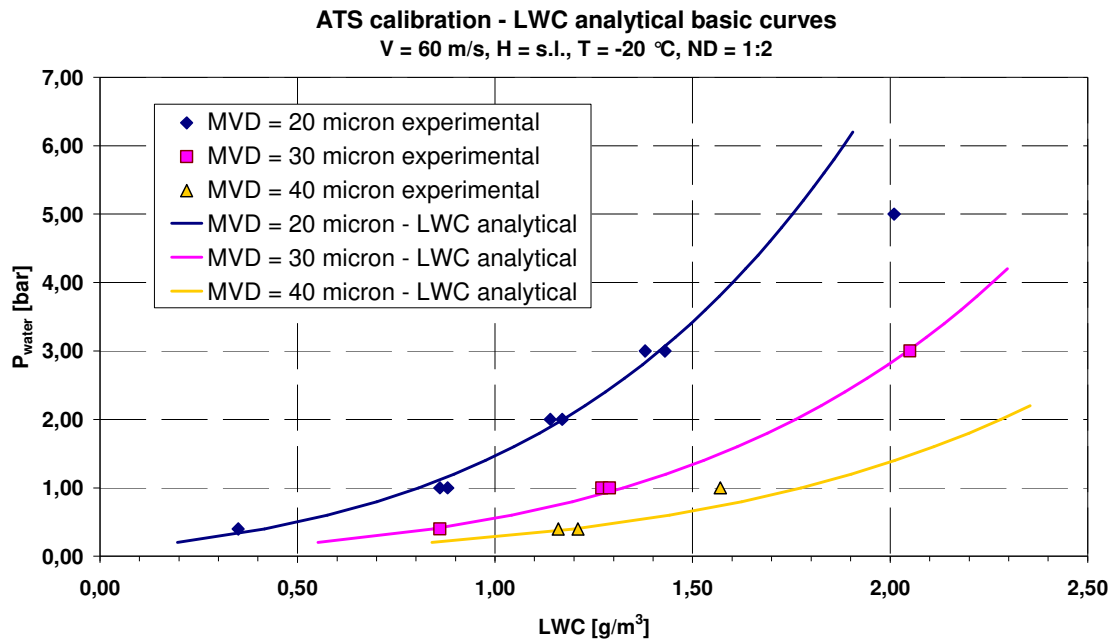


Fig. 8.43: LWC calibration curves at different MVD

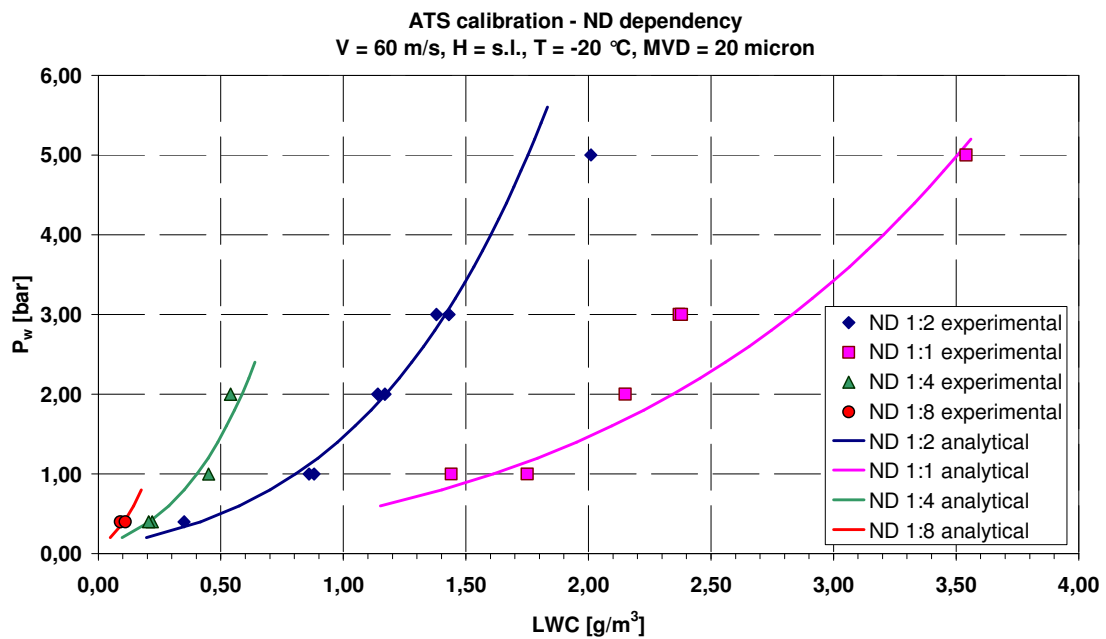
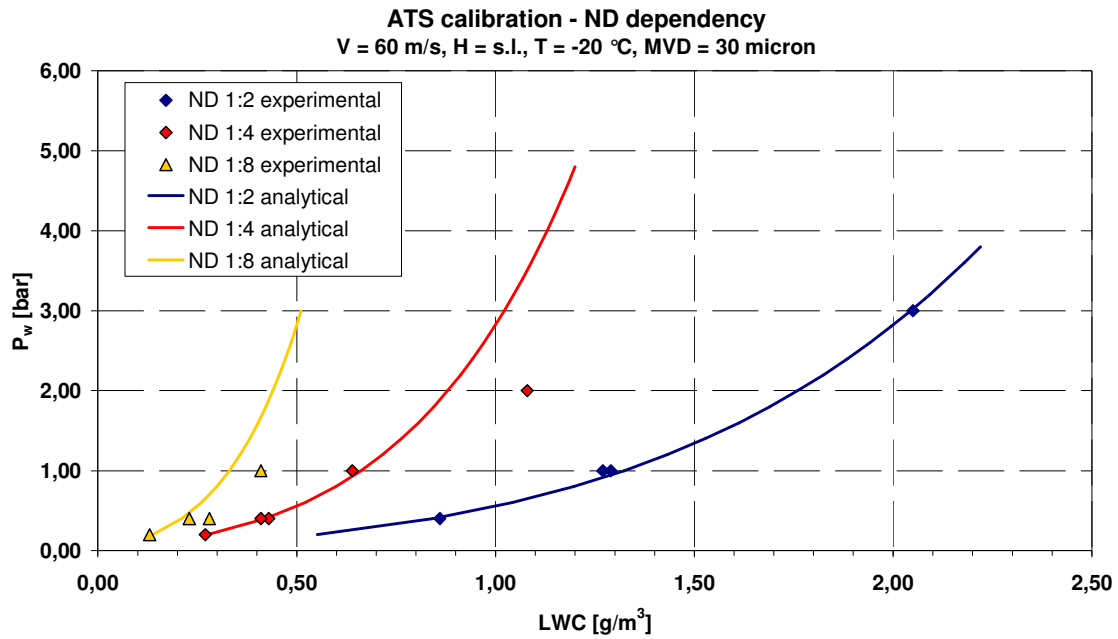
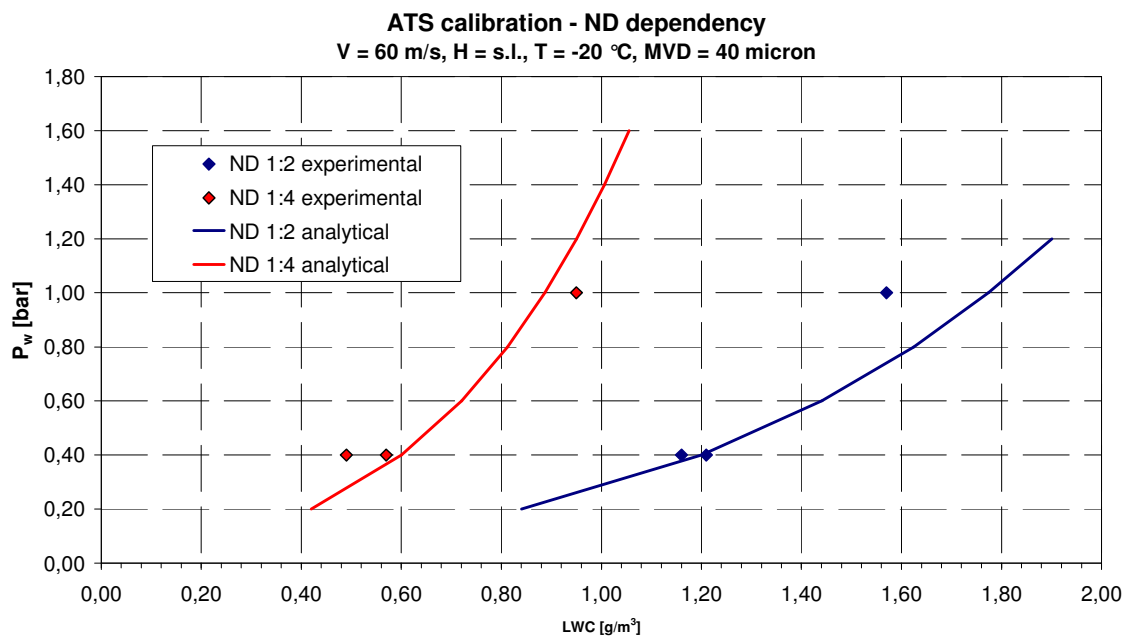


Fig. 8.44: LWC calibration curves at different nozzle density at 20  $\mu\text{m}$



**Fig. 8.45:** LWC calibration curves at different nozzle density at 30  $\mu\text{m}$



**Fig. 8.46:** LWC calibration curves at different nozzle density at 40  $\mu\text{m}$

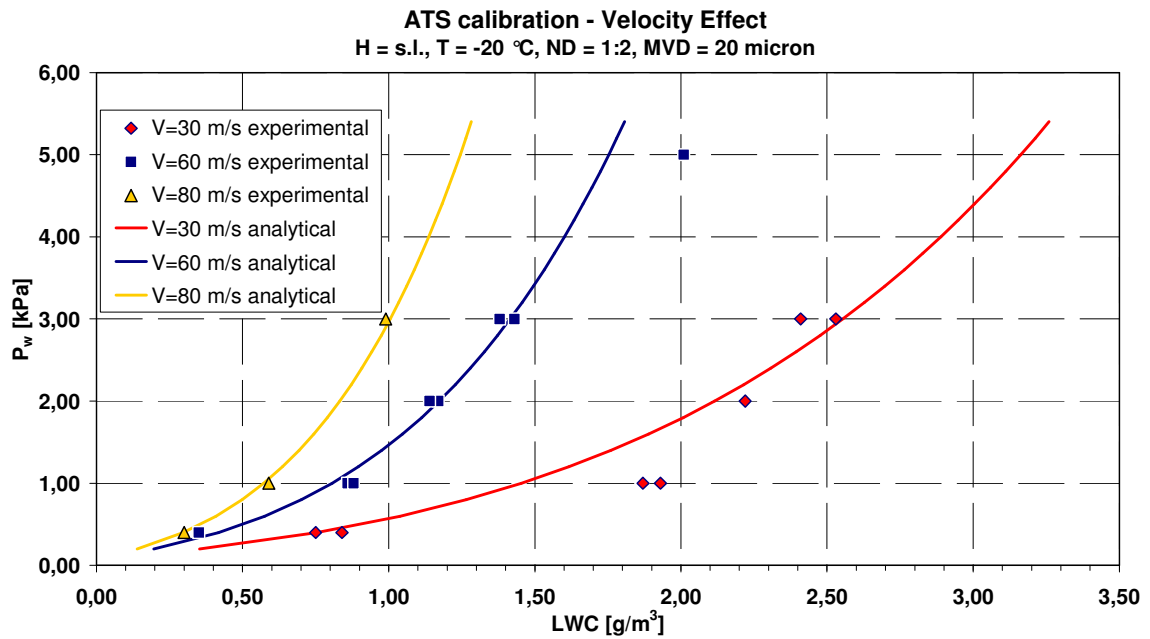


Fig. 8.47: LWC calibration curves at different velocities at 20  $\mu\text{m}$

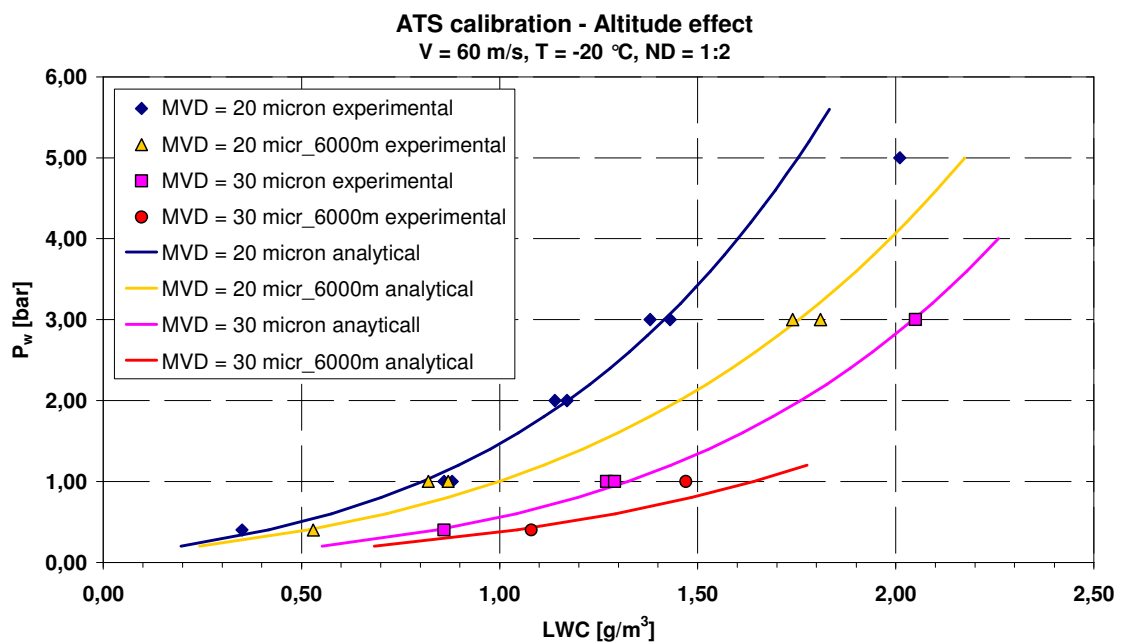


Fig. 8.48: LWC calibration curves at different altitude

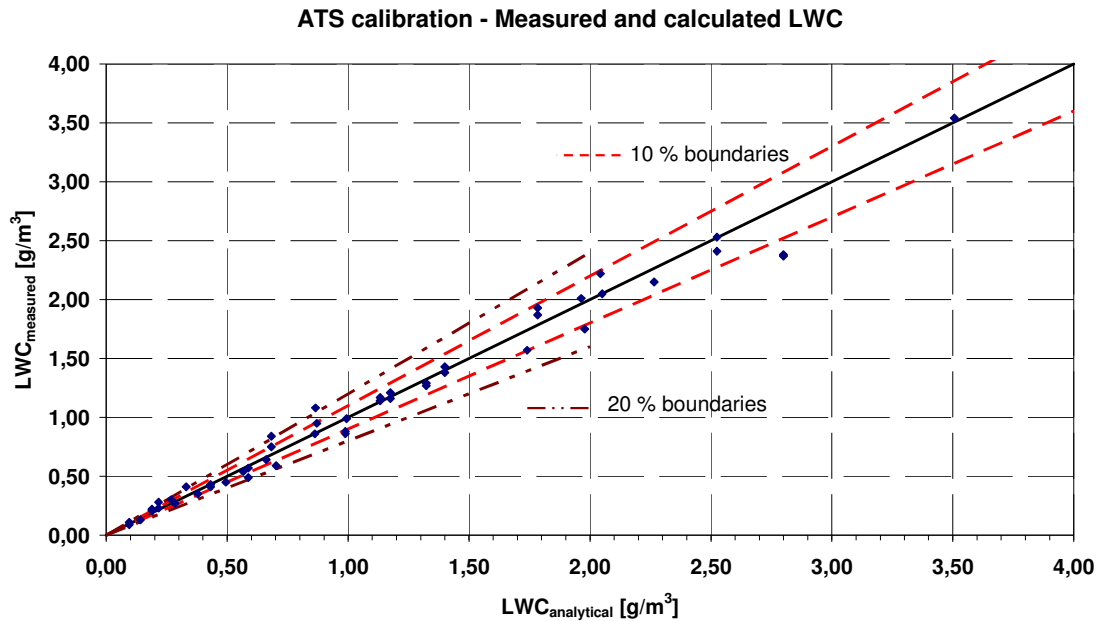
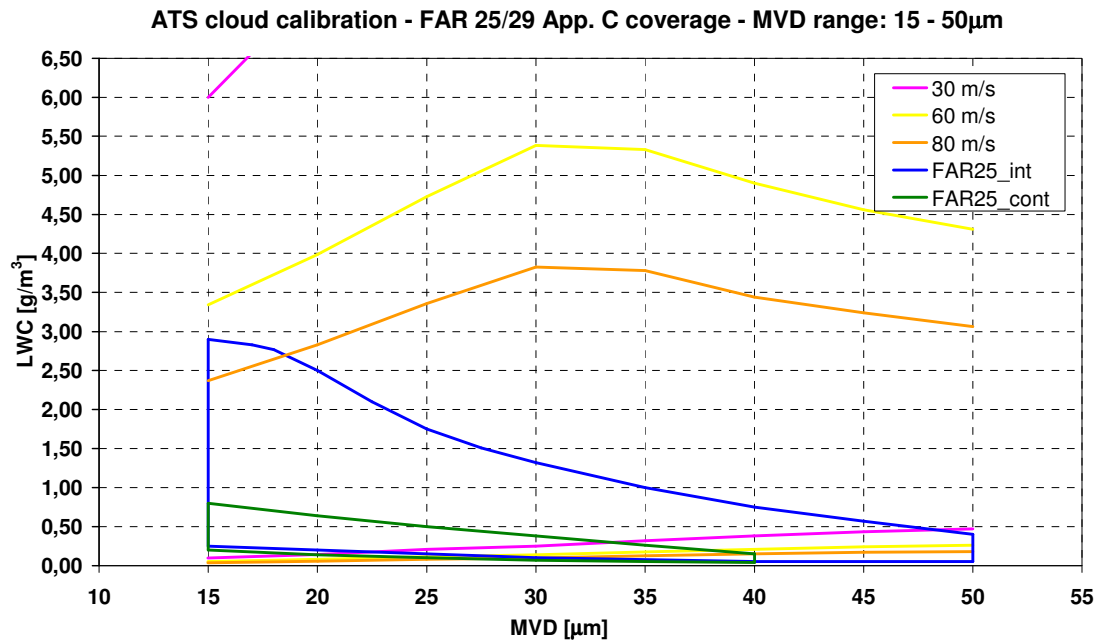


Fig. 8.49: LWC interpolation error

### 8.2.5 Icing cloud operative envelope

Figure 8.50 shows the ATS cloud envelope within the 15-50  $\mu\text{m}$ . The envelope was obtained considering the 'basic' test conditions ( $T_s = 0^\circ\text{C}$ ,  $h = 0\text{ m}$ ); differences can occur at different static pressures (altitude). On the other side is clearly shown the effect of the velocity on the envelope itself.

Finally also in the case of the ATS a remarkable coverage is obtained for the two FAR icing envelopes.



**Fig. 8.50:** LWC – ATS Spray Bar envelope versus FAR 25/29 App. C certification criteria

## 8.3 DATA COMPARISON

### 8.3.1 MVD Data Comparison: basic analysis

Analytical formulation for ATS and STS have been already reported in sec. 8.1.1 and 8.2.1, whereas figures 8.51, 8.52, showing MVD data for STS and ATS respectively, are reported again along with MTS data [22] in figure 8.53. Looking at the three different charts, it can be stated that qualitatively they are in good agreement. Also some more information can be extrapolated by looking at the red arrows added to the figures. For the STS the maximum MVD is well above the minimum target of 50  $\mu$ m (54  $\mu$ m) already at  $\Delta p$  equal to 0.25 bar and for a  $P_{\text{water}}$  of 0.4 bar. This result is quite different from the one obtained for the ATS where for the same  $P_{\text{water}}$  and the same  $\Delta p$  the MVD released by the SBS is of about 35  $\mu$ m. If it is considered the right side of pictures 8.51 and 8.52, given  $P_{\text{water}}$  of 7 bars and  $\Delta p$  equal to 2.5 bars in the center of the STS it has

been measured about 20  $\mu\text{m}$  while in the ATS for the same conditions the result turns to be less than 14  $\mu\text{m}$  in MVD. This result can be explained considering the different dimension of the two test sections and the diverse kind of mixing obtained within the single spraying nozzle cone. Figure 8.54 qualitatively shows the projection of a single nozzle spraying cone. The area of influence for each nozzle is much larger in the ATS than in the STS (it is expected to be approximately three times larger as the ratio between ATS and STS size). Therefore in the STS the mixing and droplets coalescence is most likely to happen and this explains why MVD are larger in average.

Finally the MTS data have been compared with the STS and ATS ones and they have been found in agreement with what here above reported. For example for SBS condition of  $P_{\text{water}}$  equal to 7 bar and  $\Delta p$  of 2.5 bars, the MVD is approximately 18  $\mu\text{m}$ , perfectly in between the 14  $\mu\text{m}$  and the 20  $\mu\text{m}$  of the ATS and STS. It is also important to remark that all the measurements have been performed approximately at 66% of the maximum possible velocity (free stream) for each test section. This allow data to be easily comparable although, particularly for large droplets, does not insure that any possible dynamic effect, can be always considered roughly the same [25].

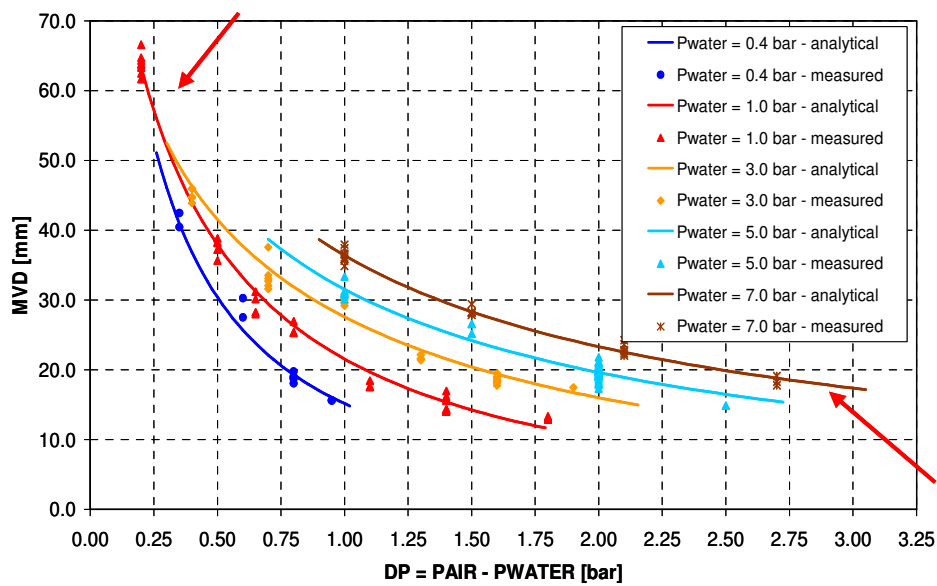


Fig. 8.51: STS MVD experimental values.

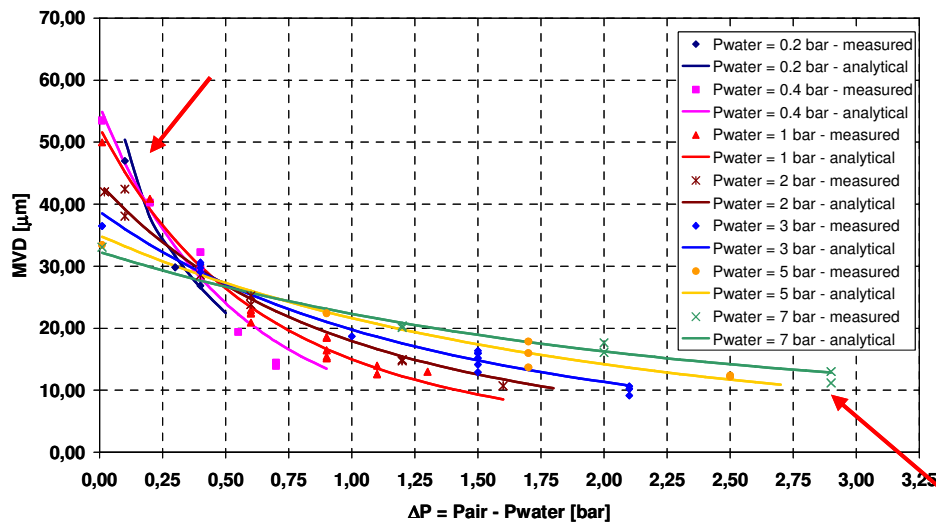


Fig. 8.52: ATS MVD experimental values

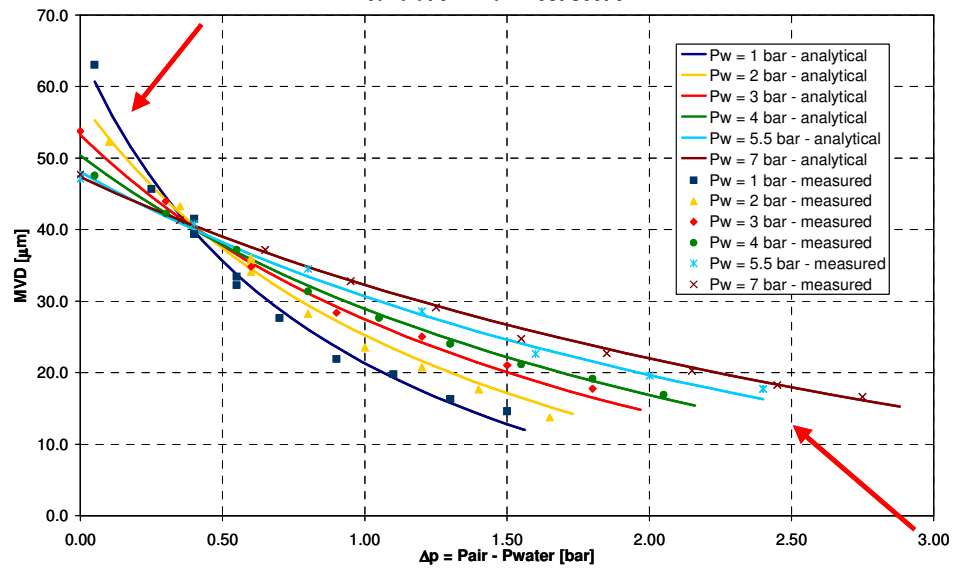
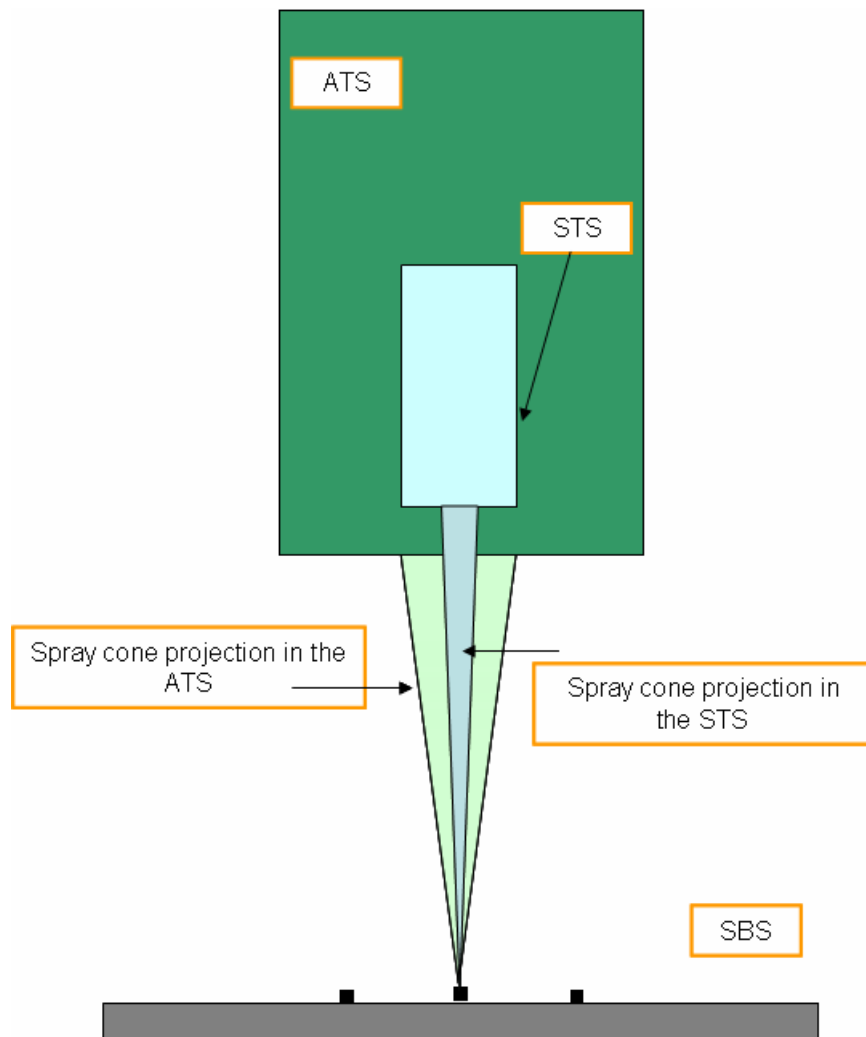


Fig. 8.53: MTS MVD experimental values





**Fig. 8.54:** Spray cone projection in STS and ATS

### **8.3.1 MVD Data Comparison: thermodynamic effects**

Altitude and temperature effects have been investigated as shown in sec. 8.1.1 and 8.2.1. In this section STS and ATS data are compared and shown in figure 8.55 and 8.56 for altitude and temperature effect respectively. As it can be seen data are coherent in both cases and it can be assessed that both altitude and temperature effect are “Test Section” independent. Specifically while temperature effect can be considered negligible, altitude (static pressure) has a quite strong impact on measurements that can be estimated to be around 30% in MVD reduction.

Being Test Section independent, these effects might be included in the MTS cloud characterization equations although these kinds of measurements were not taken at the time that test section was investigated. Of course, this effect will have to be confirmed by direct measurements in the MTS.

Finally more measurements in the range of 35-50  $\mu\text{m}$  shall be taken in the future to better assess altitude and temperature effect in that region; however no drastic differences with what measured so far are expected.

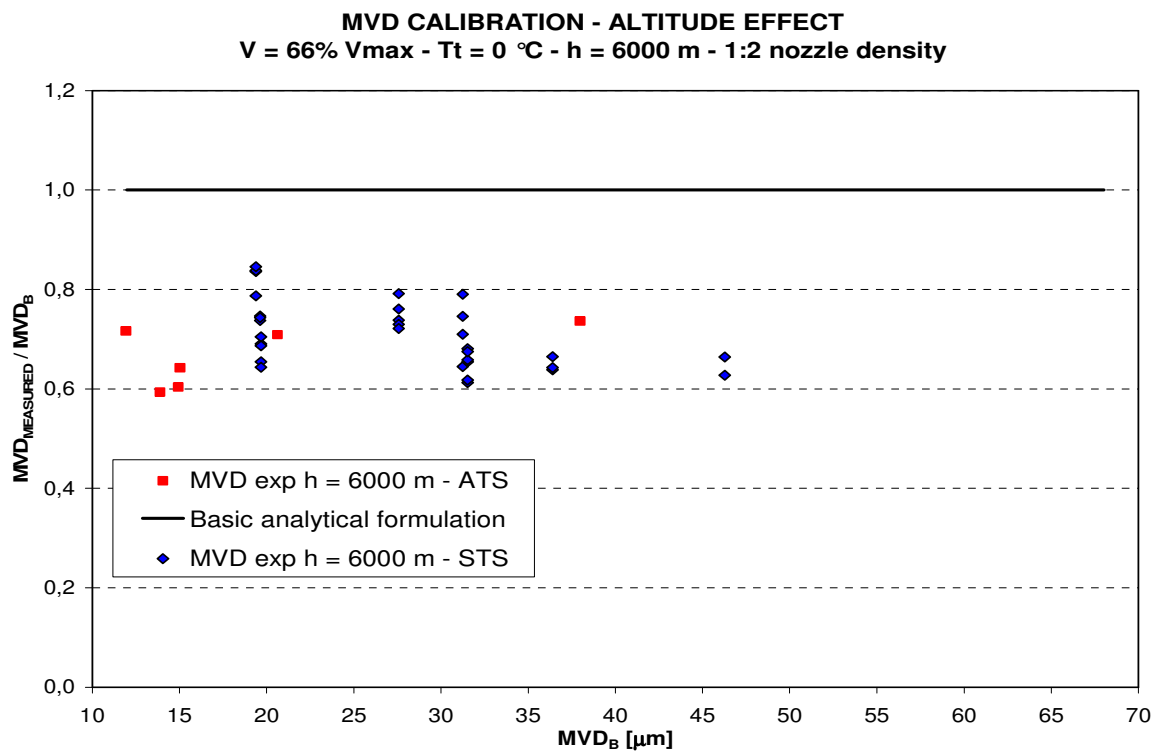


**Fig. 8.55:** STS and ATS altitude effect

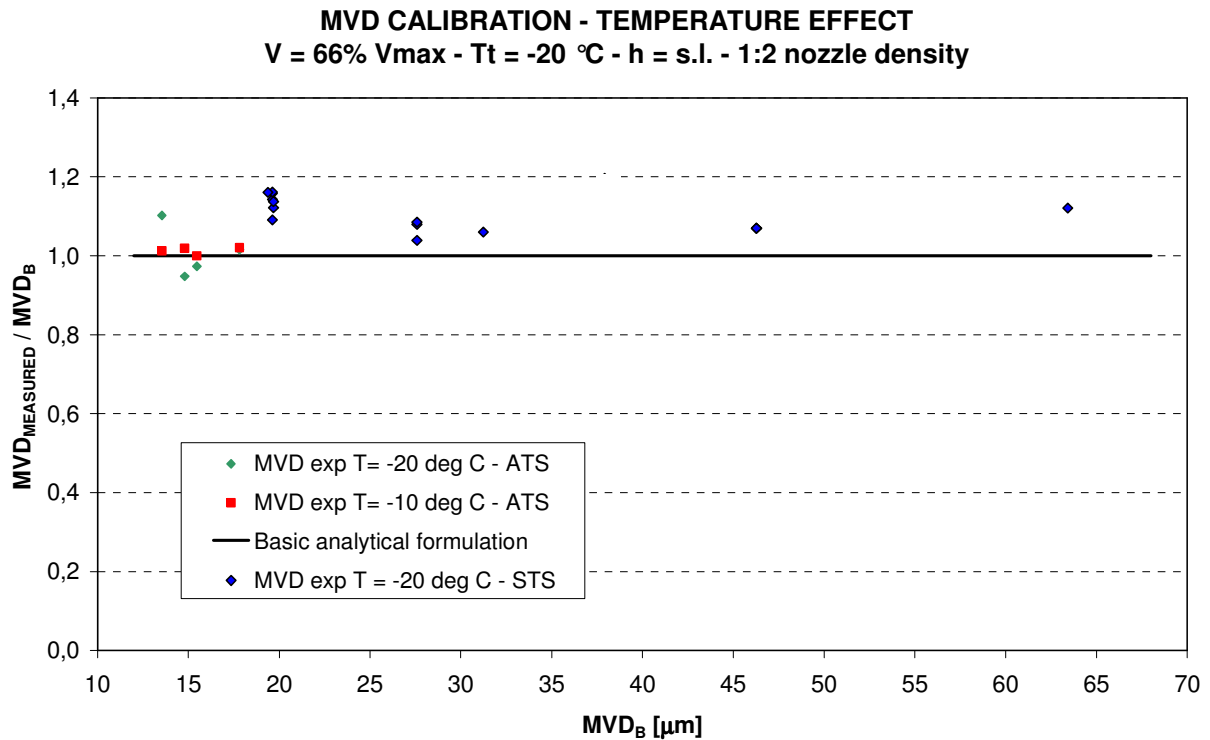


Fig. 8.56: STS and ATS temperature effect

### 8.3.2 MVD Data Comparison: Fluid Dynamic effects

Velocity and SBS spray nozzle density effects have been investigated as shown in sec. 8.1.1 and 8.2.1. In this section STS and ATS data are whenever possible compared, and they are shown in figure 8.57 and 8.58 for velocity and nozzle density effect respectively.

Figure 8.57 reports only STS velocity effect data. Data in the ATS were actually not collected since, as already stated, the ATS velocity envelope did not justify this effort also given the results previously obtained for the STS. Indeed, in the range 90-140 m/s only a small dynamic effect is observed (MVD are increasing by about 10% going from 90 to 140 m/s). MTS data for this effect are also missing and therefore no other

observation can be made; the MTS it is however expected to behave as the STS for the same range of velocity (90-140 m/s) or better (no/negligible velocity effect) due to the lower contraction ratio.

Figure 8.58 shows the result of the SBS spray nozzle effects on both ATS and STS. The effect can be easily explained considering the interaction between spraying nozzles that increases as the nozzle density increases. Figure 8.59 explains nozzle interaction giving an idea of the process that can be used to explain chart 8.58.

MTS data are missing and therefore comparison can not be done, however nozzle density is expected to have a significant effect only when all the set of active nozzles is spraying simultaneously.

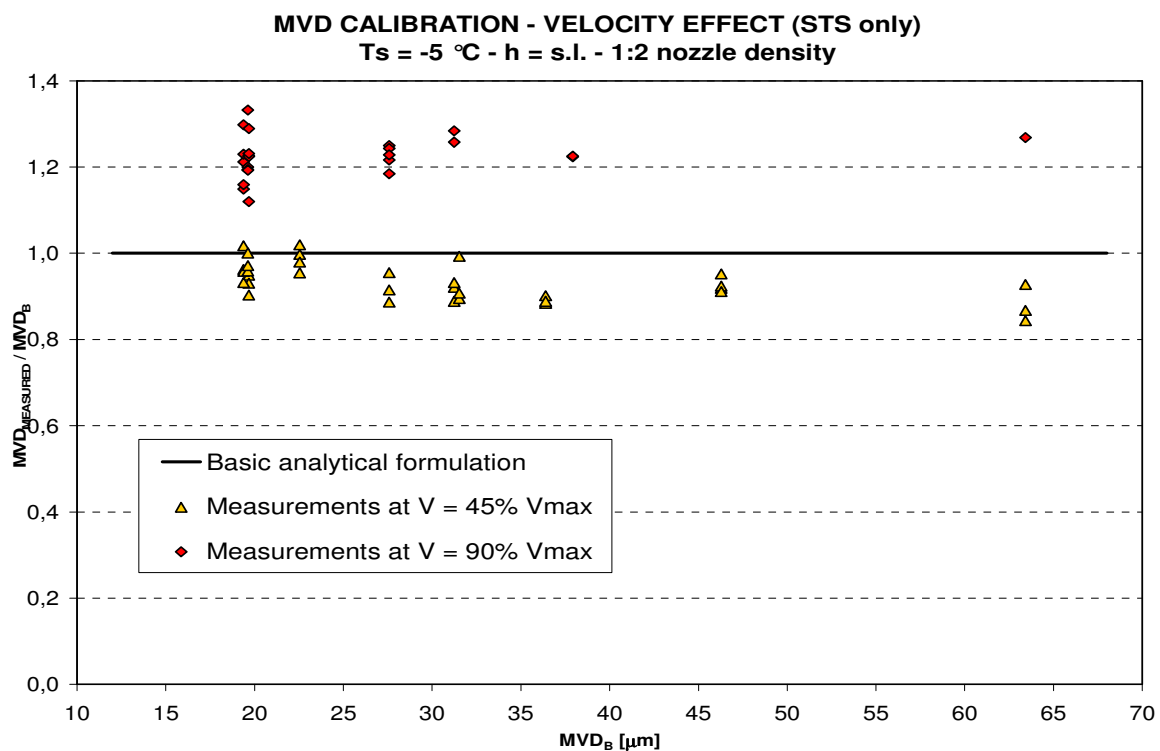
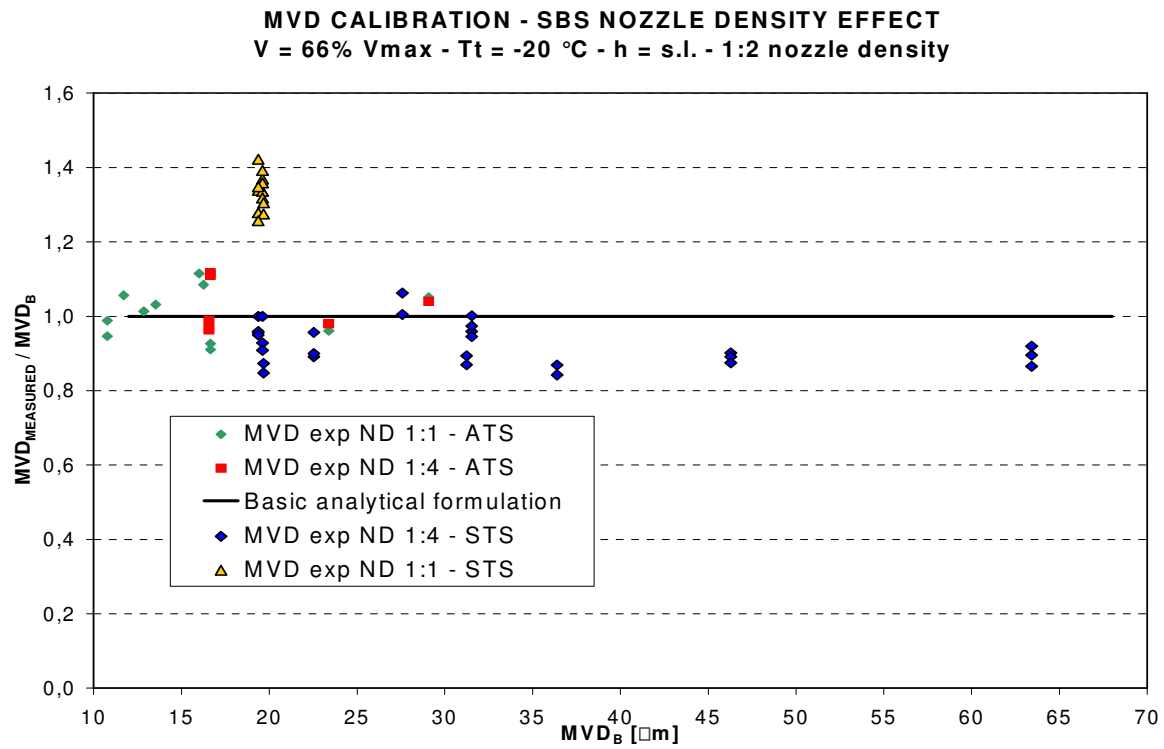
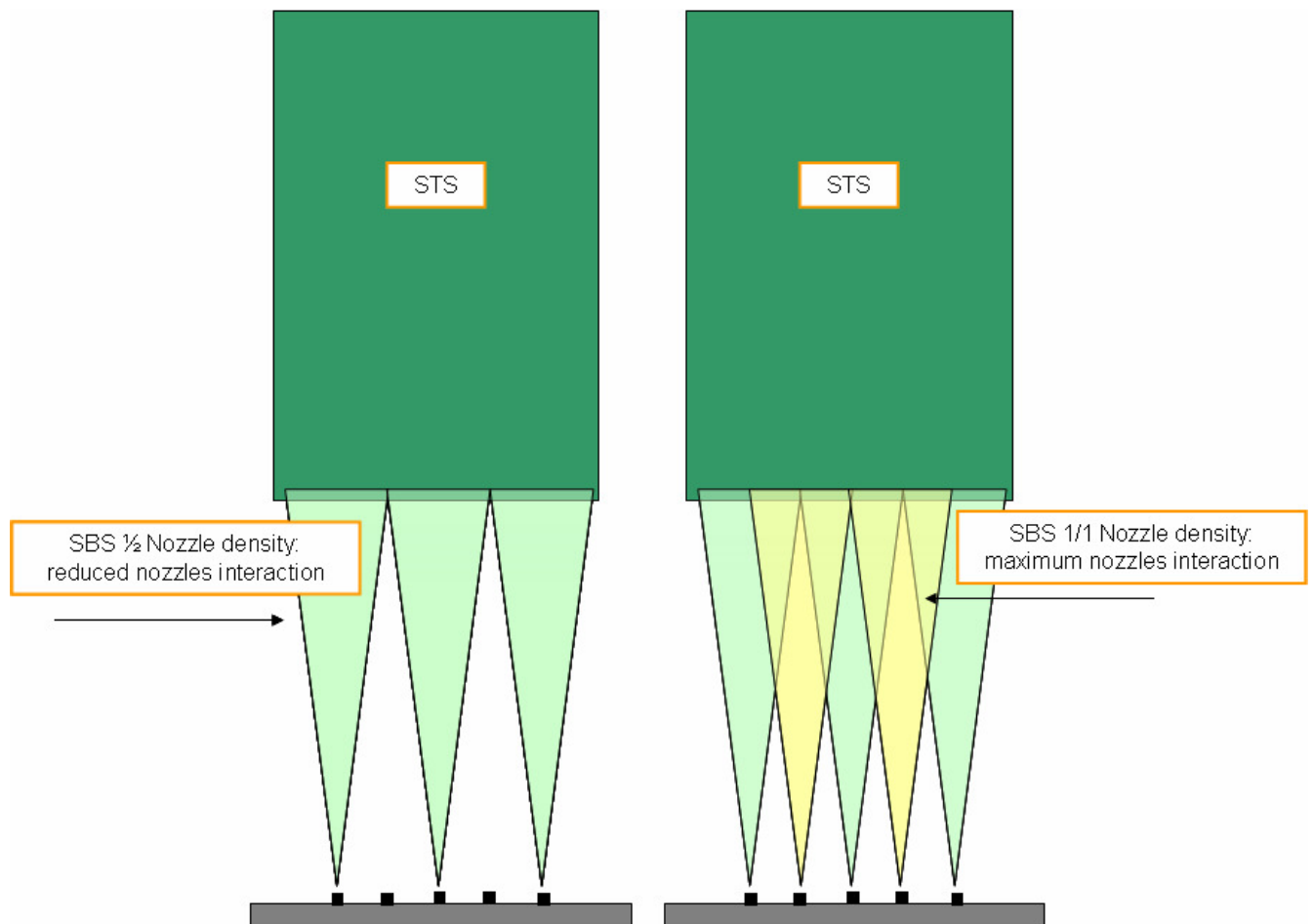


Fig. 8.57: STS velocity effect



**Fig. 8.58:** STS and ATS nozzle density effect



**Fig. 8.59:** Spray nozzles interaction in the case of the STS

### **8.3.3 SBS Temperature Envelope Comparison**

Tests and procedures for ATS and STS have been already reported in sec. 8.1.2 and 8.2.2. When comparing ATS and STS data as in figure 8.60, it is evident that data are coherent. The different behavior of the two test sections can be explained with the longer time needed for the droplets in the ATS to reach the center of the test section due to the different absolute velocities. Furthermore for fixed velocity (i.e. 66% of the maximum free stream velocity) and fixed static temperature, total temperature in the STS are well higher than the ones obtained in the ATS due to the higher values of Mach

number. The two effects qualitatively explain why, when generating droplets in the ATS, they need to be warmer if compared with the ones generated in the STS.

MTS data are missing although it is expected that data will fall between the STS and ATS ones.

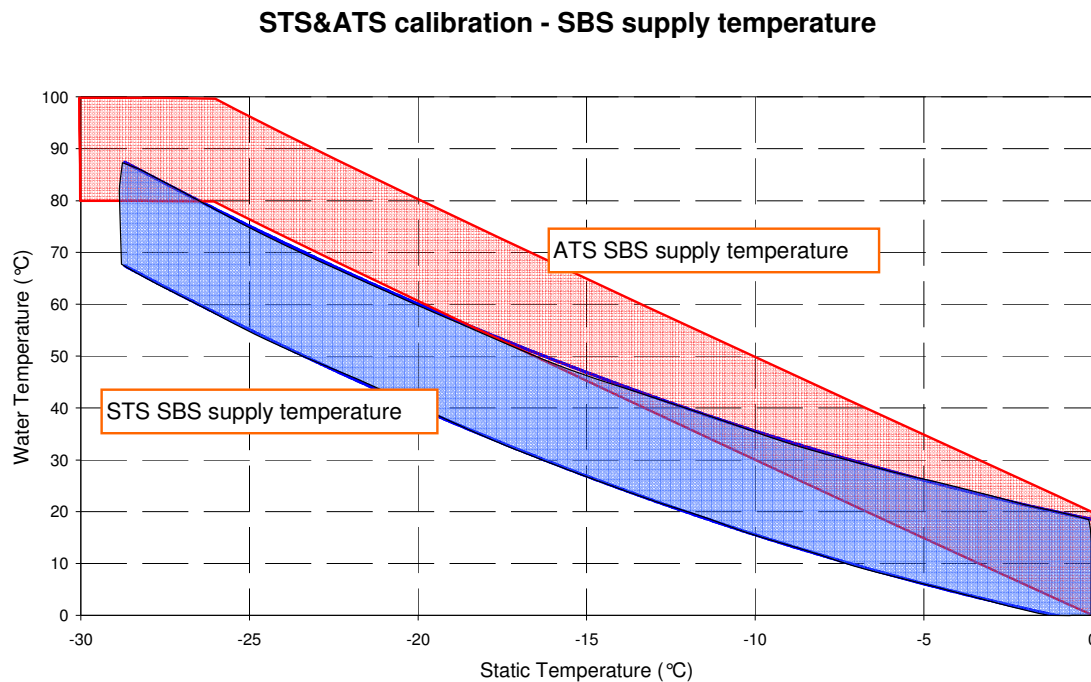


**Fig. 8.60:** STS and ATS SBS supply temperature comparison

### **8.3.4 Uniformity Measurements Comparison**

Data and procedures have been already explained in sections 8.1.3 and 8.2.3 for ATS and STS respectively. Data can not be directly compared due to the different tests sections dimensions, nevertheless some interesting consideration can be done as well.

Let is considered the influence of the SBS on flow turbulence. SBS vertical strut are located at about 50% of the horizontal mid-span (see figure 8.61), and they are well evident if it is considered turbulence level measured in the test section for both main flow field direction and for the orthogonal one. Figures 8.62 and 8.63 reports turbulence

level for the STS and ATS respectively (details on the aerodynamic measurements can be found in [24]).

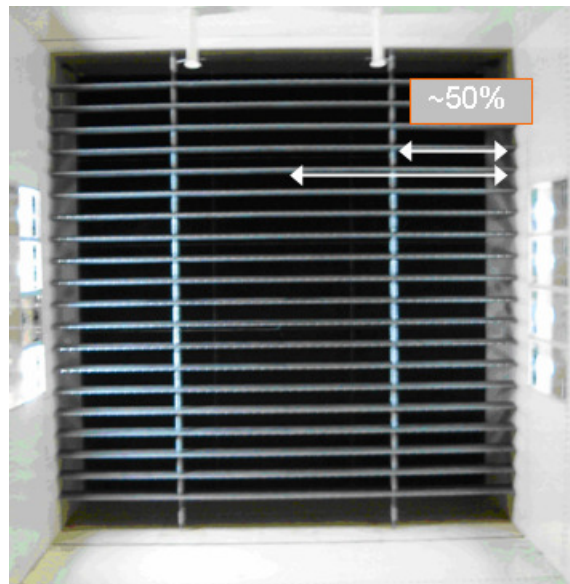


**Fig. 8.61:** SBS in the stilling chamber

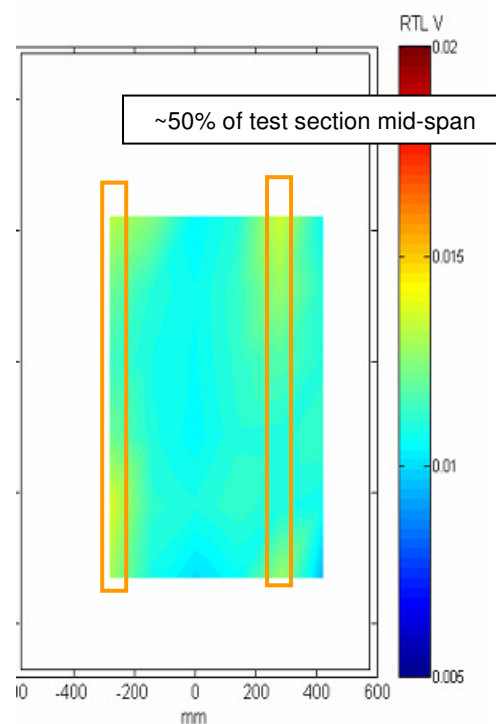


**Fig. 8.62:** Turbulence level in the STS



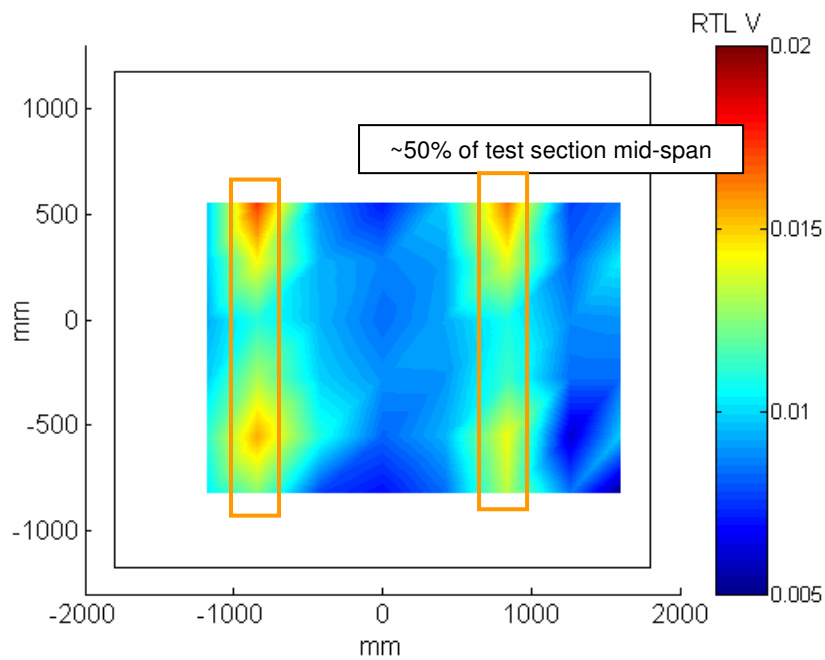


**Fig. 8.63:** Turbulence level in the ATS

It is interesting to see that approximately in the same region cloud uniformity is reduced. This effect is shown in figures 8.64 and 8.65 for the STS and ATS respectively. ATS uniformity data seems to be in better agreement with the aerodynamic ones, although this can be just due to the fact that uniformity measurements for the ATS have been taken in a much larger region of TS cross section. Indeed in the STS is quite difficult to exactly identify where the lack of cloud uniformity begins (see figure 8.64).

Although aerodynamic data for the MTS are missing, cloud uniformity results are in agreement with what measured for the STS and ATS. An example of the uniformity measured for the MTS is reported in figure 8.66.

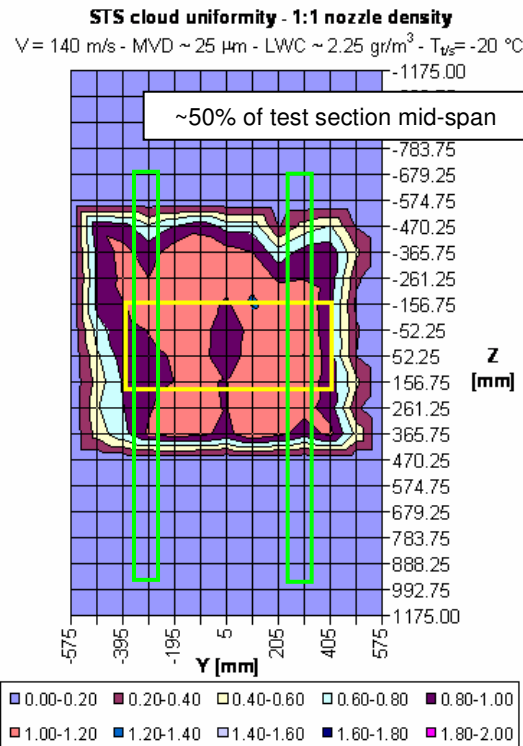


Fig. 8.64: SBS vertical strut influence on the STS uniformity

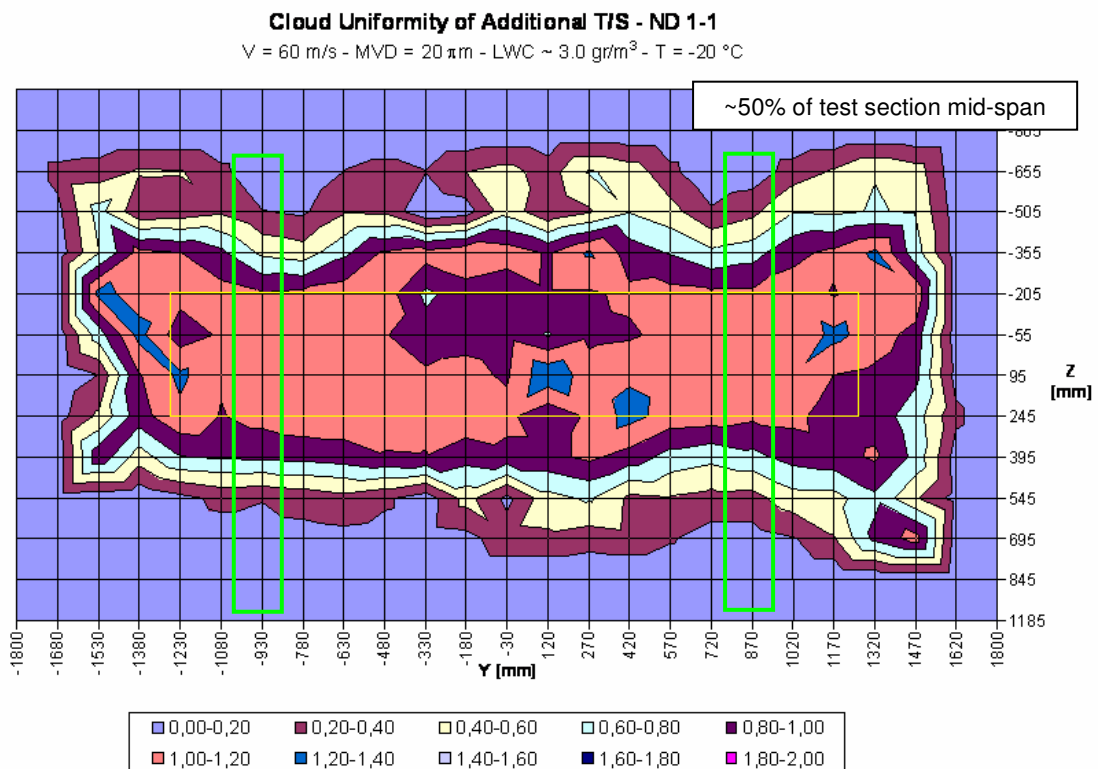
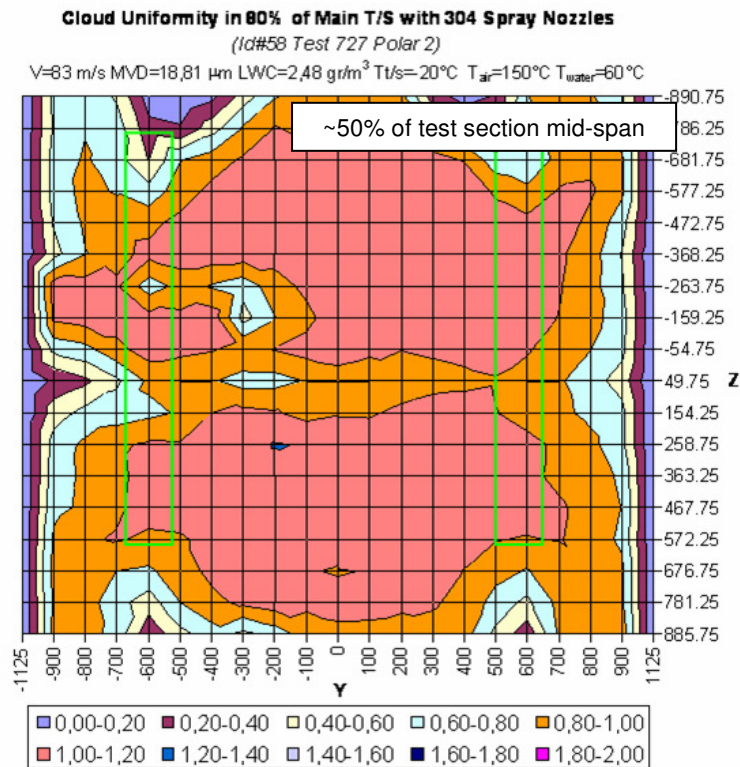


Fig. 8.65: SBS vertical strut influence on the STS uniformity



**Fig. 8.66:** SBS vertical strut influence on the STS uniformity

### 8.3.5 LWC Data Comparison

LWC measurements and procedures have been shown before in sections 8.1.4 and 8.2.4. In this section data are compared in order to check if the same behavior is shown for both STS and ATS. Specifically figure 8.67 and 8.68 report velocity and nozzle effect on the LWC. Being available some results for the MTS they have been added to the plot and compared as well. As expected from bibliography and from what stated in previous sections 8.1.4 and 8.2.4, results show very good coherence for both nozzle density and velocity effect.

Figure 8.69 shows for STS and ATS the Altitude effect on the LWC. Although only few data are available it seems that an effect is present. Since altitude is expected to be

“test section independent” (thermodynamic effect), it is suggested to collect more data in any of the three test section available to better asses this effect.

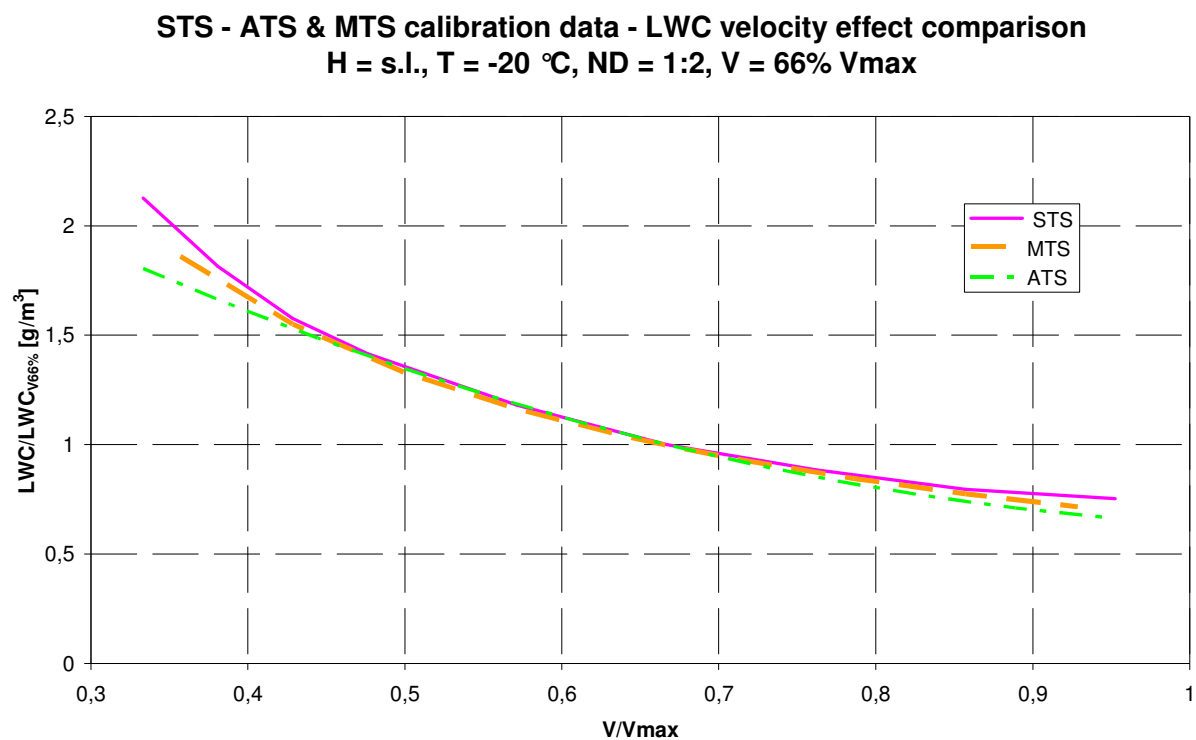


**Fig. 8.67:** ATS, MTS, and STS velocity effect on LWC comparison

**STS&ATS calibration data - LWC Nozzle Density effect comparison**  
**H = s.l., T = -20 °C, V = 66% Vmax**

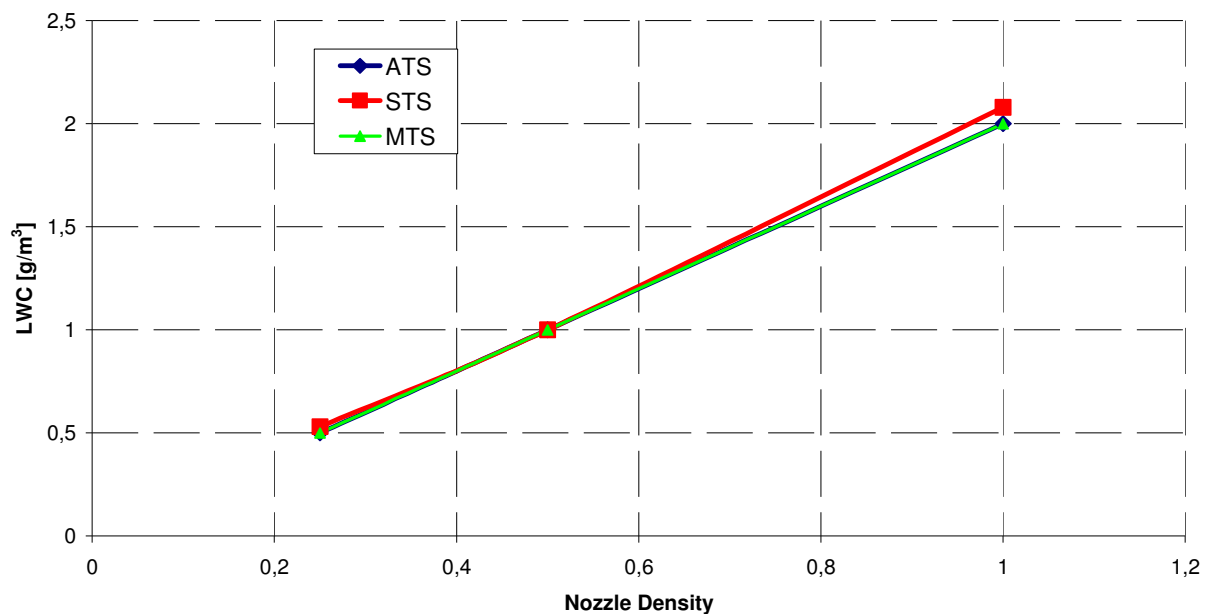


**Fig. 8.68:** ATS, MTS, and STS nozzle density effect on LWC comparison

**STS&ATS calibration data - LWC Altitude effect comparison**  
**T = -20 °C, V = 66% Vmax, ND = 1\_2**

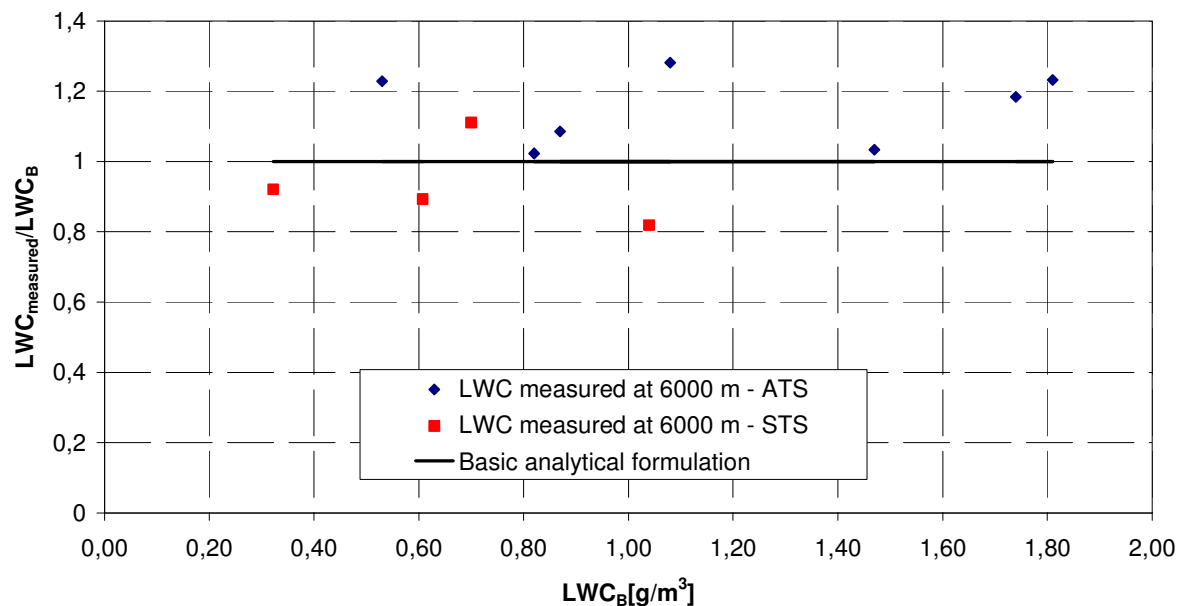


**Fig. 8.69:** ATS, and STS altitude effect on LWC comparison

# CONCLUSIONS

The steadily increasing demands for all weather flight capabilities, and a significant number of severe accidents have recently stressed the interest in aircraft icing again. Considerable research has been performed during the last decade and a large number of publications produced. The meteorological pre requisites, details of ice accretion, and the effects of performance degradation have been investigated in detail. Concerning the icing tunnel facilities, however, the SAE Aerospace Information Report *AIR 5320* issued in 1999, stated that “icing simulation ground testing plays an important role in the overall safety of civil and military aviation. While improvements are continually being made to icing simulation facilities and test techniques, the overall quality of the data produced in these facilities is still lower than desired. Much of this is due to the overall difficulty in producing a uniform cloud of known water droplet size and liquid water content. [...] However, by careful calibration and operation of icing simulation facilities, an improvement in data quality and repeatability may be achieved”.

As seen in the previous pages, this work goes in the direction of much improving the knowledge of the world’s largest icing facility and the way the cloud is generated by the Spray Bar System. Furthermore the effect of the main fluid-dynamic and thermo-dynamic parameters have been deeply investigated for both MVD and LWC, in order to provide to the icing community a well known environment with well established cloud reproduction performance.

Specifically the cloud generated by the Spray Bar System in the largest (Additional Test Section) and the smallest (Secondary Test Section) of the three test sections available at the Icing Wind Tunnel have been characterized, following the procedures

acknowledged worldwide in the icing community. Further to this, temperature, static pressure (simulated altitude), nozzle density and velocity influence have been assessed on both the MVD and LWC generation. Results turned to be very interesting mainly as far as the altitude effect is concerned for both main cloud parameters.

Equation necessary to compute the desired “cloud environment” in any test conditions have been defined. Finally the full set of data acquired for both test sections have been compared (when available) with the data acquired for the MTS. Data comparison showed a general good coherence of the measurements for all the parameters such as MVD, LWC SBS temperature assessment and cloud uniformity.

To accomplish this goal, huge efforts have been spent by CIRA IWT team and all the support staff necessary for making the facility efficient. About one and half year has been spent only to carry on the experimental activity (separated in two different test campaign, one for the STS and the other one for the ATS). Despite this effort, still much work has to be done, i.e. to more accurately investigate MTS performance and use those data to better assess data results already obtained for the STS and ATS.

Results obtained so far however, already allow to carry on some interesting industrial/research activities for some of the major aircraft manufacturers, such as AIRBUS for the A380 (full scale mock up of the air inlet leading edge installed in the STS) or the Dassault with the Falcon 7X (full scale model of the external part of the wing). Other clients such as Augusta, Eurocopter and Lockheed Martin have been using the IWT with satisfaction or are going to use it not far in the future.

## APPENDIX A:

### DE ICING AND ANTI ICING SYSTEMS

Overview of Conventional Ice Protection Systems			
De-icing systems:	Characteristics:	Advantages:	Disadvantages:
Pneumatic Impulse De-icing System	The tubes within the fabric-reinforced synthetic rubber boot are inflated alternately to fracture and to debond the ice accretion on the surface to be protected.	<ul style="list-style-type: none"> <li>- relatively cheap</li> <li>- low bleed air consumption</li> <li>- proven technology</li> </ul>	<ul style="list-style-type: none"> <li>- aerodynamic effects (inflated/deflated boots and ice build-up between cycles)</li> <li>- restrictions concerning transonic speed</li> <li>- limited life due to wear and erosion</li> <li>- low resistance to oil and hydraulic fluids</li> <li>- water ingress through pinholes in rubber</li> <li>- water ingress through air supply</li> <li>- constant suction required when not in use</li> </ul>
Fluid Ice Protection System	FPD (Freezing Point Depressant) fluid is pressed through porous skin onto the surface to be protected, to lower freezing point of the impinged supercooled water droplets.	<ul style="list-style-type: none"> <li>- no bleed air consumption</li> <li>- clean leading edge (dirt)</li> <li>- proven technology</li> </ul>	<ul style="list-style-type: none"> <li>- high weight; reservoir required</li> <li>- logistics (fluid availability and costs)</li> <li>- environmental restrictions</li> <li>- L.E. skin must remain porous (holes open)</li> <li>- drag can be caused by roughness of porous leading edge</li> </ul>
Electro Thermal Systems	Heating elements on skin surface area provide heat to melt the build-up ice	<ul style="list-style-type: none"> <li>- no bleed air required</li> <li>- proven technology</li> </ul>	<ul style="list-style-type: none"> <li>- high energy consumption (typical 12 W/in<sup>2</sup>)</li> <li>- weight (additional generator)</li> <li>- FOD (Foreign Object Damage) sensitive</li> <li>- cyclic use (controller or thermostat required)</li> <li>- (over) heating problems when used in combination with composites</li> </ul>
Hot Air Systems	Hot air is applied to raise the skin temperature to prevent freezing of the supercooled droplets or to melt the ice.	<ul style="list-style-type: none"> <li>- aerodynamically clean when it is a fully evaporative system</li> <li>- proven technology</li> <li>- reduction of bleed air consumption can be achieved by changing system into a de-icing system without major re-design/development</li> </ul>	<ul style="list-style-type: none"> <li>- weight of air distribution system, air temperature and airflow control units</li> <li>- aerodynamic degradation in icing conditions when used as de-icing system</li> <li>- significant engine performance penalty (bleedair) for advanced high bypass ratio engines</li> <li>- aerodynamic degradation caused by runback ice when it is a running wet system</li> <li>- structural implications of using hot air, e.g. for composites, adhesives, high strength alloys</li> <li>- supplement for an usual ice protection system (e.g. for improved pneumatic systems)</li> <li>- not a stand alone ice protection means</li> </ul>
Low Adhesion Coating (Kilfroast Comp.) (ICEX)	Reduces considerably the adhesive forces for ice accretions	<ul style="list-style-type: none"> <li>- simple and inexpensive</li> </ul>	



Overview of New De-icing Systems under Development			
De-icing Systems:	Characteristics:	Advantages (according to vendor):	Disadvantages:
Electro-Expulsive Separation System or Electro-Expulsive De-Icing System (EESS, EEDS)	Consists of conductors embedded in elastomeric blanket (boot) covering the ice accreting surfaces. Opposing currents in two legs create opposing magnetic fields causing a repulsive force between the top and bottom conductor layers. The top surface of the blanket is accelerated so as to destroy the ice-blanket bond.	<ul style="list-style-type: none"> <li>- effective for removing thin ice layer.</li> <li>- minimising aerodynamic penalties.</li> <li>- easy manufacturing retrofitting.</li> <li>- low power consumption.</li> </ul>	<ul style="list-style-type: none"> <li>- typical de-icing penalties (consisting of aerodynamic effects due to residual ice and ice build-up between cycles)</li> <li>- elastomeric boots tend to get pulled away from surface (smoothness)</li> <li>- unknown effects of lightning strike</li> <li>- service life: dependent on ability of elastomeric materials to withstand rain, sand, erosion, oil and hydraulic fluids</li> </ul>
Eddy Current Repulsion De-Icing Boot (ECDIB)	(same as above but use of eddy currents instead of opposing magnetic field).	[see above]	[see above]
Pneumatic Impulse Ice Protection System (B.F. Goodrich) (PIIP)	Pneumatic impulse tubes covered by titanium skin on top of aircraft leading edge skin. High pressure air is supplied to impulse valve which discharges a pulse into the impulse tubes, snapping the surface outward. The surface is stretched more than ice is capable of stretching without fracturing.	<ul style="list-style-type: none"> <li>- reduced intrusion of inflated de-icer into airstream.</li> <li>- provides a superior weather &amp; erosion resistant surface material.</li> <li>- improves ability of ice protector to remove thin ice (0.03 inch).</li> <li>- low power and low system weight.</li> </ul>	<ul style="list-style-type: none"> <li>- typical de-icing penalties</li> <li>- high pressure air required</li> <li>- cannot be bonded to aluminium skin</li> <li>- fatigue of titanium skin (aerodynamic smoothness and accuracy reduced; service life).</li> </ul>
Electromagnetic Impulse De-Icing (EIDI)	Flat-wound coils inside the leading edge induce eddy currents in metal skin, with the result that skin and ice layer are deformed.	<ul style="list-style-type: none"> <li>- low power consumption and low maintenance costs.</li> <li>- does not alter external surfaces, so no aerodynamic impacts.</li> </ul>	<ul style="list-style-type: none"> <li>- typical de-icing penalties. Does not adapt readily for retro-fitting.</li> <li>- possible fatigue and EMI (Electro-Magnetic Interference)</li> <li>- unproven for transport aircraft</li> <li>- unknown effects of lightning strike</li> <li>- maintenance of active system is a problem (lethal electric power level).</li> </ul>

### Overview of New De-icing Systems under Development (Continued)

De-icing Systems:	Characteristics:	Advantages (according to vendor):	Disadvantages:
Shape Memory Alloy Based De-Icing System (SMA). Innovative Dynamics, Inc. developed two De-Icing Systems and IDI patent is pending. For more details see Gerardi et al. (1995).	Shape Memory Alloys (SMA's) exhibit a large temperature induced dimensional change (up to 8% strain for a NiTi-alloy) over a relatively narrow transition temperature range. In addition internal stresses in the SMA generate a force during the shape change. When cooled the shape expands and returns to its original shape when heated and so an ice braking action is created.	<ul style="list-style-type: none"> <li>- SMA de-icer is designed for application on rotor blades and propellers</li> <li>- substantial power savings over existing electrothermally powered de-icing systems with greater durability and erosion resistance.</li> <li>- results of NASA Lewis IRT test results encourages further developments.</li> </ul>	<ul style="list-style-type: none"> <li>- for fixed wing application an additional system may be required to aid in the shedding of the debonded ice from the surface due to the lack of rotational dynamics that propellers and rotorblades do have to expel the debonded ice.</li> <li>- under development, not yet installed on helicopter or propeller for in-service trials.</li> </ul>
Space Age Electro-Thermal System Using Nickel Coated Carbon Fiber Mat (Thermion No-Ice™)	Very Light Very Thin Cloth-like Nickel Coated Carbon Fiber Heater Mat. Can be laid up in E-glass or sandwiched in silicon embedded cloth. Can be layered for increased power density. Used in power applications from 12 V dc to 280 V ac.	<ul style="list-style-type: none"> <li>- Very close to surface</li> <li>- Reduced power required</li> <li>- Eliminates circuit breakage discontinuities</li> <li>- Very light weight (2 lb. per 500 sqft)</li> <li>- Self regulating (design for temperature)</li> <li>- Easily tested for continuity</li> <li>- Life of airframe reliability</li> </ul>	<ul style="list-style-type: none"> <li>- Lay-up applications must be professionally done and quality controlled</li> <li>- Requires cycling circuitry for efficient power control</li> </ul>

## **APPENDIX B:**

### **OTHER CERTIFICATION/QUALIFICATION ASPECTS**

#### ***B 1.0 GENERAL ASPECTS OF CERTIFICATION AND QUALIFICATION***

The ice certification of a large (20 and more passenger) civil transport aircraft has to be performed as prescribed in JAR/FAR (Joint Airworthiness Requirements/Federal Aviation Regulations) section 25.1419 [17]. The critical icing conditions are given in Appendix C of that document. Additional advisory material is provided by FAA (Federal Aviation Administration) in the so-called 'Advisory Circulars', and in 'Orders'. Similarly the Joint Airworthiness Authority (JAA) issued the 'Interpretative Material and Acceptable Means of Compliance' ACJ (Advisory Circular Joint) 25.1419 which includes differences between some European national authorities and to the United States. Also the JAA presented a 'Notice of Proposed Amendment' NPA 25F-219 which is a draft for an 'Advisory Material Joint' Ah4J 25-1419 concerning handling characteristics and performance under icing conditions. The latter provides detailed guidance for demonstration of safe flight with realistic ice contamination on various aircraft parts. However, this material - although it is generally felt to be very useful for certification - is (yet) not fully accepted by the national authorities. Usually, the qualification of military transport aircraft adapts the civil rules just mentioned. For fighter type aircraft the requirements are normally reduced but even for this type of aircraft some concern on icing exists and is considered during qualification. For smaller transport aircraft and general aviation JAR/FAR sec. 23.1419 must be fulfilled if an ice protection system is installed and ice certification is desired. For large helicopters ('Transport Category

Rotorcraft') special guidelines can be found in FAR/JAR part 29. FAR/JAR 27 deals with smaller helicopters ('Normal Category Rotorcraft'). Appendix C of FAR/JAR part 25 on the meteorological conditions is in principle valid for all cases. However, part 29 contains its own Appendix C which allows for a 'pressure altitude limit' in icing conditions due to the limited flight altitude of helicopters. JAR/FAR part 33 and part 35 concern icing effects on engines and propellers, respectively. The ice certification program for a fixed wing transport aircraft shall determine the impact of ice accretion on unprotected parts of the aircraft as well as on parts protected by de-icing (e.g. boots) or anti-icing systems. Power or thrust losses due to the proper function of the systems and eventual losses in propeller efficiency have to be taken into account. For unprotected surfaces a maximum thickness of 3 inches (75 mm) can be assumed for the ice shape under most critical icing conditions, while on surfaces protected by a cyclically operating deicing system ice shapes of appropriately reduced height may be applied. For anti-icing systems the application of any residual ice is not needed if proper function of the ice protection system can be demonstrated under all relevant icing conditions. Also the possibility of building up runback ice has to be considered [17]. This is formed when water runs downstream and freezes after some distance or by partially melted ice pieces which travel stream-wise and freeze again on the surface. Recently interest has focused on ice ridges that may occur aft of the area protected by cyclically operating de-icing systems. These ridges may sometimes grow under very extreme meteorological conditions (e.g. large supercooled droplets of freezing drizzle up to 400  $\mu$ m diameter - outside of the meteorological certification envelope -) starting from ice remaining behind the inflating rubber boots after removal of the ice. Special attention has also to be paid to the ice shape roughness that may be present in real icing flights. The roughness is prescribed for the artificial ice shapes with respect to height and distribution of

roughness elements in the Advisory Material Joint (AMJ) 25.1419 (3 mm height normally, reduced to 1 mm for take-off ice, and 8-10 particles/cm<sup>2</sup>). Especially, the so-called 'sand paper ice' for simulation of critical ice accretion produced by large droplets hitting the aircraft surface or by hoar frost effects has to be simulated by pasting Carborundum paper with grains of prescribed size (Carborundum paper No. 40) on the aircraft surface. In any case when using artificial ice shapes it must be guaranteed that the performance degradation by natural ice accumulation does not exceed that one occurring with artificial ice. Lift, drag and pitching moment changes due to the most critical ice shapes have to be investigated with respect to performance degradation. Special attention must be paid to any increase of stall speed. Ultimately, the stall warning has to be set to lower angles of attack than without ice thus establishing a sufficient margin before stall under ice accretion. During flight tests with both artificial ice and in natural icing conditions the handling qualities will be investigated up to and including stall. Increase of stall speed due to ice accretion and corresponding decrease of stall angle of attack must be investigated. Sufficient longitudinal and lateral control capability, static longitudinal, lateral directional and dynamic stability have also to be shown. Starting from trimmed flight a 0 g (push-over) maneuver is proposed by the authorities to be flown by applying sufficient push force on the stick until 0 g - or, if this exceeds the tail plane capability, the minimum possible load factor – is reached. That maneuver can dramatically reveal any critical susceptibility of the horizontal tail to ice accretion effects. Furthermore it is said that vibrations and buffeting must be avoided. The flight in icing conditions includes take-off, climb, cruise, holding, descent and landing. Ice accretion before take-off must principally be avoided (clean wing concept). But some ice build up during take-off shall be presumed irrespective of the existence of an ice protection system if icing conditions are present at and close to the ground. It is

assumed that de-icing systems are generally not switched on prior to and during take-off except that an early switch-on is required in the AFM. In the first take-off segment the ice accretion accumulated at the time the landing gear is fully retracted has to be taken for performance analysis. For the second segment flight phase the ice accretion at the point where the aircraft reaches 400 ft height above the take-off surface is applicable. It may be presumed that an eventually installed de-icing system is switched on at this height. Of course, both take-off segments can be treated at once if the worst case artificial ice shape is used for demonstration. Corresponding safety demonstrations have to be flown under the additional assumptions of most critical thrust-power-to-weight conditions and critical engine failure. Since cumuliform clouds do not occur in ground proximity, only maximum continuous icing conditions - as given by JAR/FAR section 25.1419 Appendix C - have to be considered. For the other flight phases, protected and unprotected surfaces may be distinguished and considered similarly. The artificial ice shapes to be applied have to be defined for the most critical icing conditions during the corresponding flight segment and appropriate power setting is demanded. In addition, for protected surfaces a failure or malfunction of the ice protection system has to be considered, i.e. failure ice shapes also have to be applied. It is stated in the JAA proposal AMJ 25.1419 that one half of the ice shape size for unprotected surfaces must be applied, i.e. 1.5 inch unless another value is substantiated. However, it must also be shown for this situation that the aircraft can safely escape from the icing conditions before the ice horns grow to larger height. Also the possible delay time in crew's recognition of aircraft icing and switch-on of ice protection systems must be regarded.

## ***B 2.0 ARTIFICIAL SHAPES, WIND TUNNEL TESTS AND TANKERS***

A great variety of ice shapes can occur during aircraft operation. Safe flight and a minimum performance shall be guaranteed under all known (or forecast) icing conditions within the meteorological certification envelope defined by the certification authorities - even in special situations, as e.g. one engine inoperative. In case of failure of de- or anti-icing systems sufficient time must be available to safely escape from the icing environment before excessive ice accretion occurs. However, this escape procedure and any other change of the usual flight procedures due to icing must be thoroughly stated in the Airplane Flight Manual (AFM). Flight tests in natural icing conditions are quite expensive and time consuming, especially since well defined icing conditions corresponding to the expected critical meteorological conditions cannot easily be found. The extreme cloud developments needed for certification conditions occur rather seldom. Insufficient LWC may frequently be compensated by extended exposure time in the sense discussed in chapter 5. However, switching from glaze to rime ice can happen by this change due to changes of 'convective/latent heat ratio' in the heat balance but this modification of ice type should be avoided [17].

It is of great importance for all companies developing and manufacturing aircraft to reduce time and to lower costs for achieving ice certification and qualification of new aircraft. Although some representative flight tests under natural icing conditions are always indispensable, a great improvement can be realized by the use of possible artificial ice shapes for the flight tests and also for the corresponding wind tunnel experiments in dry air. The essential question to be answered for this methodology is: How can we predict reasonable ice shapes and to what extent can we make sure that the shapes chosen are realistic for the flight conditions to be simulated? And if a

positive answer has been found on this question, also the certification and qualification authorities must have confidence in what has been done. Fortunately, during recent years the theoretical prediction methods have been improved in capability and reliability and, in addition, some of the national authorities do more or less accept this progress for defining artificial ice shapes. Alternately, it is a frequent practice to use ice tunnel experiments for finding realistic ice shapes but this procedure also needs acceptance from the authorities since applying the similarity laws cannot fully guarantee correspondence to real in-flight ice accretion. Flight tests behind icing spray tankers are also attractive for this purpose but there exist even more problems concerning acceptance due to possible deficiencies in the artificial spray clouds and their calibration. Therefore, theoretical calculations as well as icing tunnel experiments where sub-scale tests have been performed and eventually also spray tanker tests may be used besides flight tests in natural icing environment for defining artificial ice shapes that will then be applied to aircraft components for investigating performance and handling qualities degradation in wind tunnel and flight tests. The use of artificial ice shapes essentially reduces time and costs for flight tests and is therefore extremely important for industrial certification and qualification procedures.

It has been demonstrated that in almost all interesting situations it is possible to replace the natural ice accretion shapes by artificially modeled ones. Recent developments in computational methods for predicting ice accumulations, and classical means for reproducing ice shapes observed in ice tunnel experiments, allow fabricated ice shapes to be used in dry air for most of the necessary measurements to determine performance degradation in icing. These 'dry air' experiments can be done either in wind tunnels or in flight tests. Only a few flight tests must then be performed after sufficient ice



contamination has been achieved flying in natural icing conditions. It must however be shown by these tests that the selected artificial ice shapes represent an envelope of worst cases which will not be exceeded by natural ice cases, with respect to performance degradation.

### ***B 3.0 POSSIBLE FAR EXTENSION***

Certification rules are subject to periodic review. Further changes - either for a specific aircraft type or a class of aircraft - may also be decided by the certification authorities due to actual events or serious safety concerns. An actual example is the freezing drizzle encounter of turboprop aircraft which always up to now has been outside of the certification conditions.

As part of the Special Certification Review conducted by the FAA (Federal Aviation Administration) and the DGAC (French authority) on the accident occurred to the ATR 72 American Eagle Flight 4184 (end of October 1994 close to Roselawn), crashed due to SLD, an extensive icing tanker test program was carried out. From this test program, ten changes were implemented for all ATR aircraft during operations in icing conditions and were incorporated in the airplane flight manual, AFM. Three arbitrarily selected changes will be cited: "Dispatch into known or forecast freezing drizzle is prohibited.", and "If visual cues associated with freezing rain or drizzle occur on one or both cockpit forward side windows, with any flaps extended, the flaps must not be retracted until the airframe is clear of ice. This includes missed approach, and go around.", and "As soon as visual cues associated with freezing rain or drizzle occur on one or both forward side

windows, immediately disconnect the autopilot while holding the control wheel firmly and exit these conditions. Fly manually until the airframe is clear of ice”.

Extensive discussions and research on the freezing drizzle and freezing rain topics are being conducted, which may result in similar restrictions for all turboprop aircraft in the future. The policy with respect to these exceedance encounters is to reduce the probability of such events (1:1000 icing encounters) by improving weather information and forecast for the pilots and developing means of exceedance detection (e.g. ‘visual cues’ as indicated above in the rules for ATR). Of course, also systematic pilot training may be very helpful with respect to recognition of these situations and safe escape procedures.

In the near future an extension of icing certification envelopes reported in chapter 5 fig. 5.1 to 5.4, is envisaged, finally including freezing drizzle and freezing rain.

#### ***B 4.0 CERTIFICATION/QUALIFICATION RULES***

Besides the basic demands for certification in JAR/FAR sec. 25.1419, the meteorological conditions for the worst cases in Appendix C of that document and the material of ACJ 25.1419 and various Advisory Circulars of FAA, the JAA proposal AMJ 25.1419 (1992) contains quite detailed and concrete guidance on how safe flight under performance degradation by icing shall be proved during certification. The most important aspects of all guiding material may be summarized as follows (due to different sources and national particulars it has to be viewed as a collection which is not obliging in all details) [17]:

***Meteorological Conditions*** for worst case simulations:

- a) Maximum Continuous Icing: flight through one cloud of suitable extent (standard 17.4 nm) and conditions as defined in Appendix C or continuous flight of 30 minutes duration through one cloud at given temperature and LWC combinations, corresponding to a standard droplet diameter of 20  $\mu\text{m}$ .
- b) Maximum Intermittent Icing: flight through clouds of suitable horizontal extent (standard 2.6 nm) and conditions as defined in Appendix C, or flight through 3 standard clouds of 5 km extent with intermediate 5 km clear air distances of 5 km at same temperature and droplet size (20  $\mu\text{m}$ ) combinations as a) but higher LWC values.
- c) However, for the rate of catch the full spectrum of droplet sizes has to be used (Langmuir D spectrum is agreed to be sufficient), for the impingement limits a maximum droplet diameter of 50  $\mu\text{m}$  has to be considered.

**Flight Conditions:** The most unfavorable flight conditions must be selected with respect to speed, altitude, angle of incidence, centre of gravity location, flap and trim setting and power supply.

**Natural Icing:** Tests must be carried out to validate other work for certification, e.g. to validate predicted ice shapes for artificial ice.

**Artificial Ice Shapes:** are commonly used for tests in dry air. If these shapes are added to the aircraft components step by step handling and performance degradation of the aircraft can be tested safely. Artificial ice shapes can be used for unprotected and protected surfaces as follows:

*Unprotected Surfaces;*

- a) The most critical main airfoil surface parts have to be equipped with ice shapes of 3 inches height.
- b) Other main airfoil surface parts have to be equipped with same height, unless analysis demonstrates that a smaller value is appropriate.
- c) The ice shape and its surface texture (roughness) must be realistically modeled, i.e. taken from experiments in natural icing if no other accepted approach can be taken (by analysis or experience).

*Protected Surfaces:*

- a) Ice Protection System Operating. The most critical ice shape accreted during the rest time of the de-icing system has to be applied. Typically for a commuter turboprop aircraft, the more critical intermittent maximum icing conditions produce ice shapes of about 1/2 inch.
- b) Delay in System Activation: Maximum icing exposure time prior to crew recognition and system activation must be established. A delay time of some minutes (normally 3 minutes) has to be considered.
- c) After System Failure: One half of the ice accumulation specified for unprotected surfaces has to be assumed if not another value - not exceeded during a flight time of 30 minutes - is substantiated by analysis or experiment. This time is considered to be sufficient to leave icing conditions in a case of a system failure.

***Tests Using a Simulated Icing Environment*** can be done in ground facilities (icing wind tunnels or outdoor spray rigs) or in-flight, i.e. flying behind a spray tanker. Both methods are not yet accepted as the only means of compliance for flight in icing

conditions by the authorities due to shortcomings in similarity laws or deficiencies in cloud simulation: *Icing Facility Tests* for components, e.g. airfoils, wings, engine inlets can be performed to document the ice build up, the typical shape and the resulting performance degradation. These results can be used to define the most critical ice shape which will be used for artificial ice shapes. *Icing Spray Tanker Tests* can be used for component testing in dry air. Components sensitive to icing, e.g. propellers, engine inlets, control surfaces can be tested safely because the aircraft can leave the spray cloud immediately if any problems occur. The measured ice build-up can be used for defining artificial ice shapes. For helicopters full scale tests behind icing spray tankers are possible.

***Flight Testing*** should address all phases of flight (takeoff, climb, cruise, hold, descent, landing and ground), while extraction of bleed air for ice protection and loss of propeller efficiency must be taken into account:

*a) Handling Flight Tests*

I. With Natural Ice:

- Qualitative assessment for comparison with artificial ice shape tests
- Verification of sufficiently early stall warning for various sizes and shapes of ice contamination
- Investigation that flight controls remain free from jamming due to ice

II. With Artificial Ice Shapes demonstration of adequate stability and control with the most critical ice accretion pertinent to each flight phase:

- Longitudinal 0 g maneuver to check the danger of tail stall for various speeds, configurations, power settings at most critical icing conditions and loads

- Demonstration that maneuvering capability can be maintained up to stall warning - Ability to trim has to be maintained to limit control forces for safe flight under icing conditions.

- Increase of stall speed and reduction of stall angle must be compensated by sufficiently early natural or artificial stall warning.

- Vibrations and buffeting must not excessively occur.

b) *Performance Flight Tests:* These have to be carried out if the ice contamination increases stall speed by more than 5kt or 5% (greater value) or increases drag by more than 5%:

I. With Natural Ice:

- To prove that actual performance degradation does not exceed that with artificial ice shapes.

II. With Artificial Ice Shapes:

- 1 g stall speeds should be demonstrated in each configuration for take-off, en-route, approach and landing phases.

- Drag characteristics should be determined in each configuration for the flight phases mentioned.

- Additional performance tests for take-off conditions if the above limits (5kt or 5%, the greater value) are exceeded and the aircraft is operated in accordance with the AFM.

c) *System Tests in Natural Ice:*

- Demonstration of proper function of all parts of ice protection systems, e.g. for the wing, empennage, engine inlets, propellers, windshield, probes.
- Demonstration of proper modes for de-icing systems.

***Ice Shedding*** must not affect the continuous safe operation of the engines or essential surfaces. It must be demonstrated that any pieces of ice shed are too small to cause unacceptable damage or that their trajectories are safe.

***Ice Crystal Conditions*** must not affect the turbine inlets and bends, Pitot heads, ducts supplying essential air, APU inlets etc.. Corresponding atmospheric ice crystal conditions are also prescribed in ACJ 25.1419.

***Demonstration of Compliance*** can be done by a suitable combination of the following methods:

- Flight testing using ice shapes - either accreted naturally or applied artificially
- Icing tunnel test data
- Spray tanker test data (rather limited up to now)
- Read cross from earlier version or ancestor of a/c

**Flight Manual:** all appropriate limitations, performance information and procedures for flight in icing conditions must be provided in the Airplane Flight Manual (AFM):

- Limitations under icing conditions must be stated.
- Procedures for normal operation of the ice protection system and in case of failure must be stated.
- Performance effects for all flight phases should appear in the AFM.

It has to be emphasized that not all of the rules in the JAR proposal AMJ 25.1419 are accepted by the national authorities but most of them have become the basis of an actual rule-making process.

#### ***B 5.0 THE CASE OF THE ATR 72***

The airplane with 68 persons onboard was in a holding pattern and was descending to a newly assigned altitude of 8,000 feet when it experienced a not commanded roll excursion and crashed during a rapid descent [17]. The loss of control was attributed to a sudden and unexpected aileron hinge moment reversal that occurred after a ridge of ice accreted beyond the deice boots. The manufacturer failed to disseminate adequate warnings and guidance to operators about the adverse characteristics of, and techniques to recover from, ice-induced aileron hinge moment reversal events. Furthermore it failed to develop additional airplane modifications, which led directly to this accident. The DGAC failed to require the manufacturer to take additional corrective actions, such as performing additional icing tests, issuing more specific warnings regarding the aileron hinge moment reversal phenomenon, developing additional



airplane modifications, and providing specific guidance on the recovery from a hinge moment reversal, which led directly to this accident. The ability of the FAA to monitor, on a real-time basis, the continued airworthiness of the ATR airplanes was hampered by the inadequately defined lines of communication, the inadequate means for the FAA to retrieve pertinent information, and the DGAC's failure to provide the FAA with critical airworthiness information, because of the DGAC's apparent belief that the information was not required to be provided under the terms of the Bilateral Airworthiness Agreement.

The National Transportation Safety Board determines the probable cause(s) of this accident as follows: the loss of control, attributed to a sudden and unexpected aileron hinge moment reversal that occurred after a ridge of ice accreted beyond the deice boots while the airplane was in a holding pattern during which it intermittently encountered supercooled cloud and drizzle/rain drops, the size and water content of which exceeded those described in the icing certification envelope. The airplane was susceptible to this loss of control, and the crew was unable to recover. Contributing to the accident were: 1) the French Directorate General for Civil Aviation's (DGAC's) inadequate oversight of the ATR 42 and 72, and its failure to take the necessary corrective action to ensure continued airworthiness in icing conditions; and 2) the DGAC's failure to provide the FAA with timely airworthiness information developed from previous ATR incidents and accidents in icing conditions, 3) the Federal Aviation Administration's (FAA's) failure to ensure that aircraft icing certification requirements, operational requirements for flight into icing conditions, and FAA published aircraft icing information adequately accounted for the hazards that can result from flight in freezing rain, 4) the FAA's inadequate oversight of the ATR 42 and 72 to ensure continued airworthiness in icing conditions; and 5) ATR's inadequate response to the continued

occurrence of ATR 42 icing/roll upsets which, in conjunction with information learned about aileron control difficulties during the certification and development of the ATR 42 and 72, should have prompted additional research, and the creation of updated airplane flight manuals, flight crew operating manuals and training programs related to operation of the ATR 42 and 72 in such icing conditions.

# **APPENDIX C:**

## **NOTES ON SCALING METHODS**

### ***C 1.0 REVIEW OF SIMILARITY REQUIREMENTS***

In icing tests one normally wishes to simulate natural in-flight icing situations as realistically as possible. That is, model test conditions should, ideally, be dynamically similar to full-scale conditions [17]. Dynamic similarity is often, however, difficult to achieve, particularly if the model tests are to be at reduced scale. Test facility size limitations frequently necessitate reduced or sub-scale testing; this is especially true for rotorcraft. Compromises are usually necessary and an appreciation of similarity requirements is essential to choosing the best compromises and understanding their consequences. Another application where similarity considerations are important is when flight or ground test exposures conducted in one set of environmental conditions are to be used to assess icing behavior in a different set of conditions. The similarity requirements are, of course, a direct reflection of the physical phenomena involved in ice accretion.

### ***C 1.1 SIMILARITY CONSIDERATIONS: A BRIEF OVERVIEW***

A routine dimensional analysis would begin with a list of the independent physical parameters which are judged to have an important influence on the phenomenon. In the case of ice accretion the list would be long and a large number of independent non-

dimensional parameters would have to be matched to ensure similarity between model and full-scale conditions. Simultaneous matching of all these parameters is, however, impossible except by exact replication of full-scale conditions. The routine approach is therefore not very useful in the case of ice accretion.

Ice accretion tests require proper scaling of three main phenomena: the air flow field, the particle trajectories and the impingement-freezing process. Each will be considered in turn. The streamline pattern and the aerodynamic pressure, force and moment coefficients must be the same for model and full-scale flows. The scaling requirements to achieve this are familiar to aerodynamicists. The model and full-scale bodies must be geometrically similar and, ideally, the Reynolds number based on body size and free stream velocity should be matched. In addition, if compressibility effects are significant, Mach number must be matched. It is usually not possible to match the Reynolds number, but there are well-established techniques for recognizing and alleviating problems that may stem from this. As mentioned elsewhere, icing problems usually occur in flight at relatively low Mach numbers so that compressibility effects can usually be neglected in icing studies for fixed-wing aircraft. Droplet trajectories are determined by aerodynamic drag and inertia forces acting on the droplets as they approach the aircraft. The drag forces are due to the relative velocity between the droplets and the air. Aerodynamic lift forces are negligible because shear velocity gradients are negligible in the bulk of the air flow and droplet angular velocity is negligible. Gravity forces are negligible relative to inertia forces because the ratio of inertia to gravity forces on the particles, that is, the Froude number  $V/(L \cdot g)$ , is of order 100 or more in full scale situations.  $V$  is the flight speed and  $L$  is a reference length of the aircraft (e.g. mean chord length of the wing). Application of Newton's law readily yields the equations of

droplet motion for the three axis directions. The requirements for similarity of droplet trajectories can be found by putting these equations into suitable non-dimensional form.

Finally the impingement-freezing process is also to be considered especially for glaze icing cases, where correct scaling of this process presents a very difficult challenge because of the complex dynamic, capillary and thermal phenomena that are involved.

## APPENDIX D

### DROPLET SIZE MEASUREMENTS ANALYSIS: THE CASE OF THE ATS

Since the ADA probe volume is usually larger than the injected droplets particles, it is possible to have more than one particle in the measurement volume at any given time. To avoid this situation a coincidence mode has been adopted during the data acquisition in order to correlate both velocity and droplet size information and to verify that the data from all the channels (detectors) represent one particle. With this configuration it has been possible to investigate on bi-phase flow proprieties taking into account the inertia of particles involved in the process of measurement and to carry out statistical information.

Typical raw particle data acquired during the measurements are:

-The Arithmetic Mean Diameter (D10):

$$D_{10} = \frac{\sum_{i=1}^n d_i}{n}$$

where

$d_i$  = diameter of particle  $i$

$n$  = number of particles

- Area Mean Diameter, or the mean surface area based on diameter (D20):

$$D_{20} = \sqrt{\frac{\sum_{i=1}^n d_i^2}{n}}$$

- Volume Mean Diameter, or the mean volume based on diameter (D30):

$$D_{30} = \sqrt[3]{\frac{\sum_{i=1}^n d_i^3}{n}}$$

- Velocity Mean (m/s), the average of all measured droplet velocity values:

$$\bar{V} = \frac{\sum_{i=1}^n V_i}{n}$$

- Velocity RMS (m/s): standard deviation of the droplet velocity measured:

$$V_{RMS} = \sqrt{\frac{\sum_{i=1}^n (V_i - \bar{V})^2}{n - 1}}$$

For the type of Phase Doppler Technique used, additional statistical parameters are available for the complete characterization of bi-phase flow conditions (e.g. drop turbulence intensity). Moreover to correct potential source of serious measurement error due to the detection of signal produced by the wrong light scattering component (e.g. reflection instead of refraction) by spherical drops trajectory through the Gaussian intensity profile in the probe volume, the Aerometrics/TSI Adaptive Threshold Validation Methods has been adopted. So, the above statistics data are corrected from the effect of the probe volume. After the Probe Volume Correction (PVC), the Volume Distribution Statistics data were computed considering the corrected droplets diameter distribution

per volume unit and the cumulative volume distribution plotting which behaviours were based on the following equations:

$$S(d) = \frac{\#(d)}{P_v \Delta d}$$

$$LWM(d) = \#(d) \frac{4}{3} \pi \left( \frac{d}{2} \right)^3 \rho_w$$

where:

- $S(d)$  is the droplet diameter distribution,  $\#/cm^3/\mu m$
- $\#(d)$  is the number of counts with diameter  $d$
- $PV$  is the ADA probe volume,  $cm^3$
- $\Delta d$  is the droplet diameter interval,  $\mu m$
- $LWM$ , is the liquid water mass
- $\rho_w$  is the water density

Both the above equations are representative of probability mass function and cumulative distribution function.

From the above equations the Median Volumetric Diameter (MVD) defined as the droplet diameter which divides the total water volume present in the droplet distribution in half, i.e., half the water volume will be in larger drops and half the volume in smaller drops. The value is obtained by actual droplet size measurements, were computed for each test conditions.



Typical droplets and its velocity histograms were generally acquired with 430000 samples at frequency range 0.2 kHz to 10 kHz of data rate in function of simulated LWC at size validation higher than 90 % for both velocity and size data.

An example of typical data results are referred to the test conditions reported in the table below.

Test No [#]	V [m/s]	Ts [°C]	h [m]	Pair [bar]	Pwater [bar]	Dp [bar]	Nozzle Density [#]
44	60	0	0	8,20	7,00	1,20	1:2
107	60	3	0	0,30	0,20	0,10	1:2
109	60	3	0	2,40	2,00	0,40	1:2
98	60	3	0	2,10	2,00	0,10	1:2

**Table D.1:** Test conditions

Data from both ADA probes were combined into a single droplet distribution taking into account the sample area, measurement time and bin width of each probe.

The figure D.1 shows the particle diameter spectra acquired with both ADA probes for the test n° 44 (MVD  $\approx$  20  $\mu$ m). By the difference in concentrations, it is possible to notice the different capability of ADA standard probe respect to ADA large in detecting small droplets (diameter smaller than 20  $\mu$ m). The first probe shows a higher sensibility to small droplets respect to the second one, while the second one shows a higher sensibility upon larger droplets (it shows droplets with larger diameters and lower concentrations).

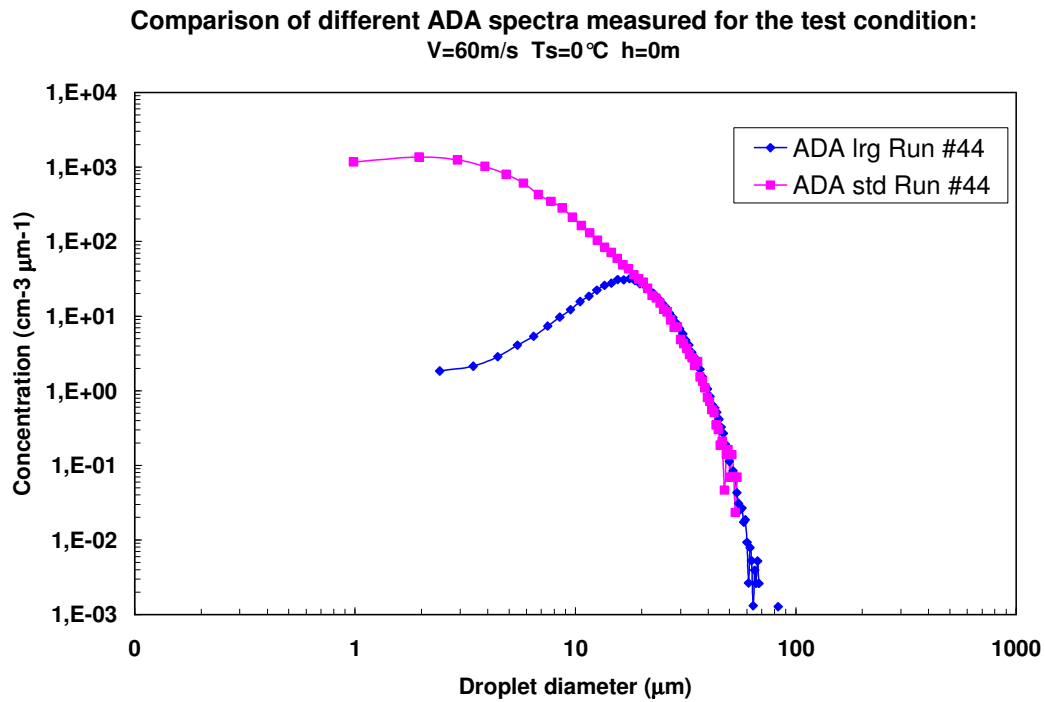


Fig. D.1: Comparison of ADA std and ADA Irg droplet spectra

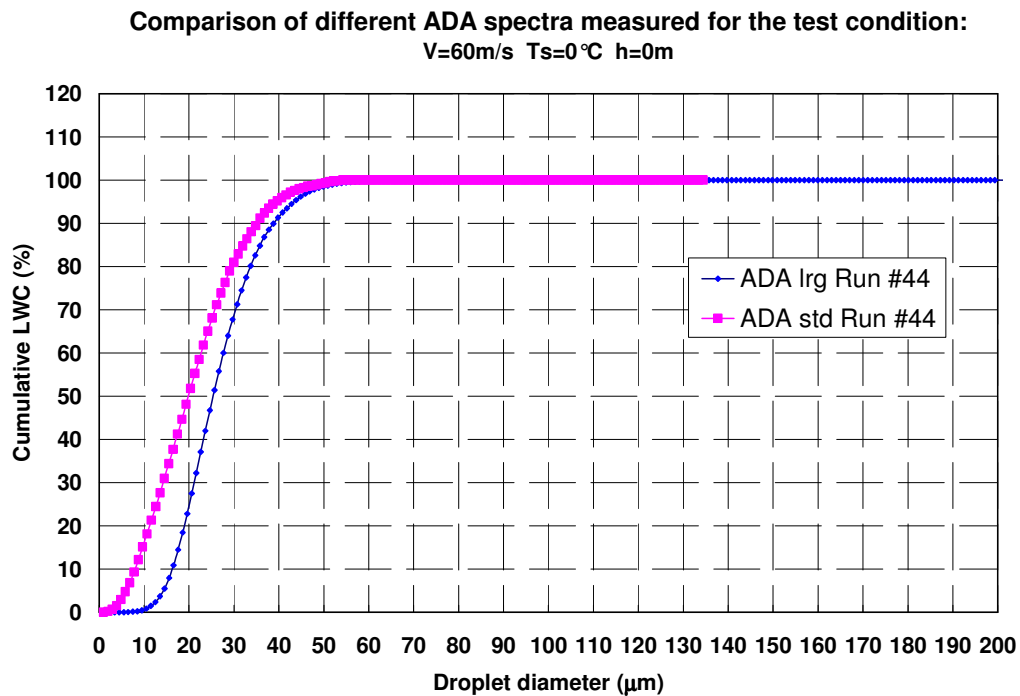
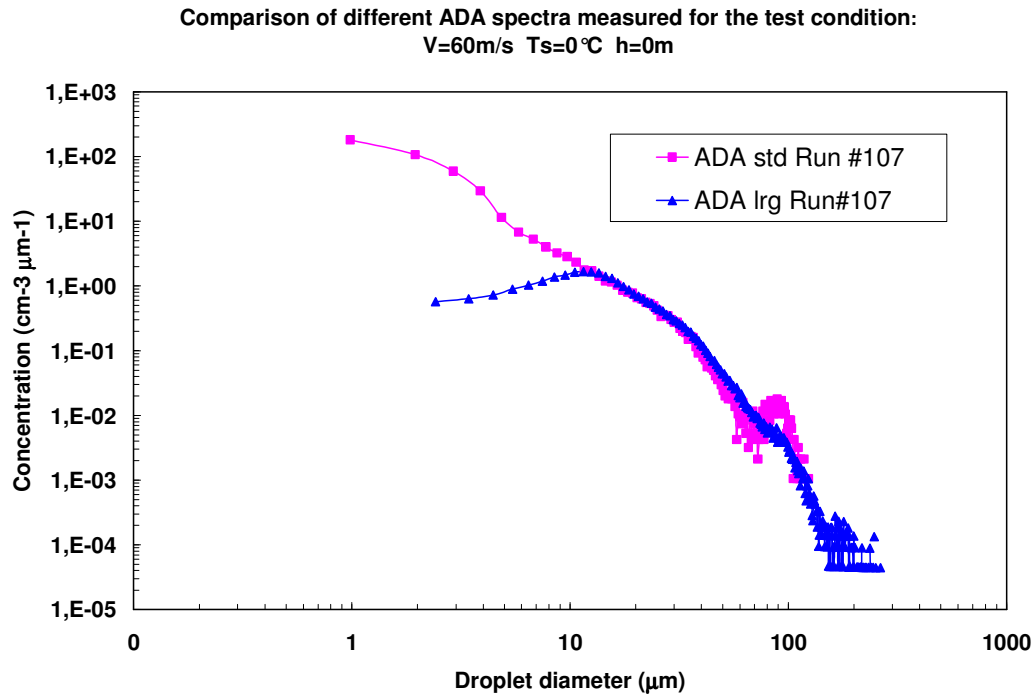


Fig. D.2: Comparison of ADA std and ADA Irg cumulative LWC

Figure D.2 shows the cumulative Liquid Water Content of both ADA probes (standard and large). As it can be seen, the effect of the low sensitivity of the ADA lrg to small droplets generates a relevant difference in the evaluated MVD, while the higher sensitivity of this system to larger droplets has not a significant effect due to the very small number of particles present in the spectrum. These particles, although not detected by the ADA std does not affect the cumulative LWC of the ADA std system, which indeed well fit the asymptotic value.

Therefore it can be stated that the ADA std system alone, is sufficient in the evaluation of the MVD when the contribution to the cumulative LWC given by large droplets is negligible.

On the contrary, when this contribution is significant, the ADA lrg system alone is the most reliable for the MVD evaluation. This can be observed in the Figure D.3, where the comparison between the ADA std and ADA lrg spectra is presented for the test n° 107 (MVD  $\approx 50 \mu\text{m}$ ). In this case the ADA std spectrum shows a significant concentration scattering for the particle diameters larger than about  $45\mu\text{m}$ . This causes an error in the MVD determination. Using the MVD obtained by the ADA lrg probe, on the contrary, the error can be significantly reduced. Indeed the influence of small droplets, although in higher concentration, on the MVD calculation, is significantly lower than the influence of the large droplets.



**Fig. D.3:** Comparison of ADA std and ADA lrg droplet spectra

Due to the considerations above mentioned, the MVD obtained by the measurements was calculated using the ADA std probe for all the spectra not showing significant scattering on large droplets diameter and a well fitting of the cumulative LWC to the asymptotic value, while the ADA lrg probe was used in all those cases in which these conditions were not verified.

The figures D.4 and D.5 show example cases in which the results given by the ADA std system were considered reliable ones. These figures show the capability of the ADA std

system to give reliable results for MVD up to about 40  $\mu\text{m}$ .

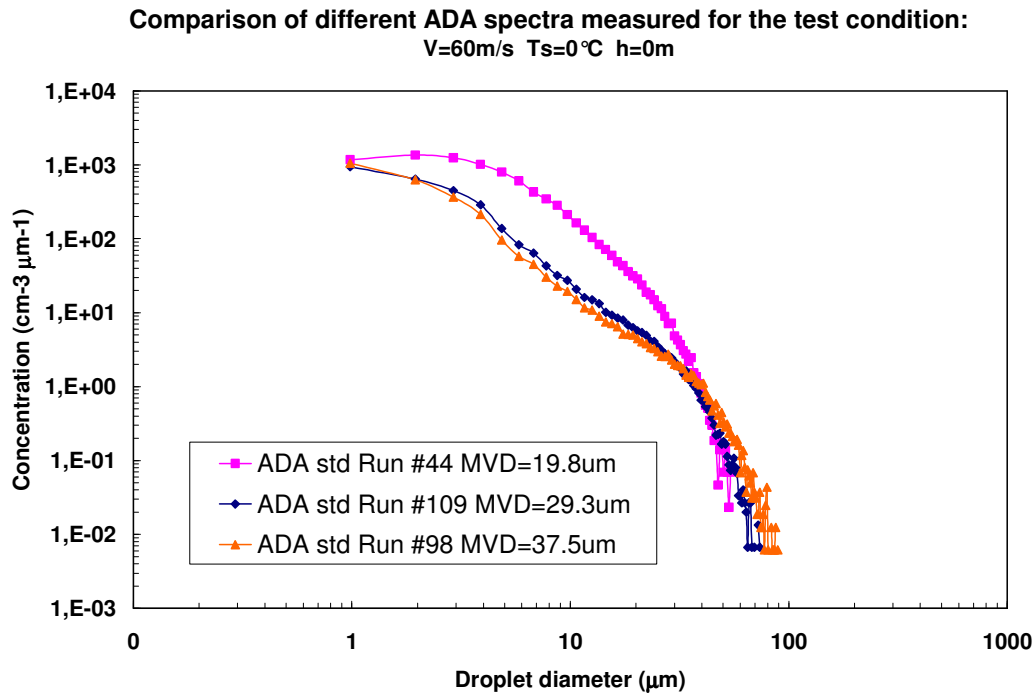


Fig. D.4: Comparison of ADA std droplet spectra for tests with different MVD

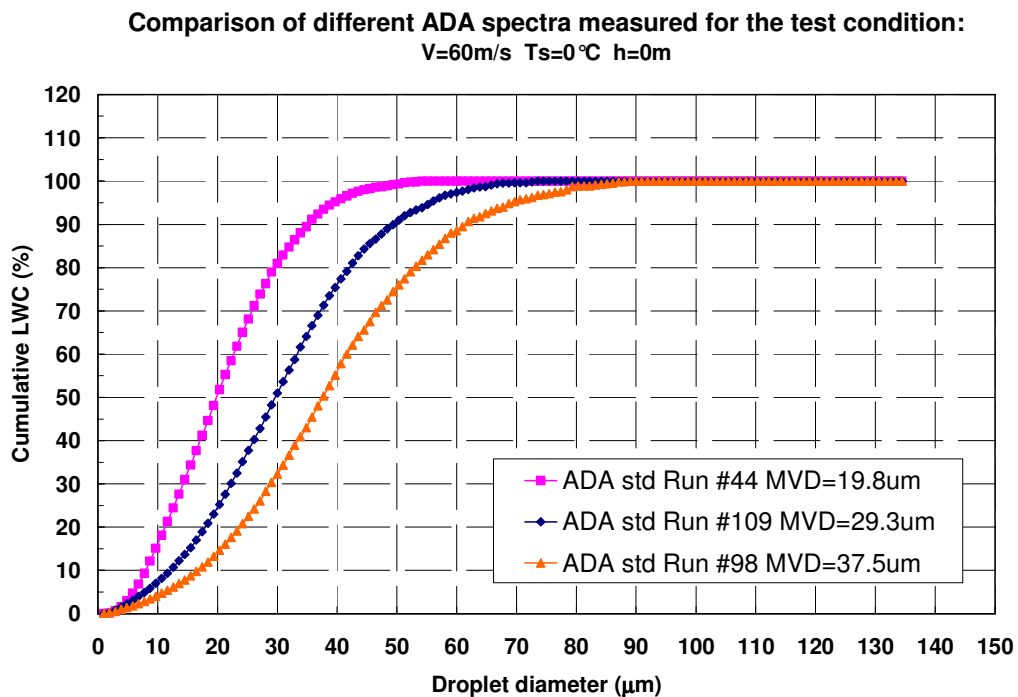


Fig. D.5: Comparison of ADA std cumulative LWC for tests with different MVD

## APPENDIX E

### SBS TEMPERATURES ANALYSIS: THE CASE OF THE STS

The analysis refers to the test conditions reported in the table below.

Test n.	V [m/s]	T <sub>0</sub> [°C]	H [m]	MVD [μm]	P <sub>WATER</sub> [bar]	T <sub>AIR</sub> [°C]	T <sub>WATER</sub> [°C]	Δt [s]
1	60	0	0	20	0.8	50	20	120
2	60	0	0	20	0.8	65	40	120
3	175	0	0	20	7	50	20	40
4	175	0	0	20	7	75	40	40
5	175	0	0	20	7	100	60	40

**Table E.1:** Test conditions

Pictures from E.1 to E.3 reports the ice accretions on the three cylinders for the test n.1.



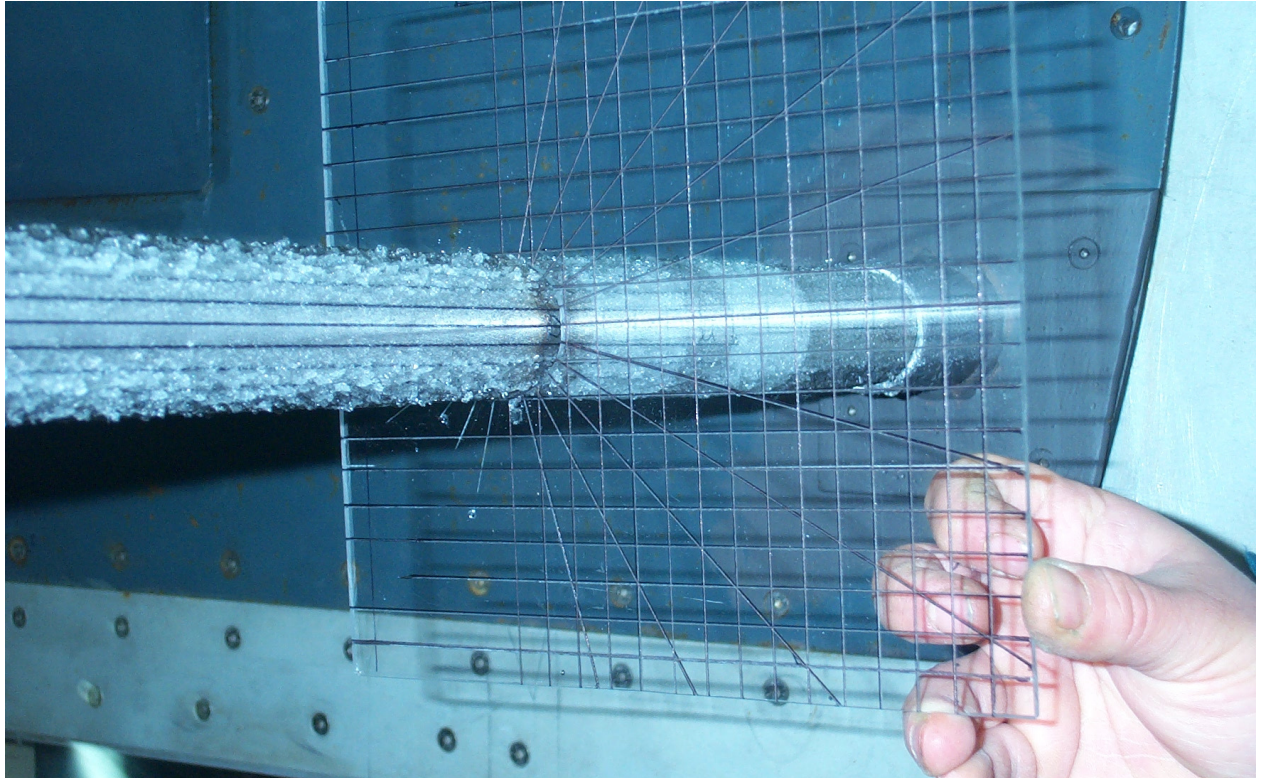


**Fig. E.1:** Ice accretion on the upstream cylinder – test n. 1

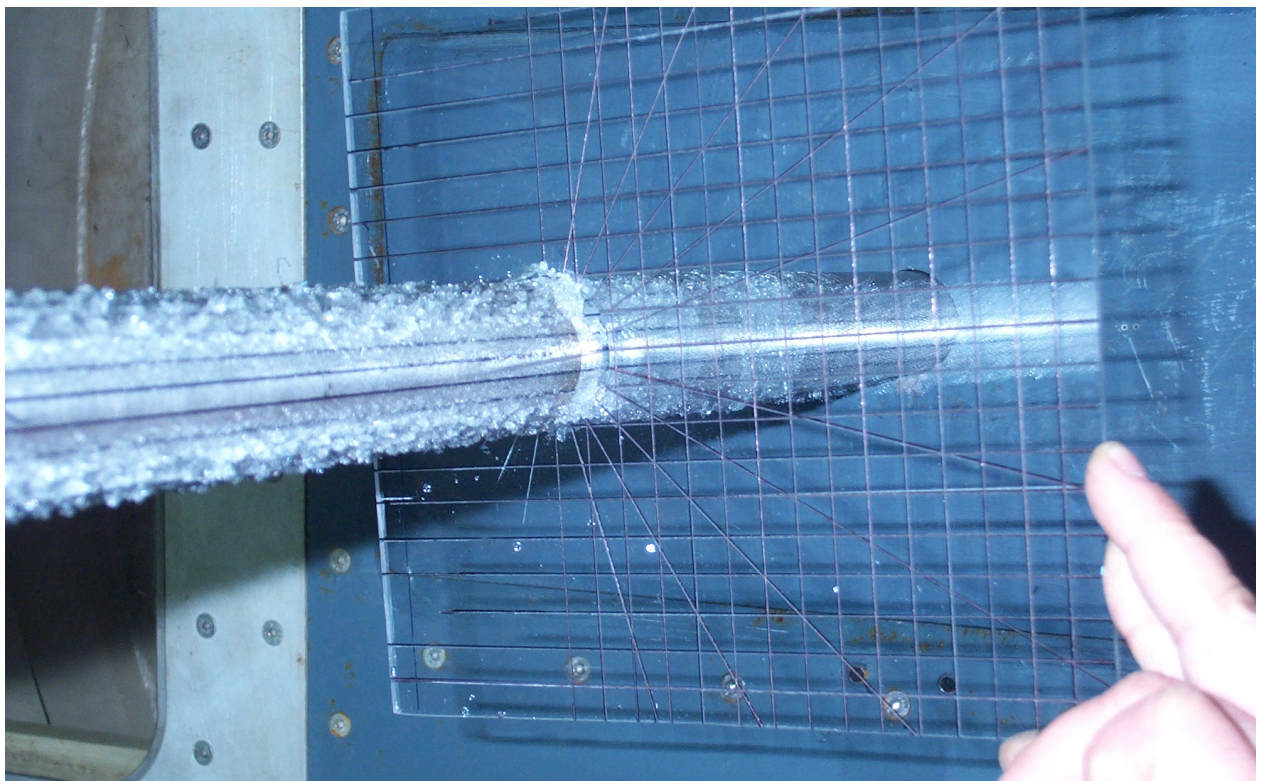


**Fig. E.2:** Ice accretion on the intermediate cylinder (test section centre) – test n. 1





**Fig. E.3:** Ice accretion on the down-stream cylinder – test n. 1

Significant differences between the three cylinders were not observed, in terms of quantity of ice, quality, adherence, transparency, etc... The third cylinder (down-stream the test section centre) showed slightly closer horns.

Pictures from E.4 to E.6 report the ice accretion on the three cylinders for the test n. 2.



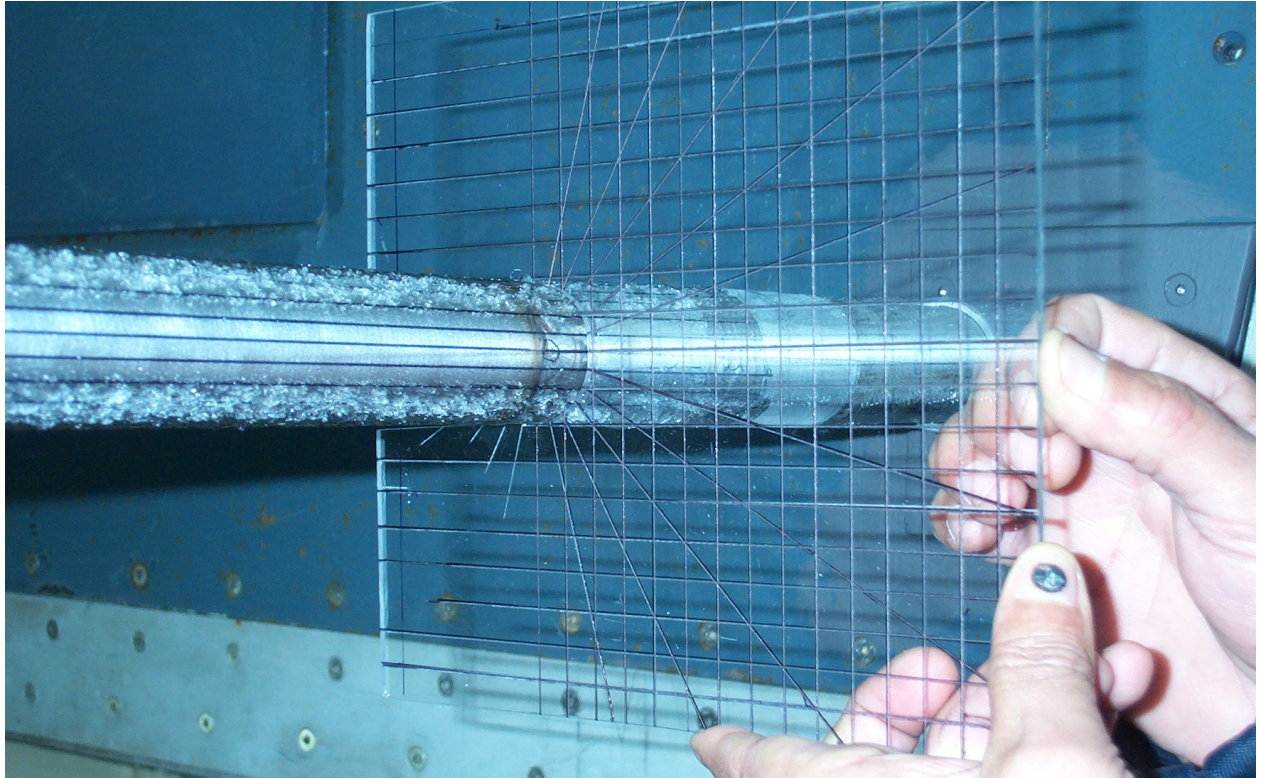


**Fig. E.4:** Ice accretion on the upstream cylinder – test n. 2

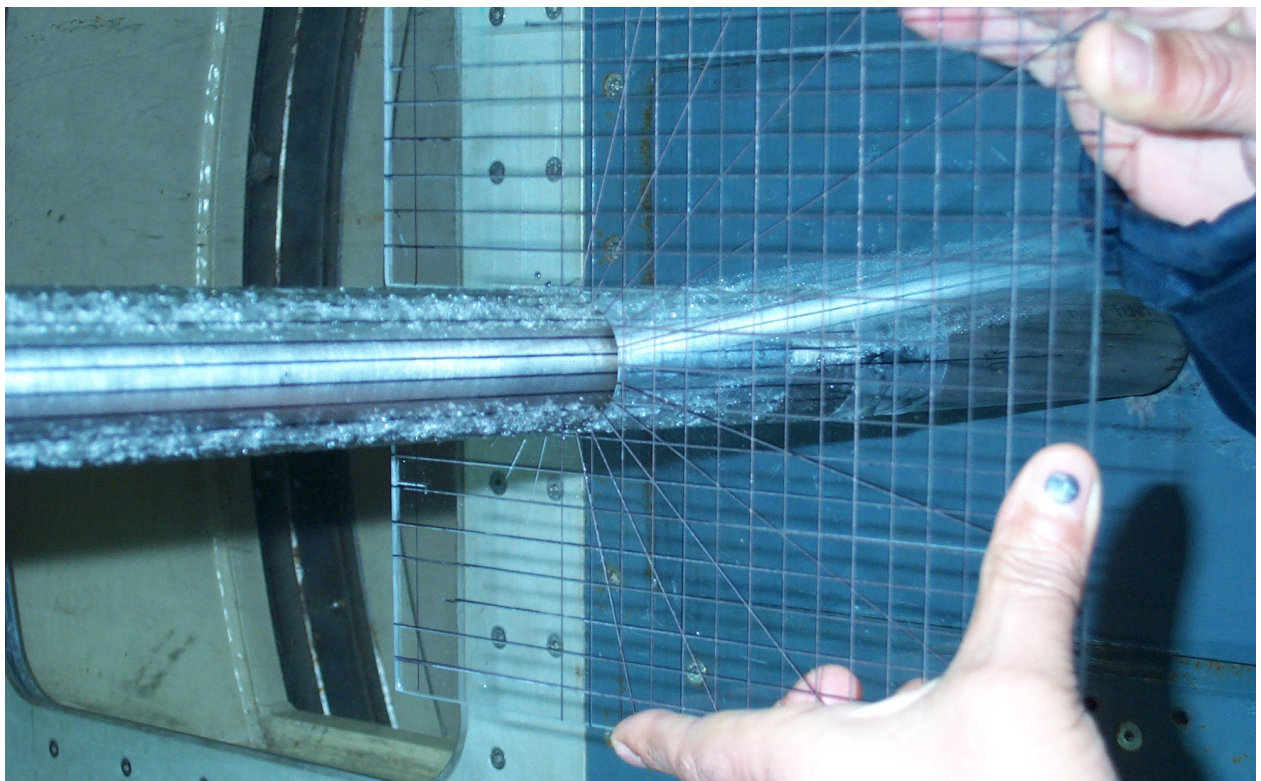


**Fig. E.5:** Ice accretion on the intermediate cylinder (test section centre) – test n. 2





**Fig. E.6:** Ice accretion on the down-stream cylinder – test n. 2

Even in this case (test n. 2), no significant differences between the three ice accretions can be observed.

Comparing the ice accretions of the two tests, it can be observed that:

- the horns' positions is almost the same in the two tests,
- test n. 2 shows a significant reduction of the ice present on the three cylinders,
- in the test n. 2, the ice present on the cylinders has a different appearance (colour and adherence) respect to the test n. 1 case,
- in the test n. 2 case, the cylinders are completely free of ice in the region of the stagnation point, up to the main horns.

From the previous considerations, the test n. 2 SBS temperatures were judged too high, so that the test n. 1 SBS temperatures are the upper limit of the optimum SBS temperatures range.

Pictures from E.7 to E.15 reports the ice accretions on the three cylinders for the tests n. 3, 4 and 5.

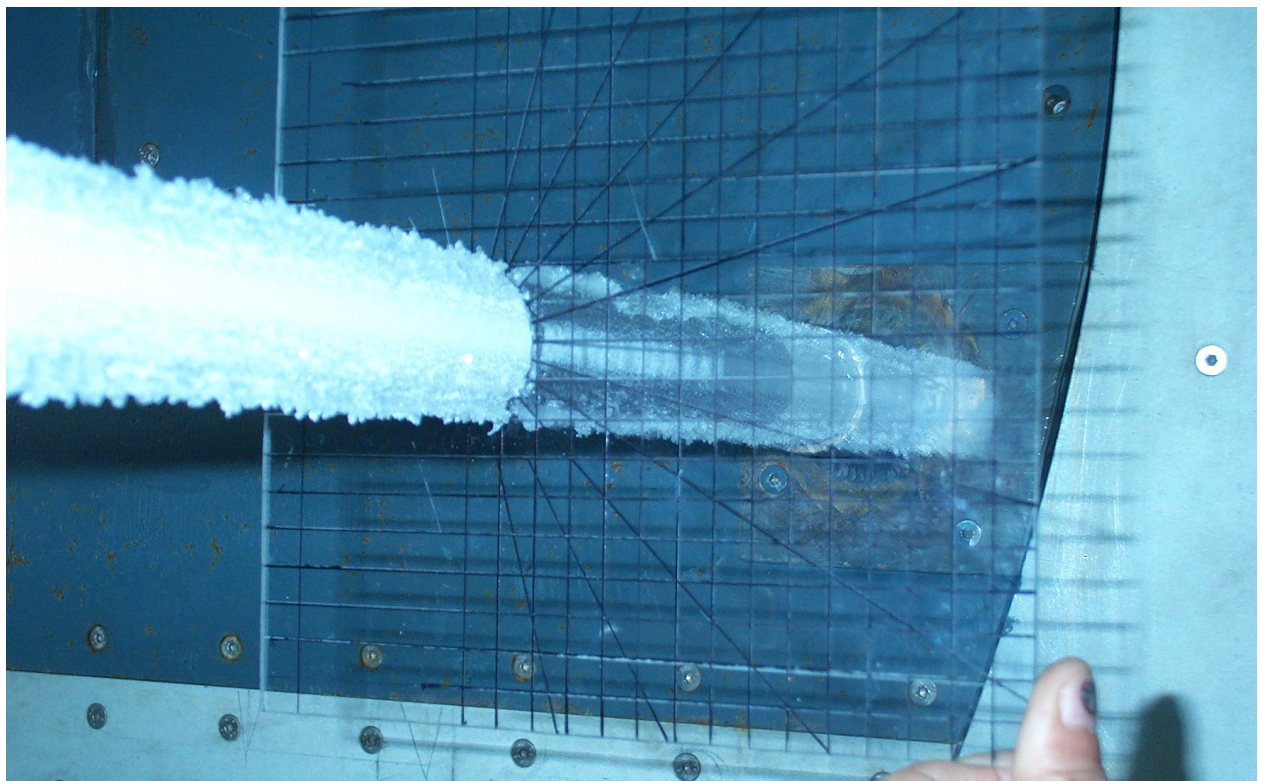


**Fig. E.7:** Ice accretion on the upstream cylinder – test n. 3



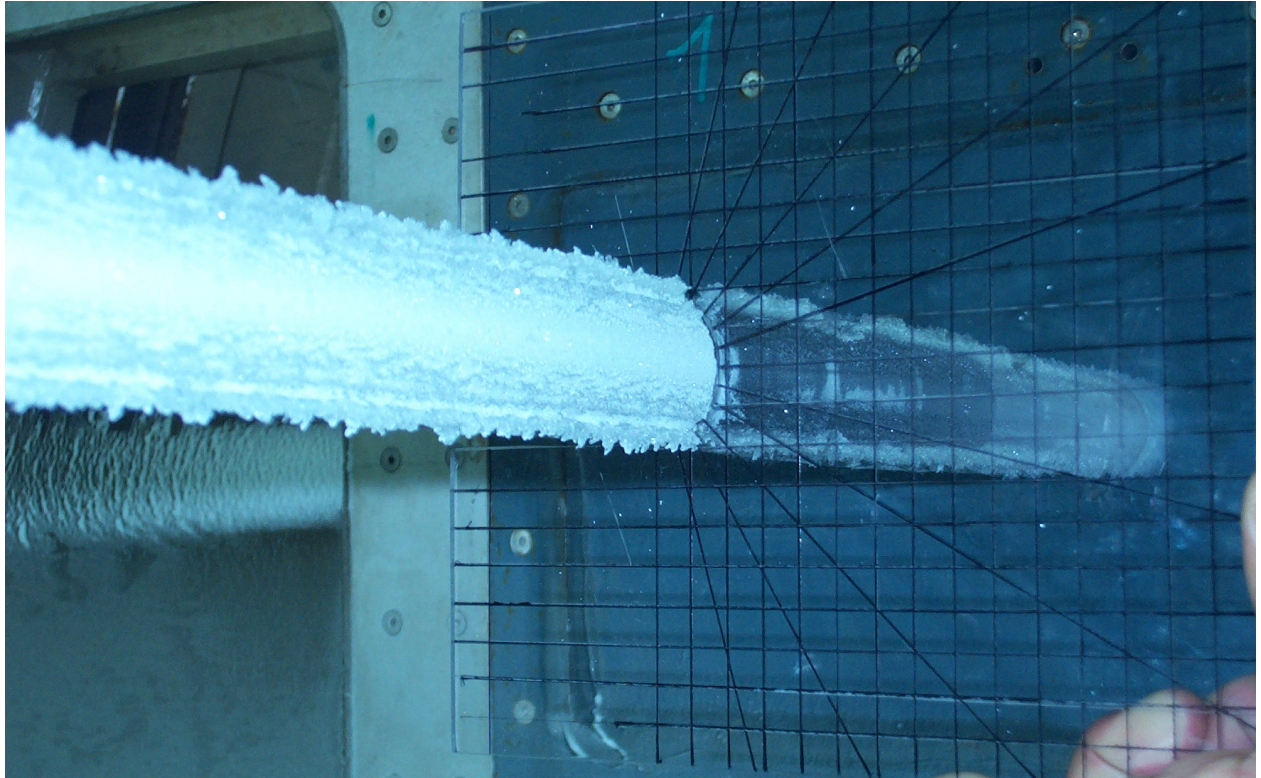


**Fig. E.8:** Ice accretion on the intermediate cylinder (test section centre) – test n. 3

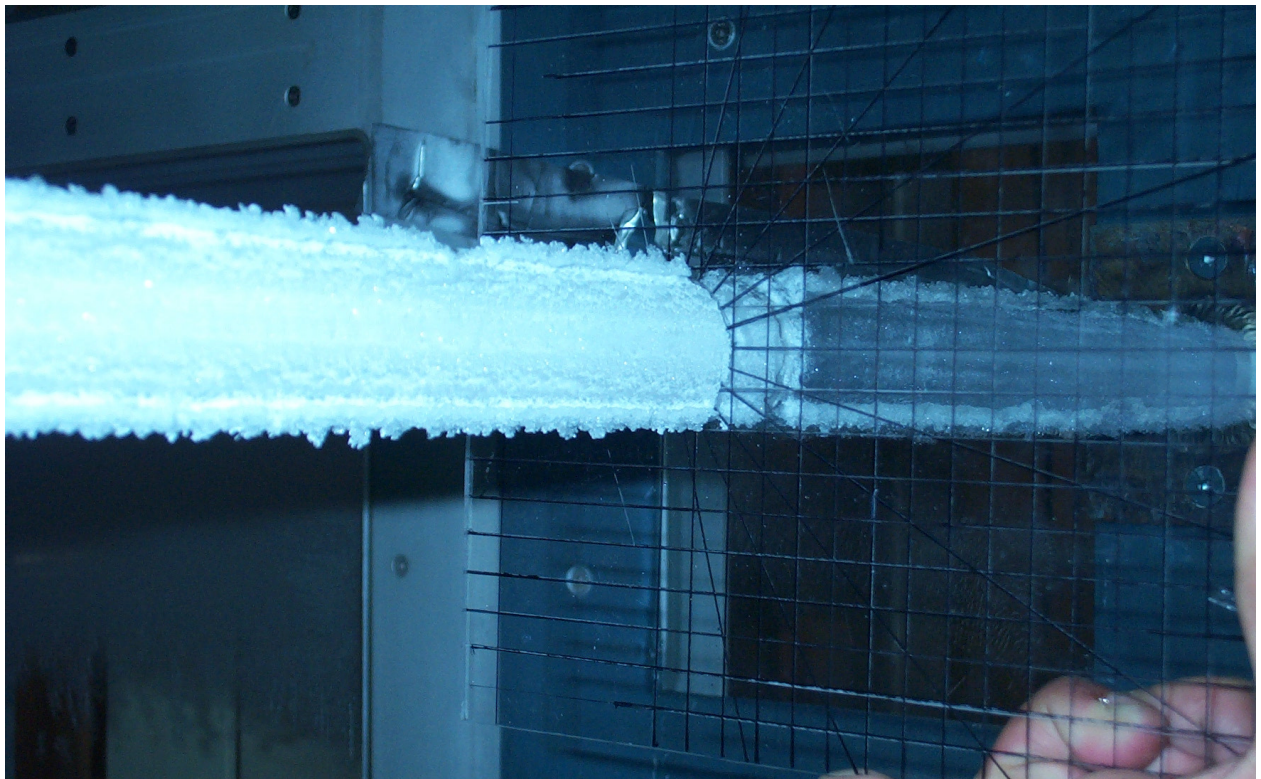


**Fig. E.9:** Ice accretion on the down-stream cylinder – test n. 3



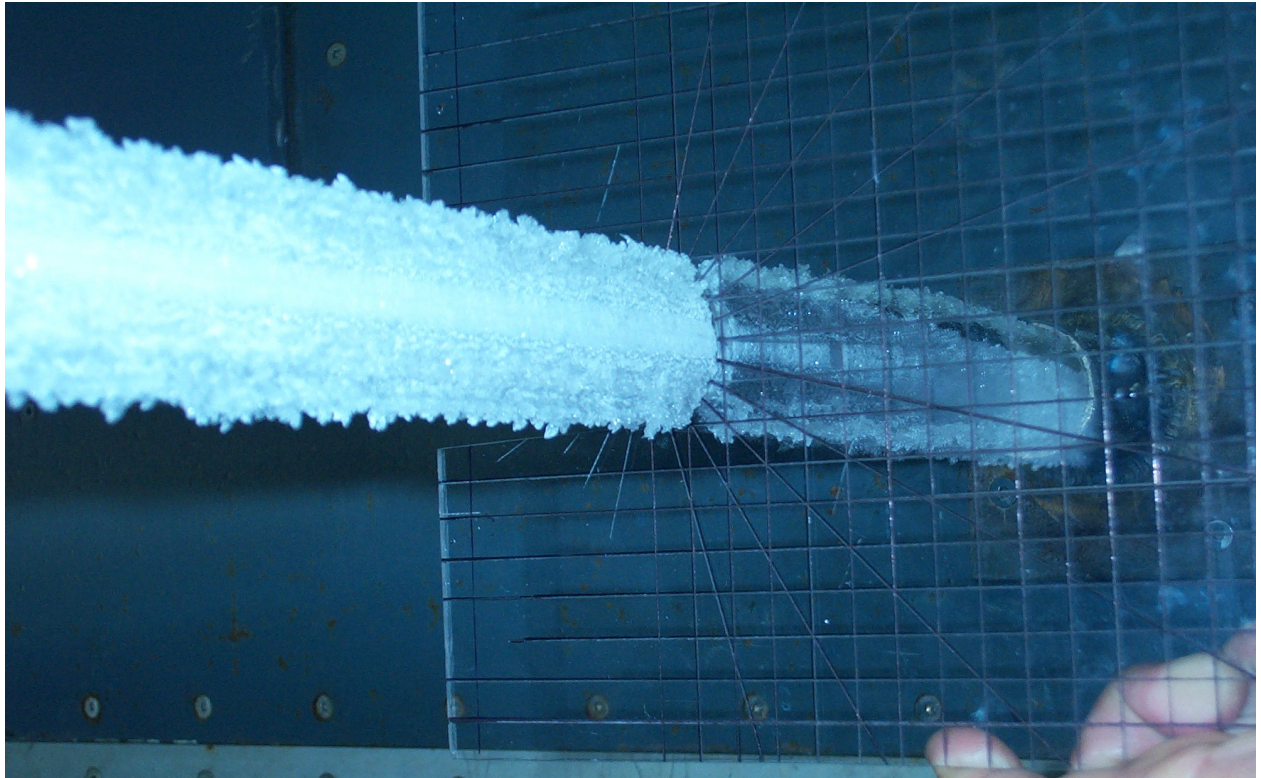


**Fig. E.10:** Ice accretion on the upstream cylinder – test n. 4

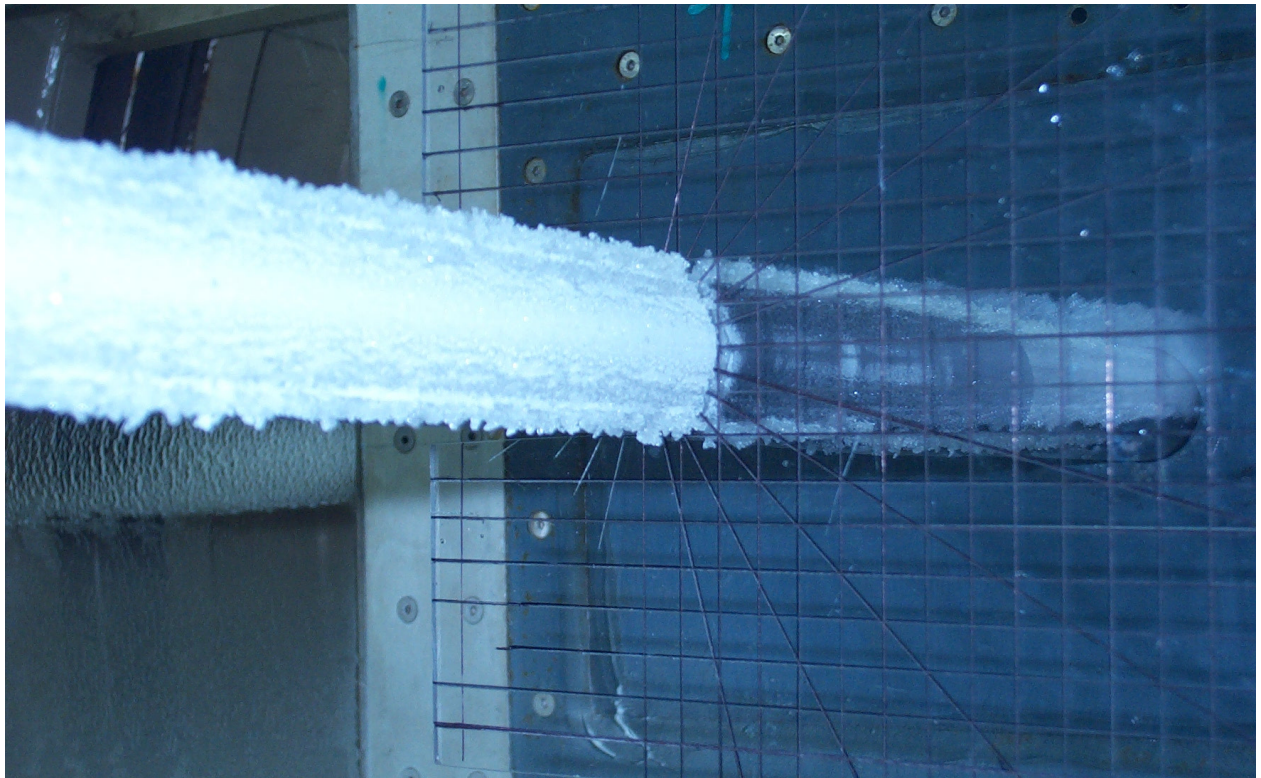


**Fig. E.11:** Ice accretion on the intermediate cylinder (test section centre) – test n. 4





**Fig. E.12:** Ice accretion on the down-stream cylinder – test n. 4

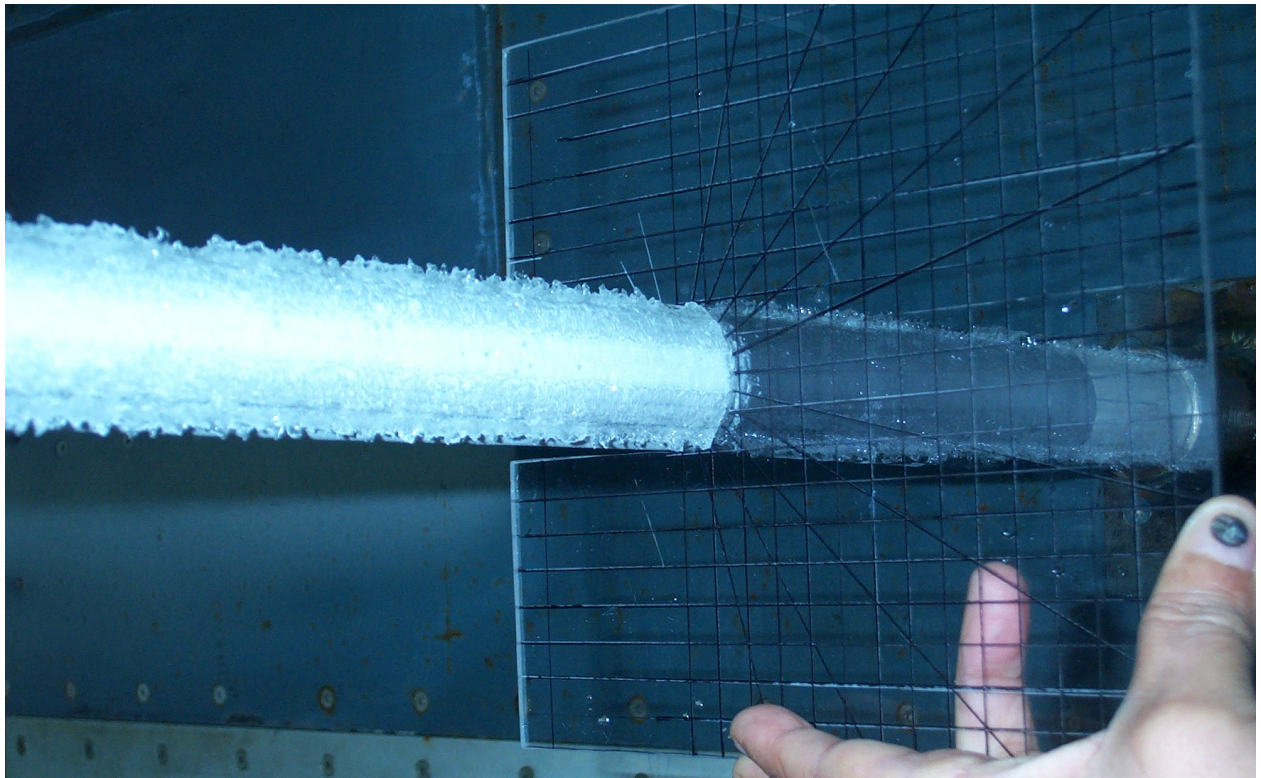


**Fig. E.13:** Ice accretion on the upstream cylinder – test n. 5



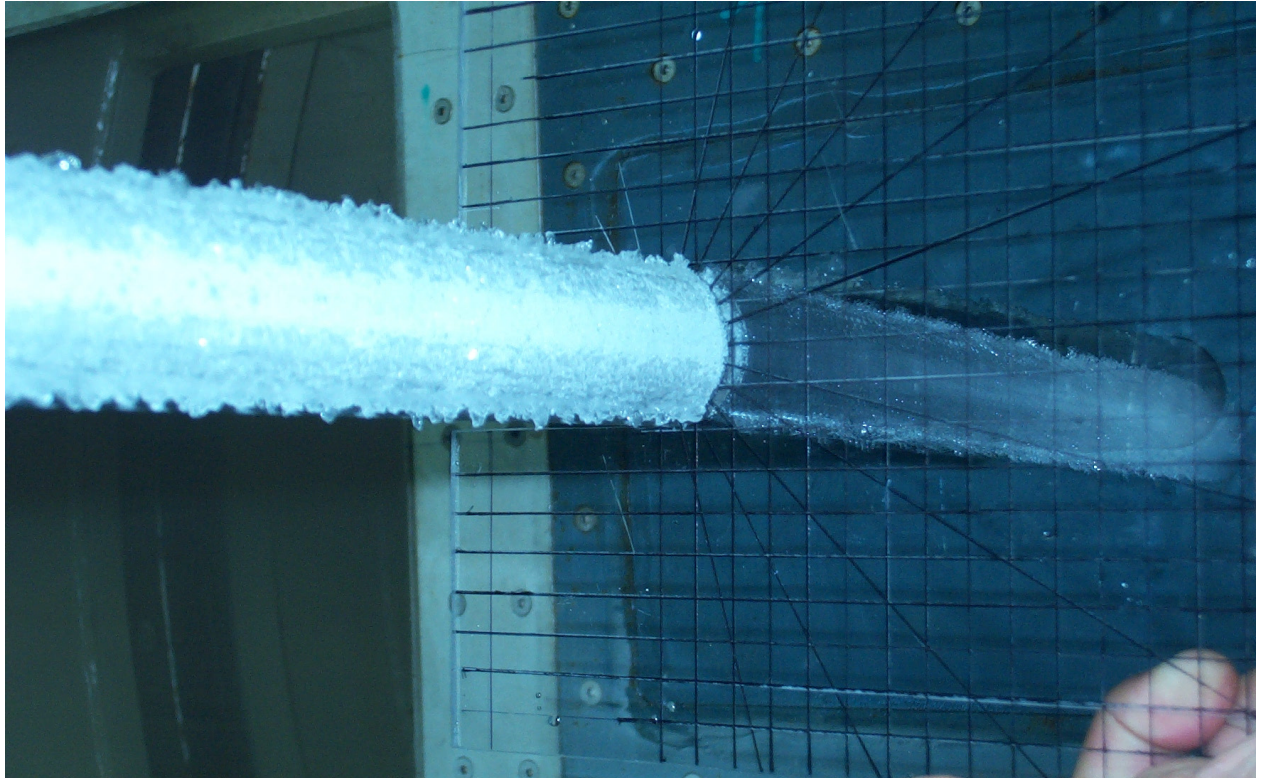


**Fig. E.14:** Ice accretion on the intermediate cylinder (test section centre) – test n. 5

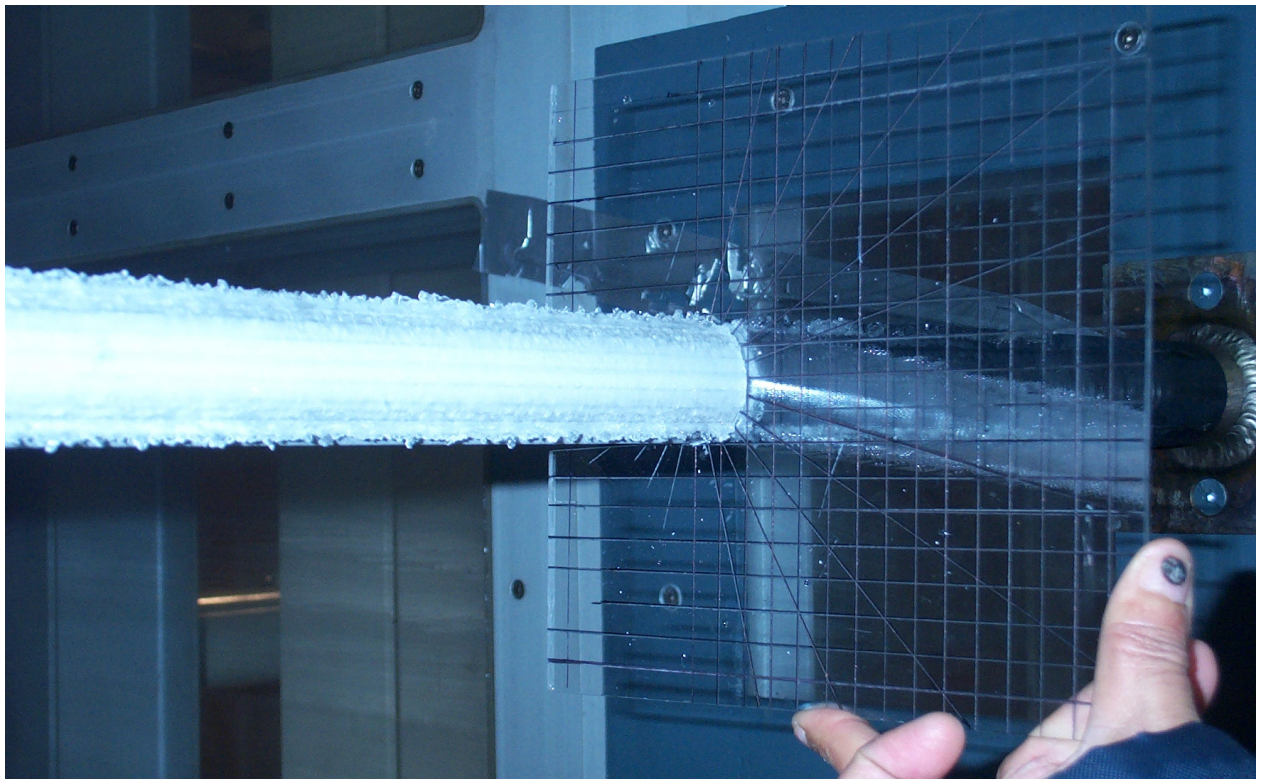


**Fig. E.15:** Ice accretion on the down-stream cylinder – test n. 5

Comparing the ice accretions of the three tests, it can be observed that:

- the horns positions do not vary significantly between the three cylinders,
- test n. 3 and 4 ice accretions do not show significant differences, in terms of quantity of ice present on the three cylinders, ice shape, etc.
- test n. 5 shows a small reduction of the ice present on the three cylinders and a slight different ice shape (the reduced quantity of ice is more evident looking at the black part of the cylinders beyond the plate).

From the previous considerations, the test n. 5 SBS temperatures were judged too high, so that the test n. 4 SBS temperatures are the upper limit of the optimum SBS temperatures range.



# BIBLIOGRAPHY

1. Paraschivoiu I., Saeed F., "Aircraft icing", John Wiley & Sons, Inc.
2. "Proceeding of the FAA International Conference on Aircraft In-flight Icing," Springfield, Virginia, May 6-8, 1996, Vol I & II, U.S. Department of Transportation, Federal Aviation Administration, DOT/FAA/AR-96/81, Final Report, August 1996.
3. Brahimi M.T., Tran P., Chocron D., Tezok F., and Paraschivoiu I., "Effects of Supercooled Large Droplets on Ice Accretion Characteristics," AIAA Paper No 97-0306, 1997.
4. Thomas S.K., Cassoni R.P., and MacArthur C.D., "Aircraft Anti-Icing and Deicing Techniques and Modeling," Journal of Aircraft, Vol. 33, No. 5, 1996, pp. 841–854.
5. Henry R., "Development of an Electrothermal De-Icing/Anti-Icing Model," AIAA Paper 92-0526, Jan. 1992.
6. Federal Aviation Administration, "Large Aircraft Ground De-icing," Pilot Guide, U.S. Department of Transportation, AC 120-58, Sept. 30, 1992.
7. Bergrun N., "Warming Trend for Icing Research," Aerospace America, Aug. 1995, pp. 22–27.
8. Potapczuk M.G., and Reinmann J.J., "Icing Simulation: A Survey of Computer Models and Experimental Facilities," AGARD CP-496, 1991, pp. 5.1–5.27.
9. Kevin R. Petty, and Carol D. J. Floyd, "A Statistical Review Of Aviation Airframe Icing Accidents In The U.S." National Transportation Safety Board, Washington, DC.
10. Lewis W., and Hoecke W.H. Jr., "Observation of Icing Encountered in Flight During 1948," NACA TN 1904, 1949.
11. Lewis W., "Icing Zones a Warm Front System with General Precipitation," NACA TN 1392, 1947.

12. Federal Aviation Administration Part 25 (FAR 25), "Airworthiness Standards: Transport Category Airplanes, Appendix C," Washington, D.C. 20591, Department of Transportation, Federal Aviation Administration, 1974.
13. Jones A.R., and Lewis W., "Recommended Values of Meteorological Factors to be Considered in the Design of Aircraft Ice-Prevention Equipment," NACA TN 1855, March 1949.
14. Anthes R.A., Panofsky H.A., and Cahir J.J., The Atmosphere, Columbus, Ohio, E. Merrill, 1978.
15. Strapp J.W., and Schemenauer R.S., "Calibrations of Johnson-Williams Liquid Water Content Meters in High-Speed Icing Tunnel," Journal of Applied Meteorology, Vol. 21, No. 1, Jan. 1982, pp. 98-108.
16. Civil Certification Authorities, "Aircraft Icing Handbook" New Zealand, 2000
17. AGARD AG 344, "Ice Accretion Simulation" Advisory Group For Aerospace Research & Development 7 Rue Ancelle, 92200 Neuilly-Sur-Seine, France, 1997
18. Cole J. A., and Sand W. R. (1991), "Statistical Study of Aircraft Icing Accidents", AIAA 91-0558.
19. Hansmann R.J., "The Influence of Ice Accretion Physics on the Forecasting of Aircraft Icing Conditions," Third International Conference on the Aviation Weather System, Anaheim, CA, Jan.-30 -Feb. 3, 1989, pp. 154-158.
20. "Calibration and Acceptance of Icing Wind Tunnels", SAE-ARP 5905.
21. Ragni A., Esposito B., Marrazzo M., Bellucci M., and Vecchione L., "Calibration of the CIRA IWT in the High Speed Configuration" Proceedings of the 43rd AIAA Aerospace Sciences Meeting and Exhibit, Reno, Nevada, Jan. 10-13, 2005 AIAA-2005-471.
22. Esposito B., Ragni A., Ferrigno F., and Vecchione L., "Cloud Calibration Update of the CIRA Icing Wind Tunnel", 2003-01-2132, SAE Transaction 2003.

23. Bellucci M., Fatigati G., Marrazzo M., Esposito B., and Ferrigno F., "Calibration of the CIRA IWT in the Low Speed Configuration" 45th AIAA Aerospace Sciences Meeting and Exhibit, Reno, Nevada, Jan. 8-11, AIAA-2007-1092.
24. Albano F., Auletta A., Bellucci M., Fatigati G., Ferrigno F., and Camussi R., "CIRA Icing Wind Tunnel Aerodynamic Calibration" Proceedings of the 2nd international conference on icing technology, Roma 7/8 settembre 2006
25. Charpin F., Prieur J., "Large Scale Icing Tests in the ONERA S1MA Windu Tunnel- Current Capabilities and new studies to generate Large Supercooled Droplets" AIAA 96-2202, June 17-20, 1996

# LIST OF ACRONYMS AND ABBREVIATIONS

ACJ	Advisory Circular Joint
ADA	Airborne Droplet Analyzer Probe
AFM	Aircraft Flight Manual
AGL	Above Ground Level
AMJ	Advisory Material Joint
APU	Auxiliary Power Unit
ARP	Aerospace Recommendation Practice
ATS	Additional Test Section
BRAIT	Boeing Research Aerodynamics and Icing Tunnel
CIRA	Italian Aerospace Research Centre
DCAC	(franch) Directorate General for Civil Aviation
EASA	European Aviation Safety Agency
EBS	External Balance System
EFS	Engine Flow Simulator
FAA	Federal Aviation Administration
FAR	Federal Aviation Regulation
FSF	Flight Safety Foundation
FSSP	Forward Scattering Spectrometer Probe
IB	Icing Blade
ICTS	Ice Contaminated Tail Plane Stall

IRT	Icing Research Tunnel
IWT	Icing Wind Tunnel
JAA	Joint Airworthiness Authority
JAR	Joint Aviation Regulation
LDV	Laser Doppler Velocimetry
LWC	Liquid Water Content
MED	Mean Effective Diameter
MSS	Model Sting Support
MTS	Main Test Section
MVD	Median Volume diameter
NACA	National Advisory Committee of Aeronautics
NASA	National Aeronautics and Space Administration
NRC	National Research Council of Canada
NTSB	National Transportation Safety Board
OAP	Optical Array Probe
PDPA	Phase Doppler Particle Analyzer
PMS	Particle Measurements System
PTS	Probe Traversing System
RH	Relative Humidity
SBS	Spray Bar System
SLD	Supercooled Large Droplet
STD	Standard

STS	Secondary Test Section
TCDS	Type Certificate Data Sheet
US	United States

# RINGRAZIAMENTI

*Anche questo treno è arrivato alla fine del suo viaggio. Un viaggio durato tre anni durante i quali sono cresciuto molto dal punto di vista umano e sicuramente non in eguale misura, dal punto di vista professionale. Come ogni viaggio molte sono state le persone che mi hanno accompagnato, alcune sono magari scese a qualche stazione intermedia, ma a tutte devo un enorme ringraziamento.*

*Primo tra tutti mi sento di ringraziare mio padre Gabriele, sceso forse dal treno troppo presto, ma che sono sicuro apprezza tutto quanto di eccezionale mi è successo in questi anni. A lui devo praticamente tutto quello che sono oggi: una persona che a sua immagine cerca in un mondo sicuramente non facile, di rimanere fedele agli insegnamenti di onestà, generosità e fedeltà che gli sono stati impartiti. Ovviamente, insieme a lui voglio ringraziare mia madre Maria e mio fratello Marco, che sempre mi sono stati vicini e compatti nel suggerirmi che strada prendere ogni volta che, durante il viaggio, si sia presentato un bivio.*

*Al Prof. Carlomagno vanno poi i miei più sentiti ringraziamenti per avermi concesso, dalla tesi di laurea ad oggi, mille opportunità di crescita, tutte di assoluto prestigio. Lo ringrazio per aver creduto in me, e spero sinceramente di poter avere il privilegio di continuare a collaborare con lui in futuro.*

*A Tommaso, persona dalle grandissime qualità tecniche oltre che umane, devo dire grazie, non solo per il supporto e l'interesse mostrato verso le attività di questo dottorato, ma soprattutto per essere riuscito a creare in laboratorio un ambiente di lavoro fatto di persone eccezionali, capaci di produrre risultati concreti e apprezzati. Ed è anche a loro, al gruppo di dottorandi-colleghi-amici, che va un grosso ringraziamento e un augurio di realizzare tutti i loro più bei sogni.*

*Al personale del CIRA che mi è stato di aiuto durante lo svolgimento di questo lavoro, e in particolare al gruppo IWT va un enorme abbraccio. Loro più di altri sono stati miei assidui compagni di viaggio in questi tre anni. Verso tutti loro nutro un infinito senso di gratitudine che porterò sempre dentro. Dall'ing. Vecchione a Rossella e Felice, da Francesco ai due "Antoni", "Marchi" e "Giovanni", Peppe, Biagio, Gianpaolo, Gennaro, Paolo, Mario, Fabrizio, Floriana, Armando, Lello, Gigino, Emilio, Enrico, Gaetano e tutti gli altri che solo per motivi di spazio non nomino. Tutti hanno contribuito a diverso titolo a questo lavoro e tutti meriterebbero molto di più di un semplice ringraziamento. Tuttavia, a parte il valore indiscutibile del loro lavoro, il mio ringraziamento più sentito va per l'affetto, la disponibilità e, in taluni casi, l'amicizia che mi hanno regalato, e che metro dopo metro, in questo lungo cammino mi ha dato grande forza e fiducia.*

*Per ultima i miei ringraziamenti vanno a colei senza la quale oggi probabilmente sarei molto ma molto meno di quel (poco) che sono. Con lei il viaggio dura ormai da oltre 13 anni e penso che questo da solo basti a far capire che quel che ci unisce è davvero qualcosa di speciale e unico. Quelli che hanno la fortuna nella loro vita di provare qualcosa del genere, chiamano questo insieme di emozioni e sentimenti Amore; tutto questo per me invece si chiama semplicemente Caterina. Non è retorica se la ringrazio per essermi stata sempre, ma davvero sempre, vicina, anche quando magari non condivideva in tutto una mia scelta. Spero di poter essere sempre alla sua altezza. So che non sarà facile, ma ci proverò sempre ogni giorno, per tutti gli altri giorni che ci vedranno vicini, in qualche parte del mondo, protagonisti di questo nostro viaggio.*